NUREG/CR-5632

Incorporating Aging Effects into Probabilistic Risk Assessment — A Feasibility Study Utilizing Reliability Physics Models

Manuscript Completed August, 2001

Prepared by
C. L. Smith, V. N. Shah, T. Kao,† G. Apostolakis †

Idaho National Engineering and Environmental Laboratory
Idaho Falls, ID 83415-3850

A. Buslik, NRC Technical Monitor

Prepared for
Office of Nuclear Regulatory Research
U.S. Nuclear Regulatory Commission
Washington, DC 20555-0001

†Massachusetts Institute of Technology

ABSTRACT

Traditional probabilistic risk assessments (PRAs), in general, do not include passive SSCs (systems, structures, and components) since they are much more reliable than the active components. Aging phenomena, however, may make passive SSCs less reliable than assumed. Further, operation of power plants over durations of decades may lead to degradation of material properties and component strength, and eventually, if not mitigated, to aging-related failures. This report documents the feasibility assessment performed by the Idaho National Engineering and Environmental Laboratory for incorporating aging information and models directly into a PRA.

The work in this report focuses on corrosion, specifically flow-accelerated corrosion. We have evaluated the feasibility of modeling aging by incorporating a flow-accelerated corrosion model into PRA. The corrosion model that we used, the KWU model developed by Kastner and Riedle, estimates wall thinning. For this purpose, we have used the PRA model developed for the Surry Individual Plant Examination. In addition, we have employed a *load-capacity* model based upon a *reliability physics* model to estimate failure caused by flow-accelerated corrosion. Also, we have shown that a rigorous treatment of both aleatory and epistemic uncertainty is a vital part of the overall methodology. Successful demonstration of the methodology embodied in this report led to the realization of both expected and unexpected results. Expected results include the calculation of core damage frequency as a function of time due to the flow-accelerated corrosion aging mechanism. Unexpected results showed that attempting to model aging-related failures via a failure rate parametric model (e.g., a linear aging failure rate model) was incomplete. We have demonstrated that the results and insights gained from the U.S. Nuclear Regulatory Commission (NRC) Nuclear Power Aging Research Program and other NRC and industry programs related to materials degradation can be integrated into existing PRA models. However, our evaluation represents the feasibility of such integration and *should not* be construed to represent either relative or absolute magnitude of risk posed by flow-accelerated corrosion in pressurized water reactors.

FIN W6329: Incorporating Aging Effects Into PRA

CONTENTS

Abstract . . . iii
List of Figures . . . viii
List of Tables . . . x
Executive Summary . . . xii
Foreword . . . xx
Acknowledgments . . . xxi
Acronyms . . . xxii

1. Introduction . . . 1
    1.1 Overview . . . 1
    1.2 Project Objectives . . . 2
    1.3 General Modeling of Aging Issues . . . 3
    1.4 Report Organization . . . 4

2. Aging Mechanisms . . . 6
    2.1 Description of Aging Mechanisms for Passive Components . . . 6
        2.1.1 Radiation Embrittlement of Ferritic Low-Alloy Steels . . . 8
        2.1.2 Thermal Aging of Cast Stainless Steels . . . 9
        2.1.3 Low-Cycle Fatigue . . . 11
        2.1.4 High-Cycle Vibrational Fatigue of Welded Piping Connections . . . 12
        2.1.5 Primary Water Stress Corrosion Cracking of Alloy 600 Components . 13
        2.1.6 Flow Accelerated Corrosion of Carbon Steel Components . . . 16
    2.2 Models and Data for Aging Damage to Passive Components . . . 17
    2.3 Field Experience Related to Aging Damage of Passive Components . . . 20

3. Risk Importance and Modeling of Flow Accelerated Corrosion . . . 24
    3.1 Overview . . . 24
    3.2 Review of FAC Failures . . . 26
    3.3 Overview of Single-Phase FAC . . . 33
    3.4 Overview of Two-Phase FAC . . . 39
    3.5 Selection of FAC Empirical Models . . . 40
    3.6 Details of KWU-Kastner FAC Model . . . 44

4. Incorporating Aging Effects into PRA Methodology . . . 49
    4.1 Introduction . . . 49
    4.2 PRA Characteristics Important to Aging Evaluations . . . 50
        4.2.1 PRA Parameters . . . 51
        4.2.2 Structural Issues . . . 51
    4.3 PRA Database Selection . . . 56
    4.4 Criteria for Selecting SSCs and Aging Mechanisms . . . 58

4.4.1 Background 58
4.4.2 Aging-Based Screening of SSCs 60
4.5 Development of Load-Capacity FAC Model 67
4.5.1 General Load-Capacity Formulation for FAC 67
4.5.2 Detailed Determination of the Capacity 72
4.5.3 Calculation of the Load-Capacity Probability 77

5. Case Studies 81
5.1 Overview of Two FAC Test Case Studies 84
5.1.1 Overview of Case 1 - Surry Unit 2 Single-Phase FAC 85
5.1.2 Event Description of Case 1 85
5.1.3 Overview of Case 2 - Trojan Single-Phase FAC 87
5.1.4 Event Description of Case 2 87
5.2 Main Feedwater PRA Calculation 88
5.3 Preheat Steam Generator PRA Calculation 97

6. Conclusions 105
6.1 General Conclusions 105
6.2 Further Considerations 107

7. References 109

Appendix A - Models/Codes Available for Quantitative Estimates of Aging Damage A-1
A-1 Radiation Embrittlement of Ferritic Low-Alloy Steels A-3
A-2 Thermal Aging of Cast Stainless Steels A-7
A-3 Low-Cycle Fatigue A-8
A-4 High Cycle Vibrational Fatigue of Welded piping Connections A-14
A-5 Primary Water Stress Corrosion of Carbon Steel Compounds A-15
A-6 Flow-Accelerated Corrosion of Carbon Steel Components A-17
A-7 References A-21

Appendix B - Field Experience Related to Damage of Passive Components Caused by Selected Degradation Mechanisms B-1
B-1 Radiation Embrittlement of Ferritic Low-Alloy Steels B-3
B-2 Thermal Aging of Cast Stainless Steels B-3
B-3 Low-Cycle Fatigue B-4
B-4 High-Cycle Vibrational Fatigue of Welded Piping Connections B-8
B-5 Primary Water Stress Corrosion Cracking of Alloy 600 Components B-11
B-6 Flow-Accelerated Corrosion of Carbon Steel Components B-16
B-7 Boric Acid Corrosion B-21
B-8 Wear B-21
B-9 References B-23

Appendix C - Modeling of Radiation Embrittlement C-1
C-1 Probability of Through-Wall Cracks in the Vessel Wall C-4
C-2 Probability Distributions Used in the VISA II-Code C-6

Appendix D - Results of PRA-Based Event Screening Using SWIM Index D-1

Appendix E - Source Code for the SAPHIRE "Compound" FAC Calculation E-1

LIST OF FIGURES

Figure 1. Simple illustration of traditional PRA versus aging-physics PRA models 5
Figure 2. Charpy V-notch surveillance data, showing radiation embrittlement effects 9
Figure 3. The flow-accelerated corrosion model 25
Figure 4. Comparison of the EPRI-CH and the KWU-KR models 35
Figure 5. The calculated influence of fluid temperature on the ferrous ion concentration and on mass transfer of ferrous ions 36
Figure 6. Schematic of a feedwater system for a Westinghouse plant steam generators equipped with preheaters 38
Figure 7. KWU-KR FAC model, comparison against single-phase laboratory data . . . 41
Figure 8. KWU-KR FAC model, comparison against single and two-phase both laboratory and plant data 42
Figure 9. EPRI-CH FAC model, comparison against single-phase laboratory data . . . 43
Figure 10. EPRI-CH FAC model, comparison against single and two-phase both laboratory and plant data 43
Figure 11. Comparison of the EPRI-CH and the KWU-KR FAC models for flow rate variations 47
Figure 12. Comparison of the EPRI-CH and the KWU-KR FAC models for dissolved oxygen content variations 48
Figure 13. Comparison of the EPRI-CH and the KWU-KR FAC models for cold pH variations 48
Figure 14. Illustration of the aging into PRA case study framework 50
Figure 15. Illustration of a load-capacity probability calculation 68
Figure 16. Example of a potential load distribution curve for nominal, steady-state pressures 70
Figure 17. Graphical illustration of the load-capacity FAC model attributes and uncertainty types 71
Figure 18. Comparison of values calculated by empirical KWU-KR model with measurements from laboratory experiments and power stations 73
Figure 19. Illustration of the logic model representing the combined FAC-caused loss-of-main-feedwater event and the nominal event 83
Figure 20. Illustration of the location and piping types for the Surry MFW PRA calculation 89
Figure 21. P&ID for the main feedwater system at the Surry plant 90
Figure 22. Probability of FW-04 pipe failure (due to FAC) as a function of time 94
Figure 23. P&ID for the AFW system at the Surry plant 98
Figure 24. Cumulative failure probability of AFW-15 pipe segment from FAC 102

LIST OF FIGURES (cont.)

Figure 25. Failure probability for AFW-15 from FAC for the i'th year of operation. . . 103
Figure 26. Cumulative core damage probability from FAC and all PRA initiators. 104

Figure A-1. Fatigue data of SA 106-B carbon steel smooth base metal specimens in air at room temperature and 288°C A-25
Figure A-2. Reference fatigue crack growth curves for carbon and low alloy ferritic steels exposed to air environments (subsurface flaws) A-25
Figure A-3. Reference fatigue crack growth curves for carbon and low alloy ferritic steels exposed to water environments A-26
Figure A-4. Coefficient "C" in equation (A-5) as a function of temperature A-27
Figure A-5. Frequency correction factor "F" as a function of cyclic frequency in the range 800° – 1,000°F A-27
Figure A-6. Ratio correction factor "S" as a function of stress ratio A-28
Figure A-7. Reference fatigue crack growth curves for austenitic stainless steels in air environments A-29
Figure A-8. Comparison of high grain boundary carbide coverage materials (>40%) with the modified Scott model A-30
Figure A-9. Comparison of low grain boundary carbide coverage materials (<20%) With the modified Scott model A-31
Figure A-10. Potential sites for the two different types of wet steam flow-accelerated corrosion damage A-32

Figure B-1. Schematic diagram of a safety injection and residual heat removal system in a three-loop Westinghouse plant B-27
Figure B-2. Location of the cracks in the base metal and welds in the safety injection piping in Tihange Unit 1 . . . . . B-28
Figure B-3. PWSCC cracks in rolled plug supplied by Babcock & Wilcox B-29
Figure B-4. Schematic of a feedwater system for a Westinghouse plant with steam generators equipped with preheaters B-30
Figure B-5. Westinghouse flux thimble tube routing B-31
Figure B-6. Westinghouse in-core instrument guides B-32
Figure B-7. Palisades core barrel wear B-33

LIST OF TABLES

Table 1. List of major LWR components evaluated in the NRC Nuclear Plant Aging Research Program 7
Table 2. Quantitative models for estimating aging damage to passive PWR components 18
Table 3. Extent of aging damage in PWR reactor pressure vessel, pressurizer, and reactor coolant pump 21
Table 4. Main PWR components and their degradation mechanisms 27
Table 5. Main BWR components and their degradation mechanisms 28
Table 6. Review of the "pipe leakage" LERs for the most recent six years 29
Table 7. Summary of 17 LER cases related to the "MSL Leakage" 31
Table 8. Aging-caused impacts to PRA parameters 52
Table 9. Aging-caused impacts to the structure of a PRA 54
Table 10. Basic event importance measure results and their applicability to the aging analysis for the Surry IPE PRA model (sorted by the SWIM index) for events with F-V > 0.005 or RIR > 2 63
Table 11. Basic events that passed the "risk significance" screening with their aging influencing factors (sorted by the SWIM index) for events with F-V > 0.005 or RIR > 2 64
Table 12. Typical stress and hoop strain parameter values for SA 516 grade 70 carbon steel 69
Table 13. Lognormal distributions for the E factor for the four regions of Figure 18 75
Table 14. Data conditions for the parameterization of the KWU-KR model 76
Table 15. Case 1 FAC parameters and epistemic uncertainty information (single phase flow) 84
Table 16. Case 2 FAC parameters and epistemic uncertainty information (single phase flow) 85
Table 17. FAC parameter and uncertainty information for the Surry main feedwater PRA analysis 93
Table 18. FAC parameters and uncertainty information for the preheater-type steam generator PRA analysis 101

Table A-1. Key regulatory changes and guidance for RPV integrity A-4

Table B-1. Summary of fatigue damage locations in major LWR components B-5
Table B-2. PWR feedwater piping cracking during 1979-1980 (1 in. = 25.4 mm) B-6
Table B-3. PWR feedwater nozzle cracking 1983 to present (1 in. = 25.4 mm) B-7
Table B-4. Summary of PWR cracking in pipes smaller than 4 inches (10.2 cm.) B-9

LIST OF TABLES (cont.)

Table B-5.	Summary of pressurizer incidents, domestic	B-13
Table B-6.	Summary of pressurizer incidents, EdF	B-14
Table B-7.	Summary of control rod drive mechanism nozzle inspection results	B-17
Table B-8.	BWRs with pipe wall thinning in the feedwater-condensate systems	B-18
Table B-9.	PWR plants with pipe wall thinning in the feedwater-condensate systems	B-19
Table B-10.	Summary of boric acid corrosion of carbon steel	B-22
Table C-1.	A comparison of three flaw-depth distributions	C-6
Table D-1.	Basic event importance measure results and applicability to the aging analysis for the Surry IPE PRA model (sorted by the SWIM index) for events with F-V > 0.005 or RIR > 2	D-5

EXECUTIVE SUMMARY

ES.1 Background

The high initial reliability of passive systems, structures, and components (SSCs) at operating light water reactors (LWRs) is being reduced as the plants are getting older. Operational experience has revealed several aging mechanisms and affecting phenomena that have caused SSC damage. Consequently, the U.S. Nuclear Regulatory Commission (NRC) sponsored the Nuclear Plant Aging Research (NPAR) program to gather data and develop insights in aging of LWR SSCs. In addition, several other NRC- and industry-sponsored projects have generated both qualitative and quantitative information related to material degradation in passive SSCs. This large collection of information, however, *has not* been used to estimate the risk impact of aging of passive SSCs.

The work embodied in this report evaluates the potential of incorporating this large body of qualitative information into probabilistic risk analysis so that the risk-impact of aging of passive SSCs can be assessed. The overall objective of the work is to assess the *feasibility* of applying the *LANL/ASCA* method for incorporation of reliability-physics based models, expert judgement, and the results of the NPAR program into an integrated aging probabilistic risk assessment (PRA). The *LANL/ASCA* method refers to the PRA methods described in NUREG/CR-6157, *Survey and Evaluation of Aging Risk Assessment Methods and Applications*. The feasibility assessment that is presented here was performed via a trial application of the NUREG/CR-6157 methodology. This application utilizes an existing nuclear power plant PRA for which a SAPHIRE computer model currently exists. The main focus of the project is on pressurized water reactor (PWR) components, but the application presented here can equally be applied to boiling water reactor (BWR) components.

Aging degradation mechanisms may be divided in two groups based on the resulting failure modes: (1) those that may cause rupture, and (2) those that may cause cracking. Radiation embrittlement, thermal aging of cast stainless steel components, and vibratory fatigue of small-diameter piping may cause rupture. Low-cycle fatigue, high-cycle thermal fatigue, and stress corrosion cracking of components (other than steam generator tubes) may cause cracking. The mechanisms that have potential to cause rupture are likely to have significantly more risk impact. Therefore, we have decided to incorporate a model for one of the degradation mechanism that may cause rupture. Specifically, we decided to incorporate flow-accelerated corrosion mechanisms into the PRA.

The flow-accelerated corrosion mechanism is characterized by a process of magnetite (Fe_3O_4) dissolving and being replaced by iron oxide. Normally, a thin layer of porous iron oxide (mostly magnetite) forms on the inside surface of carbon steel feedwater piping and limits further corrosion. However, the magnetite layer may be dissolved and be replaced by new iron oxide formed at the metal-oxide interface, resulting in pipe thinning. This process is called *single-*

phase flow-accelerated corrosion. A similar corrosion process causes wall thinning of carbon steel piping exposed to wet steam; this process is called *two-phase* flow-accelerated corrosion.

ES.2 Incorporation of Aging Reliability-Physics Model into PRA

Single-phase flow-accelerated corrosion test results have identified several factors that affect the corrosion rate: (a) hydrodynamic variables including fluid velocity, piping configuration (geometry of the flow path), and roughness of the inner pipe surface; (b) metallurgical variables including chemical composition and weight percentage of chromium, molybdenum and copper in the steel; and (c) environmental variables including temperature and water chemistry (e.g., dissolved oxygen, ferrous ion concentration, pH). These parameters were utilized in the corrosion model that was integrated into the SAPHIRE PRA software. This model was derived from existing flow-accelerated corrosion research that has been performed both within and outside the U.S. As part of the model development, we investigated existing industry computer codes algorithms including the EPRI-sponsored CHECWORKS and the Siemens/KWU WATHEC versions. We have elected to base our calculations on the KWU-KR (KR for Kastner and Riedle, the model originators) model because it is well documented in the published literature.

The KWU-KR model calculates the corrosion rate as a function of multiple parameters (as noted above). With this model, the pipe thickness can be calculated as a function of time. The wall corrosion, $W_C(t)$, is the thickness of the pipe corroded away and is calculated by

$$W_{C,calculated}(t) = \frac{\Delta\phi_R\, t}{\rho_{st}}$$

where

$\Delta\phi_R$	=	flow-accelerated corrosion rate ($\mu g/cm^2$ hr),
t	=	exposure time (hr),
ρ_{st}	=	the density of steel ($\mu g/cm^3$).

The corrosion rate, $\Delta\phi_R$, is calculated using a fairly complex analytical expression derived from operational and experimental test data. Details of this calculation are provided in the report.

To determine the risk impact of pipe rupture caused by flow-accelerated corrosion, we need to determine the probability of rupture at different locations in susceptible piping. The probability of rupture can be determined using a "load-capacity" formulation for the flow-accelerated corrosion mechanism. The loads acting on the piping may be represented by the steady state and transient pressures, and the pressure capacity of piping takes into account pipe wall thinning caused by flow-accelerated corrosion. Once both the load and capacity parameters are known, we can estimate the piping failure probability. We integrated this calculation using load (e.g., piping pressure) and capacity (e.g., pipe wall-thickness remaining at a point in time)

directly into the SAPHIRE PRA model in order to demonstrate the feasibility of "incorporating reliability-physics based models directly into PRA."

One novel aspect of the work was the specific treatment of uncertainties (both epistemic and aleatory) as part of the model development. For example, to express our uncertainty in the KWU-KR model predictions, we employ the "adjustment-factor" approach. This resulted in the utilization of a model for the corrosion rate that is a product of its *deterministic* reference model prediction and an adjustment factor. This adjustment factor accounts for the inadequacy of the calculated value and represents model uncertainty. Further, when we make predictions using the KWU-KR model, we do not know how inaccurate the model is with respect to the actual situation that we are attempting to model. In other words, we do not know what the value of the adjustment-factor is. We can say, then, that we have a population of conditions (similar to a population of plant-specific failure rates) which is aleatory.

The study did not take credit for the potential of inspections of FAC-susceptible piping locations. All plants currently have an existing inspection program for FAC. Consequently, if one were to determine that FAC was taking place at an unacceptable rate or that the thickness of a pipe was marginally acceptable, a decision could be made to replace the damaged piping. This intervention would mitigate the FAC process and usurp the potential for pipe failure (in that particular pipe). But, to take credit in the PRA for having an inspection program, one would need to determine a probability that the inspection program fails to detect and mitigate FAC. It was beyond the scope of this project to determine this non-detection probability, but we know that it is not zero since U.S. NPPs have had FAC inspection programs for several years while at the same time FAC events still are being recorded in the operational history.

The treatment of the uncertainties within the load formulation was also addressed. The load was divided into two types: (1) steady-state pressure loading and (2) transient pressure loading. The two loads are treated separately and with different model types. The steady-state pressure is modeled simply as a parameter with epistemic uncertainty. But, the treatment of the transients is more complicated because their occurrence in time must be evaluated. The occurrence of transients is an aleatory phenomenon. The magnitude of the transient pressure is represented by a parameter having epistemic uncertainty.

ES.3 Case Study Results

For the first case study, a piping segment was selected for analysis and incorporation into a full-scale PRA model. The selected pipe segment in our analysis is the same as the particular segment that failed in December of 1986 at Surry (the 18-inch suction line to the main feedwater pump A of Unit 2 failed in a catastrophic manner). In accordance with our choice to analyze the main feedwater system, we specifically modeled the pipe segment failure. Failure of this pipe in Surry's main feedwater system results in the loss of two main feedwater pumps at the same time.

The indirect impacts due to failure of the pipe segment were also considered. For the Surry plant, flooding in the turbine building was a significant plant vulnerability. But, the pipe segment is located in the basement of the turbine building. After discussions with Surry PRA and piping personnel, it was determined that there are no safety related equipment in the area. Hence, it was decided that indirect effects will not contribute to our case study.

Once the piping event was integrated into the Surry PRA model, the basic event was linked to the flow-accelerated corrosion SAPHIRE "plug-in" calculation module. With the data for the flow-accelerated corrosion parameters known, the failure probability of the pipe as a function of time can be estimated. Figure ES-1 illustrates the results of such a calculation. Note that in addition to the failure probability, the constituents to the total probability are shown. As previously discussed, these constituents come from two type of models, namely, from either the nominal steady-state pressure or transient pressures.

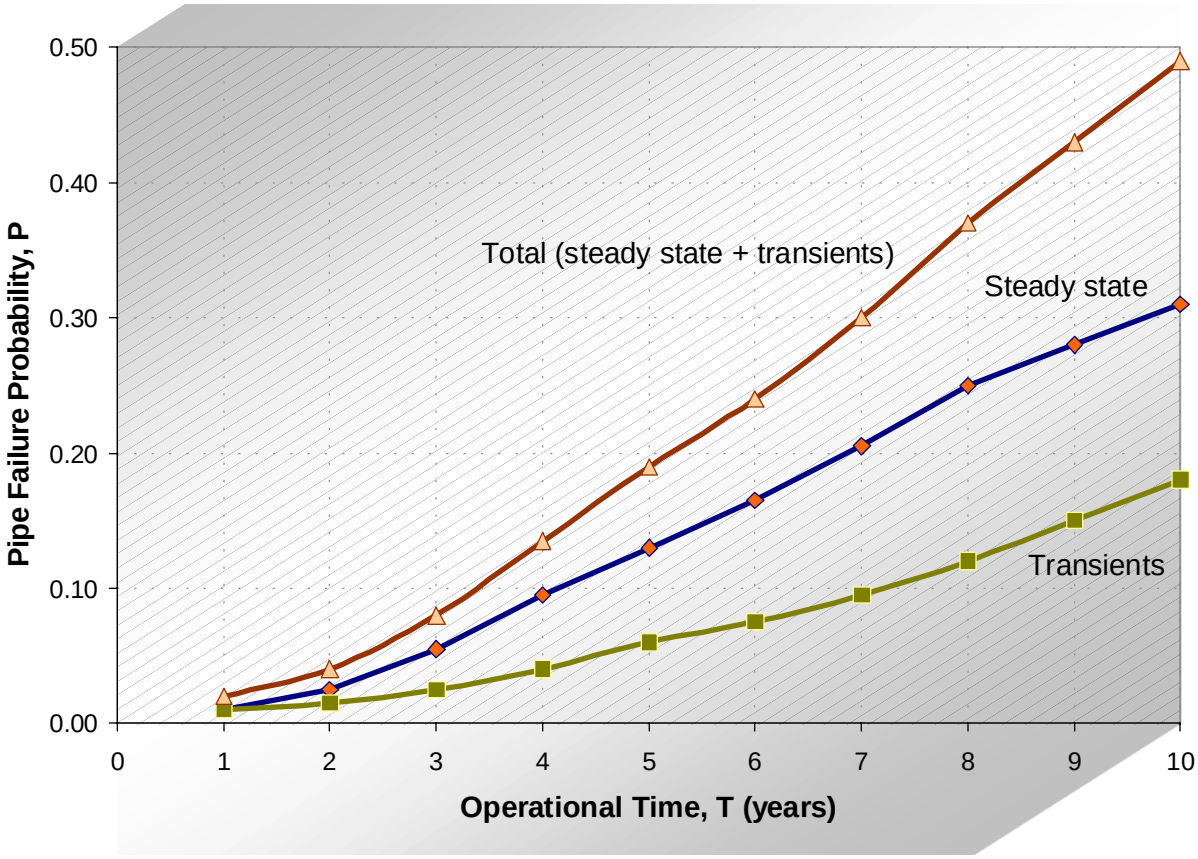

Figure ES-1. Flow-accelerated corrosion impact on the FW-04 pipe segment as modeled with the KWU-KR model.

From the PRA, the core damage probability over 10 years shows a small increase of about 20% for the loss of main feedwater event tree sequences (i.e., just the IE-T2 sequences). However, the overall impact on the overall core damage frequency over the 10 year period was found to be insignificant (less than 0.2%). This result is not surprising since the nominal loss of main feedwater sequences contribute less than 1% to the total core damage. Note though that the impact on the risk due to flow-accelerated corrosion for other plants or plant models has not been evaluated. Further, the calculations performed for this case study were somewhat conservative due to simplifications made as part of the calculation. These simplifications, their analysis implications, and suggestions for more refined calculation techniques are discussed in the body of the report.

A second case study was set up to evaluate the potential for flow-accelerated corrosion in plants equipped with preheater-type steam generators. For this second case, the auxiliary feedwater (AFW) system of the Surry IPE model was modified. Note that Surry does not have a preheater steam generator, but the nominal PRA model can be modified to represent the potential flow-accelerated-corrosion-caused failure and resultant impact on the AFW piping. For the model, the focus of the case study are pipe segments AFW-15 and AFW-16. These two pipe segments were incorporated directly into the Surry PRA, and failure of the pipe segment is represented by the flow-accelerated corrosion module within the SAPHIRE software. With the data for the flow-accelerated corrosion parameters known, the changes in pipe failure probability (due to the corrosion) as a function of time can be evaluated. Figure ES-2 illustrates the results of such a calculation. Note that for this case study calculation, we focused only on the steady-state

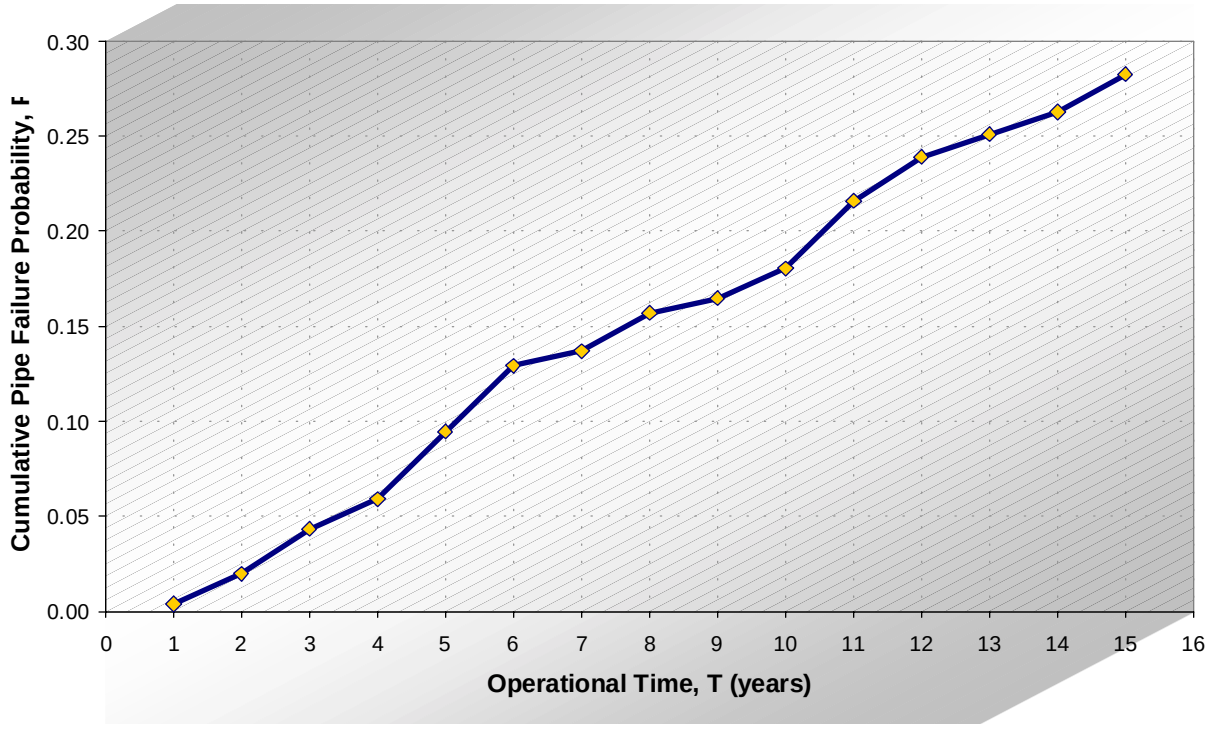

Figure ES-2. Cumulative failure probability of AFW-15 pipe segment from FAC

pressure load model. Further, no credit was taken for inspection or testing of the pipe segments. The results shown in Figure ES-2 represents the pipe failure probability from FAC (for just one pipe section). In order to obtain the pipe failure curve, we divided the operational time into 15, one-year periods. Then, the probabilities were then summed over all time periods to obtain the cumulative probability curve.

Further analysis for the pre-heater case looked at the impact on the overall core damage probability. Figure ES-3 presents the results of 15 years of operation where the core damage probability is shown (cumulatively) for each of the years. For each period, we calculate the core damage probability from both FAC and non-FAC sources and then sum over every period. The probability of core damage over 10 years from all initiators is about 7E-4, and the contribution of FAC (in the preheater section of the AFW) over the ten year period is about 0.2% of this. Although the AFW system has high importance, in the sequences where FAC causes partial loss of the AFW system the main feedwater system is initially available. Thus, the loss of AFW in these sequences does not produce a high contribution to the core damage frequency.

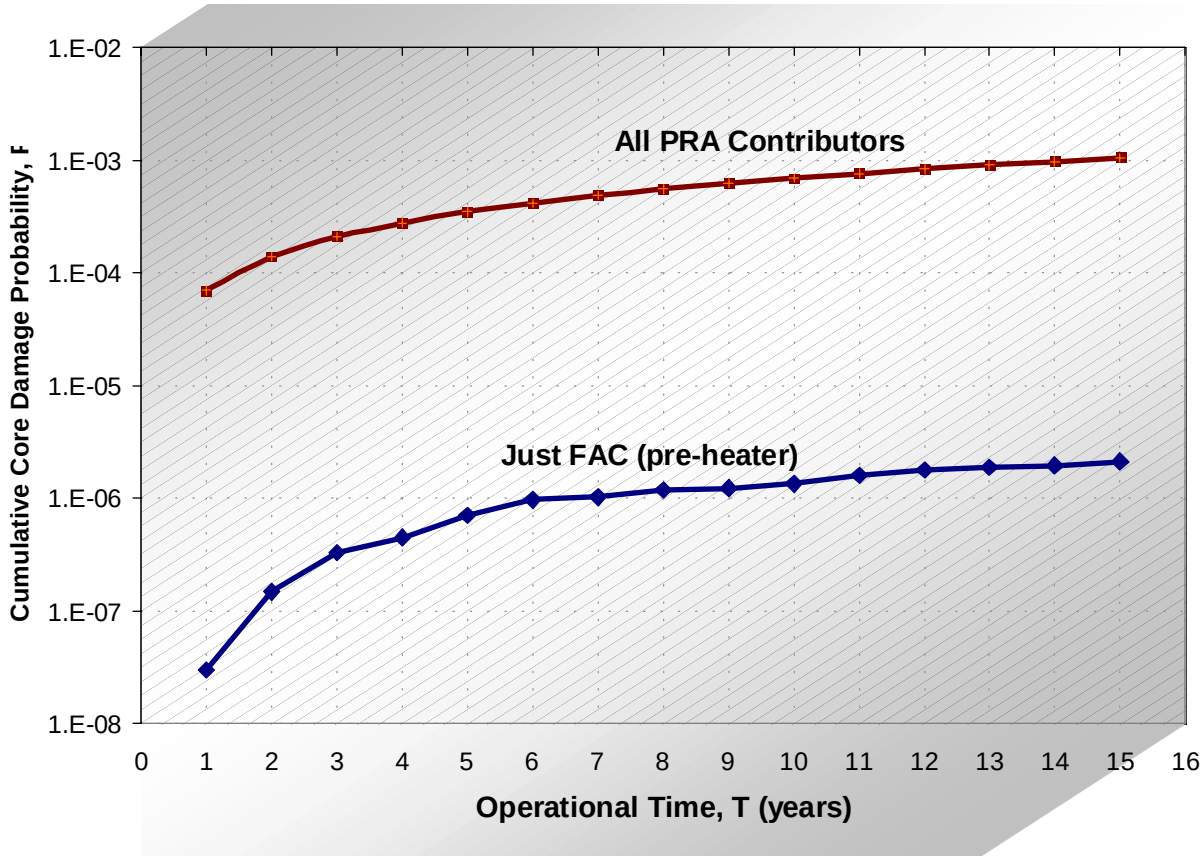

Figure ES-3. Cumulative core damage probability from FAC and non-FAC sources for the i'th year of operation.

The overall result of the work was that we successfully applied an aging reliability-physics model to the existing SAPHIRE Surry PRA risk model and subsequently determined aging-based risk insights. As part of the work, general methods were developed to facilitate the inclusion of aging mechanisms into PRA models. The outcome of development included (1) a generic process to perform the aging-to-PRA modeling, (2) a focused application of flow-accelerated corrosion failure modeling, and (3) incorporation of the flow-accelerated corrosion aging model directly into a PRA. In summary, the general methods addressed:

- The technique of screening for risk-based determination of potential aging-affected components.

- The treatment of uncertainties (aleatory and epistemic).

- The integration of deterministic models into the PRA that represents applicable aging failure mechanisms.

- The determination of component aging-caused failure probabilities via a "load-and-capacity" analysis.

Since this project is a feasibility study, it was not the objective to address all aging mechanisms, nor to provide a complete picture of the magnitude of the risk or impact on core damage frequency resulting from aging. The work did qualitatively discuss the spectrum of aging-related issues facing LWRs. Also, the work did evaluate aging impacts on the core damage frequency for FAC. But to reiterate, these evaluations are of a feasibility nature and *should not* be construed to represent the magnitude (both absolute and relative) of risk posed by aging in LWRs.

The methodology of incorporating NPAR-related aging issues into PRA was demonstrated through this feasibility study. Specifically, key issues and insights that resulted from the work include:

- The rigorous determination and management of uncertainty treatment for the aging mechanism resulted in a robust model and insightful results.

- The study demonstrated that a rigorous treatment of an important aging mechanism such as flow-accelerated corrosion need not rely on sparse failure data in an attempt to quantify a statistical failure rate.

- While the main benefits of the statistical aging rate models (e.g., the linear aging reliability model) are their simplicity and ease of application, research showed that these models do not capture the total impact or behavior of complex aging mechanisms such as flow-accelerated corrosion.

- It was found that flow-accelerated corrosion in the main feedwater piping over 10 years had only a slight impact on the risk at Surry. The predominant reason for this result is that the contribution to the total plant core damage frequency from failure of main feedwater in the Surry PRA is nominally less than 1%.

- The "risk metric" used in this report was core damage frequency and probability. But, the methodology that is described could readily adopt other risk measures (large early release frequency, off-site consequences).

- Monetary arguments were considered to be outside the scope of the feasibility assessment. The financial risk of events such as a flow-accelerated-corrosion-caused rupture of main feedwater piping may be important and could be quantified using the general methodology described in the report.

- Consideration should be given to applying the demonstrated techniques to *non-aging* issues. For example, given the availability of a failure model for reactor coolant pump seals, the failure model could be incorporated directly into the PRA rather than just imbedding the *results* of the model in a basic event in the PRA.

FOREWORD

This report presents a feasibility study for a method of incorporating the effects of the aging of systems, structures, and components (SSCs) into the assessment of the risk from nuclear power plant accidents. Earlier work on assessing the effects of the aging of SSCs on the core damage frequency and risk used age-dependent failure rates for SSCs which were based on relatively sparse failure data, and on expert judgement. The time dependence of the failure rates was based on simple assumptions as to the behavior of the failure rates, such as Taylor series expansions. Because of the sparseness of the data on failure rates, models which inferred failure rates from degradation rates were also developed. However, these models also were hampered by the sparseness of data on degradation, and on uncertainties in the models used. These earlier models are reviewed in NUREG/CR-6157, *Survey and Evaluation of Aging Risk Assessment Methods and Applications*.

Because of the lack of data on the aging of SSCs, NUREG/CR-6157 proposed a method using reliability physics models. The use of reliability physics models makes maximal use of the operational and experimental data, and information concerning aging mechanisms, that have been developed concerning the aging of SSCs. The current work is a feasibility study for the method proposed in NUREG/CR-6157.

The use of reliability physics models to infer time-dependent failure probabilities is resource-intensive. Consequently, the method in actual practice must carefully select the SSCs, and the aging mechanisms which will be treated by this method. Importance measures are useful here. Those SSCs and aging mechanisms which contribute most to change in risk with plant age would be treated by the use of reliability physics models, and the aging of other SSCs would be treated by more simplified methods.

The current study is limited in some ways, since it was only a feasibility study. The aging mechanism chosen was flow-accelerated corrosion. Although this may not be the most important mechanism from the point of view of risk significance, it serves to demonstrate many aspects of the method. The probabilistic risk assessment calculations were limited to internal events, to the full power mode of operation, and to estimates of the core damage frequency. The effects of inspection were not included. For certain SSCs, even if they have relatively high risk importance when inspection is not included, it may be desirable not to spend the resources to develop a sharper estimate of the risk using reliability physics models, but merely to depend on inspection to identify incipient failures. However, in certain cases, inspection may be expensive and it may be best to select the inspection interval depending on the results of probabilistic risk assessment calculations using reliability physics models to estimate the failure probability of the SSC as a function of time. The inclusion of inspection in the method must of course model the probability that the inspection method fails to detect degradation.

Mark A. Cunningham
Chief, Probabilistic Risk Analysis Branch
Division of Risk Analysis and Applications
Office of Nuclear Regulatory Research

ACKNOWLEDGMENTS

We would like to thank several individuals for their participation in the successful completion of this report. First, we would like to acknowledge the work of the programmatic technical monitor at the Nuclear Regulatory Commission (NRC), Dr. Arthur Buslik. His interaction with the report and the technical aspects of the analysis were very appreciated. Also of the NRC, we would like to thank Dr. Nathan Siu for his direction and thoughts provided in the initial phase of the project. Second, we would like to acknowledge the assistance provided by personnel at Virginia Power's Surry nuclear power station, especially that from David Bucheit, Alex McNeill, and Ian Breedlove. Third, we would like to acknowledge the direct and indirect contributions from our Idaho National Engineering and Environmental Laboratory colleagues including Mike Calley, Tim Leahy, James Knudsen, Jacquie Janibagian, Dana Kelly, Ken Russell, and Ted Wood.

ACRONYMS

AASHTO	American Association of State Highway Transportation Officers
ACRS	Advisory Committee on Reactor Safeguards
ANL	Argonne National Laboratory
ASCA	Advanced System Concepts Associates
ASME	American Society of Mechanical Engineers
ASTM	American Society for Testing and Materials
ATWS	anticipated transients without scram
B&W	Babcock and Wilcox
BWR	boiling water reactor
CRD	control rod drive
CRDM	control rod drive mechanism
CVN	Charpy V-notch
EDEAC	EPRI Data Base for Environmentally Assisted Cracking
EDF	Electicite de France
EDO	Executive Director for Operations
EPRI	Electric Power Research Institute
FAC	flow accelerated corrosion
F-V	Fussell-Vesely
GDC	general design criteria
HEP	human error probabilities
IGSCC	intergranular stress corrosion cracking
INEEL	Idaho National Engineering and Environmental Laboratory
IPE	individual plant examination
IST	in-service testing
KWU-KR	KWU-Kastner-Riedel
LANL	Los Alamos National Laboratory
LER	licensee event reports
LOCA	loss of coolant accident
LOSP	loss of off-site power
LWR	light water reactor
NCHRP	National Cooperative Highway Research Program
NDE	nondestructive examination
NEI	Nuclear Energy Institute
NPAR	Nuclear Power Plant Aging Research
NPE	Nuclear Plant Experience
NRC	Nuclear Regulatory Commission
OCA-P	overcooling accident-probabilistic approach
ORNL	Oak Ridge National Laboratory

ACRONYMS (cont.)

PRA	probabilistic risk assessment
PRAISE	Piping Reliability Analysis Including Seismic Events
PTS	pressurized thermal shock
PWR	pressurized water reactor
PWSCC	primary water stress corrosion cracking
RAW	risk achievement worth
RIR	risk increase ratio
RPV	reactor pressure vessel
SAPHIRE	systems analysis programs for hand-on integrated reliability evaluations
SAW	submerged arc welding
SGTR	steam generator tube ruptures
SPAR	Simplified Plant Analysis Risk
SRP	Standard Review Plan
SSC	systems, structures, and components
SWIM	Smith weighted importance measure
SWS	service water system
TIRGALEX	Technical Integration Review Group for Aging and Life Extension
TMI	Three Mile Island

This page left blank.

Incorporating Aging Effects into Probabilistic Risk Assessment — A Feasibility Study Utilizing Reliability Physics Models

1. INTRODUCTION

1.1 Overview

The operation of complex systems, such as light water nuclear reactors, over long periods of time invites the potential of age-related degradation and a reduction of the strength of passive components in light water reactors. The U.S. Nuclear Regulatory Commission (NRC) sponsored the nuclear power plant aging research (NPAR) program during 1985-1994 to gather information about nuclear power plant aging. (Vora, 1993) This program collected a large body of information, mainly *qualitative*, on plant aging and its potential effects on plant safety. Incorporating this body of knowledge into modern risk assessment techniques such as probabilistic risk assessment (PRA) has been envisioned as an effective and systematic method to assess the impact on plant risk resulting from aging of SSCs (systems, structures, and components). However, this body of knowledge had not yet been formally integrated into modern risk assessment techniques.

A number of age-related degradation mechanisms [e.g., fatigue, irradiation embrittlement, stress corrosion cracking and flow-accelerated corrosion (FAC)], not fully accounted for in the original design, have caused failures and raised questions about the safety of older nuclear power plants (Shah and Macdonald, 1993). To better capture these age-related issues for plant safety, the methods and analysis presented in this document utilize PRA techniques and models. Consequently, the process will allow for modeling of aging of passive components in a PRA so that the effect of aging on core damage frequency (and other risk metrics) can be estimated. From the incorporation of aging models into PRA, it is expected that decisions related to plant operation and maintenance will have a stronger technical basis. Further, resources geared toward plant operation can be better focused based upon the risk-informed methods presented in this document.

One question that may arise concerns the assumed robustness in nuclear power plant design and the overall impact of aging mechanisms. Since modern power plants are designed to operate for 40 years, it is often assumed that all aging-related wear would be accounted for in the original design of the plant. But, it turns out that aging is a concern for many types of components and systems in operating power plants. These concerns are illustrated by Gosselin (1997) when comparing actual aging-caused failures with the original plant design by way of a review of service experience:

> "Service experience has shown no correlation between actual failure probability and design stresses and fatigue usage predictions contained in the plant's design stress report. Failures typically result from degradation mechanism and loading conditions (i.e., intergranular stress corrosion cracking [IGSCC], flow accelerated corrosion

[FAC], thermal stratification, etc.) not anticipated in the original design. Since the likelihood of a piping failure is strongly dependent upon the presence of an active degradation mechanism in combination with service conditions and transient load conditions, it has been established that the relative rupture frequency of a pipe segment can be determined based on evaluating the type of degradation mechanism present in a pipe segment during any mode of operation and by considering associated loading and service conditions."

Given the concerns raised from aging-caused failures and their potential impacts on reactor safety and relicensing, the NRC Commissioners have become increasingly interested in aging-related issues. For example, NRC Commissioner Nils Diaz addressed the 450th ACRS (Advisory Committee on Reactor Safeguards) meeting regarding NRC's life extension policy of nuclear power plants on March 6, 1998 and stated:

> "I believe the license renewal process will be difficult unless we fully and legally incorporate risk insights into it...We have the responsibility to define and clarify what we mean and if necessary to demand that certain issues be risk-informed, to be able to set them in the proper context (NRC, 1998)."

1.2 Project Objectives

The overall objective of the work discussed in this report is to assess the *feasibility* of applying the "LANL/ASCA" method for incorporation of reliability-physics based models, expert judgement, and the results of the Nuclear Plant Aging Research (NPAR) program into an integrated aging risk assessment. The "LANL/ASCA" method refers to the application of PRA methods described in NUREG/CR-6157, *Survey and Evaluation of Aging Risk Assessment Methods and Applications*.(Sanzo et. al., 1994) The feasibility assessment that is documented in this report was performed via a trial application of the NUREG/CR-6157 methodology. This application utilized an existing nuclear power plant PRA for which a SAPHIRE computer model currently exists (Russell et al., 1994).

As part of the study, general methods were developed to include aging mechanisms into PRA models. The objective of the methods development was to both delineate the process required to perform the aging-to-PRA modeling and refine the procedures used therein. Included in these general methods are:

- A technique for risk-informed determination of potential aging-affected components. This technique relies on both knowledge of aging failure mechanisms and susceptible components and application of component PRA risk rankings.
- The explicit treatment of aleatory and epistemic uncertainties.
- The integration of reliability-physics models into the PRA that represents applicable aging

failure mechanisms. For the feasibility study discussed in this report, a single mechanism, flow accelerated corrosion (FAC), was utilized.

It was not the objective of the project to address all aging mechanisms nor to provide a complete picture into the magnitude of the risk or core damage frequency impacts resulting from aging. The project does qualitatively discuss the spectrum of aging-related issues facing light water reactors (LWR). Also, the project does evaluate aging impacts on the core damage frequency, but to reiterate, these evaluations are of a feasibility nature and *should not* be construed to represent the magnitude (both absolute and relative) of risk posed by aging in LWRs.

1.3 General Modeling of Aging Issues

Aging issues such as IGSCC and FAC are complex, multi-parameter phenomena, and the susceptibility of a given site or SSC cannot be determined by considering only a few parameters. Even though aging models can predict observed results fairly well in some cases, such calculations are subject to large uncertainty. Since the development of detailed aging models based on reliability physics is still in its infancy, an approximate model that modifies the failure rate directly has been proposed (Vesely, 1987). The failure rate of a component is written as

$$\lambda(t) = \lambda_0 + \alpha t \tag{1}$$

where

$\lambda(t)$ = total component failure rate,
λ_0 = component failure rate due to "random" failures,
α = aging related factor,
t = component age.

The linear failure rate model shown above assumes that the total failure rate, $\lambda(t)$, is the sum of random failures, λ_0, and aging, αt. This assumption of linearity in time has been questioned; in fact, it is shown in the NUREG/CR-6157 report (Sanzo et. al., 1994) that the failure mechanisms discussed earlier do not necessarily lead to failure rates that are linear in time.

A general drawback of the linearly-increasing failure rate model, equally shared by the other reliability distributions that have been proposed in the literature (Sanzo et. al., 1994), is that the model essentially represents a parametric approximation, made at a relatively high level, of failure processes and mechanisms that usually have a rather complex physical behavior. Thus, although a particular parametric reliability distribution may adequately fit the available failure data, it will always constitute a drastic simplification when examined from the point of view of the underlying physical phenomena. The obvious danger under these conditions is that a careless or superficial choice and application of parametric reliability models may obscure the understanding of the role played by important physical processes and may inhibit the management of aging.

Besides the information that the NPAR Program has collected, there has been extensive use of expert opinions. In 1986, the Executive Director for Operations (EDO) of U.S. NRC established the TIRGALEX (Technical Integration Review Group for Aging and Life Extension) to structure a plan to integrate the NRC's aging and life-extension activities. One of the major results of the TIRGALEX plan has been the identification of the safety-related structures and components that should receive high priority in the subsequent phase of the NPAR program.

The TIRGALEX expert panel utilized a set of risk criteria to set priorities in the evaluation of aging structures and components. The same data set used in this process (now called the TIRGALEX database) was also used as the database in later PRA studies under NPAR program.

The modeling technique discussed in the remainder of this report is an extension of modern PRA techniques. Physical aspects of aging mechanisms are incorporated into the PRA model using basic events contained in fault or event trees. As part of this incorporation of physical aging models into the PRA, it may be necessary to augment the existing fault or event trees to encompass the additional aging mechanisms. For example, if sections of piping are susceptible to FAC, the system fault trees containing these sections of piping may need to be modified to account for the pipe segments. Once the pipe segments are incorporated into the PRA, the physical aging model representing FAC could be "tied" to the pipe segment basic events, thereby allowing an analyst or regulator access to physical parameters (e.g., fluid velocity, steam quality, temperatures, pH) that drive the FAC phenomenon. Consequently, having the physical process incorporated directly into the PRA yields risk insights based upon the aging process rather than an abstraction of failure data into a statistical probability parameter. This general concept of incorporating a physical aging model is illustrated at a high level in Figure 1.

1.4 Report Organization

The report is divided into six major sections. Section 1 includes this overview. Section 2 discusses the important aging mechanisms. Included in this discussion are details of the mechanisms, reliability-physics models for the mechanisms, and field experience related to the mechanisms. Section 3 discusses the FAC aging mechanism that is evaluated in this report. Included in this discussion are examples of the risk significance of FAC, and overview of single and two-phase FAC, empirical models, and details of the chosen model utilized in the analysis for this report. Section 4 discusses the general reliability-physics modeling approach used in this report. Included in this discussion are aspects of the PRA implications of aging analysis, a proposed screening technique, and details on the development of the load-capacity FAC model. Section 5 discusses the PRA analysis cases that were conducted to demonstrate the feasibility of incorporating reliability-physics models into PRA. Section 6 provides conclusions and recommendations from the work. Section 7 lists the references used in the main body and the appendices of the report.

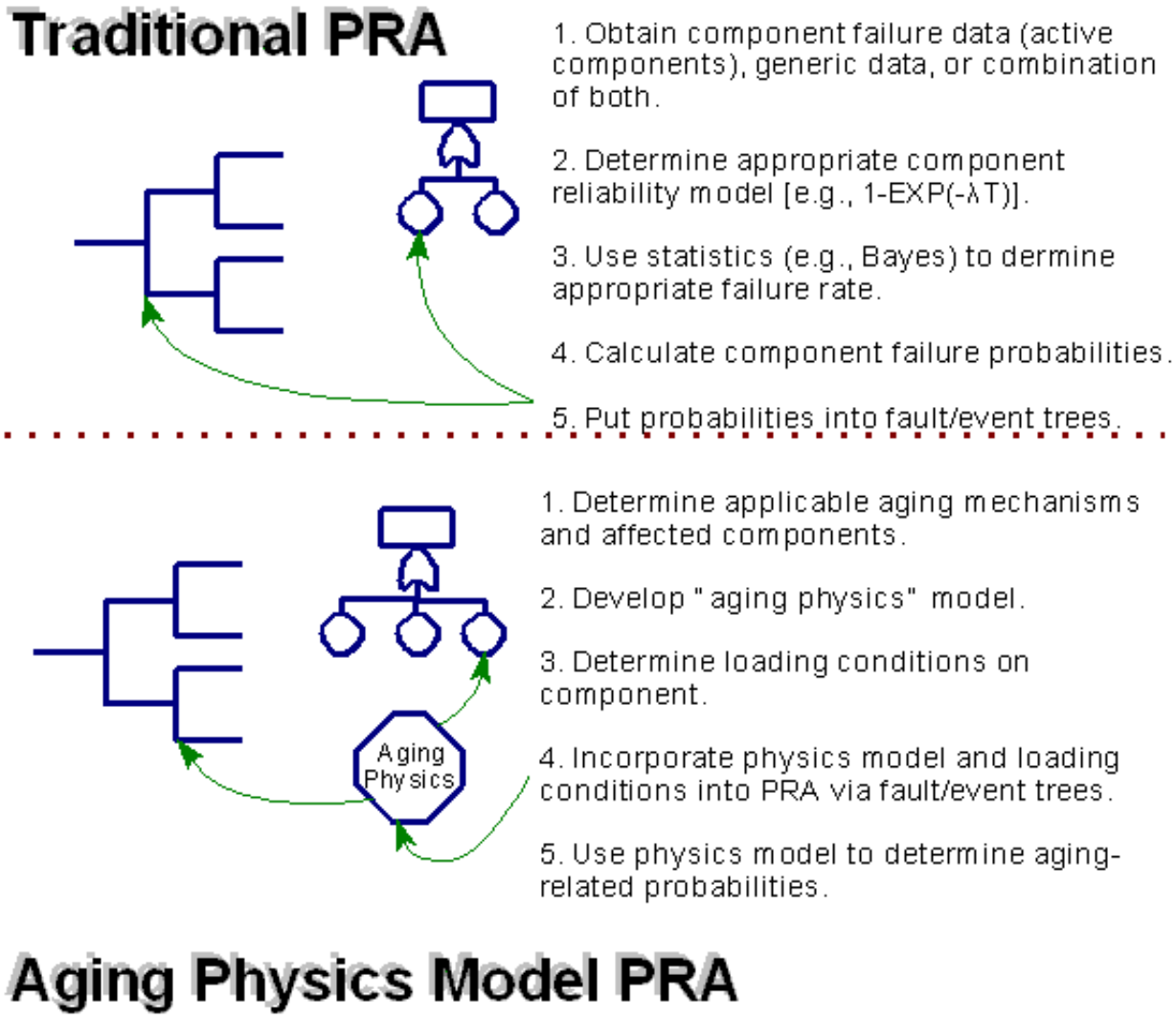

Figure 1. Simple illustration of traditional PRA versus aging-physics PRA models.

2. Aging Mechanisms

Several aging (degradation) mechanisms have degraded the material properties or reduced the strength of the passive components in light water reactors (LWR). In addition to these mechanisms, several stressors and degradation mechanisms, not fully accounted for in the original design, have caused failures (Shah and MacDonald, 1993). Examples of these failures include corrosion of piping, degradation of steam generator tubes, and cracking of cable insulation. These failures have raised questions about the continued safety and increased risk of the older nuclear power plants and, in particular, about the structural integrity of the passive pressure boundary components and containment. Therefore, it is desirable to include the aging of passive components in a PRA, so that the effect of aging on core damage frequency can be estimated and the decisions related to plant operation and maintenance can be made with a stronger or bolstered technical basis.

In-depth aging assessment of 22 components has been performed as part of the Nuclear Plant Aging Research (NPAR) program during 1985-1994 (Shah and MacDonald, 1993). Table 1 lists these components; it includes 12 pressurized water reactor (PWR) and 10 boiling water reactor (BWR) components. Ten of these are primary pressure boundary components; others include reactor pressure vessel internals, vessel supports, main feedwater and steam piping, primary containments, cables and connectors, and emergency diesel generators. In addition, aging assessment of several active components and systems has been performed as part of NPAR (Kondic, 1992). We have reviewed the database developed in NPAR and presented it here so that it can be used in incorporating aging effects in a PRA.

One difficulty with the incorporation of aging effects into an integrated risk study is the sparseness of data especially for passive components and structures needed to estimate the failure probabilities as a function of aging (or time). One way of alleviating this difficulty is to develop the needed information by analyzing the models describing the physics of aging damage and estimating the frequency of transients that will consequently lead to failure.

The aging mechanisms for passive components are described in Section 2.1. Models for analyzing these mechanisms are summarized in Section 2.2. Related field experience is presented in Section 2.3.

2.1 Description of Aging Mechanisms for Passive Components

The aging mechanisms active in the primary pressure boundary components and in the main feedwater and steam piping may be divided into four categories: (a) embrittlement mechanisms causing loss of material fracture toughness - radiation embrittlement and thermal aging, (b) fatigue mechanisms, (c) stress corrosion cracking mechanisms, and (d) corrosion and wear mechanisms. These mechanisms along with the factors affecting the extent of damage are discussed here.

Table 1. List of major LWR components evaluated in the NRC Nuclear Plant Aging Research Program.

Major PWR Components
1. Reactor pressure vessel
2. Containment and basemat
3. Reactor coolant piping and safe ends
4. Steam generator tubes
5. Reactor coolant pumps
6. Pressurizer
7. Control rod drive mechanisms
8. Cables and connectors
9. Emergency diesel generators
10. Reactor pressure vessel internals
11. Reactor pressure vessel supports
12. Feedwater piping, nozzles and steam generator shell

Major BWR Components
1. Containment and basemat
2. Reactor pressure vessel
3. Recirculation piping and safe ends
4. Recirculation pumps
5. Control rod drive mechanisms
6. Cables and connections
7. Emergency diesel generators
8. Reactor pressure vessel internals
9. Reactor pressure vessel supports
10. Feedwater and main steamline piping

2.1.1 Radiation Embrittlement of Ferritic Low-Alloy Steels

The main component affected by the radiation embrittlement is the reactor pressure vessel, which is fabricated from ferritic low-alloy steel, also called pressure vessel steel. The pressure vessel steel includes SA302B, SA302B (modified), SA533B, SA508-2, and SA508-3. Neutron radiation also embrittles vessel internals, which are made from stainless steels and Nickel-based alloys, at higher fluence levels. This section focuses on the damage caused to pressure vessel steel.

Irradiation can produce several types of microstructural changes in the low-alloy steels, which include small fine-scale precipitates, vacancy clusters (microvoids), and interstitial clusters (dislocation loops). Copper-rich precipitates, possibly alloyed with elements such as manganese and nickel, or vacancies are believed to be a dominant hardening feature in pressure vessel steels containing a small amount of copper, for example, 0.2 wt% Cu. Other possible types of radiation-induced or -enhanced precipitates are phosphides and small carbides. The major effects of irradiation are enhanced diffusion rates and defect clustering. These microstructural changes are kinetic phenomena and are functions of flux and temperature, as well as composition and microstructure. In general, the changes in the microstructure can be understood from basic principles of alloy thermodynamics and precipitation kinetics, coupled with rate theories of radiation damage (Odette 1983, Odette and Lucas 1986, Lucas and Odette 1986).

The radiation-induced microstructural changes cause an increase in the yield and ultimate tensile strengths, a decrease in the fracture toughness, and an increase in the ductile-to-brittle transition temperature. The change in toughness generally is monitored by using specimens that have been irradiated in surveillance capsules and then subjected to Charpy V-notch (CVN) testing (ASTM 1985). The results from irradiated CVN testing show both (a) an increase in the ductile-to-brittle transition temperature [measured at the 41 J (30 ft-lb) energy and often referred as T_{30}], which is equated to a change in the reference ductile-to-brittle transition temperature (RT_{NDT}), and (b) a drop in the upper shelf energy (USE). Figure 2 illustrates these changes from the unirradiated condition for an actual set of surveillance specimens subjected to CVN testing. Both the shift in T_{30} and the drop in USE are key NRC parameters for reactor pressure vessel operation.

The shift in the ductile-to-brittle transition temperature of vessel materials including base metal, weld metal, and heat-affected zone, depends on chemical composition (especially presence of trace elements, copper, nickel, and phosphorous), post-weld heat treatment, operating temperatures, and neutron fluence (with $E > 1$ MeV). The typical copper and nickel contents in the vessel materials are, respectively, in the range of 0.0 to 0.4 and 0.0 to 1.2 wt%. Copper and nickel have more detrimental effects on the weld metal than on the base metal.

Postweld heat treatment time can have an effect on the measured value of initial RT_{NDT} for weld material (Stout 1985). The use of shorter postweld heat treatment time (< 50 hr) may enhance

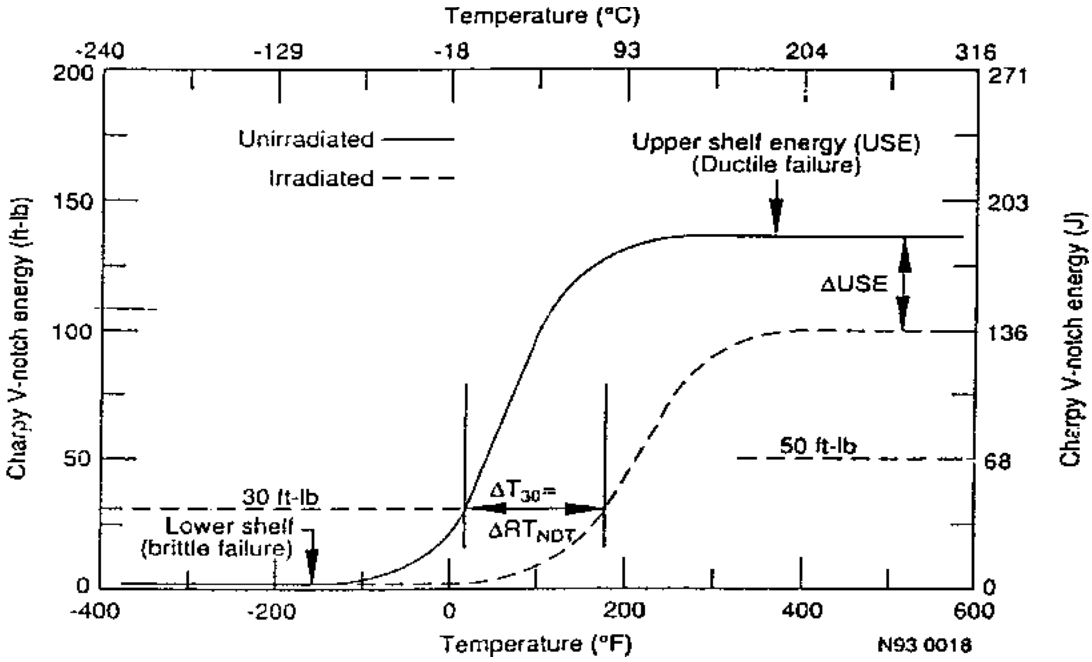

Figure 2. Charpy V-notch surveillance data, showing radiation embrittlement effects.

or degrade Charpy V-notch and tensile properties. Normal operating temperature corresponds to a temperature at the inside surface of the vessel wall of approximately 288°C (550°F). Radiation embrittlement rates are sensitive to changes in temperature near the normal operating temperature. Lower temperature irradiations [even 14°C (25°F) lower] can result in higher rates of embrittlement even though the fluence level stays about the same (Steele, 1975). The shift in the transition temperature is not significant for fluence less than 10^{17} n/cm^2 (E > 1 MeV). The shift increases as the fluence increases from 10^{17} to 10^{20} n/cm^2.

The drop in the Charpy upper shelf energy depends on fast neutron fluence, copper content and operating temperature. The upper shelf energy decreases as fast neutron fluence and copper content increases. Lower temperature irradiation can also result in decrease in upper shelf energy (Hoge 1979). The Linde 80 welds have lower initial upper shelf energy.

2.1.2 Thermal Aging of Cast Stainless Steels

Nuclear power plant main coolant piping is made from either austenitic stainless steel or carbon steel. Austenitic stainless steel piping material includes both wrought and duplex austenitic-ferritic stainless steels, whereas the pump and valve body materials include the duplex stainless steel only. The duplex austenitic-ferritic stainless steels are often referred to as *cast* stainless steels. The ferrite (delta ferrite) phase is not present in the wrought stainless steel but is present in the cast stainless steel and also in the stainless steel weld metal. The ferrite phase improves the resistance

of the duplex stainless steels to sensitization, intergranular corrosion, and stress corrosion cracking, and resistance of the weld metal to hot cracking. However, the presence of ferrite also causes upward shift in ductile-to-brittle transition temperatures and reduction in fracture toughness after long-term exposure to LWR operating temperatures. This degradation mechanism is termed *thermal aging*.

Cast austenitic-ferritic (duplex) stainless steels with delta ferrite content greater than about 10% will experience an increase in the transition temperature and a reduction in toughness when aged at elevated temperatures; both room-temperature and operating temperature toughnesses decrease. The maximum effect occurs when aged at 475°C (885°F), and the general phenomenon is often referred to as 475°C embrittlement. This temperature is well above the maximum temperatures of PWR main coolant piping (318°C for hot leg and 288°C for cold leg); nevertheless, a reduction of toughness does take place at the PWR operating temperatures, but requires longer exposure (aging) times.

Only Westinghouse-designed PWR plants use austenitic stainless steel for the main reactor coolant piping.[†] PWR plants in other countries, such as France, Sweden, and Japan, that are based on the Westinghouse design, also use the stainless steel piping material. The material for the straight portion of the main coolant piping is either wrought or cast stainless steels, 28 U.S. plants have wrought stainless and 27 U.S. plants have cast stainless steel piping; and the material for all fittings is cast stainless steel (Egan et al., 1987). The other cast stainless steel components include pump and valve bodies, present in all PWR plants. The straight portions of the piping is centrifugally cast, whereas all other cast stainless steel components are statically cast. The cast stainless steel components do not need any cladding.

Basic Mechanisms Causing Thermal Aging. The loss of toughness of the cast stainless steels during elevated-temperature operation is related to (a) the formation of a Cr-rich alpha-prime phase and a Ni-rich and Si-rich G phase in the ferrite and (b) precipitation of carbides or nitrides in high-nitrogen steels at the austenite-ferrite phase boundaries. The formation of the alpha-prime phase in the ferrite is the primary factor involved in the thermal aging of cast stainless steel at PWR operating temperatures. The phase-boundary carbides play a significant role in thermal aging at temperatures greater than 400°C (750°F), but have smaller effect on the aging at exposure temperatures less than 400°C.

Because only the ferrite phase is embrittled by long-term service at PWR operating temperatures, the overall thermal aging of cast stainless steel piping depends on the amount and morphology of the ferrite present. For LWR applications, the traditional guideline has been that

[†] Combustion Engineering- and Babcock & Wilcox-designed PWR plants use carbon steel piping cladded with stainless steel for the main coolant loop. This piping is not susceptible to the thermal aging damage. The material of reactor coolant system piping other than main coolant piping is typically wrought stainless steel.

low-temperature aging is a major concern only when the volume fraction of the ferrite exceeds approximately 15 to 20% (Copeland and Giannuzzi, 1984). However, where ferrite levels are greater than 15%, there is a greater tendency for a continuous path of embrittled material to exist through the thickness of the cast component, which would greatly reduce its toughness if the ferrite regions were embrittled (Chopra and Chung, 1986). The statically cast components are more susceptible to thermal aging than the centrifugally cast components.

2.1.3 Low-Cycle Fatigue

Fatigue is defined by ASTM (1972) as:

> *The process of progressive localized permanent structural change occurring in a material subjected to conditions which produce fluctuating stresses and strains at some point or points and which may culminate in cracks or complete fracture after a sufficient number of fluctuations.*

The term "progressive" implies a time or usage process, while the term "localized" implies that the fatigue process operates at local areas rather than throughout the component. These local areas can have high stresses and strains due to fabrication defects in material, geometric discontinuities, or metallurgical discontinuities.

Fatigue damage occurs only in regions that deform plastically under the influence of fluctuating loads. Thus, smooth specimens free of stress risers that are subjected to elastic stress fluctuations do not experience fatigue damage. On the other hand, fatigue damage does occur under elastic stress fluctuations if the component contains stress risers where the localized stresses and strains exceed the elastic limit of the material. After a certain number of load fluctuations, the accumulated fatigue damage at the regions of stress concentration causes initiation and subsequent propagation of fatigue cracks in the plastically deformed region.

It is known that fatigue, in general, occurs in four stages: (1) early fatigue damage, (2) fatigue crack initiation, (3) fatigue crack growth, and (4) fracture. Most structural metals are polycrystalline and thus consist of a large number of individual ordered crystals or grains. The early fatigue damage generally consists of dislocations, dislocation loops, and vacant lattice sites, which have accumulated into slip bands of dislocations within the grains. Some grains are oriented such that the planes of easy slip are in the direction of the maximum applied shear stress. Slip occurs in ductile metals within these individual grains by the dislocations moving along the crystallographic planes. This creates an appearance of one or more planes within a grain sliding relative to each other (Fuchs and Stephens, 1980).

The progressive nature of slip band development has been observed (Kennedy, 1963). Initially, only a few slip bands are present in a few grains. As the fatigue cycling continues, more slip bands are observed in the grains with planes of easy slip in the direction of the maximum applied

shear stress, and more grains with slip bands are observed. Then, microscopic fatigue cracks generally grow from the persistent slip bands which intersect the component surface or the grain boundaries in the plane of the maximum shear stress range (Forsyth, l969). Crack initiation occurs when a microscopic crack grows to a detectable size or when several microscopic cracks join and form a detectable crack.

Generally, a fatigue crack initiates at the surface of a component and grows across several grains controlled mainly by shear stresses, and then grows in a zigzag manner essentially perpendicular to, and controlled mainly by, the maximum tensile stress range. Most fatigue cracks generally grow across the grain (transgranular growth), but some may grow along the grain boundaries (intergranular growth). When the crack reaches a critical size, applied stress intensity factor at the crack tip becomes equal to or greater than the critical stress intensity factor, sudden fracture occurs (Fuchs and Stephens, 1980).

Pressure and thermal stresses imposed during system transients, including heatup and cooldown, cause low-cycle fatigue damage. The susceptible sites in the PWR primary coolant systems are the nozzles, dissimilar metal welds, and elbows. There have been no reported failures, not even discovered cracks, in existing PWR main coolant piping. One of the reasons for this defect-free performance has been that the main coolant piping has not experienced significant transients that were not included in the original fatigue design. However, PWR branch lines have experienced thermal fatigue cracking caused by the phenomena not accounted in the original fatigue design. More information about the thermal fatigue cracking of the branch lines may be found in the NUREG report by Shah et al. (1998).

2.1.4 High-Cycle Vibrational Fatigue of Welded Piping Connections

Fatigue failures of piping occur predominantly at the socket welds commonly used for joining small diameter piping (i.e. < 2-in.) and at the fillet welded attachments under high-cycle vibrational conditions. Three characteristics of welded joints contribute to these failures: weld geometry, weld discontinuities, and residual stresses. Geometric discontinuities caused by localized change in section intensify the stresses in a very local area. The magnitude of the stresses decay rapidly to applied nominal stress values away from the discontinuities. The magnitude of the stress concentration depends on the geometry of the discontinuity. The various imperfections and crack like discontinuities present in weld metal or heat-affected zone also act as stress raisers and drastically reduce weld joint fatigue strength.

Fatigue cracks in a weldment initiate where localized stress range is maximum. This location may not correspond to the location where stress concentration factor is maximum. Fatigue cracks may initiate either at surface discontinuities such as at weld toe rather than at embedded discontinuities such as inclusions. Presence of discontinuity such as lack of penetration at the weld root can degrade the fatigue strength. But, it should be noted that the mere existence of discontinuities does not automatically make a weldment defective or unsuitable for a given application.

Residual stresses are introduced in a weldment because of the inability of the deposited molten weld metal to shrink freely as it cools and solidify. The magnitude of the residual stresses depends on several factors including size of the deposited weld beads, weld sequence, total volume of deposited weld metal, weld geometry, strength of deposited weld metal and of the adjoining base metal and other factors. These stresses have little effect on fatigue crack initiation but can have significant effect on crack propagation. Fatigue cracks can initiate under nominal tensile or compressive stress fluctuations. As fatigue crack initiation is governed by the stress range rather than the magnitude of static or steady-state (applied or residual) stresses, tensile residual stresses usually have little effect on the behavior of structural component.

2.1.5 Primary Water Stress Corrosion Cracking of Alloy 600 Components

Primary water stress corrosion cracking (PWSCC) of Alloy 600 (Inconnel 600) was identified in the laboratory as early as 1959, when Coriou et al. (1959) reported cracking of this material in "high purity" water at 350°C (662°F). The mechanism was first observed in the field in 1971 when PWSCC was observed in hot-leg tube roll transitions[†] at Obrigheim. Increasingly, steam generator tubes have been removed from service as a result of primary-to-secondary leaks caused by PWSCC at high stress locations such as expansion transitions, tight radius (i.e., Rows 1 and 2) U-bends, and tube dents at tube support plate intersections (Theus, 1986; Hunt and Gorman, 1986). In last twelve years, other Alloy 600 components such as pressurizer instrument penetrations and heater sleeves, steam generator tube plugs, control rod drive mechanism (CRDM) nozzles, and reactor coolant piping penetrations have experienced PWSCC damage. As a result, significant research and development efforts have been expended to determine the factors affecting the PWSCC mechanism.

The PWSCC phenomenon has been verified and its understanding was expanded by 1966. By 1973, it had been largely defined with respect to its dependence on stress, temperature, pH, electrochemical potential, heat treatment, and alloy composition. This work has been summarized elsewhere (Tatone and Pathania, 1985; Theus, 1986; Hunt and Gorman, 1986). The research has shown that PWSCC is an intergranular cracking mechanism requiring at least the following three conditions to be present simultaneously:

- High applied or residual tensile stress or both
- Susceptible tubing microstructure (few intergranular carbides)
- High temperature.

Effect of Stress The PWSCC damage rate increases as a function of stress to an exponent. Test results have shown this exponent to be in the range of 4 to 7 (Hunt and Gross 1994). An exponent of 4 is typically used, i.e., damage rate $\propto \sigma^4$, where σ is the maximum principal tensile stress, which includes both applied and residual stresses. This correlation suggests that a 50% reduction in the

[†] Roll transition region of the tube located in the hot-leg side of the steam generator.

effective stress will result in a sixteen-fold decrease in the damage rate and a corresponding increase in PWSCC initiation time. A threshold stress, that is, a stress below which PWSCC does not initiate, has not been determined experimentally for Alloy 600. However, use of the strain rate damage model, which is based on slow strain rate test data, leads to an estimated threshold stress of about 241 MPa (35 ksi) at the operating temperature of about 315°C (600°F) (Begley 1988).

All the PWSCC failures reported in the field, including CRDM nozzle cracking, resulted from high residual tensile stresses; the applied operating stresses are generally low. High residual stresses are generally introduced during fabrication or installation of the Alloy 600 components, such as CRDM nozzles. Cold work increases the residual stresses on the inside surface, which is exposed to primary reactor coolant, and thereby reduces the resistance to PWSCC. The magnitude of residual stresses at the affected sites are of yield strength level; in the cold-worked steam generator tube, the residual stress can be as high as 690 MPa (100 ksi). Similarly, the residual stresses in the thin layer of cold-worked material on the inside surface of the CRDM nozzle are high and the PWSCC initiation time is short. However, these stresses are only skin deep and do not affect PWSCC crack growth.

Effect of Microstructure Field experience and research results show that the PWSCC resistance of Alloy 600 is highest when the grain boundaries are covered with continuous or semicontinuous carbides. The PWSCC resistance is lower when the grain boundaries are covered with widely spaced, discrete carbides. The PWSCC initiation time increases by a factor of five as the grain boundary carbide coverage increases from 0 to 100% (Rao, 1994). The reasons for this beneficial effect of the intergranular carbides are not yet fully understood. According to Bruemmer, Charlot, and Henager (1988), the intergranular carbides act as a source of dislocations, resulting in plastic strains that cause crack tip blunting and, thus, reduce PWSCC susceptibility. Another possible explanation, according to Smialowska of the Ohio State University, is that the Alloy 600 material passivates more readily in the presence of intergranular carbides (Hunt and Gross, 1994).

The percentage of the grain boundary covered with intergranular carbides depends on the heat treatment temperature and time, carbon content, and grain size. During the heat treatment, if the temperature is high enough, the Alloy 600 material recrystallizes, and new grain boundaries are formed. If all the carbides are dissolved during the heat treatment, the carbon is then in solution, and the carbides will precipitate at the new grain boundaries during subsequent cooldown. As a result, the grain boundaries maybe fully covered with carbides and the material becomes resistant to PWSCC. If all the carbides are not dissolved, then the undissolved carbides remain as intragranular carbides (at old grain boundaries), and during subsequent cooldown the additional carbides will preferentially precipitate at the sites of these intragranular carbides. As a result, the grain boundaries are not fully covered with carbides, and the material is less resistant to PWSCC.

The solubility of carbon in Alloy 600 is fairly low and depends on its carbon content. The temperature at which all the carbides are dissolved increases as the carbon content increases (Scarberry, Pearman, and Crum, 1976). For example, for a carbon content of 0.03 wt%, all the

carbides will be dissolved at a heat treatment temperature of 980°C (1800°F). For a carbon content of 0.15%, the corresponding temperature is 1204°C (2200°F). So, if the heat treatment temperature is not high enough or the carbon content is too large, such that all the carbides are not dissolved, the resulting microstructure will be less resistant to PWSCC. Review of several PWSCC failures supports this observation (Campbell and Fyfitch, 1994).

Alloy 600 material is more resistant to PWSCC if its grains are larger. This is so because a larger grain size is associated with a lower yield strength and also with a smaller total grain boundary, which requires a smaller amount of carbide for complete coverage. If the heat treatment temperature is high enough [>925°C (1700°F)], recrystalization takes place (Tillack and Fernsler, 1981). The final grain size depends on the heat treatment temperature and time. Higher heat treatment temperature and longer heat treatment time result in a larger grain size. The size of the recrystallized grains also depends on the amount of cold working of the material before the heat treatment. The greater the amount of cold work, the finer the grain size.

Effect of Operating Temperature PWSCC is a thermally activated process that can be described by an Arrhenius relationship of the form

$$\text{damage rate} \propto e^{-Q/RT} \tag{2}$$

where Q is the activation energy, R is the universal gas constant, and T is the temperature in degrees Rankine. Various estimates for Q for Alloy 600 tube materials have been derived from laboratory studies and field experience. The estimates range from 163 to 272 kJ/mole (39 to 65 kcal/mole), with a best-estimate value of 209 kJ/mole (50 kcal/mole) (Gorman et al., 1991; Stein and McIlree, 1986). Estimates for activation energy for Alloy 600 components fabricated from different product forms, for example, bar and tubing, may be different.

PWSCC initiation and growth are very sensitive to temperature. For example, in any affected steam generator, the PWSCC has been first reported in the tubes on the hot-leg side, not on the cold-leg side. Similarly, PWSCC has been first reported in Alloy 600 penetrations in pressurizers, where the operating temperature of the primary coolant is the highest [343°C (650°F)].

Effect of Coolant Chemistry Tests over the range of high temperature pH values from 6.9 to 7.4 show that the primary coolant chemistry has a secondary effect on PWSCC initiation in Alloy 600 material (Lott et al. 1992). Some preliminary results show that PWSCC initiation is sometimes accelerated when the lithium content is high. For example, PWSCC initiation time was reduced by about a factor of two when the lithium concentration was increased from 2.2 ppm to 3.5 ppm at a constant boron concentration of 1200 ppm. Some tests are being performed to determine the lithium concentration above which the PWSCC risk begins to decrease (Berge et al. 1992). A recent Japanese study show that PWSCC damage is minimized at 2-ppm lithium, compared to damage at 1 ppm and 3.5 ppm (Millett and Wood 1994). EPRI-sponsored studies indicate that increasing the hydrogen concentration in the primary coolant increases the rate of PWSCC. Consequently, PWR

Primary Water Chemistry Guidelines (Rev.2) recommend that utilities maintain hydrogen concentrations in the range of 25 to 35 cm^3/kg, which is near the lower end of the typically used range of 25 to 50 cm^3/kg (EPRI 1990, Gorman 1989).

2.1.6 Flow-Accelerated Corrosion of Carbon Steel Components

Flow-accelerated corrosion affects carbon steel piping, thermal sleeves, J-tubes, and feedrings carrying single phase, subcooled feedwater and steamlines carrying wet steam. A brief description of flow-accelerated corrosion is as follows. A thin layer of porous iron oxide [mostly magnetite (Fe_3O_4)] forms on the inside surface of carbon steel feedwater piping exposed to deoxygenated water in the temperature range of about 95 to 260°C (200 to 500°F). Generally, this layer protects the underlying piping from the corrosive environment and limits further corrosion. However, the magnetite layer may be dissolved at the oxide-water interface and be replaced by new iron oxide formed at the metal-oxide interface, resulting in material removal and thinning of the piping. The corrosion process is strongly influenced by the fluid velocity, chemistry and temperature, piping configuration, and alloy content of the steel as discussed below. This process is called *single-phase flow-accelerated corrosion* (FAC).

FAC is often called *erosion-corrosion* in the United States. But, this process is primarily a corrosion process enhanced by chemical dissolution and mass transfer, rather than a mechanical process involving removal of the oxide layer by erosion or cavitation. No evidence of the removal of surface oxide by mechanical shear forces has been found during any macroscopic or microscopic examination of the damaged inside surfaces of the feedwater piping. Hence, the term *"flow-accelerated corrosion"* is more appropriate for the observed wall thinning of carbon steel piping exposed to deoxygenated feedwater (Chexal et al., 1996). Laboratory results show that the fluid velocities associated with the removal of the oxide layer by mechanical processes are higher than those associated with the dissolution of an oxide layer. Also, the kinetics of metal removal by a mechanical process are either quasi-linear or nonlinear, whereas the kinetics of metal removal by an oxide dissolution process are linear (the corrosion rate is constant in time). The corrosion rates (wall thinning rates) observed in the field are almost constant when the influencing factors do not vary.

The flow-accelerated corrosion process is an extension of the generalized carbon steel corrosion process in stagnant water. In stagnant water, the carbon steel corrosion rate is low and decreases parabolically with time due to the formation of a protective oxide film at the surface. FAC takes place at low flow velocities and, as mentioned earlier, the corresponding corrosion rate is constant. The difference between generalized corrosion and FAC is the effect of water flow at the oxide-feedwater interface.

A similar corrosion process causes wall thinning of carbon steel piping exposed to wet steam; this process is called *two-phase FAC*. If the piping is exposed to dry or superheated steam, no FAC takes place; a liquid phase must be present for FAC damage to occur. Corroded surfaces produced by single-phase FAC have a different appearance than those formed by the two-phase FAC. When

the single-phase FAC rate for a large-diameter piping is high, the corroded surface is characterized by overlapping *horseshoe pits* that give an orange peel appearance. The corroded surface of a large diameter piping exposed to two-phase flow has a well known *tiger striping* appearance.

2.2 Models and Data for Aging Damage of Passive Components

The objective of this section is to summarize the models and codes available for *quantitative* estimates of aging damage so that their use in the PRA analysis can be evaluated. Note that in the context of this section, a single "code" could includes several models. Summary of models for selected aging mechanisms is presented in Table 2. Summary for other aging mechanisms including those for steam generator tubes will be developed later in the project. For each code or model, type of data used for its development, its current status, and its limitations are listed. All the models are deterministic.

The VISA II code has capabilities for both deterministic analysis and probabilistic analysis to calculate the probabilities for vessel failure under pressurized thermal shock (PTS) conditions. The models are generally based on the specimens having representative material characteristics and tested in the simulated field environment. Development of some of these models is completed, whereas others are being developed. Some of these models have been adopted by the ASME code. Most of the models have been verified and several of them validated with the field results or with the representative laboratory results. Limitations of some of these models have been identified in the Table 2.

Table 2. Quantitative models for estimating aging damage to passive PWR components.

Aging Mechanism		Code/Model	Basis	Status	Limitations
Radiation Embrittlement		VISA-II[a] code, both deterministic and probabilistic analysis, estimates, probability of vessel failure under PTS conditions	Analytical models for basic physical processes; field and laboratory data for flaw distribution	Verified	
Thermal Aging		ANL has developed a procedure.	Laboratory test results	Limited validation	
Low-Cycle Fatigue	Initiation	ASME Section-III fatigue design procedures	Laboratory test results	Limited validation. Used in the field.	Does not include effect of LWR environment. Generally provides conservative estimates for fatigue life usage.
	Propagation	ASME Section XI, Appendix A - carbon and low-alloy ferritic steels; Appendix C - austenitic stainless steels	Laboratory test results	Validated with the laboratory test results. Used in the field.	Models for stainless steel do not include effect of LWR environment.
High-Cycle Fatigue of Welded Piping Connections		ASME Section III fatigue design procedures	Fatigue test data for small polished specimens and use of fatigue strength reduction factors	EPRI has an ongoing project.	Does not always ensure conservative design. Requires complex stress analysis.
		AASHTO fatigue design approach	Requires fatigue test data for full-size components		Empirical model. Testing of full size components may be expensive.
Primary Water Stress Corr. Cracking of Alloy 600 Penetrations	Initiation	Industry models	Laboratory and field data	Models are used to predict susceptibility of a penetration to cracking.	Needed data on residual stress and grain boundary carbide distribution may not be available.
	Propagation	Industry models	Laboratory data	Being developed	
Flow-Accelerated Corrosion		CHECWORKS WATHEC	Laboratory and field data	Development completed. Verified and validated. Used in the field.	Adequate training and appropriate application of the model are required.

a. VISA-II (Vessel Integrity Simulation Analysis) code has been developed by Pacific Northwest Laboratory for the NRC.

Even though crack initiation/propagation models presented in Table 2 are deterministic, they can be incorporated in a probabilistic system code such as PRAISE (Piping Reliability Analysis Including Seismic Events) to estimate probability of pipe failures caused by fatigue and stress corrosion cracking as a function of time. The PRAISE code uses deterministic fracture mechanics analysis for estimating crack growth. Some of the input, such as initial crack size and inspection detection probability, are considered to be random variables. PRAISE generates the pipe failure probability as a function of time by Monte Carlo simulation, that is, by performing a series of deterministic lifetime calculations for different sets of input drawn from their respective statistical distributions (Harris et al. 1992). (VISA-II code also uses Monte Carlo simulation.) Two leak models have been recently incorporated in the PRAISE Code, one for leak through a fatigue crack and one for a stress corrosion crack. The surface roughness for these two cracks are different, and, therefore, the leak rates are different. So the PRAISE code can be used for generating statistical data on the leak rates.

The review of field experience indicates that the passive components have experienced through-wall cracks, leaks, and ruptures. However, the number of failures are few except of steam generator tubes; the data are insufficient to estimate failure probabilities needed for PRA. The probabilistic analyses of passive components subject to aging mechanisms may be performed to estimate these probabilities. Thus, the probabilistic codes such as PRAISE or VISA-II may be modified and used for these analyses. Note that each of the models listed in Table 2 are described in additional detail in Appendix A. U.S. NRC guidelines for estimating the extent of damage and requirements for acceptable damage are identified where applicable in Appendix A.

2.3 Field Experience Related to Aging Damage of Passive Components

Radiation embrittlement and thermal aging cause degradation of material properties but do not initiate any physical damage such as cracking. No failure caused by these two mechanisms have been reported. Potential failure modes associated with these mechanisms have been identified in this section. The remaining mechanisms *have* caused cracking or wall thinning of pressure boundary components. The field experience related to these mechanism is summarized in Appendix B.

The degradation mechanisms may be prioritize according to the type and the extent of damage they have produced in the field or have a potential to produce during the 60 years of plant operation. The damage may be a physical damage to a component or performance degradation of a system. Physical damage includes cracks, wall thinning, leaks, and rupture. The frequency of occurrence may be taken into account in the prioritization.

The following seven levels could be used to prioritize the potential aging-related damage (note that this prioritization is based upon aging degradation and is not specifically risk-based).

1. Mechanism has caused rupture in the field
2. Mechanism has caused significant wall thinning or cracking and has a potential to cause single or multiple ruptures (common-mode failures) during 60 years of operation
3. Mechanism has caused leakage in the field
4. Mechanism has caused significant damage to material properties and has a potential to cause rupture during 60 years of operation
5. Mechanism has caused cracking, wastage, or localized wall thinning and has a potential to cause through-wall cracking and leakage during 60 years of operation
6. Mechanism has significantly reduced material resistance to fatigue and SCC and has a potential to initiate cracking and then cause through-wall cracking
7. Mechanism has no potential to cause cracking or rupture during 60 years of operation

The seven levels identified above could be utilized as a "condition indicator" parameter and used to indicate performance for components susceptible to aging mechanisms such as FAC. An indication level of 7 implies acceptable performance while, alternatively, a level of 1 implies unacceptable performance. Note though that this level identification is only used in this report as a screening metric.

Table 3 summarize the damage levels for passive components including: PWR reactor pressure vessel, pressurizer, and reactor coolant pump; PWR reactor coolant piping; PWR steam generators; and PWR main and auxiliary feedwater lines and main steam lines. Within Table 3, the numbers listed for a particular component and aging mechanism represent one of the seven levels discussed on the previous page.

Table 3. Extent of aging damage in PWR reactor pressure vessel, pressurizer, and reactor coolant pump.

Major components		Aging mechanisms												
		Embrit-tlement		Fatigue			Stress corrosion cracking (SCC)			Corrosion/wear				
Component	Subcomponent	Radiation Embrittlement	Thermal aging	Low-cycle thermal fatigue	High-cycle thermal fatigue (†)	High-cycle mechanical fatigue	Primary water SCC	Intergranular SCC	Transgranular SCC	Flow-accelerated corrosion	Boric acid corrosion	Pitting	Wear/fretting	Erosion
PWR reactor pressure vessel, pressurizer, and reactor coolant pump components.														
Reactor pressure vessel	Beltline region	4												
	Outlet/inlet nozzles			6										
	Instumentation nozzle						6							
	Flange closure studs			6							5			
Vessel internals	Thimble tubes												3	
Control rod drive	Housing								3					
	Nozzles						3							
Pressuizer	Vessel shell			6										
	Instrumentation penetrations						3							
	Heater sleeve/sheath						3							
	Manway bolts										3			
Reactor coolant pump	Pump body		7											
	Closure studs										3			
PWR reactor coolant piping														
Main coolant loop	Branch nozzle/elbow			6										
	Cast stainless steel piping and elbows		7											
	Dissimilar metal welds			6				5						
	Stainless steel welds		7											
Surge and spray lines	Nozzles			6										

Major components		Aging mechanisms												
		Embrit-tlement		Fatigue			Stress corrosion cracking (SCC)			Corrosion/wear				
Component	Subcomponent	Radiation Embrittlement	Thermal aging	Low-cycle thermal fatigue	High-cycle thermal fatigue (†)	High-cycle mechanical fatigue	Primary water SCC	Intergranular SCC	Transgranular SCC	Flow-accelerated corrosion	Boric acid corrosion	Pitting	Wear/fretting	Erosion
Surge and spray lines	Horizontal sections and elbows			6	6									
Branch lines and nozzles	High pressure safety injection line			3										
	Residual heat removal line			3										
	Other lines connected to primary coolant loop			3										
Small diameter lines	Instrumentation lines					1	5							
	RCP leakoff lines					1								
PWR steam generator (Westinghouse and CE designs)														
Primary side shell	Manway cover studs								3		3			
Secondary side shell	Feedwater nozzle bore, blend radius, and shell face beneath the surface		5	5	5									
	Girth welds			5					5					
	Inspection ports							3						
Tubes	Inside surfaces - U bends, roll-transitions, dented tube regions					1								
	Outside surfaces - Tube-sheet crevice, sludge piles, tube-support plate, and free span regions						1					3	1	
	Tubes in antivibration bar and preheater region												5	
Tubes (cont.)	Inadequately supported tubes above upper support plate					1								

Major components		Aging mechanisms												
		Embrit-tlement		Fatigue			Stress corrosion cracking (SCC)			Corrosion/wear				
Component	Subcomponent	Radiation Embrittlement	Thermal aging	Low-cycle thermal fatigue	High-cycle thermal fatigue (†)	High-cycle mechanical fatigue	Primary water SCC	Intergranular SCC	Transgranular SCC	Flow-accelerated corrosion	Boric acid corrosion	Pitting	Wear/fretting	Erosion
PWR feedwater and main steam lines														
Main feedwater piping	Piping inside containment			3	3					2				
	Piping outside containment									1				
Auxiliary feedwater piping	Piping inside containment									4 (‡)				
	Piping outside containment													
Main steam line	Up to main steam isolation valve and safety valve													
	Downstream of main steam isolation valve and safety valve									1				

(†) High-cycle thermal fatigue generally causes crack initiation, but no crack growth. One exception is thermal cycling which can cause both crack initiation and growth.

(‡) Rupture of the bypass line in pre-heat steam generator may not be isolatable.

Note: The values in the table refer to one of the seven damage levels identified on page 21, 65.

The component types and aging mechanisms that have a level six value or above would be "cross-referenced" with the PRA model importance measures to identify those basic events that (A) are susceptible to aging mechanisms and (B) are important to the plant (from a core-damage perspective). The results of this cross-referencing of aging mechanisms to basic event importance are presented in Section 4.

3. Risk Importance and Modeling of Flow Accelerated Corrosion

3.1 Overview

Reviews of Licensee Event Reports (LERs), the Nuclear Plant Experience (NPE) database, and associated literature indicate that FAC is an important aging mechanism for investigation. A particular FAC problem area is the wall thinning of carbon steel pipe, a passive component. FAC in carbon steel pipe systems is characterized by the simultaneous dissolution of iron from the iron oxide-fluid interface and the formation of an iron oxide film at the oxide-metal interface. Bulk flow plays a vital role in providing a sink for dissolution. Under stagnant conditions, corrosion products would concentrate in the aqueous solution reducing the concentration gradient driving force for the corrosion process. Flow inhibits this concentration process and enhances the concentration gradient.

For single-phase FAC, wear patches often start as "horseshoe or scallop" shapes expanding to wide troughs of dimension less than the order of the pipe. Two-phase material degradation appears as "tiger striping" occurring in bends and downstream from flow disruptions in which separate patches on the order of the pipe diameter experience significantly greater material loss than immediately adjacent sections (Chexal, et al., 1996).

Increased fluid velocity, approaching sonic velocity, accelerates FAC. An additional acceleration may occur when rapid flashing of water to vapor occurs. This phenomenon is aggravated by system pressure fluctuations. (Nedelko and Kastner, 1991).

Over the past several years, several FAC models have been developed by utilities and nuclear steam supply vendors. The two main ones are the KWU-KR (Kastner and Riedle, 1986) and the EPRI-Chexal-Horowitz models (EPRI-CH) (Chexal, et al., 1996). While the formulation of the EPRI model is not documented in detail due to its proprietary nature, the formulation of the FAC material loss rate used in the KWU-KR model (Kastner, 1987) is well documented. A third empirical model, part of the BRT-Cicero code, was developed at the Electricité de France (EDF) and is based on experimental data taken on the Cicero test loop (Chexal, et al., 1996). The EDF's BRT-Cicero code is not documented in detail possibly because of its proprietary nature. Consequently, the FAC analysis presented in this work will center around the KWU-KR model.

FAC is a complex, multi-parameter phenomenon, and the susceptibility of a given site cannot be determined by considering only a few parameters. Even though the models can predict observed results fairly well in some cases, such calculations are subject to large uncertainty. The two models discussed above are limited in their ability to consider the effects of complex pipe geometries. The behavior at a particular location depends not only on the geometry at that location, but also on the upstream flow geometry. These individual parameter uncertainties can be propagated through the model using Monte Carlo methods. Even if the input parameters for the model were known

perfectly, the model prediction would be still imperfect. The issues associated with quantification of uncertainty in the predictions of the FAC physical model will also be included in this work.

The FAC phenomena follows a simple two-step process illustrated in Figure 3 (Remy and Bouchacourt, 1992). The first step consists of production of soluble ferrous ions and their accumulation at the oxide-water interface and the second step consists of mass transfer of these ions into the bulk coolant. In the second step, the flowing water removes the soluble ferrous ions by a convective mass transfer mechanism, which is a diffusion gradient driven process. Generally, the concentration of ferrous ions in the bulk water is very low compared to their concentration at the oxide-water interface. Therefore, the ferrous ions present at the oxide-water interface can diffuse very rapidly into the solution.

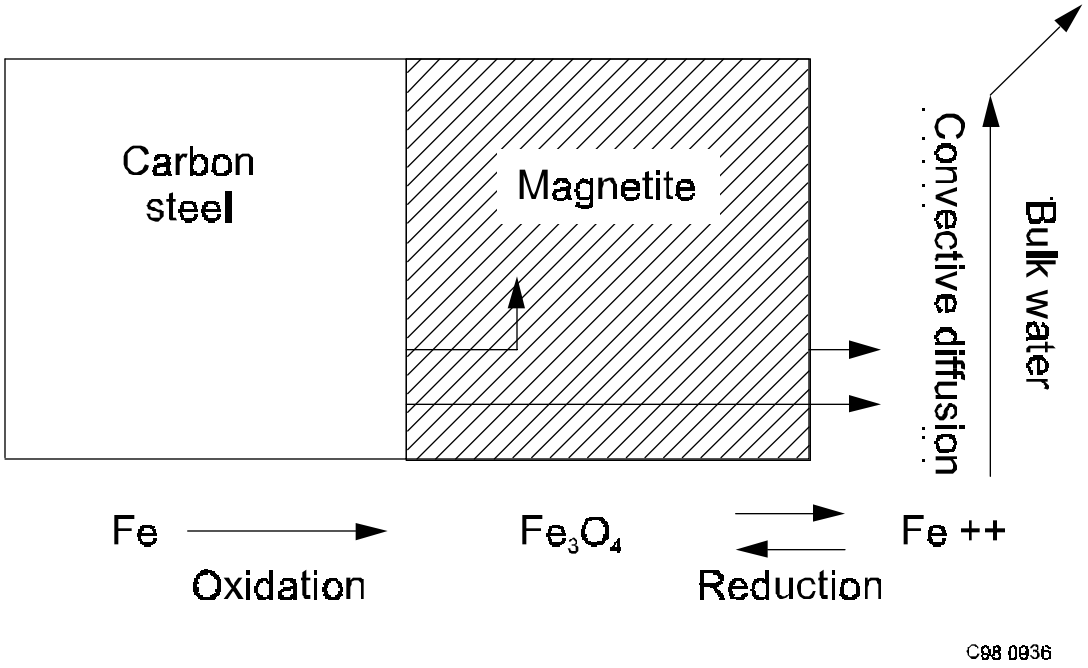

Figure 3. The flow-accelerated corrosion model (Remy and Bouchacourt, 1992).

3.2 Review of FAC Failures

As mentioned, reviews of LERs, the NPE database, and associated literature indicate that FAC is a candidate among aging mechanisms [see Table 4 and Table 5, main PWR and BWR components and their degradation mechanisms (Shah and Macdonald, 1993)] for investigation and modeling. Using the SCSS (Sequence Coding and Search System) database, ORNL searched for *"Pipe Leakage"* problems to retrieve the most recent LERs (from 1990 to April 1996). There are a total of 880 LERs (740 pages) associated with leakage problems of pipe systems (Poore, 1996). Of these, 30 recent cases have been reviewed. Table 6 shows a summary of this review. Note that 11 cases are related to passive components, 11 cases are related to active components, and the remaining 8 cases are not related to components. Service Water Systems (SWS) play an important role in these pipe leakage locations. This was also found in the Nuclear Plant Aging Research (NPAR) program (Jarrel, et al., 1989).

Using the SCSS database (Poore, 1996), the keywords of "PWR and Pipe/Pipe and Steam Leak/Leakage/Rupture/Ruptured/Crack/Fracture/Fractured" has been searched to retrieve the recent LERs (from 1980 to April 1996). There are a total of 89 LERs associated with steam leakage problems of PWRs' pipe components. Table 7 shows a summary of 17 LERs. The LERs are reported to the NRC within 30 days. Generally, the degradation mechanisms or root causes of LERs will be clearly identified a few months later after events. It is assumed that most of the degradation mechanisms in Table 7 were unclear when the LER were issued.

All the FAC-related field experience in PWR plants is associated with piping outside the containment. But single-phase FAC has also caused significant wall thinning of ceratin carbon steel piping located inside the containment at one BWR (USNRC, 1991). Since this piping constitutes a primary pressure boundary, the event has raised a concern that the rupture caused by FAC may lead to a loss-of-coolant accident. In general though, FAC may have following four types of risk impacts:

1. May increase the frequency of transients.

2. May increase the unavailability of safety system.

3. May contribute to LOCA in certain BWR plants.

4. May increase the frequencies of certain overcooling events responsible for generating pressurized thermal shock.

Table 4. Main PWR components and their degradation mechanisms

Components \ Degradation Mechanisms	Radiation Embrittlement	Time-Dependent Relaxation (Creep)	Hydrogen Embrittle-ment	Stress Corrosion Cracking	Low-Cycle Thermal Fatigue	High-Cycle Mechanical and Thermal Fatigue	Corrosion Fatigue	Thermal Embrittle-memt	Mechanical Wear, Fretting and Fatigue	Corrosion and FAC
Reactor Pressure Vessel (RPV)	X			X						X
Containment and Basemat		X	X	X						X
Reactor Coolant Pipe, Safe ends, and branch					X	X		X	X	
Steam Generator tubes				X		X	X		X	X
Reactor Coolant Pump (RCP)						X		X		X
Pressurizer				X	X					
Control Rod Drive Mechanisms				X				X	X	
Safety-related Cables and Connections	X							X		X
Emergency Diesel Generators									X	X
Reactor Internals		X		X		X			X	
Reactor Pressure Vessel Supports	X			X						
Feedwater Pipe and Nozzles, and Steam Generator Shell				X	X	X				X

Table 5. Main BWR components and their degradation mechanisms

Components \ Degradation Mechanisms	Radiation Embrittle-ment	Time-Dependent Relaxation (Creep)	Stress Corrosion Cracking	Low-Cycle Thermal Fatigue	High-Cycle Mechanical and Thermal Fatigue	Corrosion Fatigue	Thermal Embrittlement	Mechanical Wear, Fretting and Fatigue	Corrosion and FAC
Containment			X			X			X
Reactor Pressure Vessels (RPV)	X		X	X	X				X
Recirculation Pipe and Safe Ends			X				X		
Recirculation Pumps			X		X		X		
Control Rod Drive Mechanisms	X		X				X	X	X
Safety-related cables and connections in containment	X	X					X		X
Emergency Diesel Generators	X							X	X
Reactor Pressure Vessel Internals	X		X		X	X	X		
Reactor Pressure Vessels Supports				X					
Feedwater and Main steam Pipe					X			X	X

Table 6. Review of the "pipe leakage" LERs for the most recent six years.

Case no.	LER no.	Type	Pipe Leakage Location	Active/ Passive
1	APL-90-010	PWR	Pipe joints and threaded connections to Check valve of air supply system to 2 dampers used for MCR normal ventilation.	P
2	DUQ-91-002	PWR	Pipe to loop 1B cold leg vent valve	P
3	DUQ-90-001	PWR	SG tube leak	P
4	APL-90-001	PWR	Reactor building cooling isolation valve keakage.	A
5	CWE-92-012	PWR	S/D, leakage of feedwater check valve	A
6	TVA-93-004	BWR	Operator error, no physical leakage	n/a
7	CPL-92-008	BWR	S/D, a through-wall leak in jacket water cooler service water supply line of EDG	P
8	NEB-94-010	BWR	S/D, leakage through RHR shutdown cooling isolation valve	A
9	NEB-93-005	BWR	S/D, reactor feedwater check valve leakage	A
10	NEB-93-005	BWR	S/D, backflow through the check valve in non-regenerative heat exchanger and RWCU pipe. Design error.	A
11	FPC-91-005	PWR	Inter-stage packing leakoff of a makeup and purification system valve	A
12	PGE-92-001	PWR	VCT outlet check valve didn't test. TS violation.	n/a
13	PGE-90-010	PWR	A crack in the positive displacement charging pump suction pipe. The cause of crack is vibration induced high cycle fatigue.	P
14	PGE-91-004	PWR	Calculation error in TS associated Unidentified Leakage Rate.	n/a
15	CWE-94-001	BWR	The undocumented plant modification, a sampling line isolation valve leakage.	A
16	CWE-91-015	BWR	The isolation valve in a primary containment penetration line leakage.	A
17	CWE-94-002	BWR	One primary containment isolation valve didn't perform LLRT.	n/a

Table 6. (cont.)

Case no.	LER no.	Type	Pipe Leakage Location	Active/ Passive
18	CW5-92-015	BWR	LPCI testable injection check valve leakage.	A
19	FIT-95-010	BWR	A packing leak on Reactor Recirculation system valve.	A
20	PNY-92-022	BWR	S/D, failure to perform ISI in emergency service water and EDG.	n/a
21	OPP-92-018	PWR	S/D, a modification revealed severe corrosion of carbon steel fasteners on the boric acid pump flanges and pipe support.	n/a
22	OPP-92-002	PWR	Condensate from nearby component cooling water pipe dripping onto the inner PAL (Personnel Air Lock) door bulkhead structure and upper latch bolt bracket causing surface corrosion.	P
23	HOP-95-013	BWR	Failure to perform ISI for some pipe line.	n/a
24	GPC-90-022	BWR	Operator error, no actual system leakage occurred.	n/a
25	PEG-90-035	BWR	A 30" pipe section on the "A" Service Water System loop had developed minor through wall flaw (in the internal pipe epoxy coating which allowed pipe corrosion to begin and subsequent erosion to occur.)	P
26	PEG-90-025	BWR	S/D, a leak at a joint weld (vibration induced fatigue) on a reactor Recirculation instrument line.	P
27	IND-95-014	PWR	S/D, a Service Water leak was detected inside containment occurring at Fan Cooler discharge flow element weld . This transition weld resulted in galvanic interaction and corrosion of the carbon steel and stainless steel.	P
28	DPC-90-025	PWR	A packing leak of Pressurizer PORV header Hi point vent valve.	A
29	NEU-94-023	BWR	A small leakage in the Service Water discharge pipe from Reactor Building Closed Cooling Water heat exchanger.	P
30	NEU-93-021	BWR	A through wall defect in the Service Water pipe in the Turbine Building. The root cause is erosion/corrosion of carbon steel pipe.	P

Table 7. Summary of 17 LER cases related to the "MSL Leakage".

Case no.	LER no. (plant type)	Plant -Unit	Commercial Operation Date	Date of Damage	Damage Component/Extent of Damage and Comments	Degradation Mechanisms	Active/ Passive
1	APL-90-019 (PWR)	Arkansas Nuclear One-2	3/26/80	8/21/90	MSIV closure due to the failure of a normally energized solenoid valve. Also found S/G-A small leak.	Not mentioned	A
2	DUQ-93-001 (PWR)	Beaver Valley-2	11/17/87	1/26/93	Extensive engineering analysis identified the stress of the AFW pipe to S/G-C, for combined water hammer and seismic events, exceeded the design stress allowable.	n/a	n/a
3	CWE-91-012 (PWR)	Braidwood-1	7/29/88	11/6/91	Significant leakage identified on main FW motor-operated isolation valve.	Not mentioned	A
4	CWE-90-010 (PWR)	Byron-2	8/21/87	12/20/90	A severe steam leak reported in main steam tunnel. The weld for main steam probe improperly repaired during outage cause a one inch hole in MSL.	SCC	P
5	NEU-94-018 (PWR)	Connecticut Yankee	1/1/68	7/11/94	No MSL leak. #3 RCP motor oil leak due to a cracked PVC coupling on the line caused a small fire.	SCC	P
6	NEU-93-012 (PWR)	Connecticut Yankee	1/1/68	7/14/93	S/D, operator error to isolate all four MSL flow transmitters. No actual MSL leakage occurred.	n/a	n/a
7	FPC-92-015 (PWR)	Crystal River-3	3/13/77	7/17/92	A steam leak occurred from the packing of a manual isolation valve associated with OTSG-A.	Not mentioned	A
8	CEC-93-010 (PWR)	Indian Point-2	8/1/74	8/18/93	No physical leak, an engineering analysis identified two regulating valves in instrument air system for main steam PORV & AFWS were not fully capable perform their function.	Not mentioned	A
9	TOL-94-002 (PWR)	Davis-Besse-1	7/31/78	7/28/94	A minor steam leak on a vent line for MFP.	Not mentioned	P

Table 7. (cont.)

Case no.	LER no. (plant type)	Plant -Unit	Commercial Date	Date of Damage	Damage Component/Extent of Damage and Comments	Degradation Mechanisms	Active/ Passive
10	NEU-91-012 (PWR)	Millstone-2	12/26/75	11/6/91	An 8 inch diameter pipe ruptured in a drain line from the first stage preheater drain tank to high pressure FW heater.	Not mentioned	P
11	VEP-92-005 (PWR)	Surry-1	12/12/72	4/2/92	S/D, No physical leak. TS violation for a potential leakage path from CTMT to safeguards building.	n/a	n/a
12	NEU-92-003 (PWR)	Millstone-3	4/23/86	1/30/92	No physical MSL leak. Inadequate work planning caused loss enclosure building integrity.	n/a	n/a
13	VEP-92-007 (PWR)	North Anna-2	12/14/80	8/6/92	A leak on the downstream weld of a LHSI (Low Head Safety Injection) isolation vent valve. An overstress condition when LHSI pump started caused valve weld failure.	SCC	P
14	TVA-93-001 (PWR)	Sequoyah-2	6/1/82	3/1/93	A steam leak on the extraction line to the feedwater heater ruptured caused a 3- by 6- inch hole in the line. The root cause of this event was a programmatic failure of the erosion/corrosion program resulting from insufficient management of the program.	Not mentioned	P
15	NEU-95-032 (PWR)	Millstone-2	12/26/75	8/8/95	A steam leak in a secondary system within the turbine building. The steam leakage occurred revealed a 14" vertical rupture in the 8" diameter recirculation line from the discharge of the B Heater Drains Pump (HDP) to Heater Drain Tank.	Not mentioned	P
16	VEP-90-003 (PWR)	Surry-1	12/12/72	4/2/92	A leak developed downstream of a low pressure heater drain pump in Unit 2 releasing steam and water into the Unit 1 turbine building. The leak was a result of a pipe failure due to excessive thinning of the wall.	Not mentioned (pipe thinning)	P
17	SCE-90-011 (PWR)	San Onofre-2	8/8/83	6/1/90	This voluntary licensee event report is being submitted to describe SCE's actions in response to a recent occurrence of pipe wall thinning as a result of erosion-corrosion (E-C) processes.	FAC (Flow-Accelerated Corrosion)	P

FAC has been a most destructive corrosion mechanism for high-energy [fluid temperature between 212 ºF to 482 ºF (100ºC to 250 ºC)] carbon steel pipe in light water reactors. It has caused rupture of large-, medium-, and small-diameter pipes carrying either single phase or two-phase flow. Single-phase FAC has also caused significant wall thinning of carbon steel J-tubes and feedrings within the recirculating steam generators (Shah, et al., 1997). FAC is the only mechanism that has significant potential for large leaks (Gosselin, et al., 1996; Gosselin, 1997).

FAC has caused rupture of carbon steel secondary piping at several PWRs. The most notable rupture of feed water piping occurred at Surry, Unit 2, on December 9, 1986. Another noteworthy event associated with single-phase FAC is the rupture of a drain pump discharge piping (350-mm diameter) at Trojan on March 9, 1985. A pressure transient caused the ultimate rupture of feedwater piping already significantly degraded by FAC at both plants. In neither case were there a leak or any other warning signs indicating incipient failures.

3.3 Overview of Single-Phase FAC

Single-phase FAC tests have been conducted at several British, French, and German laboratories to identify the factors affecting the FAC rates (rate of metal loss) and to provide data for development of empirical models to estimate these rates (Chexal and Jones, 1988; Chexal and Horowitz, 1995). An evaluation of the test results from the operating plants data has identified several factors that affect the FAC rate. These factors may be divided into three groups: (a) hydrodynamic variables - fluid velocity, pipe configuration (geometry of the flow path), and pipe roughness of pipe inside surface; (b) metallurgical variables - chemical composition including weight percentage of chromium, molybdenum and copper in the steel; and (c) environmental variables - coolant temperature and water chemistry including dissolved oxygen, ferrous ion concentration, metallic impurities in water, and pH (Shah, et al., 1997).

The hydrodynamic variables affect the rate of mass transfer of the iron ions and other corrosion products to the bulk coolant and thus affect the FAC rate. *Fluid velocity* affects the mass transfer. At a relatively low flow velocity, the FAC rate is controlled by the rate of mass transfer, whereas at higher velocity (still lower than the critical velocity above which metal removal by mechanical process takes place), the mass transfer rate is higher and the FAC rate is controlled by the chemical reactions at the oxide-coolant and metal-oxide interfaces. FAC is less frequently observed in straight lengths of pipe free from hydro-dynamic disturbances unless the bulk fluid velocity is high. Laboratory studies of the effect of bulk flow velocities, varied from 2 to 18 m/s (6.6 to 59 ft/s), on the FAC of carbon steel in 150°C (300°F) circulating water show that the FAC rate increases with an increase in the flow rate and (for a given flow rate) the FAC rate is almost constant. The variable *pipe configuration* takes into account the hydrodynamic disturbances (elbows, tees, branch connections, reducers, valves, flow control orifices, etc.) that produce high local fluid velocities and result in a further increase in mass transfer. Experiments have shown that local-flow

velocities in elbows can be two to three times the bulk-flow velocities (Bosnak, 1987; NRC, 1987). A rough surface produced by the FAC process can be very damaging. The micropits formed by the initial selective attack on the carbon steel microstructure grow until they touch, and thus the surface becomes rough. The dependence of mass transfer on the velocity is greater for a rough surface than for a smooth surface.

Generally, the FAC monitoring programs concentrate on inspection of pipe elbows and tee fittings, i.e., the sites where local high velocities may be present. However, FAC has caused rupture at other feedwater pipe sites, such as in the flange of a flow measuring device downstream of an orifice at Loviisa Unit 1 in Finland and in the straight portion of a pipe, located immediately downstream of a level control valve, at Surry Unit 1 and at Millstone Unit 3. FAC has caused significant wall thinning of the feedwater control valve bypass line at both the San Onofre and Diablo Canyon plants. It was surprising to find significant wall thinning and failures of the startup feedwater system pipe at both the Wolf Creek and Callaway plants because these systems were used for a very short time period during startup. Investigation of these failures showed that the cause was the flow resulting from the leaking valves on the pipe (Chexal, et al., 1996).

Trace amounts of chromium, molybdenum, and copper in carbon steel provide resistance to FAC. The FAC rate is most sensitive to the weight percent (wt%) of the chromium in the steel. For example, the FAC rate dependence on chromium content as predicted by the EPRI-CH model for a 90-degree carbon steel elbow is equal to about 3.9 mm/yr (0.155 in/yr) for 0.03 wt% Cr and about 0.4 mm/yr (0.016 in/yr) for 0.50 wt% Cr (Chexal and Horowitz, 1995). Thus, a small amount of chromium significantly reduces the FAC rate. The corresponding FAC rate in the case of 0.03 wt% Cr predicted by the KWU-KR model through our calculations (and verified against the current version of the KWU software) is *significantly smaller* and equal to about 1.14 mm/yr (0.045 in/yr). This deviation between the EPRI-CH and KWU-KR model is shown in Figure 4.

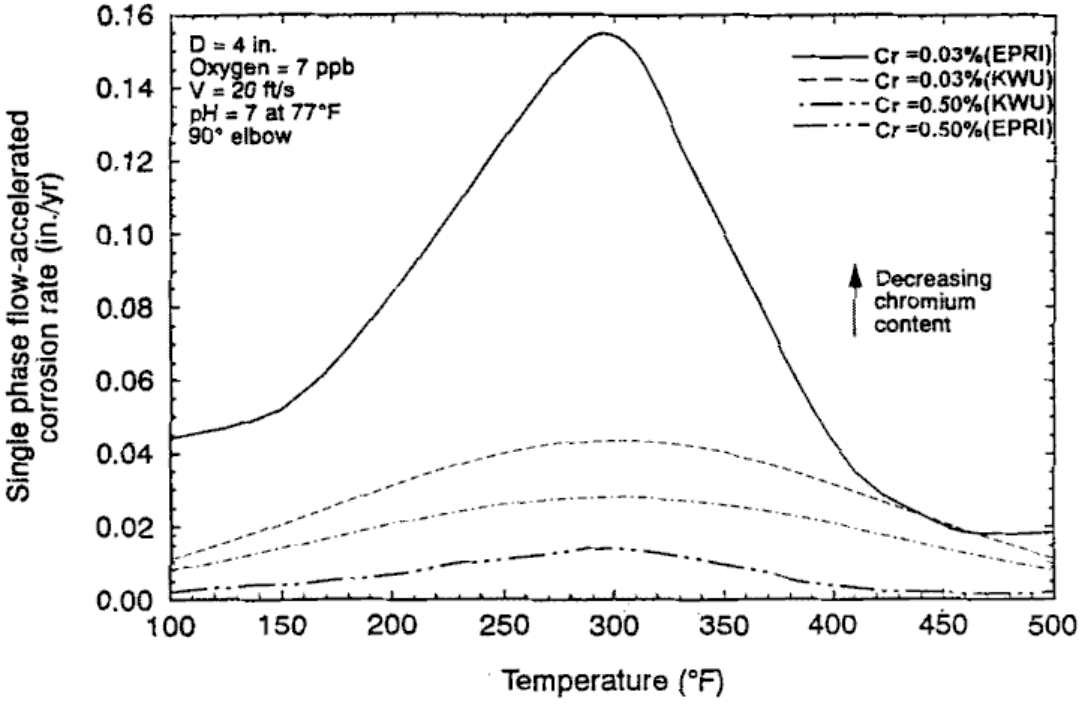

Figure 4. Comparison of the EPRI-CH and the KWU-KR models.

The two main environmental variables that affect the FAC rate are the fluid temperature and chemistry. The water chemistry includes dissolved oxygen, ferrous ion concentration, metallic impurities, and cold pH level. The *fluid temperature* influences both the ferrous ion production and the mass transfer of these ions into the bulk water (Remy and Bouchacourt, 1992). As the temperature increases, the ferrous ion concentration at the oxide-water interface decreases almost linearly. On the other hand, as the temperature increases, the ferrous ion diffusivity into the coolant increases, resulting in a mass transfer coefficient that increases almost linearly. The resulting FAC rate variation with temperature is a bell-shaped curve as Figure 5 shows.

The temperature at which the maximum FAC rate occurs depends upon the other environmental conditions. For most feedwater pipe conditions, the maximum FAC rate occurs at about 150°C (300°F) (Chexal and Horowitz, 1995).

The FAC rate varies inversely with the level of *dissolved oxygen* in the fluid. As the level of oxygen increases above a threshold value, a less porous oxide layer of hematite, instead of magnetite forms. Because the solubility of hematite in the feedwater is several orders of magnitude

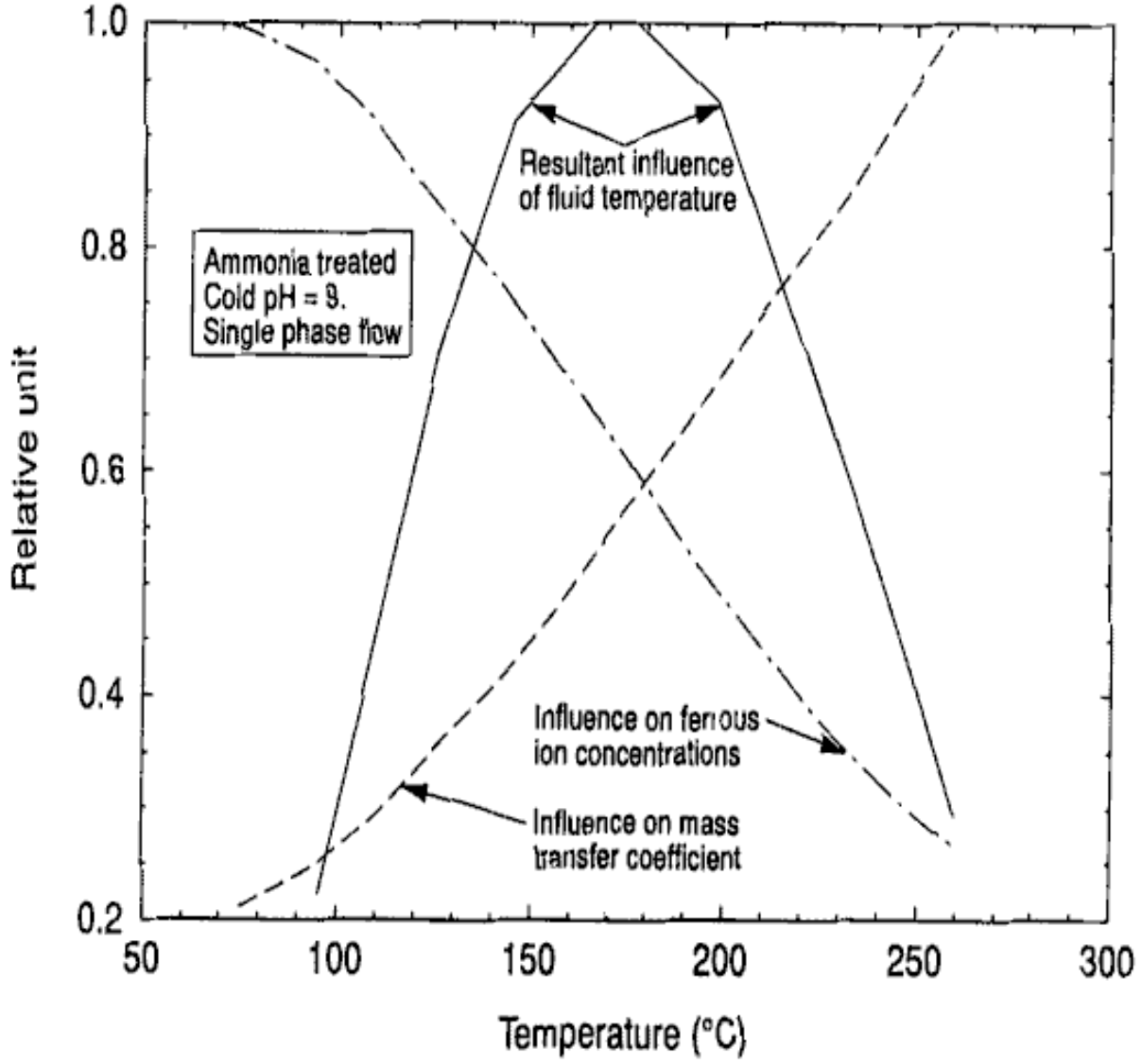

Figure 5. The calculated influence of fluid temperature on the ferrous ion concentration and on mass transfer of ferrous ions (Remy and Bouchacourt, 1992).

lower than that of magnetite, the FAC rate decreases significantly. Some laboratory test results show that the threshold value for dissolved oxygen is less than 15 ppb (Remy and Bouchacourt, 1992). Using the EPRI-CH model shows a reduction in the maximum FAC rate from about 3.2 to 0.89 mm/yr (0.125 to 0.035 in./yr) as dissolved oxygen content increases from 10 to 30 ppb.

Ferrous ion concentration and metallic impurities in the water affect the FAC rate. The increase in the *ferrous ion concentration* in the bulk fluid reduces the mass transfer of ferrous ions from the oxide-coolant interface to bulk coolant. An increased ferrous ion concentration can reduce or suppress FAC when mass transfer controls the process. FAC rates vary by an order of magnitude over the cold pH[†] range of 8.5 to 9.5, which is typical for feedwater systems (Jonas, 1988).

FAC has caused rupture of carbon steel secondary piping at several PWRs. The most notable rupture of feed water piping occurred at Surry, Unit 2, on December 9, 1986. Another noteworthy event associated with single-phase FAC is the rupture of a drain pump discharge piping (350-mm diameter) at Trojan on March 9, 1985. A pressure transient caused the ultimate rupture of feedwater piping already significantly degraded by FAC at both plants. In neither case were there a leak or any other warning signs indicating incipient failures.

Two examples of events associated with two-phase FAC include ruptures of the fourth stage steam extraction piping, one at Millstone Unit 2 in October, 1986, and another one at Fort Calhoun on April 21, 1997. Single-phase FAC has also caused significant wall thinning in auxiliary feedwater piping at Catawba Unit 2, which has preheat steam generators. Ten Westinghouse-designed PWRs with Models D4, D5, and E of preheat steam generators are susceptible to such wall thinning (USNRC 1992). The preheater bypass line arrangement is shown in Figure 6. The pipe rupture is a risk-significant event because it may cause reactor trip. In addition, some of the rupture events, such as a break of a small steam line, may represent a dominating overcooling event that may contribute to pressurized thermal shock (PTS) risk to reactor pressure vessel (Selby et al. 1985). The PTS risk associated with steam line break is, however, small; therefore, the PTS risk associated with FAC-induced steam line rupture will be quite small.

It is important to note that FAC events still happen (e.g., Fort Calhoun, April 1997) even though the nuclear power generation industry in the U.S. has a very active FAC evaluation and control program in place at every plant. Consequently, to model FAC in a probabilistic way (e.g., via a PRA), one would need to quantify the effectiveness of existing FAC programs.

[†] Cold pH is taken at temperature 25^0C (77^0F). A lower cold pH provides the same desired pH at the operating temperature.

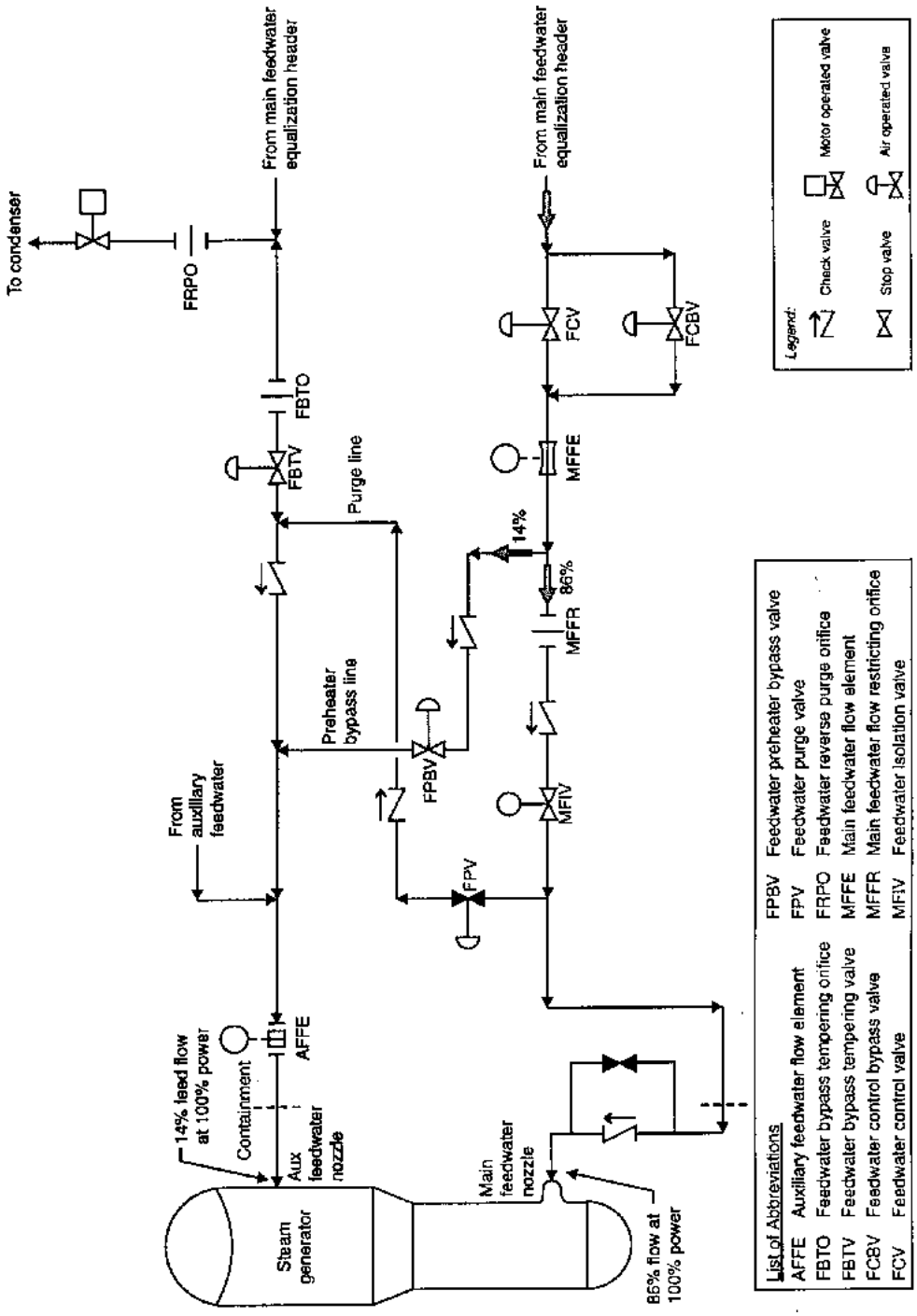

Figure 6. Schematic of a feedwater system for a Westinghouse plant steam generators equipped with preheaters (Shah, et al., 1997).

3.4 Overview of Two-Phase FAC

Examination of worn extraction pipe has identified two distinct mechanisms causing damage in the system carrying two-phase coolant: oxide dissolution and droplet-impact wear (Keck and Griffith, 1987). The oxide dissolution mechanism is similar to the single-phase FAC mechanism discussed above with one exception. Two-phase FAC has been observed in pipe carrying wet steam. Its occurrence has not been observed in pipe carrying dry steam (100% quality). Moisture in the wet steam is essential to dissolve the oxide film. Test results show that the FAC rate in a two-phase flow varies with the quality of the steam. It is zero at 100% quality and equal to the single-phase (water) flow value at 0% quality. The FAC rate peaks at some intermediate value of quality (Chexal and Horowitz, 1990). Field data indicated that the greatest degradation was seen in pipe containing steam with the highest moisture content, such as the turbine crossover pipe and the exhaust and extraction pipe connected to the high-pressure turbines.

The droplet-impact wear mechanism may be explained as follows. The liquid phase in a steam line generally flows in a thin layer near the main steam line pipe wall, while the vapor forms the core of the flow and moves much faster than the liquid phase. This velocity difference creates shear forces at the liquid-vapor interface; if this force is greater than the surface tension force at the interface, some liquid will be sheared off the liquid layer and carried over with the vapor. This liquid will form droplets, which will be accelerated by the vapor and become entrained in the vapor core. A fraction of the entrained liquid droplets will impinge on the oxide film on the main steam line inside the surface. The impact of liquid droplets on carbon-steel oxide films can produce a matrix of cracks and subsequent fatigue failure of the films, and expose the underlying metal surfaces to the corrosive action of the coolant. The parameters that determine film failure are the oxide hardness, the critical strain to oxide failure, and the fatigue loads required to fracture the oxide film. This wear mechanism occurs under certain conditions at elbows and fittings where the flow changes direction, predominantly on the outside radius of the bend in the direction of the flow (Keck and Griffith, 1987). In contrast, damage caused by oxide dissolution occurs on the inside radius of the bend where flow separation causes turbulence. The droplet impact wear mechanism requires the presence of droplets, so this mechanism occurs only in pipes carrying two-phase flow.

Keck and Griffith (1987) provide simple models for estimating oxide dissolution and droplet-impact wear. The model developed to describe droplet-impact erosion does not depend strongly on temperature, but does depend strongly on flow velocity (fourth power dependence). Therefore, droplet-impact wear is expected to be of importance at high flow velocities.

FAC has caused ruptures in two-phase systems at some PWRs. The following are three examples: Oconee Unit 2 in 1982 , Arkansas Nuclear One Unit 2 in 1989, and Sequoyah Unit 2 in 1993. The FAC caused a 1219-mm (4-ft) rupture of a 609.6-mm (24-in.)-diameter, long-radius elbow in the feedwater heat extraction line that is supplied steam from the high-pressure turbine

exhaust at the Oconee Unit 2 in 1982 (NRC, 1982). The utility established a pipe inspection program for two-phase (steam/water) systems after this incident. After the feedwater pipe rupture accident at Surry Unit 2 in 1986, the utility augmented this program to include single phase systems (NRC, 1991).

In 1989, following the 18 April rupture of a 355.6-mm (14-in) diameter steam extraction line at Arkansas Nuclear One Unit 2, pipe inspections revealed significant thinning of other sections of the two-phase steam extraction pipe at the plant. The pipe wall was worn from the nominal 9.52-mm (3/8 in) thickness to a thickness of about 0.79-mm (0.031-in). The 180 degree fishmouth rupture was about 76.2-mm (3-in.) wide. That prompted the utility to replace more than 30.48-m (100 ft) of carbon steel pipe with 2.5% chrome alloy material (Stroller, 1989).

A third incident occurred at Sequoyah Unit 2, a 1,148 MWe PWR that has been in commercial operation since 1982. The extraction line to the feedwater heater ruptured and caused a 76- by 152-mm (3- by 6-in.) hole in the line. The cause of this event was a programmatic failure of the FAC program resulting from insufficient management of the program (Stoller, 1993). To prevent recurrence, an independent review of the FAC program for adequacy and completeness was to be performed. The utility was to evaluate appropriate pipe systems on both Units 1 and 2 again. Inspections, as well as repair and replacements, were to be performed based on the results of the evaluation. This resulted in a long shutdown for both units.

3.5 Selection of FAC Empirical Models

Of the three most-used models proposed to describe FAC, two will be briefly discussed in this section. Those models are empirical, the KWU-KR model (Kastner and Riedle, 1986 ; Kastner, 1987) and the EPRI-CH model (Chexal, et al., 1996). The KWU-KR model is the FAC model within the WATHEC code produced by Siemens/KWU as a program to aid utilities in managing pipe degradation caused by the FAC process. This KWU-KR model is derived from both single- and two-phase flow data. Single-phase flow data taken in the lab were used to derive the original relationships among the parameters. The derived relationships were then adjusted as needed to fit two-phase plant data (Kastner, 1987). A similar method was used for the EPRI-CH model which is the FAC model within the CHECWORKS code, an EPRI product that competes with WATHEC. The lab data used in the KWU-KR model were generated at Siemens/KWU and the plant data used consists of approximately 6,000 single- and two-phase data points (Chexal, et al., 1996). The data used by EPRI includes British, French and German lab data, U. S. plant data, and EPRI sponsored lab data (Chexal, et al., 1996).

Both the KWU-KR and EPRI-CH model report better model predictions when compared to laboratory single phase data than when compared to all data within the respective databases. Figures 7 and 8 give the comparison, respectively, of single phase laboratory data and of single and two-phase both lab and plant data to the KWU-KR model (Kastner and Riedle, 1986). For single and two-phase both lab and plant data in Figure 8, the empirical calculated FAC rate in 85% of 1,049 cases are greater or equal to the measured FAC rate. Figures 9 and 10 give the comparison, respectively, of single-phase lab and of single and two-phase both lab and plant data to the EPRI-CH model (Chexal and Horowitz, 1995; Chexal, et al., 1996). For the performance of the EPRI-CH correlation against single-phase lab data, the measured FAC rate lies within a range of ±50% compared with the predicted FAC rate. However, lab and plant data shows the measured FAC rate lies within a range of +100/-50%[†] compared with the predicted FAC rate.

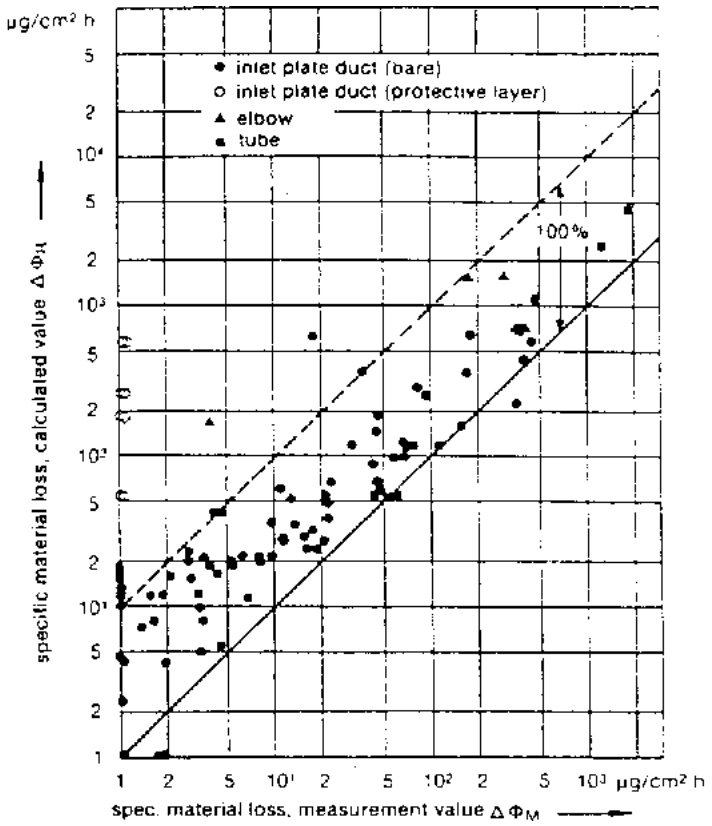

Figure 7. KWU-KR FAC model, comparison against single-phase laboratory data (Kastner and Riedle, 1986). Permission to use this copyrighted material is granted by VGB PowerTech Service GmbH.

[†] The associated plots, either in the Chexal and Horowitz 1995 paper or Chexal and et al. 1996 book, were mistaken to say "the accuracy of the wear rate predication is generally within ±50%". Actually, the two ±50% lines as indicated in Figure 10 were +100/-50% lines.

We have elected to base our calculations on the KWU-KR model because it is well documented in the published literature. Similar documentation for the CHECWORKS model is not available because of its proprietary nature. A third model, part of the BRT-Cicero code, is based on the test data taken at the Cicero test loop and was developed by the Electricité de France. But the documentation of this model is also not available because of its proprietary nature.

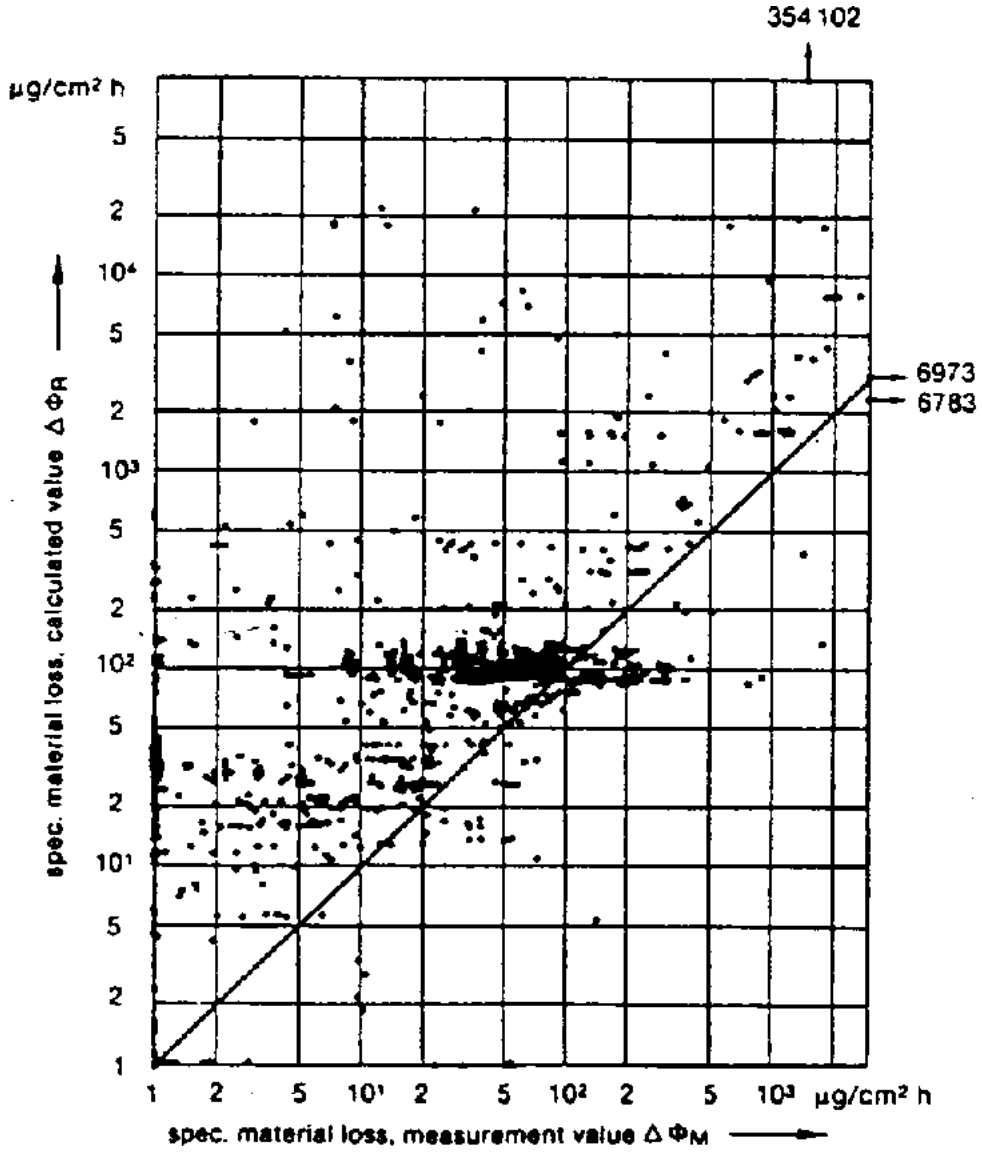

Figure 8. KWU-KR FAC model, comparison against single and two-phase both laboratory and plant data (Kastner and Riedle, 1986). Permission to use this copyrighted material is granted by VGB PowerTech Service GmbH.

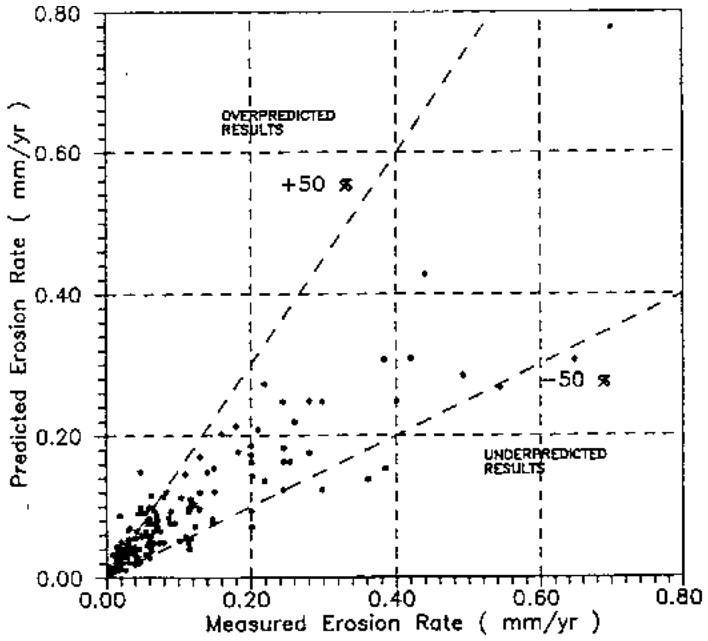

Figure 9. EPRI-CH FAC model, comparison against single-phase laboratory data (Chexal and Horowitz, 1995; Chexal, et al., 1996). Permission to use this copyrighted material is granted by EPRI.

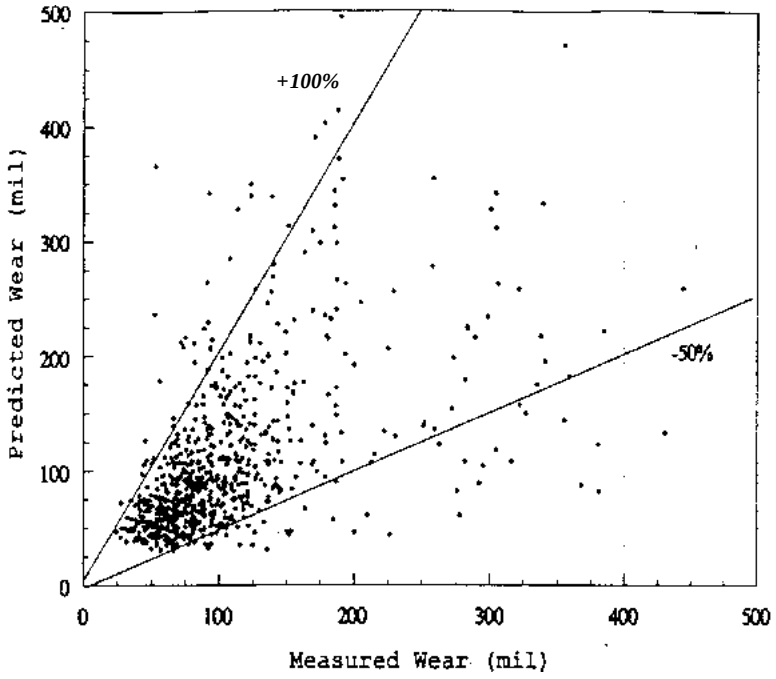

Figure 10. EPRI-CH FAC model, comparison against single and two-phase both lab and plant data (Chexal and Horowitz, 1995; Chexal, et al., 1996). Permission to use this copyrighted material is granted by EPRI.

3.6 Details of the KWU-KR FAC Model

The KWU-KR model calculates the corrosion rate as a function of Keller's geometry factor, flow velocity, fluid temperature, material chemical composition, fluid chemistry (pH at 25°C and dissolved oxygen), exposure time, and, in the case of two-phase flow, steam quality. With this model, the pipe thickness can be calculated as a function of time. The wall corrosion, $W_C(t)$, is the thickness of the pipe corroded away and is given by

$$W_C(t) = \frac{\Delta\phi_R\, t}{\rho_{st}} \tag{3}$$

where

$\Delta\phi_R$ = FAC rate ($\mu g/cm^2$ hr),
t = exposure time (hr),
ρ_{st} = the density of steel ($\mu g/cm^3$).

Kastner and Riedle's work (1987) is the basis for estimating the FAC rate, $\Delta\phi_R$. Once the FAC rate is estimated, the wall thickness as a function of time can be calculated. This wall thickness is be found by

$$W_{pipe}(t) = W_{original} - W_{C,calculated}(t) \tag{4}$$

where

$W_{pipe}(t)$ = pipe wall thickness at time t (cm),
$W_{original}$ = original, nominal pipe wall thickness (cm),
$W_{C,calculated}(t)$ = calculated thickness of pipe corroded away at time t (cm).

The corrosion rate, $\Delta\phi_R$, is calculated via the following steps.

Using the KWU-Kastner model, the pH, oxygen content, liquid velocity, geometrical factor, total content of chromium and molybdenum in steel, and operating temperature are known. We can calculate FAC rate as the following equations (Kastner, 1986):

$$\Delta\phi_R = 6.35\, k_c\left(B\cdot e^{N\cdot w}\cdot\left[1 - 0.175\cdot(pH-7)^2\right]\cdot 1.8\cdot e^{-0.118\,g} + 1\right)\cdot f(t) \tag{5}$$

with

B = $-10.5\sqrt{h} - \left(9.375\times10^{-4}\,T^2\right) + \left(0.79\,T\right) - 132.5$
N = $-0.0875\,h - (1.275\times10^{-5}\,T^2) + (1.078\times10^{-2}\,T) - 2.15$ *(for 0% ≤ h ≤ 0.5%)*
N = $(-1.29\times10^{-4}\,T^2 + 0.109\,T - 22.07)\,0.154\,e^{-1.2\,h}$ *(for 0.5% ≤ h ≤ 5%)*

and

$\Delta\phi_R$ = calculated specific rate of material loss ($\mu g/cm^2$ h),
k_c = geometrical factor,

w = flow velocity (m/s),
pH = pH value,
g = oxygen content (μg/kg),
h = content of chromium and molybdenum in steel (total %),
T = temperature (°K)
f (t) = a time correction factor.

Note that the time correction factor, f (t), of the FAC rate equation is a function of exposure time in the KWU-KR model (Kastner and Riedle, 1986). Exploring the behavior of this factor, it can be shown that the factor f (t) has a value of 1 in small operating periods and tends to the value of 0.79 for an operating period of 9.6×10^4 hrs (around 11 years). Note that for longer operating periods ($t \geq 9.6 \times 10^4$ hrs), f (t) equals 0.79. The time correction factor is given by

$$f(t) = C_1 + C_2\, t + C_3\, t^2 + C_4\, t^3 \qquad (6)$$

where

t = the exposure time (hr),
C_1 = 9.999934×10^{-1},
C_2 = -3.356901×10^{-7},
C_3 = $-5.624812 \times 10^{-11}$,
C_4 = 3.849972×10^{-16}.

The geometry factor, k_c, is given by one of the following values:(Kastner, 1986)

0.04 for "straight tube"
0.08 for "leaky joints" or "labyrinths"
0.15 for "behind junctions"
0.16 for "behind tube inlet (sharp edge)"
0.23 for "elbow R/D=2.5"
0.30 for "elbow R/D=1.5"
0.30 for "in and over blades"
0.52 for "elbow R/D=0.5"
0.60 for "in branches #2"
0.75 for "in branches #1"
1.0 for "on tubes," "on blade," or "on plate"

This FAC model was developed in 1980s and, therefore, the further understanding developed since then is not incorporated in the model. The following assumptions are employed in the model. Comments based on the current understanding of the FAC phenomena are also presented, if appropriate, along with each assumption.

1. The model has no restriction on the flow velocity up to the critical velocity which metal removal takes place by mechanical processes.

2. The FAC rates are insignificant at water temperature greater than 240°C, and the resulting material losses can be ignored. This assumption is consistent with our current understanding.

3. The lower and upper limits for the cold pH are 7.0 and 9.39, respectively. Note that the typical limits for PWR are 8.5 and 9.5. The model assumes that the corrosion rate is very small (1μg/cm^2/h) and constant if the pH is greater than 9.39. But the test results show that at higher pH values, the corrosion rate increases with increasing pH value.

4. The oxygen concentration is less than 30 ppb. For higher concentration, the rate is constant and very small. The test results and plant data show that the rate is very small for the oxygen concentration greater than 15 ppb.

5. The chromium and molybdenum content is less than 0.5 wt%. No material loss takes place if the content is higher. This is conservative because the field data show that there is no material loss if the content is greater than 0.1 wt%.

6. The model is valid only for operating periods longer than 200 h. Very high losses can occur in the start-up phase.

7. The two-phase FAC model uses the mean velocity in the water film on the inside surface of the piping instead of the velocity of a two-phase fluid. The basic condition is annular flow in two-phase flow. When applying the empirical model for water flow to water/steam flows, the reference velocity used is not the velocity of a two-phase mixture, but the mean velocity in the film of water on the wall of the component, W_F. A simplified equation for this is:

$$W_F = \frac{\dot{m}}{\rho_W} \frac{1 - x_{st}}{1 - \alpha} \tag{7}$$

where

$\dot{m}$	=	mass flux (kg/m^2 s),
ρ_W	=	density of the water at saturation condition (kg/m^3),
x_{st}	=	steam quality,
α	=	void fraction.

Comparison of the KWU-KR FAC model with the EPRI-CH Code Chexal and Horowitz (1995) have analyzed four simple FAC problems using the EPRI-CH model [see Figures 3, 5, 7, and 8 in the Chexal and Horowitz' paper (Chexal and Horowitz, 1995), or Figures 52, 51, 54, and 56 in the NUREG/CR-6456 report (Shah, et al., 1997)]. The EPRI-CH model has been incorporated in the CHEC computer program and other subsequent programs developed by EPRI. Comparison of the results shows that the KWU-KR FAC rate results are generally significantly lower than those of the EPRI code. A comparison of the KWU-KR model with those of the EPRI-CH was shown in Figure 4 for variations in the chromium content. Three other associated comparisons are shown in Figures 11, 12, and 13 for variations in flow rate, dissolved oxygen content, and pH, respectively. The results of the four comparison cases show that the calculated FAC rates via the KWU-KR model are *less* conservative when compared with corresponding results of the EPRI-CH model. However, the comparison shown in Figure 8 indicates that the FAC rates calculated using the KWU-KR model are conservative as compared to actual laboratory and plant operational data.

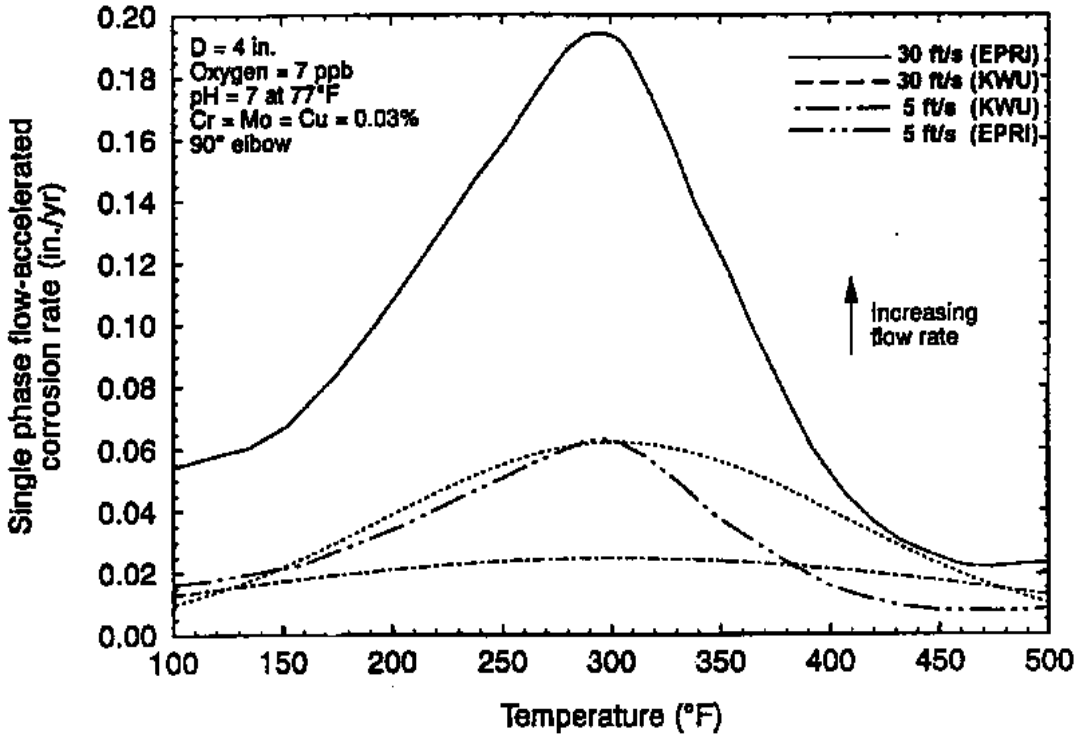

Figure 11. Comparison of the EPRI-CH and the KWU-KR FAC models for flow rate variations.

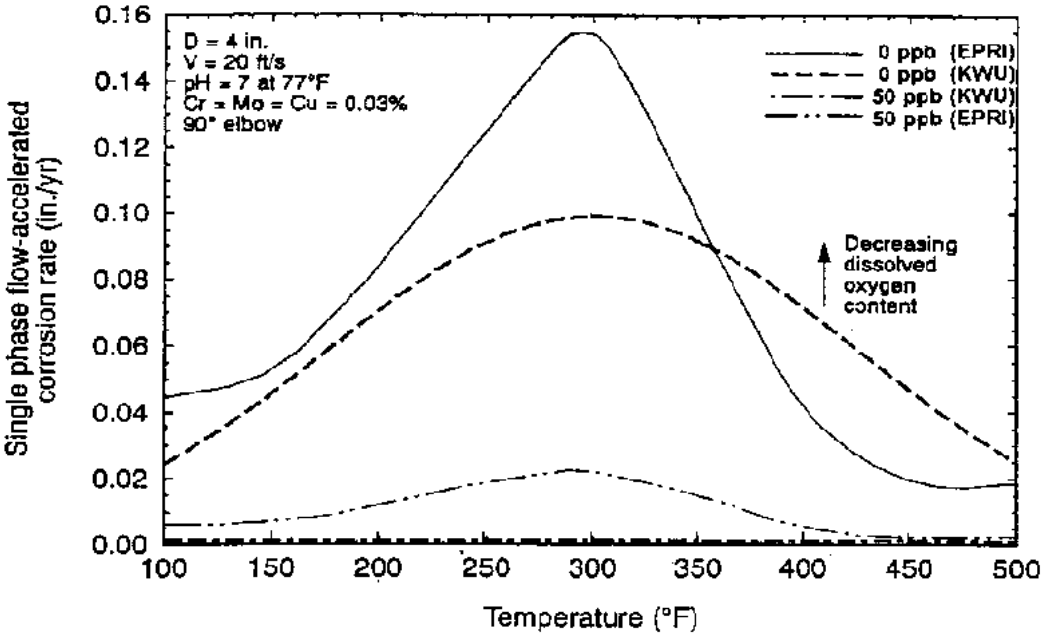

Figure 12. Comparison of the EPRI-CH and the KWU-KR FAC models for dissolved oxygen content variations.

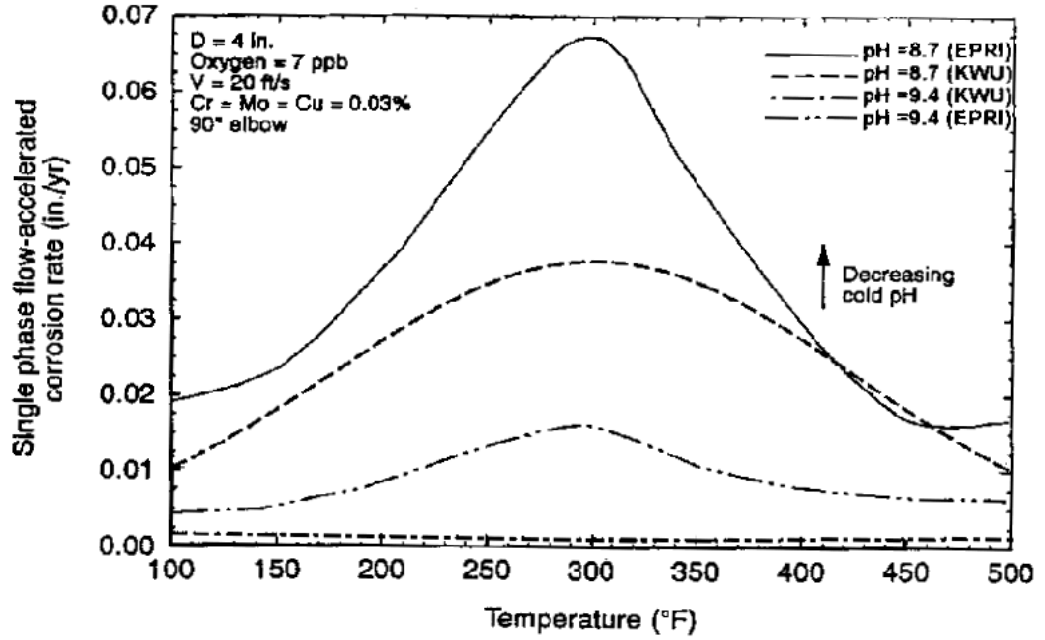

Figure 13. Comparison of the EPRI-CH and the KWU-KR FAC models for cold pH variations.

4. Incorporating Aging Effects into PRA Methodology

4.1 Introduction

As part of the feasibility demonstration to incorporate aging effects into a PRA, a case study has been identified and defined. The attributes for the mechanism of this case study are discussed in this section. Specifically, four areas of discussion that explain the selection and content of the case study are provided and they include:

- PRA model parameters and structural characteristics that might be affected by aging
- Justification for the PRA database selection
- Proposed screening methodology for selecting mechanisms and applicable SSCs
- Details on the load-capacity formulation used to obtain aging-related failure probabilities

While these four areas cover many of the areas important to the quantification of aging effects, it should be reiterated that the case study does not address all mechanisms and SSCs. Instead, the case study has been formulated to motivate a feasibility test aimed at demonstrating the practice of using a PRA to quantify and prioritize plant aging mechanisms with currently available software tools and models. It is anticipated that the case study will provide a test bed to explore aging-related issues advanced in the report *Survey and Evaluation of Aging Risk Assessment Methods and Applications* (Sanzo et al., 1994). Specifically, the four major findings of the report provide the context for the case study and the issues to be investigated. Paraphrased from NUREG/CR-6157, these four findings are:

1. Issues of aging cannot be addressed by modifying failure rates only.
2. Probabilistic aging models allow the effective use of a variety of aging information (in addition to just failure events).
3. Probabilistic aging models allow for risk management studies to be performed since the model incorporate specific aging related stressors.
4. The methodology can build upon existing PRA models.

The report by Sanzo et al. provides a critical review of existing research that incorporated aging insights or models in a probabilistic manner. Within this context, several reports have been published prior to the Sanzo report by the NRC. These reports include topics such as model

determination (Vesely, et al., 1990; Vesely 1992), data analysis (Wolford and Atwood, 1992), and utilization of PRA models for prioritization (Davis, et al., 1985).

The case study that is proposed in this report will directly address all four of findings by Sanzo et al. As a prelude to the case study definition, an overview of the case study is defined as:

> The case study starts information gathering of relevant aging mechanisms along with the selection of an appropriate, existing PRA model. After selection of the PRA model, the model is modified to include important passive (or other) components not currently in the model. In parallel with the PRA model adjustment, probabilistic aging models are utilized to determine (1) proper inputs into the PRA and (2) "links" of the aging reliability-physics models into the PRA (or PRA software) for a overall risk management framework. This framework is shown graphically below.

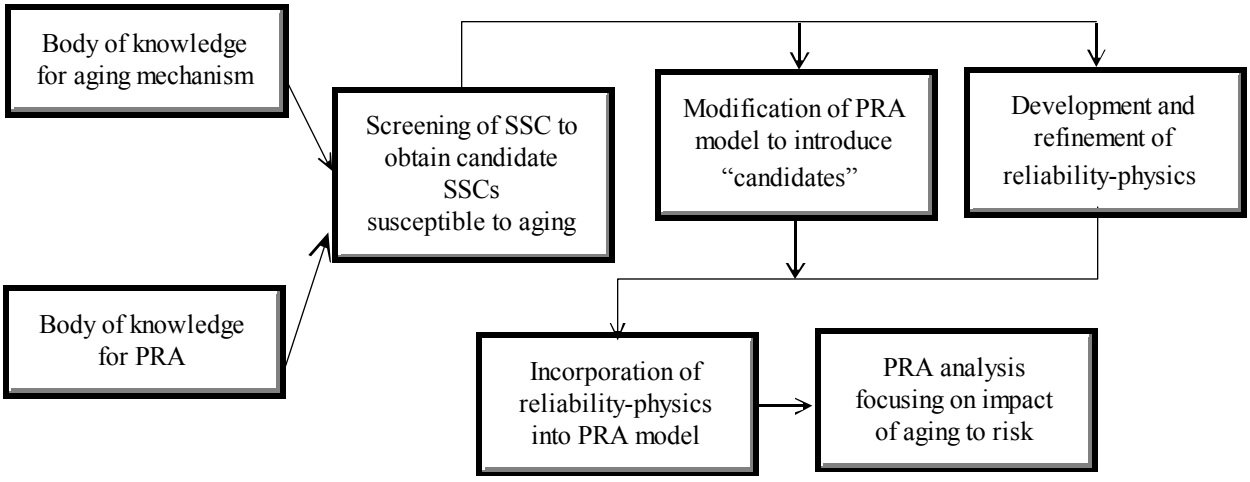

Figure 14. Illustration of the aging into PRA case study framework.

Details of the case study framework are provided in the remainder of this report.

4.2 PRA Characteristics Important to Aging Evaluations

As has been pointed out in previous studies, aging can affect the PRA model structure (e.g., sequences, success criteria) as well as model parameters (Phillips, 1993). Consequently, one must consider both effects when modeling aging impacts. This section provides a brief discussion of these aging-caused effects to the PRA model for both PRA parameters (e.g., initiator frequencies, basic event probabilities) and structural issues (e.g., success criteria within fault trees, timing on the event trees).

4.2.1 PRA Parameters

For the case study explored in this report, the failure of specific piping segments is modeled using the KWU-KR methodology. To determine the risk impact of pipe rupture, we need to determine the probability of rupture at different locations in susceptible piping. The probability of rupture can be determined using a load-capacity formulation. Ultimately, this probability will be incorporated into a PRA model. But, in general, aging mechanisms may effect a power plant in several different ways and impact more than one SSC. To account for this potential spectrum of impacts to SSCs in a risk framework, the PRA model must be modified accordingly.

As part of the framework development, we have constructed a list of applicable parts of the PRA that should be investigated for possible modifications during an aging study. The PRA parameters that may be effected due to aging impacts are listed in Table 8. For each parameter, a note is made to indicate whether or not it was necessary to model the aging-caused impact in the case study. Information is also provided for each parameter to lend insights as to why (or why not) impacts for a particular PRA parameter will be investigated. Specific issues related to each parameter are presented in the remainder of this section.

4.2.2 Structural Issues

In general, the incorporation of aging into a PRA may impact the modeling contained in the PRA (since the PRA model is only intended for "nominal" operation over a relatively short period of time, such as a year). Modeling operation of a power plant for a time period like a single year assumes that year-in, year-out that this "nominal" PRA model could be interchanged for any one year time period of operation. The incorporation of aging into the model (and hence, a time-dependent aspect) fundamentally changes the assumption of the interchangeability behind the PRA.

To account for the potential PRA modeling changes following the introduction of aging into the model, the overall structure of the PRA must be questioned. Included in the list of structural PRA issues are those identified in Table 9. For each issue, a note is made to indicate whether or not the case study modeled the aging-caused impact. Information is also provided for each issue to lend insights as to why (or why not) impacts for a particular PRA parameter should be investigated.

Table 8. Aging-caused impacts to PRA parameters.

Category	Treated in case study	Note
Initiator Frequency		
General transients	Yes	Although not generally large contributors to the core damage frequency, transients do play a part in the overall core damage model. An increase in transient frequency can lead to large increases in core damage frequency. Further, note that aging caused transients are not typically included in the PRA model.
Loss of offsite power (LOSP)	No	The aspect of trending LOSP is somewhat straightforward and, consequently, would not need to be explored in this feasibility study.
Loss of coolant accidents (LOCA)	No	Aging issues such as erosion and corrosion of primary piping may play an important role in impact to LOCA frequencies. But, the FAC analysis that was performed for the case study only impacted secondary piping.
Anticipated transients without scram (ATWS)	No	The aging impact on the reactor scram function is not clear. Since the risk increase potential (i.e., risk achievement worth) is so large for the reactor protection system, some further investigation is warranted.
Steam generator tube ruptures (SGTR)	No	Generally important from a risk perspective. Current tube rupture work may provide useable insights into aging impacts.
Internal floods	Limited review	Excluded from original scope of the analysis, but this parameter could cause significant risk impacts. Consequently, a limited case-specific analysis might be considered. For the specific piping section that was modeled for FAC, discussions were held with plant personnel as to consequential impacts from flooding.
Human Performance Probabilities		
Human error probabilities (HEPs)	No	Since organizations change over time, organizational impacts on performance could vary. Maintenance and testing practices may also change over time. But, these factors are outside the scope of the analysis and are not explored.
Recovery probabilities	No	The recovery basic event probabilities that are part of a PRA model can be affected by aging of hardware. Changes in operator performance over time and its effect on recovery actions is not quantified.

Table 8. Cont.

Category	Treated in case study	Note
Component Basic Event Probabilities		
Failure rates	Yes	As a function of a physical aging model (e.g., corrosion, fatigue, stress corrosion cracking), component failure rates can be affected. Also, the possibility of conditional aging-related failures needs to be investigated (e.g., failure given initiator, initiator given failure).
Mission times	No	The basic event mission times are determined by decay heat removal times, recovery and isolation times, arrival rates of offsite resources, etc. Aging could affect some of these parameters, but it is expected to be a secondary impact on core damage frequency. As such, this parameter is not evaluated.
Repair times and maintenance durations	No	The repair times and maintenance durations could be affected by aging. Assumed plant operational practices for repair and maintenance should be incorporated into the plant PRA model where appropriate.
Testing intervals	No	The test intervals and duration could be affected by aging. Assumed plant operational practices for testing should be incorporated into the plant PRA model where appropriate. Related to testing intervals is the positive benefit from inspections. Many aging mechanism may be managed (i.e., reduce the risk) by proper inspections. These inspections should be credited in the analysis when possible.
Common Cause Failure Modeling		
Dependent failures	Yes	It is assumed that the total failure rate for a component could be affected by aging impacts. The aging-affect on the allocation of failures (e.g., the beta, gamma, delta parameters for the Multiple Greek Letter model) is not known and is not within the scope of the analysis. Dependent failures that arise due to a common aging mechanism such as FAC are included in the study.

Table 9. Aging-caused impacts to the structure of a PRA.

Category	Treated in case study	Note
Initiating Events		
New initiators	Yes	The possibility exists to have "new" initiators become important that may have been previously excluded due to low likelihood. Examples could include pipe break or flooding scenarios that were thought to be unlikely. The quantification of the new initiating event frequencies and their subsequent inclusion into existing initiator groups is important and is addressed.
Initiator assumptions	No	Since aging could incorporate failure modes or mechanisms not previously addressed, it is important to review the existing PRA initiator assumptions. Initiators that have been grouped (e.g., transients, main steam line break) may need to be broken out.
Consequential events	Yes	Consequential events could be important given the potential for safety system degradation in conjunction with internal flooding. For example, rupture of feedwater piping may impact other important systems due to localized flooding.
Event Trees		
Sequence timing issues	No	Aging affects on batteries, seals, etc., could affect multiple basic events that rely on timing considerations (e.g., recovery actions) as part of an accident sequence.
Sequence ordering and success criteria	Yes	The accident sequence events will need to be reviewed to ensure that aging affects will not change the attributes of the sequence.
Intersystem dependencies	No	Intersystem dependencies may need to be added to the PRA model to better treat aging effect. For example, poor water chemistry control may affect multiple piping segments in more than one location.
Fault Trees		
Incorporating of passive components	Yes	The fault tree logic should be changed to represent new basic events (e.g., passive components) important to the feasibility study. Examples could include reactor vessel and piping events.
Changes to lower logic structure	Yes	Other changes to fault tree logic (e.g., change in success criteria due to heat transfer capacity or pressure capacity changes) will be made to incorporate the physical aging models that are used.

Table 9. Cont.

Category	Treated in case study	Note
Additional maintenance/testing	No	While aging of components may result in changes to maintenance and testing practices, these types of effects will not be explored as part of this feasibility study. Note that the analysis performed in this report does not credit maintenance or testing on passive components before potential failures. A larger-scope assessment should credit maintenance and testing where appropriate.
New common cause failure mechanisms	Yes	Dependent failures may be modeled as part of the fault tree adjustment to incorporate the passive components. For example, failure of a piping header may defeat redundant trains of a safety system.
Previously ignored failure mechanisms	Yes	If an ignored failure mechanism become evident during the analysis, it should be added. The feasibility study will not attempt to identify new failure mechanisms, but aging mechanisms are, in general, not accounted for in current PRA models..
Other		
Plant damage state definitions	No	The feasibility study scope of work stops at the definition of core damage.
Binning of Level 1 sequences	No	The feasibility study scope of work stops at the definition of core damage.
Treatment of non-dominant sequences	Yes	If non-dominant sequences become more important, the applicability of existing recovery rules and logic modeling will have to be evaluated.

4.3 PRA Database Selection

Modern PRAs are made up of complex logic models that have a variety of input parameters. Since the level of detail and modeling methods vary from one PRA to another, it is not easy to determine which is the "best" PRA to use for a particular analysis. Complicating the selection process is the fact that the INEEL has in-house over 20 full-scope PRAs available for use with the SAPHIRE software. Further, a single plant may have multiple, different PRA models available in SAPHIRE. For example, the Surry plant has three different SAPHIRE PRA models, the NUREG-1150 model, the utility IPE, and the Simplified Plant Analysis Risk (SPAR) model used for the Accident Sequence Precursor program. These three models vary with respect to level of modeling detail (e.g., the NUREG-1150 model has approximately 1100 basic events, the IPE has 2300 basic events, and the SRM has 150 basic events).

In order to select an appropriate model to investigate aging concerns, the measurable attributes of the PRA models could be subjectively graded to provide a relative ranking of the database merit. These attributes for the PRA models were divided into three high-level sections: (1) model ease of use, (2) model quality, and (3) representativeness to the problem. Then, after the attributes were defined, the attributes were subjectively evaluated for the available PRA models.

Since the judgement scheme was based upon an incomplete and subjective information, additional investigation into additional criteria and decision-making inputs to the weighting process may be justified. Nonetheless, since the model selection process can not be perfected, and no single, flawless PRA model exists, scrutinizing the models that were judged to be "the best" will help in the final decision-making process. Three PRA models were identified as the "best" for the feasibility study documented in this report. These three models were: Peach Bottom 1150, River Bend, and Surry IPE. It was decided that the Surry IPE model will be most appropriate for this project.

Peach Bottom 1150 — The Peach Bottom 2 and 3 plants have a lengthy operating history at 23 years each. The General Electric design is a BWR 4 type with a rated electrical output of 1080 MWe. The containment type is Mark I (62 psig design pressure). The design of Peach Bottom is typical of newer BWR plants that have a reactor core isolation cooling system. The NUREG-1150 model was completed almost 8 years ago and probably does not reflect the current configuration of the plant. While the original NUREG-1150 analysis ignored the non-dominant accident sequences, these sequences have been added (including appropriate recovery modeling) to the SAPHIRE Peach Bottom NUREG-1150 database. Even with the additional non-dominant accident sequences, the PRA model analysis takes about 10 to 15 minutes for a single evaluation. But, since many of the aging related mechanisms that have been previously explored by the INEEL center around PWRs, and since BWRs represents a minority of the plants of interest, the Peach Bottom 1150 model was precluded from potential use in the project.

River Bend — The River Bend plant has a moderate length of operating history at 11 years. The General Electric design is a BWR 6 type with a rated electrical output of 936 Mwe. The containment type is Mark III. The design of River Bend is typical of new BWR plants that have reactor core isolation cooling and high pressure core spray systems. The IPE model is from results dated 1993 and, consequently, represent the configuration of the plant six years ago. This model contains non-dominant sequences. Again, since many of the aging related mechanisms that have been previously explored by the INEEL center around PWRs, and since BWRs represents a minority of the plants of interest, the River Bend IPE model was precluded from potential use in the project.

Surry IPE — The Surry IPE generally reflects the current plant configuration with the last update to the model from 1994. The model allows all accident sequences to be quantified, including the non-dominant sequences. The model quantification time is short (less than one minute, including the application of recovery actions) which would allow for multiple analyses to be run in a short time if necessary.

The point estimate for the core damage frequency (CDF) reported in the Surry PRA for internally generated events is 7.4E-5/yr. The CDF associated with the updated station model (1994 results) is 7.2E-5/yr, which is based on 48 sequences that are above a truncation level of 1E-7/yr. The total core damage frequency for all sequences above a truncation level of 1E-10/yr is 7.3E-5/yr. This frequency is in good agreement with the PRA results. Also, it shows that the contribution from sequences less that 1.0E-7/yr is not significant to the nominal core damage frequency results.

For the majority of the PRA analysis discussed in this report, the truncation level that was used with the Surry model was set at 1E-10/yr. The only exception to this rule was for the screening step using the PRA importance measures. For the generation of importance measures, a truncation level of 1E-13/yr was used in order to provide adequate assurance that all applicable basic events would appear in the overall importance measure list.

4.4 Criteria for Selecting SSCs and Aging Mechanisms

4.4.1 Background

Various methodologies exist for prioritizing components according to particular issues of interest. Examples of such methodologies include activities for inservice inspection and testing and the NRC Maintenance Rule. Other aging-related activities have investigated mechanisms and impacts of aging failures for specific types of components. In addition, research has gone into assessing the probabilities of aging-caused failures. This section discusses some of the previous work and presents the criteria to be used for selecting SSCs and aging mechanisms for the case study.

ASME/NEI The ASME Research Task Force on Risk Based Inservice Testing (IST) along with the Nuclear Energy Institute (NEI) have recognized that current regulation and testing schemes (e.g., ASME Codes) treat components with equal safety significance. ASME and NEI further realize that a risk-informed approach will reduce the testing burden while maintaining the current level of safety. To achieve these goals, ASME and NEI propose a risk-informed IST program that includes:

- Determination of quantitative component risk — This step entails using the plant-specific PRA to categorize components based upon the Fussell-Vesely (FV) and risk achievement worth (RAW) importance measures. The threshold for classifying a component as belonging to the high safety significance category are FV $\geq$ 0.005 or RAW $\geq$ 2.

- Categorization of qualitative and quantitative component safety — This step blends probabilistic analysis with deterministic evaluations and operational experience via an expert panel process (e.g., mixing the quantitative analysis with qualitative insights).

- Test strategy formulation — This step identifies the type of tests and frequency of tests for components in the two safety categories.

- Reevaluation of aggregate risk — This step is used to reevaluate the change in risk due to the revised testing schemes and intervals.

- Implementing the testing program — This step implements the revised tests.

PLG PLG has investigated the prospect of using Bayesian analysis to estimate age-related changes in failure rates (Bier et al., 1990). While the work originally was intended to be an evaluation of aging data, the data collected did not show evidence of aging. Consequently, the work that was documented was a demonstration of one application of Bayesian analysis for aging data. Unfortunately, the work did not attempt to link aging mechanisms with changes in failure rates or probabilities, nor did it demonstrate how Bayesian aging failure rates would be used in a PRA framework.

INEEL Various programs have been conducted at the INEEL concerning aging related analysis. The majority of the aging work performed by the analysts at INEEL addressed the mechanisms of aging and related failures for specific types of SSCs. Examples of these aging mechanism and component evaluations include: safety class transformers (Roberts, Edson, and Udy, 1996), Advanced Test Reactor components (Dwight, 1990), metal containments (Shah, Smith, Sinha, 1994), class 1E batteries (Edson and Hardin, 1987, Edson, 1990), and high pressure injection systems (Meyer, 1989). While the focus of these studies has been on mechanisms of aging rather than how to incorporate aging effects into a PRA, the results obtained from these analyses provide insights into different facets of the aging issue.

NRC The U. S. NRC has had an extensive program evaluating the risks and mechanisms of aging since the early 1980s, notably through the Nuclear Plant Aging Research (NPAR) program. Numerous facets of plant aging have been investigated and are summarized in the annual NUREG-1377 reports entitled "NRC Research Program on Plant Aging: Listing and Summaries of Reports Issued Through *date*," where the "date" is the date of the last summary report.

Within the context of the NPAR program, fourteen subject areas have been defined that classify the aging investigation work. These areas include:

1. Aging, including plans, surveys, analyses, methods, and models.
2. Diesel generators and related systems
3. Electrical power systems, including cables, trays, connectors, circuit breakers, relays, switches, penetrations, and related components
4. Electrical equipment, including transformers, motors, batteries, chargers, and invertors
5. Instrumentation, measurement, and control systems
6. Maintenance
7. Major components: reactor vessels, reactor coolant pumps, steam generators, pressurizers, and structures (including basemat and containment)
8. Monitoring
9. Operating experience, field results, and related data
10. Piping, including valves, seals, supports, snubbers, and related components
11. Resources from within existing PRAs

12. Safety and protection systems (including injection systems) and their components
13. Seismic effects and aging
14. Service water, auxiliary feedwater, instrument air, and other fluid systems, including their pumps, heat exchangers, and related components; balance of plant systems and components

For the reporting year 1992, a total of 123 aging-related reports were published that fit one of the above categories. The majority of the work performed to that date (July 1992) fell under one of the 14 categories with the exception of category 11, PRA. Out of the 123 reports, only three pertained to the topic of aging and PRA. This finding follows that of work performed by other organizations. The impact of aging has been investigated and documented for a number of specific plant systems or types of mechanisms. Unfortunately, the translation of these aging impacts into SSC failure probabilities has not been investigated as throughly. Consequently, the resulting change in risk or core damage frequency due to aging impacts has not been addressed. Further work (e.g., the analysis documented in this report) will help to refine the PRA aspect of aging concerns.

Westinghouse Owners Group The Westinghouse Owners Group has developed guidance for risk-informed applications such as piping inservice inspection. In these applications, the PRA is used to assist in the "engineering" portion of the analysis. Specifically, piping segments are defined and are related to a failure probability from expert judgement and deterministic calculations. Actual modeling of piping segments is allowed via one of two methods: (1) the introduction of new events into system fault tree models or (2) simulated events using already-modeled components (e.g., surrogate components). Details of the Westinghouse methodology can be found in WCAP-14572.

4.4.2 Aging-Based Screening of SSCs

The screening of SSCs for an aging-based analysis must be performed in two steps. First, a screening should be performed based upon the *aging mechanism* that may be applicable or of interest. This screening should focus on the particular physics of the aging mechanism (e.g., FAC is not a concern for primary piping in PWRs), the likelihood of aging-caused failure over the time period of interest, and the potential risk significance of the failure. The general process and insights useful to perform this first level of screening was discussed in Section 2 of this report, particularly in the areas discussing actual aging-related impacts (e.g., Section 2.3).

The second level of screening is then based upon risk insights provided via a probabilistic risk model. Specifically, a method is demonstrated that relies on component importance measures. Note that, since most of the passive components of interest are not included in a standard PRA model, one must extrapolate from the components/systems that are included to related passive components. Also, the general "robustness" issues related to the use of importance measures are still applicable to the our screening methodology (Cheok 1998). But, since the methodology utilized in

this report only relies on importance measures to provide a "go/no-go" answer to the question on screening, it is believed that general importance measure limitations are not critical.

In general then, one could perform the screening analysis using the aging mechanisms or the PRA (via component events) or a combination of the two.

To start the selection of potential aging-important SSCs, cut sets for the Surry IPE model were generated using a truncation level of 1E-13/yr. From these cut sets, the basic event importance measures [including Fussell-Vesely (F-V) and the risk increase ratio (RIR, also known as risk achievement worth, or RAW)] were calculated. These importance measures were then evaluated to obtain a *single* ranked list of events using the Smith Weighted Importance Measure (SWIM) index. The SWIM index is a "summary" type of importance measure that allows an analyst to combine information from the F-V list of events with the RIR list of events (with a user selected weighting factor) in order to work with a single, ranked list of basic events. Advantages to using the SWIM index over separate lists of measures are (1) the results are contained in a single list rather than two (or more) importance measure lists, (2) events are ranked against each other even for cases where one event has a high F-V (and low RIR) while another event has a high RIR (and low F-V), and (3) the analyst can weight one result characteristic over another (e.g., RIR is more important than F-V so weight the RIR measures higher). Item (1) above, pertaining to the use of a single list, is relevant to minimizing analysis time when dealing with multiple "what if" scenarios or when managing lists of traditional importance measures containing hundreds of events (as we did in this analysis).

To obtain the SWIM index, the two traditional (i.e., F-V and RIR) measures to be "weighted" are initially redefined by the equations:

$$W_{FV} = I_{FV}$$
$$W_{RIR} = 1 - \frac{1}{I_{RIR}} \tag{8}$$

where I_{FV} = the F-V importance measure for the i'th event
I_{RIR} = the RIR importance measure for the i'th event

Since the RIR measure value lies between one and infinity, the W_{RIR} will fall between zero and one, just like the F-V measure (and, consequently, the W_{FV} measure). But, the scale for the W_{RIR} measure needs to be adjusted so that the risk importance threshold (e.g., F-V > 0.005 or RIR > 2 indicating a risk significant event) will correspond to the same numeric value as the W_{FV} measure. Consequently, we will need to solve the RIR weighted equation at the F-V threshold, or:

$$W_{RIR}^{x} = \left(1 - \frac{1}{2}\right)^{x} = 0.005 \tag{9}$$

Solving this equation for the "x" power yields a value of 7.64. Thus, to scale the two weighted measures to the same risk threshold (based upon the widely used F-V threshold of 0.005 and RIR of 2), we need to use the equation:

$$W_{RIR} = \left(1 - \frac{1}{I_{RIR}}\right)^{7.64} \tag{10}$$

Then, the SWIM index is defined as:

$$SWIM = \left(W_{FV}\right)^{\omega_{FV}} + \left(W_{RIR}\right)^{\omega_{RIR}} \tag{11}$$

where ω_{FV} = the weighting factor for the F-V measure
ω_{RIR} = the weighting factor for the RIR measure

The default weighting factors have a value of one. If an analyst wanted to emphasize the RIR measure over the F-V, the ω factors would need to be adjusted accordingly. The analysis performed for this report left the weighting factors at their default values of one, since the intent is only to find which events are *above* a specified risk threshold. Again, the thresholds that define an event as being important are either that F-V > 0.005 or the RIR > 2.

Since the scaled risk threshold in the SWIM derivation was chosen to be 0.005, any event with a SWIM value of 0.005 or larger can be considered to be risk significant. This value implies that the event has to be above the risk threshold based upon *only one of the two* importance measures. If an event has a SWIM greater than 0.005, the event would pass the risk-based part of the screening. But, the SWIM list still would be evaluated for those events (and their related "passive" components) with respect to applicable aging mechanisms.

The partial results of the importance measure analysis are shown in Table 10. The complete results, all events that were considered to be risk significant, are shown in Appendix D. The events shown in Table 10 represent a single sorted list of basic events from the nominal Surry IPE model sorted based upon the SWIM index. Only those events that could be considered risk significant (i.e., F-V > 0.005 or RIR > 2) are included in the table. Along with the basic event name, an event description is shown along with the event's nominal probability.

In Table 10, the events that are labeled as "n/a" are presumed (for this study) to not be affected by aging or are completely outside the current scope of the analysis demonstration. Note that for a full scope analysis, many of these excluded events may be included in the study. For those excluded events, the complete list (as shown in Appendix D) includes events such as: operator errors (e.g., 1RSHEP-SFLNG-PT6), maintenance activities (e.g., 1EEBUS-UM-1H), recovery actions (e.g., HEP-1ECA3:2), success/complemented events (e.g., C-LT02), plugging events

Table 10. Basic event importance measure results and their applicability to the aging analysis for the Surry IPE PRA model (sorted by the SWIM index) for events with F-V > 0.005 or RIR > 2.

Event	Probability	F-V	RIR	SWIM	Applicability	Event Description
IE-T8	5.9E-04	2.2E-01	3.8E+02	1.200		LOSS OF SWITCHGEAR ROOM COOLING
1FWCKV-CC-275889	6.3E-05	5.3E-02	8.4E+02	1.044		CCF 3/3 FL CHECK VALVES 1FW27
IE-VX	1.6E-06	2.1E-02	1.3E+04	1.021		INTERFACING LOCA
IE-T4	5.0E-06	1.0E-02	2.0E+03	1.006		LOSS OF RCP COOL/INJECT
IE-A	5.0E-04	6.3E-02	1.3E+02	1.005		LARGE LOCA
IE-RX	2.7E-07	3.6E-03	1.4E+04	1.003		VESSEL RUPTURE
1RPBKR-CC-RTARTB	1.3E-05	1.1E-02	8.1E+02	1.001	n/a	Common-cause failure 2/2 REACTOR TRIP BREAKERS
1RSHEP-SFLNG-PT6	8.0E-05	2.5E-02	3.1E+02	1.000	n/a	TEST FLANGES LEFT BLANKED AFTER 1-PT-17.6
1SICKV-CC-798285	6.3E-05	2.1E-02	3.2E+02	0.997		CCF 3/3 CHECK VALVES S1-79
1CSMV--PG-1CS25	4.5E-05	1.5E-02	3.4E+02	0.993	n/a	N.O. VALVE CS-25 PLUGGED IN STANDBY
1SIMOV-CC-867842	2.5E-04	4.2E-02	1.5E+02	0.992		CCF 3/3 FC OF CL HH DISCH MOVS 1867C
1RPROD-LF-CRODS	1.8E-06	1.4E-03	7.9E+02	0.992		Control rods fail to insert due to MECHANICAL BINDING
IE-S1	1.0E-03	7.1E-02	7.2E+01	0.971		MEDIUM LOCA
1SICKV-CC-224225	6.3E-05	1.1E-02	1.5E+02	0.961		CCF 2/2 FC OF CHECK VALVES SI225 AND SI224
1EEBUS-LU-1H	1.2E-05	1.6E-03	1.3E+02	0.945	n/a	4160v Bus Bar 1H Loss of Function 1-EE-BUS-1H
1EEBUS-UM-1H	7.3E-06	9.4E-04	1.3E+02	0.944	n/a	BUS BAR UNSCHEDULED MAINTENANCE
1EEBUS-LU-1H-1	1.2E-05	1.4E-03	1.2E+02	0.938	n/a	480v Bus 1H-1 Loss Of Function 1-EE-BUS-1H-1
1EEBUS-LU-1H-480	1.2E-05	1.4E-03	1.2E+02	0.938	n/a	Bus Bar Loss of Function 1-EE-BUS-1H
1EEBUS-UM-1H-1	7.3E-06	8.4E-04	1.2E+02	0.937	n/a	BUS BAR UNSCHEDULED MAINTENANCE
1EEBKR-SO-14H15	3.4E-05	3.3E-03	1.0E+02	0.929	n/a	Breaker 14H15 Spuriously Opens 1-EE-BKR-14H15
1EEBKR-SO-15H7	3.4E-05	3.3E-03	1.0E+02	0.929	n/a	Breaker 15H7 Spuriously Opens 1-EE-BKR-15H7
1EETFM-LP-1H1	1.9E-05	1.9E-03	1.0E+02	0.928	n/a	Transformers Fails To Supply Power 1-EE-TX-1H1
1EEBKR-SO-14H14	3.4E-05	2.5E-03	7.7E+01	0.907	n/a	Breaker 14H14 Spuriously Opens 1-EE-BKR-14H14
1EEBUS-LU-1H1-1	1.2E-05	9.2E-04	7.7E+01	0.906	n/a	480v MCC 1H1-1 Loss of Function 1-EE-BUS-1H1-1
1EEBUS-UM-1H1-1	7.3E-06	5.4E-04	7.6E+01	0.904	n/a	480V MCC 1H1-1 unavailable DUE TO MAINTENANCE
1EGEDG-CC-123	7.5E-05	4.9E-03	6.6E+01	0.895	n/a	COMMON CAUSE FAILURE OF EDG #1/2/3
1EGEDG-CC-13	1.1E-04	6.4E-03	5.7E+01	0.880	n/a	COMMON CAUSE FAILURE OF EDG #1 AND EDG #3
1SICKV-FC-1SI25	6.3E-04	2.7E-02	4.4E+01	0.867		CHECK VALVE 1-SI-25 FAILS TO OPEN
1SICKV-FC-1SI410	6.3E-04	2.7E-02	4.4E+01	0.867		CHECK VALVE 1-SI-410 FAILS TO OPEN
1RSMOV-CC-104AD	2.5E-04	1.2E-02	4.9E+01	0.867		CCF 4/4 FC OF INLET ISO VALVES 1-SW-MOV-104A/D
1RSMOV-CC-105AD	2.5E-04	1.2E-02	4.9E+01	0.867		CCF 4/4 FC OF OUT ISO VALVES 1-SW-MOV-105A/D
1EE-LOOP-24	2.1E-04	1.0E-02	4.9E+01	0.864	n/a	Loss of offsite power within 24 HRS OF REACTOR TRIP
1SIMV--PG-1SI24	5.5E-04	2.4E-02	4.4E+01	0.863	n/a	MANUAL VALVE 1-SI-24 PLUGGED IN STANDBY
1EGEDG-CC-12	1.1E-04	5.2E-03	4.6E+01	0.851	n/a	COMMON CAUSE FAILURE OF EDG #1 AND EDG #2
1SIMOV-CC-1115BD	2.5E-04	1.1E-02	4.4E+01	0.850		CCF 2/2 FC OF LCV 1115B AND LCV 1115D TO OPEN
1SIMOV-CC-1115CE	2.5E-04	1.1E-02	4.4E+01	0.850		CCF 2/2 FO OF LCV-1115C AND 1115E TO CLOSE
1SWCKV-PG-1SW130	3.0E-06	1.4E-04	4.8E+01	0.850	n/a	CHECK VALVE 1-SW-130 PLUGS DURING MISSION
1CESTR-CC-SUMPPG	5.0E-05	2.0E-03	4.2E+01	0.834		COMMON CAUSE BLOCKAGE OF CONTAINMENT SUMP
1EEBUS-LU-1J-480	1.2E-05	5.0E-04	4.2E+01	0.833	n/a	Bus Bar 1J 480v Loss of Function 1-EE-BUS-1J
1EEBUS-LU-1J-1	1.2E-05	5.0E-04	4.2E+01	0.833	n/a	480v Bus 1J-1 Loss of Function 1-EE-BUS-1J-1
1EEBUS-LU-1J	1.2E-05	5.0E-04	4.2E+01	0.833	n/a	4160v Bus Bar 1J Loss of Function 1-EE-BUS-1J
1EEBUS-UM-1J-1	7.3E-06	2.9E-04	4.1E+01	0.829	n/a	BUS BAR UNSCHEDULED MAINTENANCE
1EEBUS-UM-1J	7.3E-06	2.9E-04	4.1E+01	0.829	n/a	BUS BAR UNSCHEDULED MAINTENANCE

Table 11. Basic events that passed the "risk significance" screening with their aging influencing factors (sorted by the SWIM index) for events with F-V > 0.005 or RIR > 2.

Event	Probability	SWIM	Embrittlement	Fatigue	Stress	Corrosion	Event Description
1FWCKV-CC-275889	6.3E-05	1.044		3	1/2/4		CCF 3/3 FL CHECK VALVES 1FW27
IE-VX	1.6E-06	1.021	7	3/6	5		INTERFACING LOCA
IE-T4	5.0E-06	1.006	7			3	LOSS OF RCP COOL/INJECT
IE-A	5.0E-04	1.005	7	3/6	5		LARGE LOCA
IE-RX	2.7E-07	1.003	4	6	6	5	VESSEL RUPTURE
IE-S1	1.0E-03	0.971	7	3/6	5		MEDIUM LOCA
1FWCKV-LEAKAGE	1.0E-04	0.724		3	1/2/4		UNDETECTED LKG THRU CKVS 27
1FWCKV-CC-131136	6.3E-05	0.723		3	1/2/4		CCF 2/2 FC CHECK VALVES 1FW131
1FWCKV-CC-425772	6.3E-05	0.717		3	1/2/4		CCF 3/3 FC CHECK VALVES 1FW142
1FWMOV-SO-24H60B	1.2E-05	0.712		3	1/2/4		Motor operated valve transfers open - 24 H1-FW-MOV-260B
1FWMOV-SO-24H60A	1.2E-05	0.712		3	1/2/4		Motor operated valve transfers open- 24 H1-FW-MOV-260A
IE-S2	2.1E-02	0.609	7	3/6	5		SMALL LOCA
IE-T7	1.6E-02	0.529	5	1/5	1/3/5	1/3/5	STEAM GENERATOR TUBE RUPTURE
1FWPSB-CC-MDP3AB	7.0E-04	0.153		3	1/2/4		CCF 2/2 FS MDP - COMMON CAUSE FAILURE
1FWCKV-FC-1FW273	6.3E-04	0.143		3	1/2/4		CHECK VALVE FAILS TO OPEN 1-FW-273
1FWCKV-FC-1FW272	6.3E-04	0.143		3	1/2/4		CHECK VALVE FAILS TO OPEN 1-FW-272
2FWMOV-CC-160AB	2.5E-04	0.141		3	1/2/4		CCF 2/2 FC CCF FTO 2-FW-MOV-160A/B
1FWPSB-FR-24HP3A	7.9E-04	0.127		3	1/2/4		MD PUMP -STNDBY SYS FAILS TO RUN - 24 HR1-FW-P-3A
1FWCKV-FC-1FW157	6.3E-04	0.122		3	1/2/4		CHECK VALVE FAILS TO OPEN 1-FW-157
1FWCKV-FO-1FW172	3.4E-03	0.062		3	1/2/4		CHECK VALVE FAILS TO CLOSE 1-FW-172
1FWCKV-FO-1FW157	3.4E-03	0.039		3	1/2/4		CHECK VALVE FAILS TO CLOSE 1-FW-157
2FWTRB-FR-24HP2	1.1E-01	0.032		3	1/2/4		TURBINE DRIVEN PUMP FAILS TO RUN - 24 HR 2-FW-P-2
1FWTRB-FS-1FWP2	2.5E-02	0.024		3	1/2/4		TURBINE DRIVEN PUMP FAILS TO START 1-FW-P-2
1FWTRB-FR-24HP2	1.1E-01	0.022		3	1/2/4		TURBINE DRIVEN PUMP FAILS TO RUN - 24HR1-FW-P-2
1FWTRB-FR-12HP2	5.7E-02	0.022		3	1/2/4		TURBINE DRIVEN PUMP FAILS TO RUN - 12HR1-FW-P-2
IE-TS1	4.4E-06	0.010				1	STEAM BREAK IN CONTAINMENT
2FWTRB-FS-2FWP2	2.5E-02	0.010		3	1/2/4		TURBINE DRIVEN PUMP FAILS TO START 2-FW-P-2
IE-T2A	6.5E-01	0.009		3	1/2		RECOVERABLE LOSS OF MFW
1FWPSB-FS-1FWP3A	7.0E-03	0.009		3	1/2/4		MD PUMP -STNDBY SYS FAILS TO START 1-FW-P-3A
1FWCKV-FC-1FW58	6.3E-04	0.008		3	1/2/4		CHECK VALVE FAILS TO OPEN 1-FW-58
1FWCKV-FC-1FW89	6.3E-04	0.008		3	1/2/4		CHECK VALVE FAILS TO OPEN 1-FW-89
1FWCKV-FO-1FW142	3.4E-03	0.008		3	1/2/4		CHECK VALVE FAILS TO CLOSE 1-FW-142
1FWCKV-FC-1FW27	6.3E-04	0.008		3	1/2/4		CHECK VALVE FAILS TO OPEN 1-FW-27
IE-T2	1.5E-01	0.007		3	1/2		LOSS OF MFW
1FWPSB-U2-SBOQS	8.0E-02	0.005		3	1/2/4		U2 IN SBO WITH A STUCK OPEN SG RV

Note: The following seven levels are used to denote the potential aging-related damage indicated in the embrittlement, fatigue, stress, and corrosion columns.

1. Mechanism has caused rupture in the field.

2. Mechanism has caused significant wall thinning or cracking and has a potential to cause single or multiple ruptures (common-mode failures) during 60 years of operation.

3. Mechanism has caused leakage in the field.

4. Mechanism has caused significant damage to material properties and has a potential to cause rupture during 60 years of operation.

5. Mechanism has caused cracking, wastage, or localized wall thinning and has a potential to cause through-wall cracking and leakage during 60 years of operation.

6. Mechanism has significantly reduced material resistance to fatigue and SCC and has a potential to initiate cracking and then cause through-wall cracking.

7. Mechanism has no potential to cause cracking or rupture during 60 years of operation.

(e.g., 1SIMV--PG-1SI24), and electrical systems (e.g., 1RPBKR-CC-RTARTB). Events that are left blank under the "applicability" column could be candidates for further aging-related investigations. Notice that passive piping components are *not* included in the events shown in Table 10 (and Table D-1 in Appendix D). These events do not currently exist within the Surry model. After these event are incorporated into the PRA model, they could be sorted and evaluated based upon their individual risk significance if so desired.

The events shown in Table 10 represent (primarily) active components. For these events, potential aging mechanism needs to be identified in order to associate a physics-based reliability model to the particular basic event. It may be possible that some of these events could be susceptible to corrosion, fatigue, or wear mechanisms. Table 11 shows the type of aging related "influencing factors" (i.e., those mechanisms that have or could cause failures) for the components that passed the "risk significance" PRA screening level. Note that no passive components appear in the list. These components will be added to the PRA as needed and will be evaluated based upon the aging mechanisms identified in Section 2.

The events shown in Table 10 should be utilized to provide the analyst a mechanism of where to focus the modeling efforts for passive components. The analyst should consider incorporating passive components associated to the active components where the active component has a high SWIM index value. For those events with low SWIM index values, the implication is that the component is not risk-significant. Consequently, any associated passive components would also be

considered to be not risk-significant. But, this knowledge of the lack of risk-significance should be tempered with two facts.

- The importance measures that are utilized in this demonstration and most current PRA analyses focus on a limited risk measure, namely the core damage frequency. Consequently, components (especially passive) that may be important to containment response or consequence reduction are not guaranteed to be important to core damage frequency.

- Consequential and spacial effects from both active and passive components may turn out to be important from a core damage frequency perspective, but many of these types of interactions are not modeled in the nominal PRA. Knowledge of the plant systems and potential interactions after failure will be required to make a judgement for SSCs that fall into this second category.

In addition to the metrics already identified, other so-called "risk-informed" PRA importance measures could be utilized where appropriate. These measures include the "combination importance measure" and the "cumulative risk contribution." While some of these measures have been incorporated into version 6.x of the SAPHIRE software, we do not address their use in this report.

Lastly, one other issue related to the screening of aging mechanisms is that of the effectiveness for existing programs to control aging. Included in these programs are activities such as inspection (both by the utility and the regulator), component replacement (or repair), and engineering analyses. For example, if a certain pipe section were regularly inspected, and if the inspection program was very effective, the probability of experiencing a failure due to FAC of this pipe section may be negligible. But, to model the inspection probabilistically (e.g., in a PRA), one would want to have the effectiveness defined in terms of a basic event probability. Further, for the analyses performed and described in this report, we do not credit any inspection or analysis programs. Other "non-demonstration" type of evaluations should consider the incorporation of relevant, formal programs that could reduce the probability of component failure.

4.5 Development of Load-Capacity FAC Model

4.5.1 General Load-Capacity Formulation for FAC

To obtain the probability that a pipe segment subject to FAC will rupture, the wall thinning must be used to determine the remaining pressure capacity. This pressure capacity would then be "balanced" against the pressure loading that the pipe segment would see over the course of operation. This type of "load versus capacity" evaluation is prevalent in the reliability literature and falls under various names such as load-capacity, probabilistic factor of safety, or stress-strength (Modarres, 1993; Ang and Tang, 1975).

Using the pressure-based approach in the classical analysis involving system strength or capacity, the pressure capacity is P_C (in our case, the system maximum allowable pressure is a function of time due to the thickness of the pipe that has been eroded away). The stress or load is P_L [i.e., either (1) a static load from the system operation pressure at the full power or steady state operation condition or (2) dynamic load from the changed system pressure which is a function of time in the transient condition]. The probability of failure of the applicable piping can be computed from

$$P_f(t) = P\left[\psi_C(t) < \psi_L(t)\right] = 1 - \int_0^\infty F_L(x,t)\, f_C(x,t)\, dx = \int_0^\infty \left(\int_x^\infty f_L(y,t)\, dy \right) f_C(x,t)\, dx \tag{12}$$

where

$P_f(t)$	=	pipe failure probability,
$\psi_C(t)$	=	representative function of the capacity,
$\psi_L(t)$	=	representative function of the load,
$F_L(x, t)$	=	the load cumulative distribution function,
$f_C(x, t)$	=	the capacity probability density function (ksi^{-1}),
$f_L(y, t)$	=	the load probability density function (ksi^{-1}),
t	=	operational time (hr),
x	=	capacity pressure (ksi),
y	=	load pressure (ksi).

A representative plot of $f_L(y, t)$ and $f_C(x, t)$ is shown below in Figure 15.

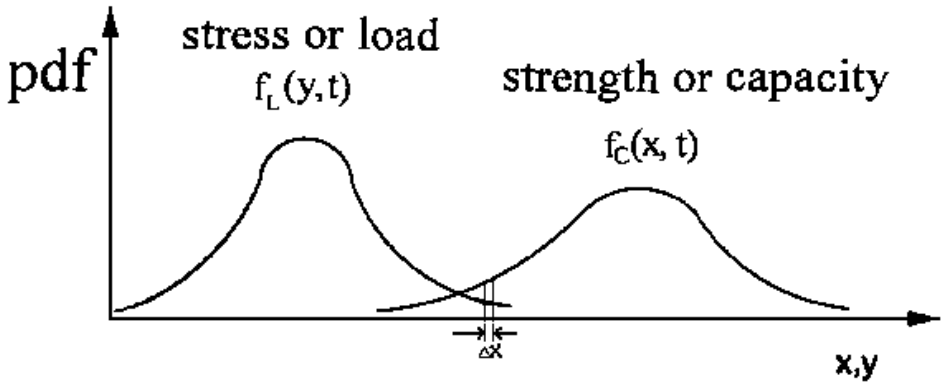

Figure 15. Illustration of a load-capacity probability calculation.

Equation 12 is based on the simple observation that failure occurs when the load exceeds the capacity. The capacity probability density function, $f_C(x, t)$ can be determined from the remaining pipe wall thickness, $W_{pipe}(t)$, as defined in Equ. (4). The KWU model for the corroded wall thickness, $W_{C,calculated}(t)$, has already been defined in Equ. (3). The pipe pressure capacity evaluation would then incorporate the thinning wall (which is a function of time) to determine the expected pressure capacity. To perform this evaluation, we made the assumption that the wall thinning is uniform around the circumference. Then, the failure pressure as a function of time can be calculated from the following equation given by Wesley et al. (1990).

$$ps_f = \frac{\sigma_f \cdot W_{pipe}(t)}{\left[r + W_{C,calculated}(t)\right]\left(1 + 0.25\,\epsilon_f\right)} \qquad (13)$$

where

ps_f (t)	=	pressure capacity (at time t) that will result in pipe failure (ksi),
σ_f	=	failure stress (ksi),
$W_{pipe}(t)$	=	pipe wall thickness at time t (cm),
r	=	initial inside radius (cm)
$W_{C,calculated}(t)$	=	calculated thickness of pipe corroded away at time t (cm) [Equ. (3)]
ϵ_f	=	median hoop strain at failure (failure strain).

The above equation defines the failure pressure for a straight pipe in terms of hoop stress and includes some provision for the biaxial stress-state in pipe wall and strain concentration effects. Failure stress and hoop strain at failure are determined from 51-mm (2-in.) uniaxial tensile test specimens. Both the

failure stress and strain should be treated as random quantities because of variability in the stress-strain relationship, uncertainty related to biaxial stress condition, necking, and effective gage length. Mean values for failure stress, σ_f, and failure strain, ϵ_f, for SA 516 grade 70 carbon steel are shown below in Table 70 carbon steel are shown below in Table 12 (Wesley et al. 1990). Although the above equation is for a straight pipe, we have assumed that it is applicable to pipe fittings such as elbows.

Table 12. Typical stress and hoop strain parameter values for SA 516 grade 70 carbon steel.

Temperature (°F)	Failure stress (σ_f), ksi	Hoop strain (ϵ_f), %
77	75.6	6.2
400	78.3	3.7
600	76.5	5.8
800	63.9	7.9

The failure pressure, ps_f, is the pressure that would cause pipe rupture. Thus, in the capacity-load framework (page 68), the calculated failure pressure is the "capacity" of interest, or

$$ps_f(t) = x \tag{14}$$

and represents the capability of a pipe wall to withstand an internal pipe pressure. This capability is given by the deterministic calculation of Equ. (13). Consequently, for a known model of the world [e.g., the calculation for $W_{C,calculated}(t)$] and known capacity parameter values (e.g., σ_f, ϵ_f), the capacity pressure resistance (in ksi) can be estimated. This pressure could then be compared to the expected internal piping pressure to determine a pipe failure probability. Additional details of the capacity development are provided in Section 4.5.2.

The load distribution, $f_L(y, t)$, represents the actual and anticipated pressures for a particular section of piping. Normally, the majority of this distribution will be at the nominal system operational pressure. For example, if nominal system pressure operation is approximately 900 psig and is experienced 95% of the time during operation, the load distribution would have 95% of the distribution centered on or around 900 psig. Transient pressures that cause system pressure to exceed nominal pressures would need to be incorporate into the load distribution. But, transient pressures are represented by an *aleatory* type of model. Incorporating these pressures would entail determining the anticipated pressures and likelihood of experiencing such a pressure as a function of time. A hypothetical steady-state load distribution may then look similar to the curve shown in Figure 16. Alternatively, the load distribution could be discretized into a discrete distribution where, during the load-capacity calculation, the load values would be sampled from one of the discrete points.

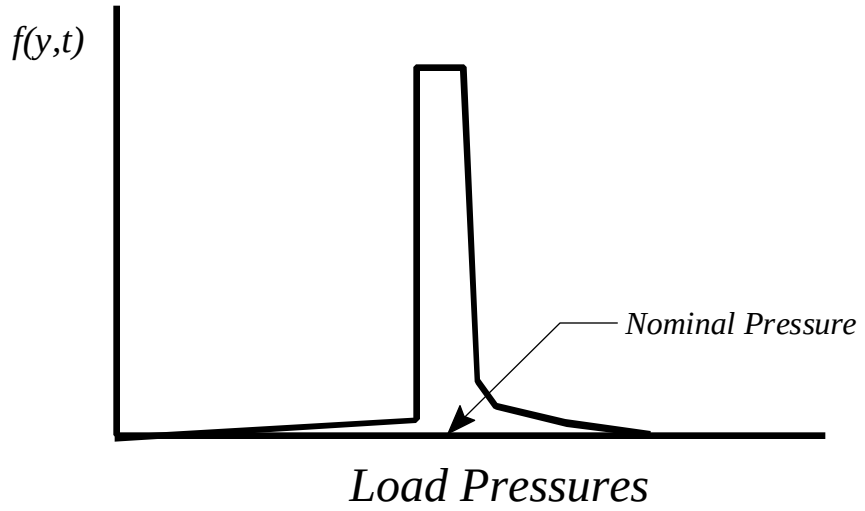

Figure 16. Example of a potential load distribution curve for nominal, steady-state pressures.

Once both the load and capacity distributions are known, two options are available to estimate failure probabilities. First, the density functions for the distributions could be utilized to obtain an analytic expression for the pipe reliability as a function of time. This approached was used by Kao in his work on FAC (Kao, 1998). A second approach is to utilize a Monte Carlo simulation routine to determine the fraction of time that the load pressure is larger than the capacity pressure. This fraction then directly represents the failure probability of the pipe due to FAC. Both techniques were utilized for the work discussed for this project.

The second approach mentioned above was incorporated into the NRC's SAPHIRE risk assessment code via the "compound" event type.† Consequently, the parameters that are contained in the capacity-load calculations (e.g., time, flow rate, pressure loads, pH) will be accessible directly in the PRA model. These parameters then potentially have a direct impact on the overall plant core damage frequency. Appendix E contains the source code utilized in the SAPHIRE compound event for calculation of the FAC rate, the capacity pressure, and the load-capacity failure probability.

At this point in the discussion, an overview of the complete load-capacity model formulation from the perspective of the types of models and associated uncertainties is provided.

† In SAPHIRE, a "compound" event is a basic event that is linked to a user-defined calculation program (i.e., a compiled dynamic link library). This basic event can be used in any fault tree or event tree that may exist in the PRA database.

Looking at the "top-most" modeling level, the load-capacity FAC model† is comprised of two parts. First, the *deterministic* aspect is included and is numerically determined by using the pipe wall thickness [$W_{pipe}(t)$] calculation as described in Section 3. A second, and equally important part of the load-capacity model, is an aleatory model representing the arrival of transient overpressure loadings (where "overpressure" indicates a pressure transient above the nominal steady-state pressure). Beneath these top-level models, we introduce applicable *epistemic* uncertainties (Apostolakis 1995). As illustrated in Figure 17, under the deterministic portion of the model are epistemic uncertainties of two types, model and parametric. Specifically, these include the E factor (model); the fluid parameters, including the nominal, steady-state pressure (parametric); and the piping parameters. Under the aleatory portion of the model are epistemic uncertainties of a single type, parametric. The parametric uncertainty in this case only refers to the rate of occurrence of transient pressure events. These aspects of the load-capacity model are clearly delineated since they will dictate how the model is solved (as will be discussed later in this section) as part of the PRA.

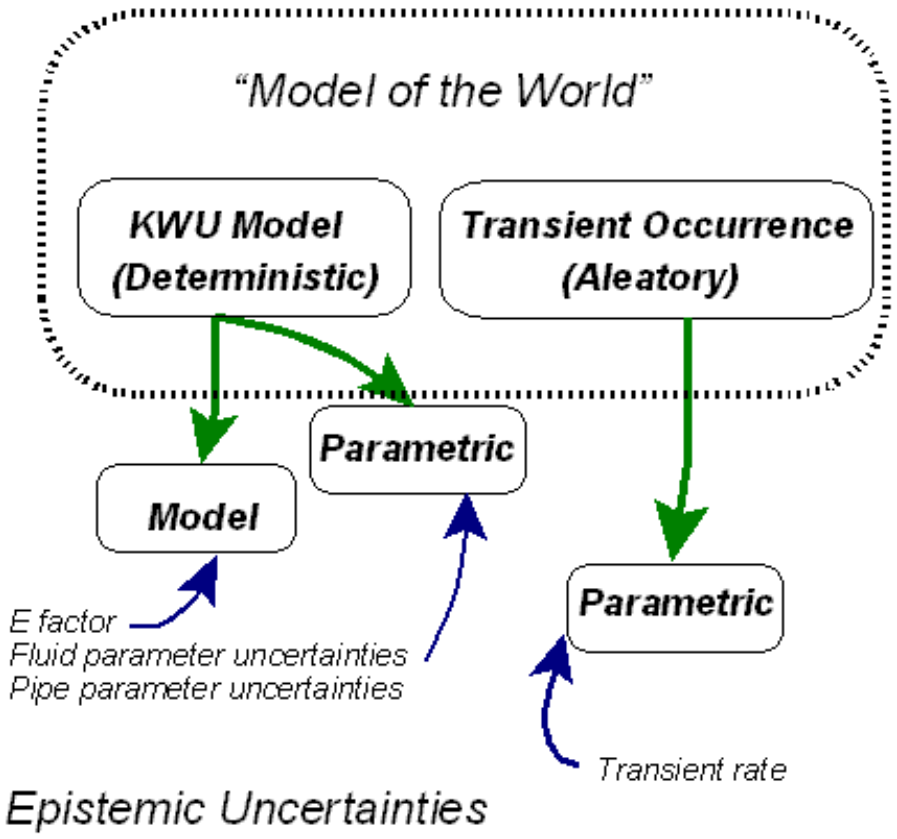

Figure 17. Graphical illustration of the load-capacity FAC model attributes and uncertainty types.

† The "model of the world" in the terminology of Apostolakis (1995).

4.5.2 Detailed Determination of the Capacity

The capacity probability density function, $f_c(x, t)$, can be determined using Equ. (3), (4), and (5) along with the KWU model for $\Delta\phi_R$. The uncertainties in the quantities on the right-hand side of Equ. (5) determine $f_c(x, t)$. Of these, the most important is the uncertainty in the prediction of the KWU model itself.

From the published literature (Kastner and Riedle, 1986), the relationship between the empirical model predictions and the measured FAC rates in laboratory studies or in power plants can be determined. This relationship is shown in Figure 18. From the data, it appears that the KWU-KR model was developed to over-predict the FAC rate (a majority of the data points are above the "one-to-one" line in Figure 18). In other words, it is designed to err mostly on the conservative side and is typical of models utilized for power plant safety where factors of safety (not best estimate) is the *de rigueur*. But, this feature of the model can be used to determine an "adjustment" factor that would express our uncertainty in the calculated results. Referring to Figure 18, there is a total of 1,049 cases where the variability reflected on individual data points is due to both parameter uncertainties and the uncertainty due to the model itself.

To express our uncertainty in the KWU model predictions, we employ the "adjustment-factor" approach discussed by Siu and Apostolakis (1982) and Apostolakis (1995). To begin this approach, we first take the available model, the so called deterministic reference model, and introduce a multiplicative factor E to modify its results. Referring to Equ. (3), the FAC rate is expressed as

$$\Delta\phi_R = \Delta\phi_{R,\,KWU\text{-}KR} \times E \qquad (15)$$

where

$\Delta\phi_R$	=	the specific FAC rate to be used in Equ. (3) ($\mu g/cm^2$ h),
$\Delta\phi_{R,\,KWU\text{-}KR}$	=	the specific FAC rate as predicted by the KWU-Kastner-Riedle model (the deterministic reference model) ($\mu g/cm^2$ h),
E	=	the adjustment factor.

Thus, Equ. (3) becomes:

$$W_{C,calculated}(t) = \frac{E\left(\Delta\phi_{R,\,KWU-KR}\right) t}{\rho_{st}} \qquad (16)$$

We note that the actual specific FAC rate can be considered to be the product of its deterministic reference model prediction and an adjustment factor E which accounts for the inadequacy of the calculated value. The question is now what type of uncertain variable is E. To determine this, we look at the evidence contained in Figure 18.

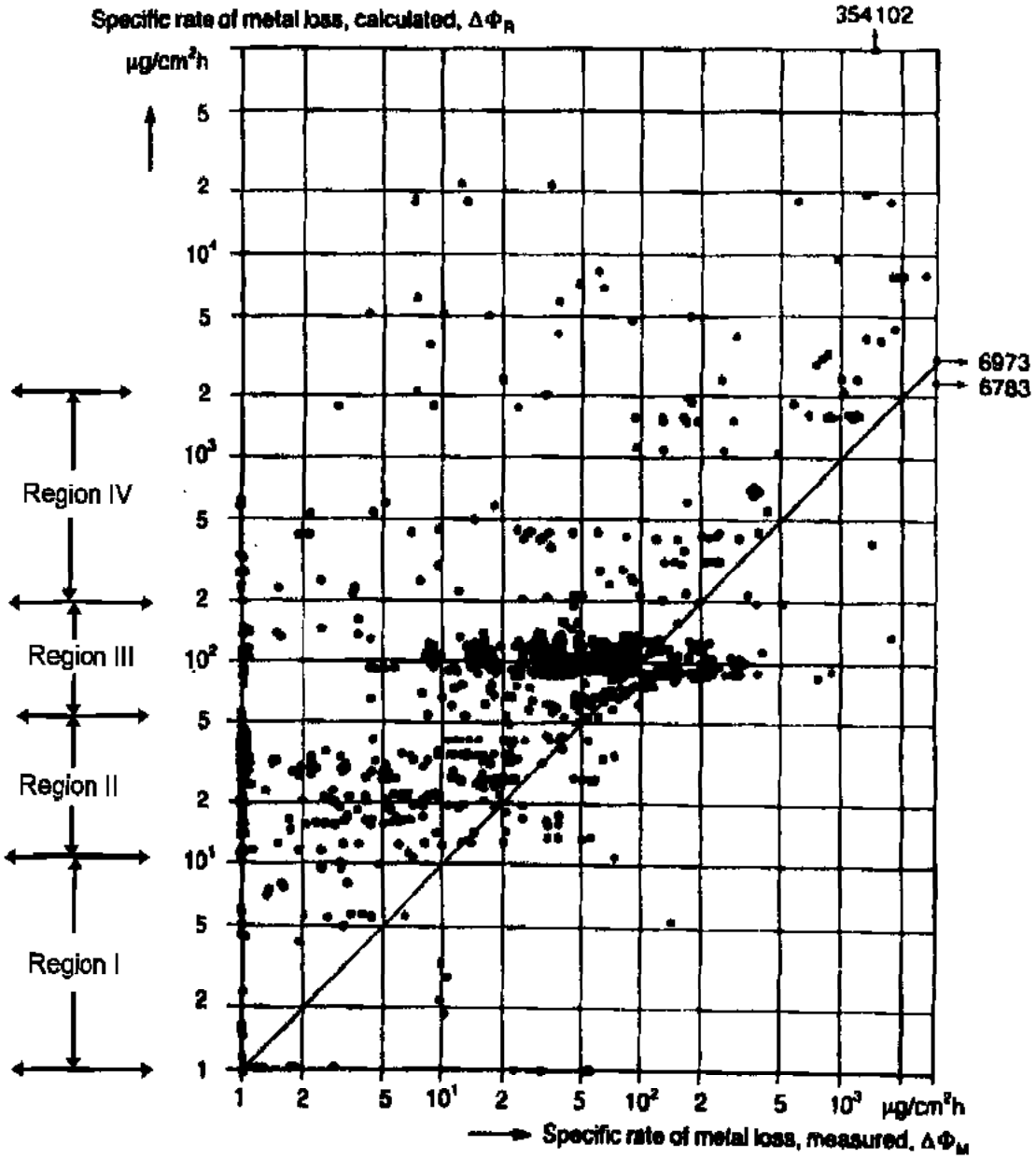

Figure 18. Comparison of values calculated by empirical KWU-KR model with measurements from laboratory experiments and power stations. (Kastner and Riedle, 1986) Copyright VGB PowerTech Service GmbH; reprinted with permission.

Region I: 1 to 10 µg/cm²h (29 data points)
Region II: 10 to 50 µg/cm²h (184 data points)
Region III: 50 to 200 µg/cm²h (653 data points)
Region IV: 200 to 2,000 µg/cm²h (92 data points)

If there were no model and parameter uncertainties in the KWU equation, the points in Figure 18 would fall on the straight line with a slope of one. This would indicate that the calculated (on the ordinate) and the actual (on the abscissa) values of the specific FAC rate were the same. Clearly, this is not the case. There are a number of measured values that correspond to a given calculated value. Presumably, the authors of the paper in which this figure appeared originally made every effort to ensure that the parameter values in the experiments and the power stations from which the measured values were taken were very close to the parameter values that were input to the KWU model to generate the calculated values. In other words, the discrepancies should be *primarily* due to model uncertainty.

When we make predictions using the KWU model, we do not know how inaccurate the model is with respect to the actual circumstances that we are attempting to model, even though the parameter values (pH, flow rate, etc.) that are input to the model are (almost) the same as those anticipated in the actual circumstances. In other words, we do not know what the value of E (the ratio of the actual over the calculated value of the specific FAC rate) is. We can say, then, that we have a population of circumstances similar to Kaplan's (1983) population of plant-specific failure rates. This "circumstance variability" is aleatory, i.e., the particular circumstances of interest to us will be one of the many circumstances shown in Figure 18 (always for the same parameter values). The relative frequency of the points with the same calculated value of the specific FAC rate determines the likelihood that the factor E will have the corresponding value. This variability will be there as long as we use the KWU model (as described by Kastner and Riedle, 1986) to produce the calculated value and it is due to the approximations made to develop this model, i.e., it is an aleatory variability.

The recognition that there is "circumstance variability" leads us naturally to the idea of a "two-stage" Bayesian analysis, as Kaplan (1983) has recommended. Siu and Apostolakis (1985) have proposed an approach to estimate the distribution of E when evidence becomes available. The aleatory probability distribution of the factor E is assumed to be lognormal with parameters μ and σ. The epistemic uncertainty is, in this case, described by a probability density function over the parameter vector $[\boldsymbol{\mu}, \boldsymbol{\sigma}]$. Each value of this vector specifies one aleatory distribution for E. The average of these aleatory curves is used in the second stage as the *epistemic* distribution of E for a specific set of circumstances.

In the present case, we note that Figure 18 contains a fairly large number of points. Consequently, the "two-stage" calculations (and the attendant calculational complexity) are not really needed, since the average aleatory distribution of E can be derived by simply using standard software packages to fit distributions to data. But, we cannot do this for every possible value of the calculated FAC rate. Instead, we divide the range of the calculated values of specific rates of metal loss in Figure 18 into four regions (denoted Region I through Region IV). Points above the calculated specific rates of metal loss of 2,000 $\mu g/cm^2h$ and points below the measured rate of 1 $\mu g/cm^2h$ are excluded from the calculations (note that the actual analyses discussed later in this report did not fall close to either of these excluded regions). From these classical statistics calculations, a lognormal distribution was found

to fit the data in each region very well (Kao, 1998). The parameters μ, σ of the distribution, as well as several characteristic values, are shown in Table 13.

Table 13. Lognormal distributions for the E factor for the four regions of Figure 18.

Parameter	Region I	Region II	Region III	Region IV
5th percentile	0.20	0.05	0.09	0.009
50th percentile	1.39	0.31	0.49	0.13
95th percentile	9.47	2.06	2.66	1.99
Mean	1.43	0.61	0.83	0.51
Error Factor	6.83	6.62	5.46	14.99
μ	0.33	-1.17	-0.72	-2.03
σ	1.17	1.15	1.04	1.65

The data for each region resulted in a lognormal distribution for E by the goodness-of-fit tests. Once the distribution of the E parameter is known for the four regions, they can be introduced into the pressure capacity equation as discussed. In the SAPHIRE calculations, the mean value and error factors are used with the lognormal distribution for the E parameter.

As an example, suppose that we perform our calculations with the KWU model and the result is 25 $\mu g/cm^2h$. The actual value of the specific FAC rate will be

$$\Delta\phi_R = \Delta\phi_{R,\ KWU\text{-}KR} * E_{II} \qquad (17)$$

where E_{II} is the factor corresponding to Region II. The actual specific FAC rate will also be lognormally distributed with parameters

$$\mu_{\Delta\phi R} = -1.17 + \ln(\Delta\phi_{R,\ KWU\text{-}KR}) = 2.050 \qquad (18)$$

and

$$\sigma = 1.15 \qquad (19)$$

Then, several characteristic values of the actual specific FAC rate are ($\mu g/cm^2h$):

5th percentile	1.17	50th percentile	7.77
95th percentile	51.5	Mean	15.1

We observe that the evidence shown in Figure 18 leads to the observation that, even though the calculated value of the specific FAC rate is 25 $\mu g/cm^2h$, the 5th and 95th percentiles of the *actual* rate

are 1.19 $\mu g/cm^2h$ and 52.2 $\mu g/cm^2h$, respectively. This represents the uncertainty in the FAC prediction. Also, note that the 50th percentile and mean of the actual rate are much lower than the calculated rate; there is a probability of 0.84 that the actual value is less than the calculated value of 25 $\mu g/cm^2h$. It is evident from the data in Figure 18 that the KWU-KR model predictions are conservative.

It should be pointed out that the data shown in Figure 18 encompasses both plant and laboratory FAC experience over a wide range of conditions. Of these points, about two-thirds are from laboratory experiments and one-third are from power plant equipment. Complicating this ratio though is the fact that of the original 1777 data points, only 1049 were used to develop Figure 18 (the discarded data points were eliminated due to incomplete parameter data). It was not reported as to the fraction of experimental versus plant data points that were discarded. Nonetheless, Table 14 lists the parameters that are represented and their range that is expressed by the data. The information presented in this Table demonstrate the variations in configurations that were used for the FAC data collection effort.

Table 14. Data conditions for the parameterization of the KWU-KR model.

Parameters	Laboratory and plant data range
Temperature	20 - 220°C
Pressure	1 - 220 bar
Chromium and molybdenum contents (sum)	0 - 100%
Velocity	0.01 - 999 m/sec
Oxygen	0 - 5200 ppb
pH (cold)	5.54 - 10.65
Geometry factors (as per Keller)	0 - 1.0
Diameter	1 - 1020 mm
Ratio of Radius to Diameter in Pipe Bends	0.5 - 4
Steam quality	0 - 1.0
Age (exposure time)	4-80,000 hr

4.5.3 Calculation of the Load-Capacity Probability

As discussed in Section 4.5.1, the "load" in the load-capacity FAC model represents the actual operating pressures that will be seen by the pipe undergoing the FAC process. In our nomenclature, the load distribution, $f_L(y, t)$, is given by two different types of pressures.

- Nominal, steady-state pressures
- Transient pressures

These two loads are treated separately and with different model types. The steady-state pressure is modeled simply as a parameter with epistemic uncertainty and, for this report, was evaluated separately from the transient loads. A component cannot fail (for the first time) from steady-state loads if it has failed previously from transient loads, and vice-versa. Therefore, treating the steady-state loads and the transient loads independently is an approximation.

The treatment of transients loads and their potential for causing failure of a pipe due to FAC is complicated because their occurrence in time must be included in Equ. (12). This occurrence of transients is an aleatory phenomenon that is modeled using the Poisson distribution. A series of calculations leads to the following expression for the reliability of a component (Kao, 1998)

$$R(t_L) = \exp\left(-\lambda t_L \left[1 - \frac{1}{t_L} \int_0^{t_L} F_L\left(ps_f(t)\right) dt \right] \right) \tag{20}$$

where

λ = the mean occurrence rate of transient pressure loads (hr^{-1}),
t_L = the operational time (hr),
F_L = the aleatory cumulative distribution function of the load,
$ps_f(t)$ = the pressure capacity, at time t, that will result in pipe failure (ksi).

We note that this is the aleatory model for the reliability, i.e., this is the model of the world for transients (Apostolakis 1995). The predictive reliability will be the average over the epistemic distributions (e.g., E, flow velocity, pH, temperatures) with the load and capacity formulation, i.e.,

$$\overline{R(t_L)} = \int_{-\infty}^{\infty} dE \int_0^{\infty} d\boldsymbol{p} \left[\exp\left(-\lambda t_L \left\langle 1 - \frac{1}{t_L} \int_0^{t_L} F_L\left(ps_f(t; E, \boldsymbol{p})\right) dt \right\rangle \right) \pi(E, \boldsymbol{p}) \right] \tag{21}$$

where

λ = the occurrence rate of transient pressure loads (hr^{-1}),
t_L = the operational time (hr),
F_L = the aleatory cumulative distribution function of the load,

$ps_f(t)$ = the pressure capacity, at time t, that will result in pipe failure (ksi),
t = the time at which a transient (hr),
E = the KWU-KR model epistemic uncertainty factor,
p = the vector of parameters applicable for the KWU-KR model (e.g., pH, flow velocity, temperature),
$\pi(E, \mathbf{p})$ = the epistemic probability density function of pressure capacity at time t.

The probability density function of the pressure capacity is a function of many things [see Equ. (13)] including: the failure stress, initial pipe wall thickness, initial pipe radius, pipe material density, and hoop strain. Each of these parameters have an uncertainty associated with them, resulting in a probability density function on the capacity. Note that this is the distribution of the capacity *for a given time*. Time is *not* a random variable in this portion of Equ. (21). As such, one must be careful as to the evaluation of the integral during the averaging process. The proper steps, as indicated in the averaging equation, are

1. First choose a p and E, thereby determining the capacity as a function of time.

2. For the (now) fixed capacity, determine the time-conditional piping failure probability.

3. Perform the averaging to obtain the piping failure probability.

An alternative procedure to the potentially complex calculation given by Equ. (21) would be to simulate the occurrence of transients (and then calculate the FAC rate for that particular time period). In general, the treatment of the *transient* pressures is more difficult (even when using simulation) than the *steady-state* pressures since the *time* to an transient overpressure is a random variable. But, either of the two methods will provide an appropriate analysis method.

The alternative approach to address the transient events is to model the events directly using Monte Carlo simulation. If we assume that transient events follow the Poisson conditions, then the time to a transient is a random variable and can be represented by:

$$P(T < t) = 1 - e^{-\lambda t} \qquad (22)$$

where
λ = the mean occurrence rate of transient pressure loads,
T = the time until the occurrence of a transient,
t = the operational time (i.e., pipe exposure time).

Using the probability integral transformation theorem, we know that parameter t can be simulated using the expression:

$$t = \ln(1 - P(T < t)) / (-\lambda) \quad (23)$$

but 1 - P(T < t) is a uniform random variate from 0 to 1 (denoted as U), so

$$t = \ln(U) / (-\lambda) \quad (24)$$

Consequently, if we know the distribution for the magnitude of the pressure given a transient [denoted as M(y)], the transient pressure distribution is:

$$f_L(y, t) = M(y) \quad (25)$$

given that the time of pipe exposure (up to a transient), t, is less than the mission time τ (where this "mission time" is total pipe operational time). Note that the mission time τ is typically measured in years of operation and should not be confused with the mission times typical of PRA (e.g., 24 hours). Now that we have defined the requisite time intervals, the Monte Carlo simulation for transient pressures will follow the steps:

1. Determine a simulated value of t (the time to a transient) using Equ. (24).

2. Compare the simulated time (t) against the mission time (τ).

   A. If $t > \tau$, then the transient arrival is after the FAC mission time. Consequently, this transient can not cause a failure and, as a result, increment the counter recording the total number of trials.

   B. If $t < \tau$, then the transient arrival is less than the FAC mission time. Consequently, this transient *may* cause a failure. Therefore, we need to calculate the pipe capacity at time t (not time τ) and compare it to the load. The load is the magnitude of M (the transient pressure, which is also a random variate).

      If the load M is *larger* than the capacity, the pipe is assumed failed with probability of one and, as a result, increment the counter recording the total number of trials and increment the counter recording the total number of failures.

      If the load M is *smaller* than the capacity, the pipe is assumed to not be failed with probability of one. Then, the time to next transient is calculated (e.g., repeat step 1) and added to the previous time (for a cumulative time simulation). Again, we need to check

to see if $t < \tau$. If it is and the load M at this new time is larger than the capacity, the pipe is assumed to be failed. If the load is smaller than the capacity, the pipe is assumed to not be failed. This iteration is continued until the cumulative time is larger than τ.

C. After a specified number of iterations, the probability of pipe failure is given by the ratio of the failure counter to the counter for the total number of trials.

3. After obtaining the probability of pipe failure for a mission time τ, this probability represents the probability of the pipe failing in any time from 0 to τ years. But, the failure probability to be used in the PRA should be specific to the i'th year of interest.

4. In addition to the load/capacity determination above, credit should be taken for testing and inspection where applicable. This testing/inspection credit could be introduced either in the PRA as a "non-failure" probability (similar to a non-recovery probability) or in the simulation as an extra barrier to failure. Note that the step 2-B above assumes that only one failure of a pipe segment is possible in the mission time τ. This assumption may be justified in that if a pipe does indeed experience a FAC failure, it will be replaced (possibly with a non-FAC susceptible pipe) and may be inspected or tested frequently. Also, other corrective measures may be implemented.

5. Case Studies

This section illustrates the analysis cases that were run using the reliability-physics FAC models with the Surry IPE model. These case studies are intended to illustrate the nature of performing this type of calculation with an actual full-scope PRA model. In general though, several steps must be performed in order to incorporate aging effects into a PRA. A summary of these steps are show below for the FAC analysis.

1. Select the SSCs to be addressed. For this step it may be useful to evaluate nuclear power plant results from the associated FAC in-service inspection program. For the selected specific systems, review the isometric drawings, piping and instrumentation drawings (P&ID), and balance-of- plant heat balance diagram of the associated system. Then, identify the relevant pipe segment boundaries.

2. Select candidate pipe segments within the system to be analyzed. Locations susceptible to FAC are elbows, pipe bends, reducers, tees, pipe entries, and straight pipes where downstream of components or obstacles turbulence occurs (e.g., downstream of flow control orifices, valves). To assist in screening for this step, knowledge of the plant component level risk prioritization results (e.g., SWIM index) and the results suggested by the expert panel review for the individual plant may be utilized.

3. Gather applicable data for the load-capacity failure probabilistic analysis. Use the KWU-KR model and the E factor to determine the capacity at specific time intervals for each relevant pipe segment. Then, determine the load conditions of the associated pipe segment.

4. Calculate the failure probability from the initial use to the *i'th* year. For the analysis presented in the report, we conservatively assume that the piping systems are not inspected or are ineffectively inspected over the total exposure time. The total failure probability of a relevant pipe segment due to FAC, is simply:

$$FPFAC = P_{ss} + P_{tr} \qquad (26)$$

where

P_{ss} = pipe failure probability from steady state load
P_{tr} = pipe failure probability from transients loads

5. Any impacts from the FAC on initiating events must be accounted for in the PRA. Generally speaking, in a PRA, the initiating event frequency represents the expected number of initiating events per unit time. For example, for a loss of main feedwater, we assume a Poisson process. A loss of MFW occurs, with the time to failure being exponentially distributed. The MFW system is repaired, and then fails again with the same time to failure distribution. For the case of FAC failure of a pipe causing an initiating event, we will here consider only the first failure of the pipe. In other words, the replaced pipe will be assumed to be subject to inspection and the failure probability will be assumed to be greatly reduced. Perhaps other steps will also be taken to reduce the failure probability of the pipe, once the failure mechanism has been revealed. Since we are considering only the first failure of the pipe, the expected number of failures in an interval of time is equal to the probability of the pipe failure in that time period. Then, if we denote by $\lambda(i)$ the initiating event frequency associated with FAC failure of pipe, we have

$$\lambda(i) = [\, P_{FAC}(i) - P_{FAC}(i - 1)] / \Delta T \qquad (27)$$

where

λ	=	FAC initiator rate (per year)
$P_{FAC}(i)$	=	failure probability of the pipe from FAC over the time period of operation (from t=0 to the end of the i'th year)
ΔT	=	one year

The rate λ would be incorporated into either an entirely new initiator with its own event tree or it would be added to an existing initiator frequency. For example, if FAC can cause a loss of main feedwater, the rate of FAC-caused main feedwater event could be added directly to the Surry IE-T2 initiator. This step is illustrated in Figure 19.

Alternatively, the non-FAC initiating events can all be recast as *probabilities* for the exposure time of interest. Then, the FAC probability can be added directly to the corresponding initiator probability. For example, for a 10 year duration, we could determine the probability of a loss of main feedwater from non-FAC initiators. This probability would then be added to the probability of FAC-caused initiators over the same exposure time to obtain a new probability of losing main feedwater over the 10 year duration.

For the main feedwater case study, the second of these methods was used and the contribution to the core damage probability from FAC initiating events was calculated for time periods ranging from 1 to 10 years. For the second case study, evaluating the pre-heater configuration, the first method was used and an initiating event frequency for the FAC initiators was calculated.

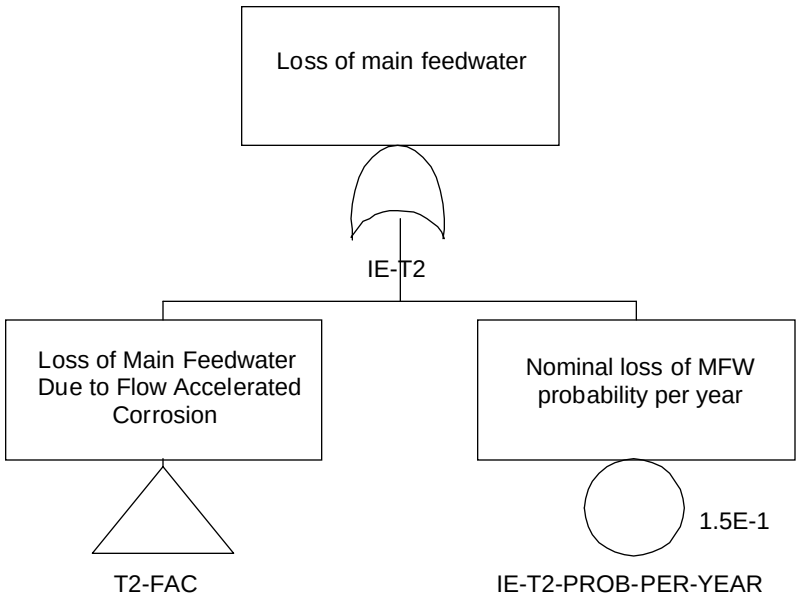

Figure 19. Illustration of the logic model representing the combined FAC-caused loss-of-main-feedwater event and the nominal event.

6. The analyst should specifically account for and model (as necessary) potential environmental impacts from FAC-caused piping failures. For example, locations of important components near FAC sites may have to be evaluated for possible damage to these components. Further, flooding from the FAC rupture location may impact components and should be accounted for in the overall analysis.

7. Assess the impact due to FAC on the core damage frequency and compare it with the nominal core damage frequency. At this point, the PRA model is available for sensitivity studies wherein questions that may be answered include:

   "What happens to the core damage frequency if the plant chemistry processes are not well controlled?" (That is, the flow pH value varies.)

   "How much does the core damage frequency change if the flow velocity in the steam generator preheater section increases 50%?"

   "What does the core damage frequency look like if I extrapolate out to 20 years?"

5.1 Overview of Two FAC Test Case Studies

Before proceeding directly to the PRA-based calculations, we evaluated FAC cases from actual operational events in order to determine the ease of use and applicability of the KWU-KR FAC model. To explore the utilization of the this model, two cases representing FAC-caused ruptures at power plants were evaluated. This evaluation included a treatment of the associated epistemic uncertainties. These two cases, and the power plants that experienced the events, are:

Case 1 Surry Unit 2, ruptured elbow downstream of tee in feedwater (18 in.) piping.

Case 2 Trojan, heater drain pump discharge (14 in.) piping.

Using the cases, the application of the FAC rate deterministic model with associated epistemic uncertainties can be investigated. The individual distributions for the epistemic uncertainties are shown in Tables 15 and 16. These parameter data are used with Monte Carlo sampling methods (10,000 iterations) to obtain the associated uncertainty on the overall FAC rate specific to each case.

Cases 1 and 2 are single phase flow. For two cases, the calculation used the following baseline parameters: 102-mm (4-in.) diameter carbon steel elbow, 7 ppb oxygen content, 6.1-m/s (20-ft/s) flow velocity, room temperature [25°C (77°F)] pH of 7, and 0.03 wt% of chromium, molybdenum, and copper content (note that deviations are noted as appropriate). The pH level at the room temperature is also referred to as *cold pH*.

Table 15. Case 1 FAC parameters and epistemic uncertainty information (single phase flow).

Parameter	Mean value	Standard deviation	Distribution
Operational time (hr)	117,360	n/a	constant
Piping Material (Cr + Mo in %)	0.08	0.0053	normal
Piping geometry (elbow after tee)	0.75	n/a	constant
Fluid velocity (m/sec)	5.1816	0.0345	normal
Dissolved oxygen concentration	1.2	0.08	normal
Water chemistry (pH)	8.9	0.089	normal
Water temperature (°K)	463	0.772	normal
Steam quality	0	n/a	none

Table 16. Case 2 FAC parameters and epistemic uncertainty information (single phase flow).

Parameter	Mean value	Standard deviation	Distribution
Operational time (hr)	76,320	n/a	constant
Piping Material (Cr + Mo in %)	0.02	0.00	normal
Piping geometry (straight pipe after	0.16	n/a	constant
Fluid velocity (m/sec)	7.26	0.05	normal
Dissolved oxygen concentration	10	0.67	normal
Water chemistry (pH)	8.7	0.09	normal
Water temperature (°K)	449.7	0.75	normal
Steam quality	0	n/a	none

5.1.1 Overview of Case 1 - Surry Unit 2 Single-Phase FAC

The most notable failure attributed to FAC in the United States occurred at Surry Nuclear Unit 2 on December 9, 1986. The Surry 1 and 2 plants are located near Gravel Neck, Virginia. Unit 1 entered service in 1972 and Unit 2 in 1973. The Westinghouse design for Surry is a 3-loop model with a rated electrical output of 823 MWe with a subatmospheric (45 psig design pressure) containment. Although the design is of the 3 loop type, Surry is considered to be somewhat atypical when compared to other PWRs. The component that failed was an 18-inch (457 mm) elbow in the condensate system.

The elbow, which had a nominal thickness of 0.500 inches (12.7 mm), was thinned to 0.048 inches (1.22 mm) (Jonas, 1988) at the point of failure. As a result of the rupture, steam and water flowed into the turbine building, fatally injuring four workers and severely burning several others. The rupture also caused damage to plant systems and triggered the fire protection system. The failure occurred just upstream of the feedwater pumps when a plant transient caused a pressure increase in the feed train.

5.1.2 Event Description of Case 1

In December 1986, an 18-inch suction line to the main feedwater pump "A" for the Surry Unit 2 power plant failed in a catastrophic manner. The condensate feedwater system flows from a 24-inch header to two 18-inch suction lines, each of which supplies one of two feedwater pumps. The line temperature at this location is approximately 188°C (370°F), with a pressure of approximately 370 psig and a maximum flow rate of 5 million lb./hr. The fluid in the pipe at this point is considered to be liquid

phase with no vapor present (Cragnolino, et al., 1988). Other relevant information from the Brookhaven National Lab (BNL) failure investigation include:

1. The pipe material is ASTM A-106 Grade B carbon steel. The pipe is 18-inch (46cm) diameter with a nominal wall thickness of 0.500 inches (1.27cm). The elbow is also with a nominal wall thickness of 0.500 inches (1.27cm).

2. Localized areas measured on the elbow were thinned to as low as .046 inch (1.17mm).

3. The flow velocity of the header was 12 fps (3.66 m/s) while the pipe was 17 fps (5.18 m/s).

4. The elbow developed two ruptures. Both ruptures in the elbow were separated by four inches and approximately two inches from the weld.

The BNL failure investigation revealed that the chemical and mechanical properties of the pipe, elbow and weld materials involved in the Surry failure were consistent with the expected properties of the specified materials. The report concluded that the overall thinning of the elbow and pipe material at Surry 2, in addition to the ductile tearing on all of the fractures examined, were a clear indication that the Surry Unit 2 feedwater pipe failed as a result of the FAC mechanism under single phase conditions.

This case was evaluated using the FAC rate equations developed in Section 3. The nominal results of this evaluation are shown below. Note that the model uncertainty factor E was not included for the nominal results of this test calculation (the last line below does show the analysis results including the model uncertainty factor E). From the Case 1 analysis results, there is around 96% probability that the calculated FAC thickness will be larger than the actual damaged piping loss thickness.

Observed FAC thickness	0.45 in.
Calculated FAC thickness	0.51 in. (10th percentile)
Calculated FAC thickness	0.63 in. (mean value)
Calculated FAC thickness	0.76 in. (90th percentile)
Ratio of calculated mean/observed	1.4
Ratio of E*calculated mean/observed	1.2

As shown by the E adjusted value, the calculated FAC thickness is only overpredicted by 20% for the scenario describe in Case 1.

5.1.3 Overview of Case 2 - Trojan Single-Phase FAC

The Trojan plant is a 1,095 MWe PWR located on the Columbia River near Prescott, Oregon. It was permanently shut down in January of 1993. During the refueling outage in 1987, extensive thinning was found in the feedwater system. This thinning was considered serious because some of the affected fittings were part of the safety-related feedwater system within the containment. Although there was no leak or rupture, the Trojan experience confirmed that FAC could be a problem in single-phase systems.

Interestingly, the inspection program at Trojan was prompted by a March 1985 failure of a 14-inch (356 mm) pipe at the discharge of the heater drain pump. The pipe, which had a nominal wall thickness of 0.375 inches (9.53 mm), had been thinned to approximately 0.098 inches (2.5 mm). Unfortunately, this failure did not prompt a program of inspections throughout the nuclear utility industry.

5.1.4 Event Description of Case 2

At the time of the failure investigation, it was believed that the Surry incident described in Case 1 was the first case of single phase FAC at a nuclear plant. However, a review of the literature revealed that Surry Unit 2 was not the first nuclear unit to have a rupture caused by single phase FAC. The first event took place at the Trojan Station and is described in part by NUREG/BR-0051 as follows (Cragnolino, et al., 1988):

> "...On the evening of March 9, 1985, the plant was operating at 100% power. Average coolant temperature was 585 ^{o}F and reactor coolant system (RCS) pressure was 2235 psig. At about 9:50 p.m., a reactor trip occurred from automatic actuation of the reactor protection system, due to a main turbine trip. The turbine trip was caused by a spurious main turbine bearing high vibration signal. The reactor protection system and plant safety systems functioned as designed during the transient. Following the turbine trip, the resulting automatic main feedwater isolation produced a pressure pulse to approximately 875 psig in the heater drain and feedwater systems, as expected. However, the pressure surge caused an eroded section of the 14-inch diameter heater drain pump discharge piping to rupture, resulting in the release of a steam-water mixture of approximately 350 ^{o}F into the 45-foot (ground-level) elevation of the turbine building. In addition to the fire suppression (deluge) system actuation by heat sensors in the turbine building and damaged secondary plant equipment, one member of the plant operating staff received first and second degree burns on 50% of his body from the high temperature fluid. He was treated at a local hospital for three weeks before being released..."

The failure occurred very close to a weld on the pipe. A "scalloped" surface typical of FAC was seen on the inside surface of the pipe. The failure investigation documented that the microstructure of the pipe material was normal for A 106 Grade B material. This failure was considered by the utility to be caused by FAC in a single phase system (450 psig and 350°F, with a bulk flow rate of 20-24 fps) (Cragnolino, et al., 1988).

From the Case 2 analysis (see results below), we may conclude that either (1) the KWU-KR model cannot be applied for the scenario in case 2 or (2) the FAC rate calculated from the reliability-physics model, being smaller than the actual damaged piping loss thickness, is a non-conservative prediction (possibly due to parameter value section). During the analysis for Case 2, there was some discussion on the specific geometry factor to be used for the analysis. The geometry factor that was used does not exactly represent the actual geometry at Trojan, but was considered to be a best estimate given the lack of detailed (with respect to an applicable geometry factor) plant-specific information for this case.

Observed FAC thickness	0.23 in.
Calculated FAC thickness	0.057 in. (10th percentile)
Calculated FAC thickness	0.067 in. (mean value)
Calculated FAC thickness	0.078 in. (90th percentile)
Ratio calculated mean/observed	0.29
Ratio E*Calculated mean/observed	0.17

5.2 Main Feedwater PRA Calculation

The selected pipe segment in our case study is the same as the particular segment that failed in December of 1986 (13.6 years after commercial operation). This pipe shown in Figure 20. A simplified P&ID for the same system with piping designators is shown in Figure 21. The 18 inch suction line to the main feedwater pump A of Unit 2 failed in a catastrophic manner. The condensate feedwater system flows from a 24 inch header to two 18 inch suction lines, each of which supplies one of two feedwater pumps.

In accordance with our choice to analyze the MFW system, we specifically model the single pipe segment (FW-04) failure due to FAC in Surry's MFW system because this event also caused two main feedwater pumps to lose suction heads at the same time. Thus, we may assume that the event was a loss of the MFW system (corresponding to the IE-T2 initiating event in the Surry-IPE) which caused a plant transient (Virginia Power, 1991). The FW-04 pipe segment was not subject to inspection, consequently, no credit was taken for the potential of inspection or replacement of the piping system.

The study evaluated the impacts of transient pressures and steady-state pressures independently, when in fact they should be analyzed in an integrated fashion. If a pipe fails from transient pressures then it cannot fail at a later time from steady-state pressure loads. The coupling of the two failure modes should be accounted for in a more realistic analysis.

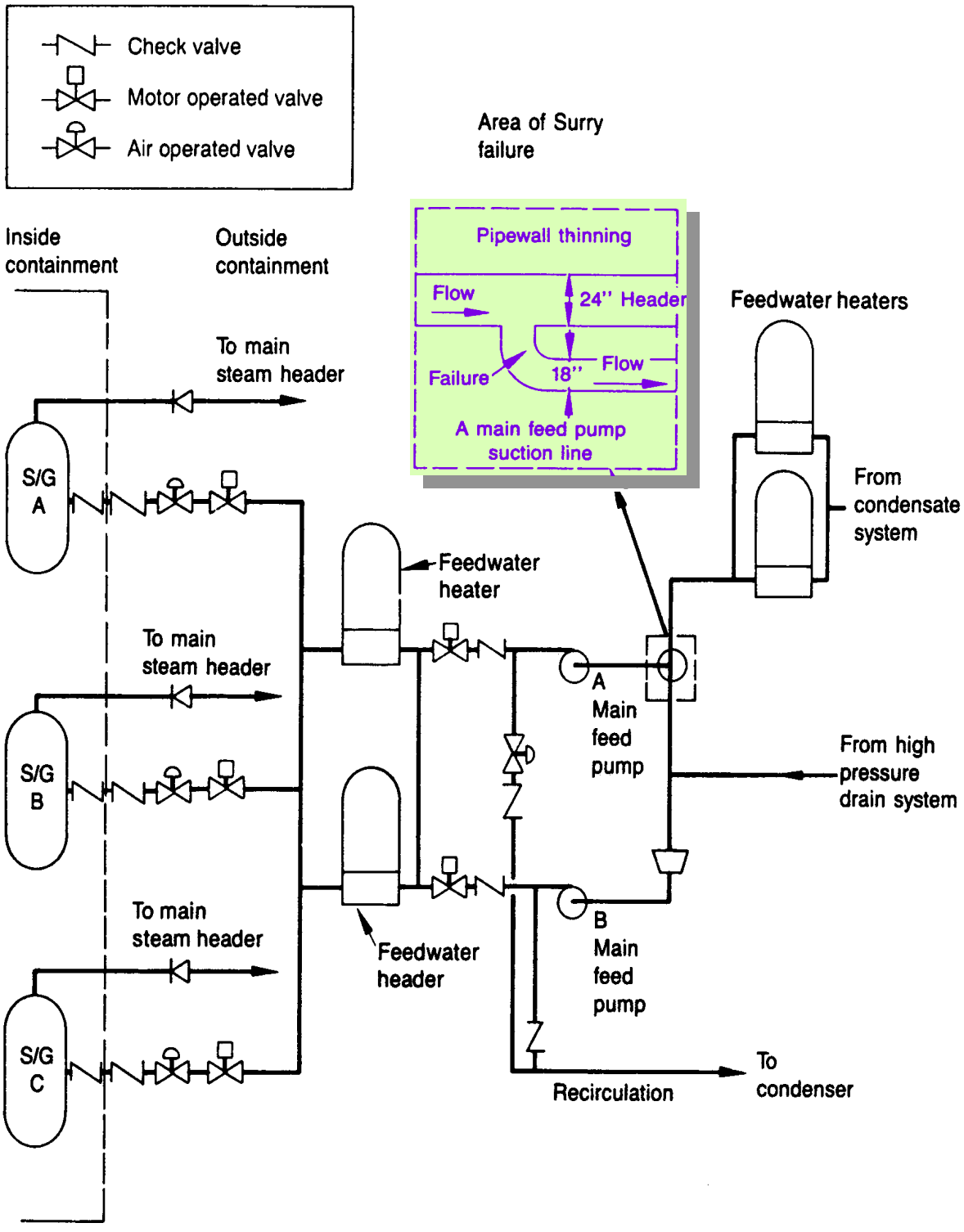

Figure 20. Illustration of the location and piping types for the Surry MFW PRA calculation.

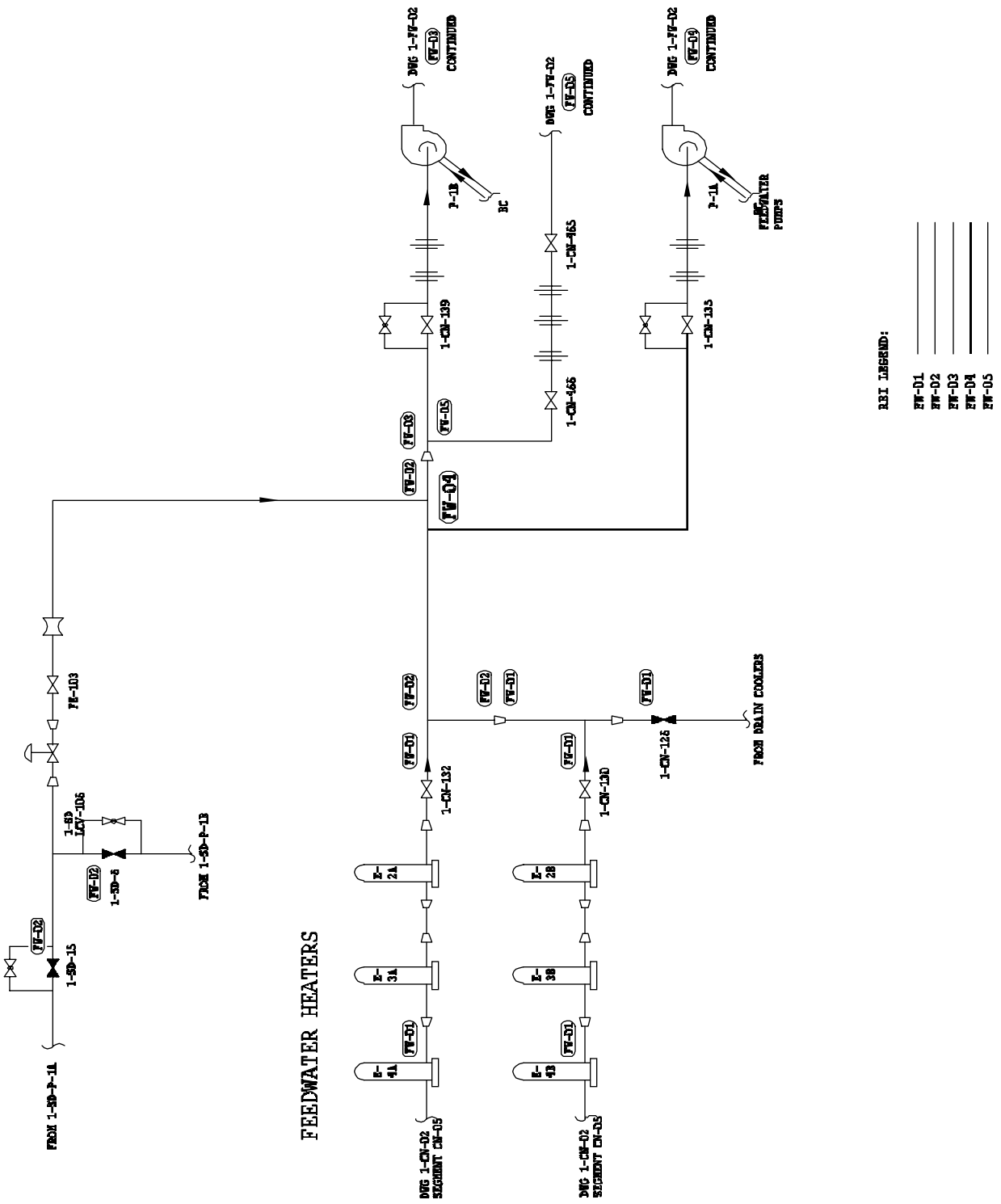

Figure 21. P&ID for the main feedwater system at the Surry plant.

The failed suction line in the P&ID drawing and other associated diagrams were reviewed in order to gain an understanding on how to model this pipe segment in the PRA. The pipe segment, noted as "FW-04," was incorporated directly in the SAPHIRE Surry PRA model by the following steps:

1. In the PRA, we identified the corresponding "surrogate" events related to FW-04. These events include failure of the feedwater pumps 1A and 1B. Applicable basic events in the PRA are:

   1FWPAT-FR-1FWP1A
   1FWPAT-FR-1FWP1B
   1FWPAT-FS-1FWP1A
   1FWPAT-FS-1FWP1B.

2. Using the SAPHIRE "cross-referencing" feature, we identified the fault trees that utilized the basic events noted in step 1. Two fault trees were found, GMF1112 and GMF2112.

3. Using the SAPHIRE logic editor, an FAC piping failure event called "FW-04" was inserted at the same level of the fault trees as those basic events identified in step 1.

4. Again using the SAPHIRE "cross-referencing" feature, we determined all of the fault trees that were used by the event tree top events related to main feedwater failure. The relevant top events for main feedwater failure are: M01, M02, and M03. In addition, a search of the initiating events identified IE-T2 as the only initiator applicable to FAC failure of the FW-04 piping.

5. Evaluating the M01, M02, and M03 fault trees, it was noted that M01 and M03 both utilize the GMF1112 and GMF2112 subtrees, so no further modifications were needed for these fault trees. Fault tree M02 did not use these two fault trees. Consequently, M02 was modified directly to use the FW-04 event.

6. Lastly, the initiating event IE-T2 was modified so that its value would be calculated using a fault tree rather than just a single basic event. Inputs into this new initiating event include the nominal frequency of loss of main feedwater and the FW-04 FAC event. By focusing on the T2 portion of the PRA, we are assuming that only losses of main feedwater will result in the transient pressure load on the FAC-susceptible piping. If other (general) transients also cause similar load on this piping, then the initiating event rate should be increase to account for these additional impacts.

For the main feedwater, the normal operating system pressure is 370 psig. This pressure represents the steady-state load pressure. The pressure during the transient (of the 1986 event) was approximately 440 psig. Thus, we used a value of 440 psig as the load.

The indirect impacts due to failure of the "FW-04" pipe segment were also considered. For the Surry plant, flooding in the turbine building (91% contribution to core damage frequency) was a significant plant vulnerability. Flooding may occur as a result of failures in the circulating water and service water systems in the turbine building. Both of these water systems are gravity fed from the intake canal (20 feet above the Turbine Building basement floor) (Virginia, 1991). The "FW-04" pipe segment is located in the basement of the turbine building. After discussions with Surry PRA and piping personnel, it was determined that there are no safety related equipment in the area. Hence the indirect effects do not contribute to our case study.

After the FW-04 piping event was integrated into the Surry PRA model, the basic event was linked to the FAC "compound" plug-in calculation. The parameters for the FAC model are shown in Table 17. With the data for the FAC parameters known, the failure probability of FW-04 as a function of time can be calculated. Figure 22 illustrates the results of such a calculation. Note that in addition to the total FW-04 failure probability, the constituents to the total probability are shown. As previously discussed, these constituents come from two type of models for the load part of the load-capacity formulation. For FAC failures in piping, the two loads arise from either the nominal steady-state pressure or transient pressures.

There are two types of models of the world, deterministic and aleatory (Apostolakis, 1990; 1995). An example of a deterministic model is the KWU-KR methodology to calculate the FAC rate as described in Section 3. An example of an aleatory model is the occurrence of transients (this type of model is sometimes referred to as "randomness"). Of course, each model of the world is conditional on the validity of its model assumptions and on the numerical values of its parameters. Since there may be uncertainty associated with these conditions, we introduce the epistemic probability model which represents our knowledge regarding the numerical values of parameters and the validity of the model assumptions.

Table 17. FAC parameter and uncertainty information for the Surry main feedwater PRA analysis.

Parameter	Symbol	Mean value	Standard deviation	Distribution
Operational time (hr)	t	117,360	N/A	point estimate
Piping Material (Cr + Mo in %)	h	0.08	0.0053	normal
Piping geometry (elbow after tee)	k_c	0.75	N/A	point estimate
Fluid velocity (m/sec)	w	5.1816	0.0345	normal
Dissolved oxygen concentration (ppb)	g	1.2	0.08	normal
Water chemistry (pH)	pH	8.9	0.089	normal
Water temperature (°K)	T	463	0.772	normal
Density steel pipe (kg/m^3)	ρ_{st}	8500	N/A	point estimate
Pipe failure stress (ksi)	σ_f	61	N/A	point estimate
Pipe hoop strain (%)	ϵ_f	6	N/A	point estimate
Pipe radius (cm)	r	22.9	N/A	point estimate
Pipe initial thickness (cm)	$W_{pipe}(t = 0)$	1.27	N/A	point estimate
Steam quality	x_{st}	0	N/A	none

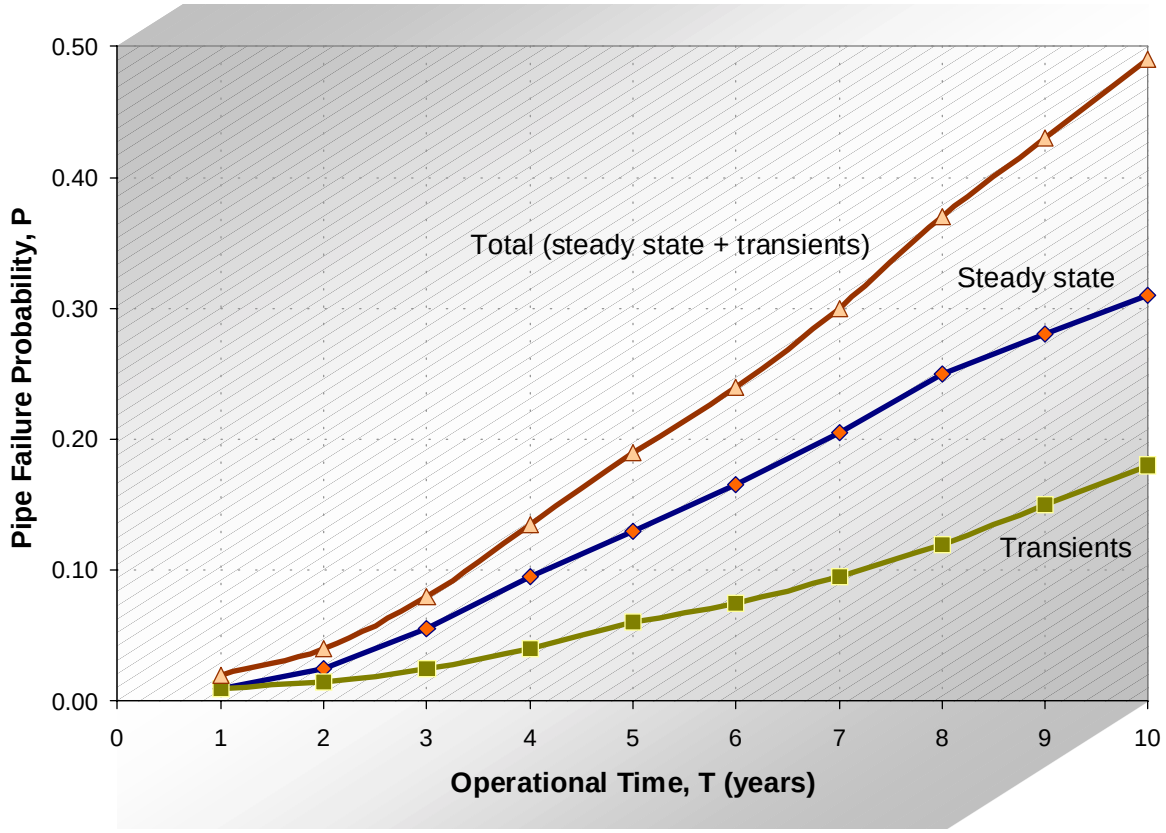

Figure 22. Probability of FW-04 pipe failure (due to FAC) as a function of time.

As an integral part of the FAC rate calculation, we introduced the model adjustment factor E, which has variability due to both parameter and model uncertainties. The uncertainties in the steady state model are primarily due to model uncertainty which is a purely epistemic uncertainty. Thus, the capacity (in the load-capacity formulation) of the pipe to withstand the load (i.e., fluid pressure inside the pipe) at steady state is dominated by epistemic uncertainties. Since the hazard function is meaningful for aleatory failures, we cannot obtain a hazard function (failure rate) directly from the failure probability calculations. Note that we can obtain a failure rate from the transient portion of the analysis because this model involves an aleatory formulation. But, it is important to note that this failure rate does not represent the total impact of FAC since the failure due to the steady-state pressure is not included.

Our results can be used to check the validity of the linear failure rate model (Vesely, 1987). This model asserts that the failure rate of a component is a linear function of time, i.e.,

$$\lambda(t) = \lambda_0 + \alpha t \qquad (28)$$

The term "α t" accounts for (potential) aging effects.

We can calculate the failure rate due to transients using the standard definition of failure rate,

$$\lambda(t) = -\frac{\frac{dR(t)}{dt}}{R(t)} \tag{29}$$

where R(t) is the reliability of Equ. (16), i.e., the probability of surviving the transients.

We note that this failure rate, Equ. (29), must be calculated within the model of the world. In other words, it must be calculated *before* the averaging process [similar to that of Equ. (21)] is performed (equivalently, the failure rate can not be calculated directly from the curve corresponding to transients shown in Fig. 22). The average failure rate can be found, in general, from the predictive calculation

$$\overline{\lambda(t)} = \int_0^\infty \lambda(t)\ \pi(ps_f)\, dps_f = -\int_0^\infty \frac{\frac{dR(t)}{dt}}{R(t)}\, \pi(ps_f)\, dps_f \tag{30}$$

where

$\lambda(t)$ = the piping failure rate due to transients,

$ps_f(t)$ = the pressure capacity, at time t, that will result in pipe failure (ksi),

$\pi(ps_f)$ = the probability density function of pressure capacity at time t.

Our results for our examples show that the assumption of linear (with time) failure rate (due to transients) *seems* reasonable, i.e., Equ. (29) is approximately linear with respect to $\lambda(t)$. The (epistemic) average value of α (from the case study) is equal to about $3 \times 10^{-3}/yr^2$. Consequently, the linear model may be a reasonable model to use in this case (assuming, of course, that the value of α could be obtained by other means, e.g., by expert opinion elicitation). But, the failure rate noted in Equ. (30) can only be calculated for the aleatory FAC model of the world (i.e., for transient pressures); the deterministic model of the world (i.e., steady-state pressures) does not have such a quantity. And, consequently, the overall failure probability for a pipe section could not exclusively utilize a linear failure rate model.

The model of the world for steady-state pressures is deterministic, i.e., failure occurs when the capacity has deteriorated below the static pressure. Consequently, a failure rate similar to Equ. (29) **does not exist**. We note that it would be incorrect to calculate a failure rate using the curve labeled "steady state" in Figure 22, just as it would be inappropriate to calculate the average failure rate for transients from the curve corresponding to transients, as discussed above. And, for the deterministic model, averaging over the epistemic uncertainties via the predictive calculation like Equ. (30) does not yield a failure rate either.

The *conclusion is that*, if one were to use the linear model of Equ. (28), assuming that α could be determined by methods other than those of reliability physics, one would model the probability of failure due to transients but would leave out the probability of failure due to steady-state loads (because these are not aleatory and the concept of a failure rate does not exist in this case). One may be tempted to derive a failure rate due to existence of the probability density function for pressure capacity. But, this temptation would be inappropriate because this density function *does not* represent uncertainty about time. Time is simply a parameter. The aleatory model, on the other hand, does model time as a random variable (the time of occurrence of transients is random). Consequently, a failure rate is a meaningful quantity within this model.

If one were to fit the transient portion of Figure 22 to a linear curve representing the failure rate, the α can be calculated to have a value of 3.4E-7/hr/year. We note that the stainless steel used in most safety-related pipe segments is not susceptible to FAC, so the comparison of the α value to other TRIGALEX values is probably not meaningful. Of course, the principal conclusion from the analysis is that the linear aging model fails for the steady state case because the uncertainties are purely epistemic. A linear aging model may *approximate* the calculated FAC probabilities because the model has both aleatory (occurrence of transients) and epistemic (distribution of pressures, pipe capacity) portions. But, the linear failure rate model does not allow insights into drivers of the aging failure probabilities.

The core damage probability due to FAC over a total of 10 years has a small increase of about 20% for just the loss of main feedwater event tree sequences (i.e., just the IE-T2 sequences). The expected number of losses of main feedwater is approximately 1.5 since the yearly rate is 0.15/yr. But, as shown in Figure 22, the FAC-caused loss probability over 10 years is approximately 0.3. Consequently, the increase in losses of main feedwater from FAC over the 10 years is 0.3/1.5, or about 20%. Since the loss of main feedwater is just one of the initiating events, the FAC contribution to *core damage* over 10 years will then be less than 20%. In fact, the core damage frequency from loss of main feedwater, without the FAC contribution, is only about 5E-7 per year (less than 1% of the total core damage frequency), so that the probability of core damage in ten years from loss of main feedwater is only about 5E-6. This value is increased by about 20%, or by about 1E-6 over the ten year period, because of the FAC-induced losses of main feedwater. But, without FAC, the core damage frequency from all initiators is about 7E-5 per year, so that the probability of core damage from all initiators over the ten year period is about 7E-4. The contribution of the FAC-induced loss of main feedwater to the core damage probability over the 10 year period is thus less than 0.2%.

The impact on the *overall* core damage frequency over the 10 year period is therefore insignificant. Note though that the impact on the risk due to FAC for other plants or plant models has not been evaluated and needs further investigations.

5.3 Preheat Steam Generator PRA Calculation

To evaluate the potential for FAC in the systems equipped with preheater-type steam generators, the auxiliary feedwater (AFW) system of the Surry IPE model was modified. Note that Surry does not have a preheater steam generator, but the nominal PRA model can be modified to accommodate the potential FAC-caused failure and resultant impact on the AFW piping.

Since this calculation is a temporary one, the modification will be accomplished via a "change set" in the SAPHIRE software so that the modification can be turned off or on as needed. To accomplish the modification, several piping segments were incorporated directly into the AFW fault trees. Specifically, the piping segments to be added are:

AFW-10
AFW-11
AFW-13
AFW-14
AFW-15
AFW-16
AFW-17
AFW-18
AFW-19

These modifications represent the preheater bypass line and will be utilized to explore the potential wall-thinning from the high-velocity feedwater flow during normal, at-power operation (Shaw, 1997). For Surry, critical sections of the AFW that will be the focus of this study are AFW-15 and AFW-16. Figure 23 shows the flow diagram for these two piping segments.

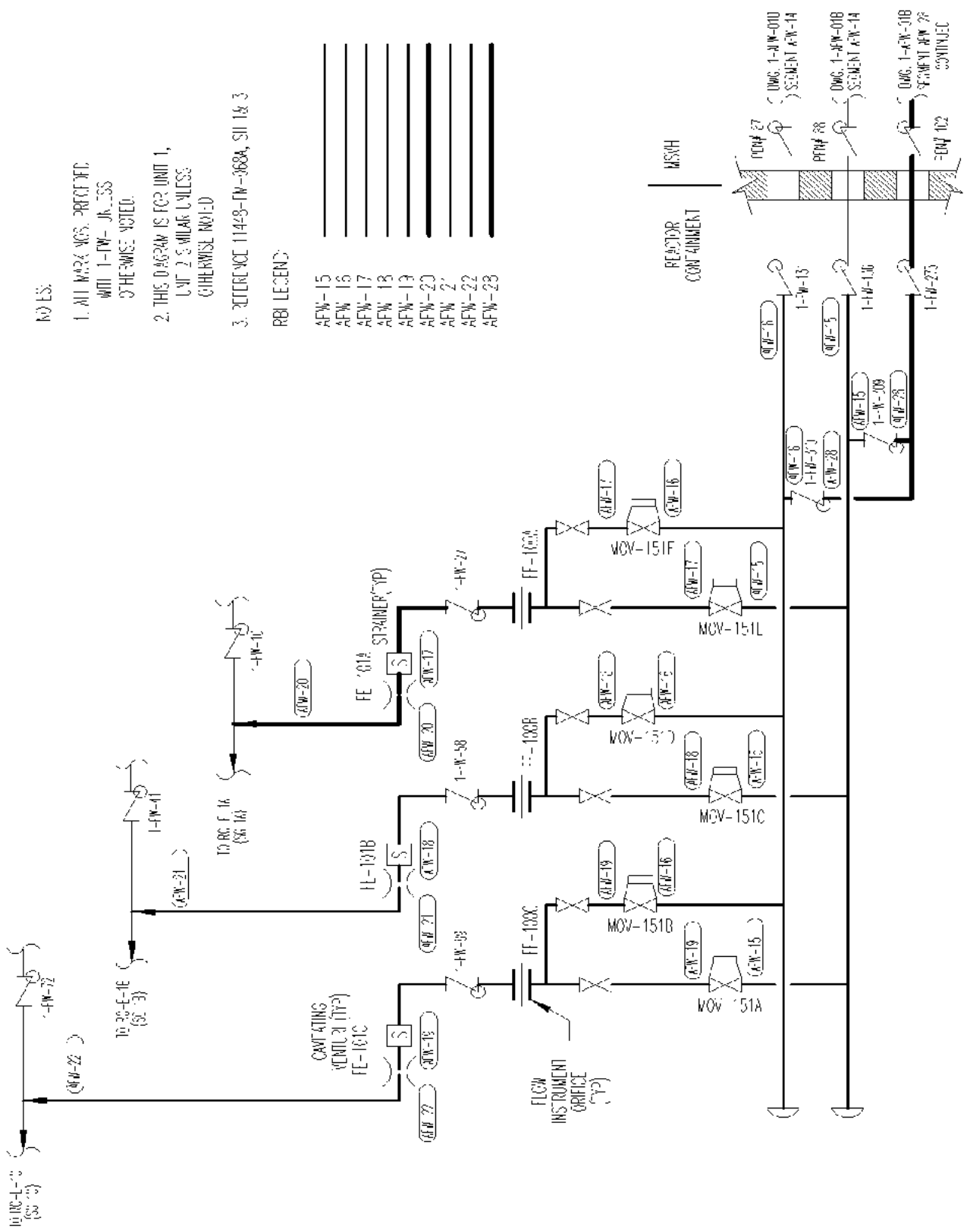

Figure 23. P&ID for the AFW system at the Surry plant.

The steam generator pre-heater operates like the system shown in Figure 6 (page 38) . With the information from this figure, the P&ID drawing and other associated diagrams for the Surry plant were reviewed in order to gain an understanding on how to model this group of pipe segments in the PRA. The pipe segments, noted as "AFW-13" through "AFW-19," were incorporated directly in the SAPHIRE Surry PRA model by the following steps:

1. In the PRA, we identified the corresponding "surrogate" events related to the applicable AFW pipe segment. Applicable basic events in the PRA, and their associated pipe segments, are:

Basic Events	Pipe Segments
1FWCKV-FC-1FW131	AFW-14, AFW-16
1FWCKV-FC-1FW133	AFW-14, AFW-11
1FWCKV-FC-1FW136	AFW-13, AFW-15
1FWCKV-FC-1FW138	AFW-13, AFW-10
1FWCKV-FC-1FW27	AFW-17
1FWCKV-FC-1FW58	AFW-18
1FWCKV-FC-1FW89	AFW-19
1FWMOV-FO-FW151E	AFW-17, AFW-15
1FWMOV-FO-FW151F	AFW-17, AFW-16
1FWMOV-PG-FW151A	AFW-15, AFW-19
1FWMOV-PG-FW151B	AFW-16, AFW-19
1FWMOV-PG-FW151C	AFW-15, AFW-18
1FWMOV-PG-FW151D	AFW-16, AFW-18

2. Using the SAPHIRE "cross-referencing" feature, we identified the fault trees that utilized the basic events noted in step 1. A total of 11 fault trees were found.

3. Using the SAPHIRE logic editor, an FAC piping failure event called "AFW-XX" (where XX represents the particular piping segment of interest) was inserted at the same level of the fault trees as those basic events identified in step 1.

For the main feedwater, the normal operating system pressure is 370 psig. This pressure represents the steady-state load pressure. Note that no indirect effects due to failure of the "AFW" piping segments were evaluated since this preheater-type system does not actually exist as Surry.

After the AFW piping events were integrated into the Surry PRA model, the basic event were ready to be linked to the FAC "compound" plug-in calculation. For this analysis, only AFW-15 and AFW-16 were evaluated since these two pipe segments are critical to the AFW system. It was assumed that if a pipe ruptured in one of these segments, a plant transient would result. In a more realistic calculation, one would note that rupture of different pipe segments at various locations may result in different initiating events (e.g., plant trip, loss of feedwater, loss of AFW). But, in this case study, we assumed that rupture would initially cause an upset condition to the main feedwater system. Further, we assumed that since the preheater section is isolatable and only carries a fraction of the total feedwater flow (about 14%), that recovery of the main feedwater is relatively straightforward. Consequently, we used a main feedwater non-recovery probability of 0.05. If the main feedwater system is not recovered, then the PRA T2 sequences are applicable (loss of main feedwater). Otherwise, the PRA T3 sequences are applicable (transient with main feedwater available).

The frequency of FAC rupture is found from the pipe failure probability as a function of time. For the preheater analysis, only two pipe sections (AFW-15 and AFW-16) were modeled. Consequently, the total FAC rupture frequency would be the summation of both the AFW-15 and AFW-16 rupture frequencies. This aggregate frequency was used to represent the general repture-induced transient initiator for both the T2 and T3 PRA sequences.

Two other PRA adjustments for the preheater case were the exclusion of multiple, simultaneous ruptures and adjustments to common-cause failure probabilities. We assumed that given rupture of one pipe segment, the other pipe segment would not rupture or be affected by the initial pipe rupture. If rupture of one pipe could cause excessive loading of the other pipe (or related components) then this impact should be addressed. Also, after rupture of one pipe, PRA basic events that represent common-cause failure of redundant components in the piping sections must be adjusted since only components in the "non-failed" pipe section need to fail in order to disable the AFW system.

The parameters for the FAC model that were used are shown in Table 18. With the data for the FAC parameters known, the core damage frequency (or probability) changes due to FAC as a function of time can be evaluated. Note that for the analysis in this case study, we (1) utilized only the stead-state, deterministic pressure load model and (2) did not credit testing/inspection as preventing potential FAC failure over the duration modeled.

Table 18. FAC parameters and uncertainty information for the preheater-type steam generator PRA analysis.

Parameter	Symbol	Mean value	Standard deviation	Distribution
Operational time (hr)	t	variable	N/A	point estimate
Piping Material (Cr + Mo in %)	h	0.08	0.004	normal
Piping geometry (elbow after	k_c	0.23	0.05	normal
Fluid velocity (m/sec)	w	9.91	0.5	normal
Dissolved oxygen concentration	g	1.2	0.1	normal
Water chemistry (pH)	pH	8.9	0.04	normal
Water temperature (°K)	T	463	2.0	normal
Density steel pipe (kg/m^3)	ρ_{st}	8000	100	normal
Pipe failure stress (ksi)	σ_f	75	1	normal
Pipe hoop strain (%)	ϵ_f	6	0.1	normal
Pipe radius (cm)	r	5.08	0.02	normal
Pipe initial thickness (cm)	$W_{pipe}(t = 0)$	0.856	0.003	normal
Steam quality	x_{st}	0	N/A	point estimate

The first result presented for the pre-heater case study looks at just the failure probability of a single pipe segment (AFW-15). Figure 24 presents the results of the pipe failure probability analysis from FAC. In order to obtain the pipe failure curve, we divided the operational time into 15, one-year periods. For each period, we calculate the FAC failure probability of the pipe. These probabilities were then summed over all time periods to obtain the cumulative probability curve shown in Figure 24. Note that the cumulative curve is not a smooth line primarily due to the fact that the probability calculation for FAC (in this case study) was performed via Monte Carlo simulation. Thus, from one interval to the next, there will be slight variations in the probability of failure.

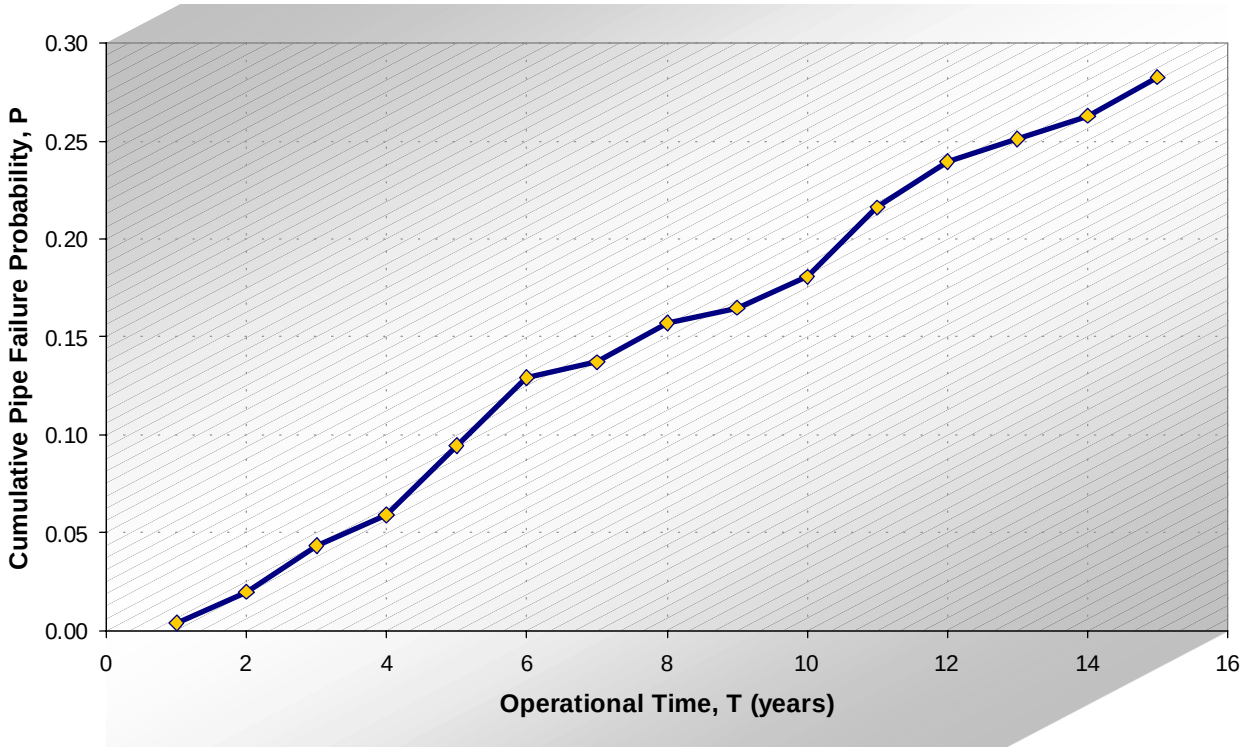

Figure 24. Cumulative failure probability of AFW-15 pipe segment from FAC

The second result presented for the pre-heater case study looks at the individual failure probabilities of a pipe segment AFW-15 for individual years. Figure 25 presents the results of the i'th year pipe failure probability analysis from FAC. Again, in order to obtain the pipe failure contributions, we divided the operational time into 15, one-year periods. For each period, we calculate the FAC failure probability of the pipe in that time period. These probabilities are shown in Figure 25. Note that the larger the "slice" of the pie, the larger the pipe failure probability for that year. The FAC-caused failure probability ranges from 0.004 in the first year to 0.035 in the 11^{th} year. Recall that the 11^{th} year probability here is not the probability of failure over 11 years of continuous operation. Instead, the 0.035 probability represents the probability the pipe fails (from FAC) within the 11^{th} year.

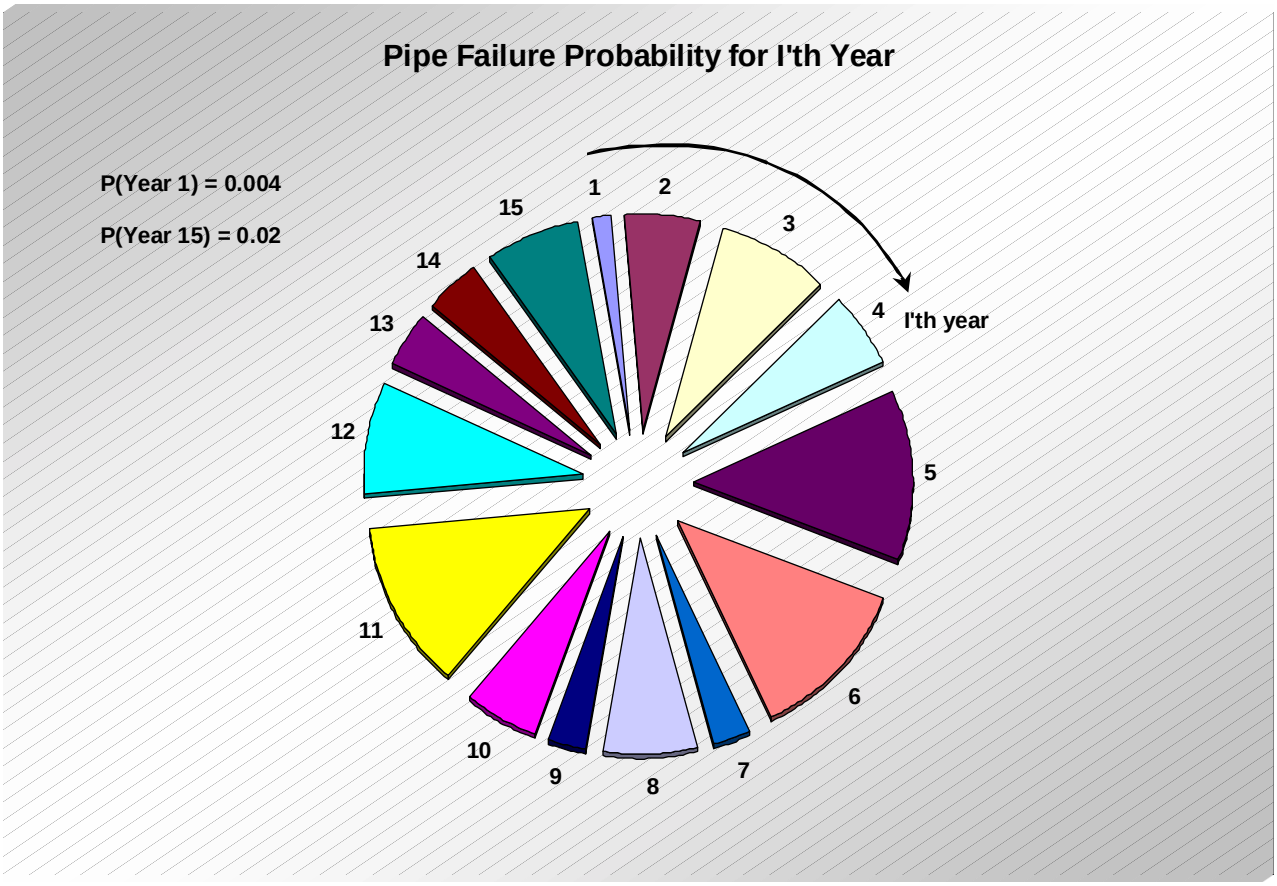

Figure 25. Failure probability for AFW-15 from FAC for the i'th year of operation.

The third, and final, result presented for the pre-heater case study looks at the impact on the overall core damage probability from just FAC failures. Figure 26 presents the results of 15 years of operation where the cumulative core damage probability is shown for each of the years. For each operational period, we calculate the core damage probability from just FAC and then the total for all PRA initiating events. Then, these core damage probabilities are summed to obtain the curve in Figure 26. The probability in the figure represents the probability that core damage will occur at any time from t = 0 to t = T. From the figure, the probability of core damage from FAC over the first ten years is approximately 1E-6. Since the probability of core damage from all initiators over the ten year period is about 7 x 10^{-4}, the FAC contribution to the core damage probability is about 0.2%. Although the AFW system has high importance, in the sequences where FAC causes partial loss of the AFW, the main feedwater system is generally available.

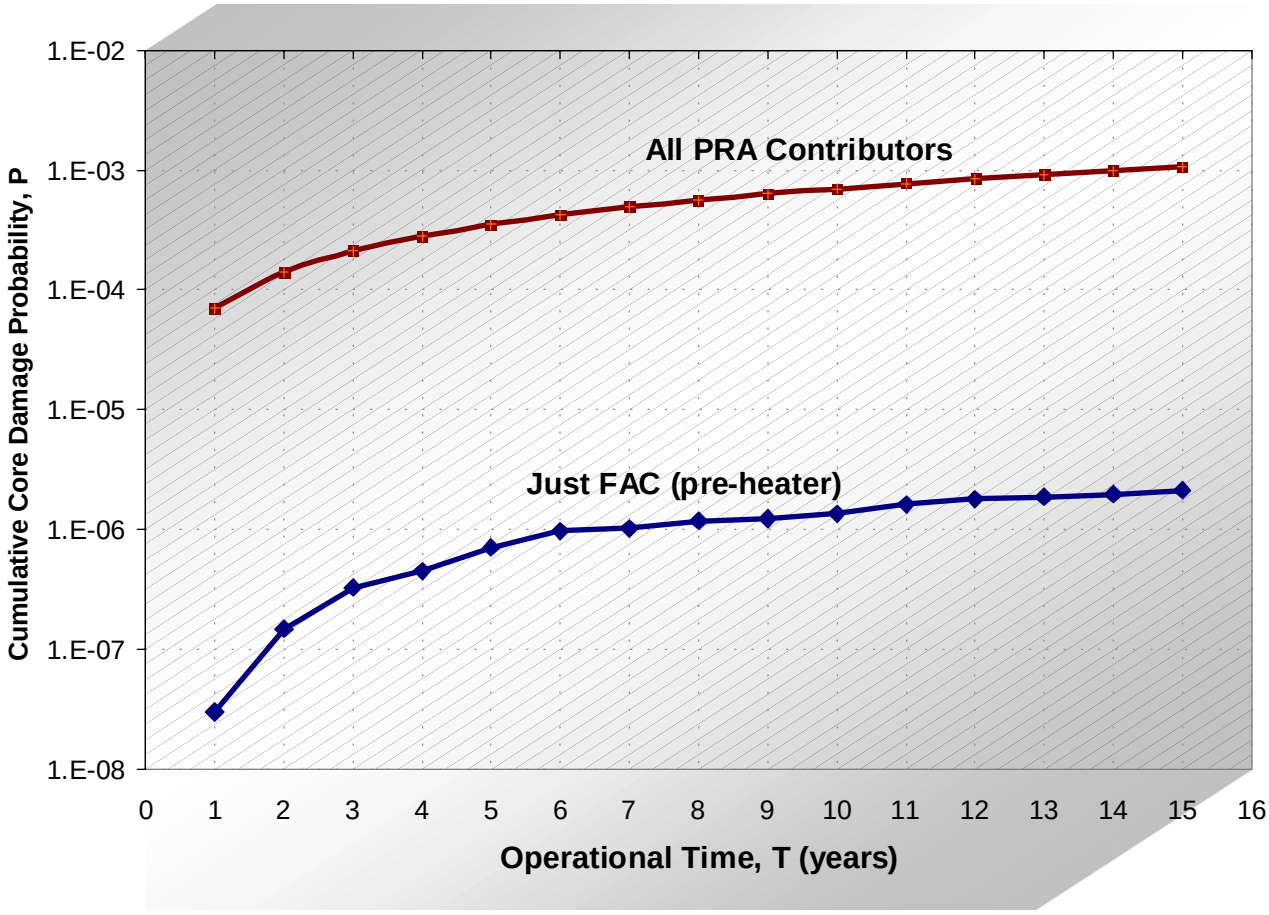

Figure 26. Cumulative core damage probability from FAC and all PRA initiators.

6. Conclusions

The overall objective of the work documented in this report was to assess the *feasibility* of applying the "LANL/ASCA" method for incorporation of reliability-physics based models, expert judgement, and the results of the NRC NPAR program and other NRC or industry programs into an integrated aging risk assessment. The "LANL/ASCA" method refers to the application of PRA methods described in NUREG/CR-6157, *Survey and Evaluation of Aging Risk Assessment Methods and Applications.*(Sanzo et. al., 1994) As documented in this report, we successfully applied an aging (FAC) reliability-physics model to the existing SAPHIRE Surry IPE risk model and subsequently determined aging-based risk insights.

6.1 General Conclusions

As part of the work, general methods were developed to facilitate the inclusion of aging mechanisms into PRA models. The outcome of development included (1) a generic process to perform the aging-to-PRA modeling, (2) a focused application of FAC failure modeling, and (3) incorporation of the FAC aging model directly into a PRA. In summary, the general methods addressed the areas of:

- The technique of screening for risk-based determination of potential aging-affected components.
- The treatment of uncertainties (aleatory and epistemic).
- The integration of deterministic models into the PRA that represents applicable aging failure mechanisms.
- The determination of component aging-caused failure probabilities via a "load-and-capacity" analysis.

Again, since this is a feasibility study, it was not the objective of the project to address all aging mechanisms nor provide a complete picture into the magnitude of the risk or core damage frequency impacts resulting from aging. The work did qualitatively discuss the spectrum of aging related issues facing LWRs. Also, the work did evaluate aging impacts on the core damage frequency. But to reiterate, these evaluations are of a feasibility nature and *should not* be construed to represent the magnitude (both absolute and relative) of risk posed by aging in LWRs.

We successfully demonstrated that the results and insights gained from the NRC's NPAR program can be integrated into existing PRA models. While we focused solely on FAC for the feasibility study, the methodology embodied in this report can be applied to other SSCs and aging mechanisms, for example, fatigue, cracking, and embrittlement.

An important aspect of the work was the determination and management of key parts of the aging mechanism failure model. For the FAC failure model, a combination of deterministic and aleatory modeling was required. The deterministic portion of the failure model was provided by using the KWU-KR FAC rate model. The KWU-KR model was used to specify the piping capacity as a function of time. The loading on the piping was provided by utilizing two models, one deterministic (for steady-state pressures) and the other aleatory (for transient pressures). Epistemic uncertainties on the model parameters, as well as the KWU model itself, were treated and incorporated directly in the analysis. It is envisioned that, in general, other aging-related reliability-physics models must be constructed in a similar fashion.

One of the important epistemic uncertainties was the model uncertainty on the FAC rate deterministic model. An adjustment factor "E" was utilized to address this uncertainty and plays a key role in the both the reliability-physics model and the resulting load-capacity model. The data that we used to assess the variability of the adjustment factor E included uncertainties due to the KWU-KR model itself and due to the numerical values of its parameters. These uncertainties were impossible to separate. In the future, when similar data are collected, an effort should be made to separate the two types of uncertainty (model and parameter) so that more accurate reliability-physics calculations can be obtained.

For the numerical determination of piping failure probabilities, two techniques were discussed. First, an analytical expression for the predictive reliability was derived [e.g., Equation (21)]. Second, a Monte Carlo simulation approach was outlined [e.g., see Equation (24)]. The work for this feasibility study evaluated both methods. We recommend that the second method, simulation, be used instead of the first method. The simulation technique for FAC was easier to implement and complemented the existing PRA framework of epistemic uncertainty propagation through fault tree models.

We demonstrated that a rigorous treatment of an important aging mechanism such as FAC need not rely on sparse failure data in an attempt to quantify a statistical failure rate. Even though the main benefit of these statistical rate models [e.g., the linear aging reliability model (Vesely, 1987)] is their simplicity and ease of application, we point out that these models do not capture the total impact or behavior of complex aging mechanisms such as FAC.

It was found that FAC in the main feedwater piping over 10 years has only a slight impact on the risk at Surry. The reason for this result is that the contribution to the total plant core damage frequency from loss of main feedwater in the Surry IPE is less than 1% of the total. Other plants may have a higher contribution to risk from FAC (if the CDF contribution from loss of main feedwater is higher). But to reiterate, this feasibility study *should not* be construed to represent the magnitude of risk posed by FAC in LWRs. While indirect effects were considered, a rigorous treatment of their impact was not performed. Considering the lack of contribution to total risk from FAC for the piping that was

studied, the indirect effects may become more important. It may be worthwhile to select piping segments located in an area susceptible to important indirect flooding effects and to find the impact on the risk. Further, note that the risk metrics used in this report were either core damage frequency or core damage probability. Other risk measures (large early release frequency, off-site consequences) could be utilized, given the availability of a PRA that provides said measures. In addition, monetary arguments were considered to be outside the scope of the feasibility assessment. The financial risk of events such as a FAC-caused rupture of main feedwater piping (which actually happened at Surry) may be important and could be quantified using the general methodology described in this report.

The impact to Surry from FAC *assuming* that it had preheater-type steam generators (which only a few plants actually have) over 15 years was evaluated in the second case study. The impact of FAC in this case was similar to the first case study. Plants with this type of preheater arrangement may have a similar contribution to risk from FAC, but this feasibility study *should not* be construed to represent the magnitude of risk posed by FAC in LWRs. For the preheater case, indirect effects were not considered since we treated the Surry model as a hypothetical plant with preheater-type steam generators.

The study did not take credit for the potential of inspections of FAC-susceptible piping locations. All plants currently have an existing inspection program for FAC. Consequently, if one were to determine that FAC was taking place at an unacceptable rate or that the thickness of a pipe was marginally acceptable, a decision could be made to replace the damaged piping. This intervention would mitigate the FAC process and usurp the potential for pipe failure (in that particular pipe). But, to take credit for an inspection program, one would need to determine a probability that the inspection program fails to detect and mitigate FAC. It was beyond the scope of this project to determine this non-detection probability, but we know that it is not zero since U.S. NPPs have had FAC inspection programs for several years while at the same time FAC events still are being recorded in the operational history.

6.2 Further Considerations

While constructing the knowledge base of information relevant to aging mechanism, details were provided for four types of important aging mechanisms: embrittlement, stress corrosion cracking, fatigue, and FAC. Of the four, only FAC was evaluated in depth. Consequently, the other three areas are fertile for a similar treatment as that performed for FAC in this report. Mechanisms such as radiation embrittlement do have well-defined reliability-physics models (e.g., the VISA-II code) available. Note that, in general, the reliability-physics models for the other mechanism could be much more complicated than that for FAC. But, given the compartmentalized structure denoted for the failure modeling described in this report, the problem of addressing other aging mechanism is solvable.

The techniques described in this report may also be applicable to non-aging issues. For example, given the availability of a failure model for pump seals (potentially leading to a loss of coolant scenario), the failure model could be incorporated directly into the PRA rather than just imbedding the *results* of the model in a basic event in the PRA. A similar application could be for embedding an off-site power recovery model directly into a PRA model. Currently, PRAs like the NRC's Simplified Plant Analysis Risk models utilize an off-site power recovery module to determine non-recovery probabilities for specific accident sequences. This type of module could be integrated directly into the PRA in the same fashion as that demonstrated for the FAC reliability-physics model, thereby giving the analyst or regulator direct access to the drivers behind these event probabilities.

Electrical component aging was deemed to be outside the scope of the feasibility assessment. Nonetheless, a preliminary investigation was made to determine the availability and types of reliability-physics models applicable to power plant electrical components. The results of the investigation showed that the reliability models which are available are focused on environmental conditions (e.g., high temperature, high humidity) causing failures. If it is desirable to evaluate electrical component aging, a concerted effort will have to be made to ensure that reliability-physics models are developed and applicable operational or testing data is available to support the models.

7. References

Ang, A. H-S. And W. H. Tang, 1975. *Probability Concepts in Engineering Planning and Design, Volume 1: Basic Principles*, John Wiley and Sons, New York.

Apostolakis, G. E., 1995. "A Commentary on Model Uncertainty," in: *Proceedings of Workshop on Model Uncertainty,"* A. Mosleh, N. Siu, C. Smidts, and C. Lui, Eds., Center for Reliability Engineering, University of Maryland, College Park, MD (also published as Report NUREG/CP-0138, US Nuclear Regulatory Commission, Washington, DC, 1994).

ASTM, 1972. "Standard Definitions of Terms Relating to Fatigue Testing and Statistical Analysis of Data," ASTM E206-72.

ASTM, 1985. "Standard Methods for Notched Bar Impact Testing of Metallic Materials," *Annual Book of ASTM Standards*, ASTM E 23-82, Vol. 03.01, American Society for Testing and Materials, Philadelphia.

Begley, J., 1988. "Application of the Gerber-Garud Strain Rate Damage Model to PWSCC," *Proceedings: 1987 EPRI Workshop on Mechanisms of Primary Water Intergranular Stress Corrosion Cracking*, EPRI NP-5987SP, Electric Power Research Institute, September, pp. D6-1 to D6-11.

Berge, P., et al., 1992. "The Effects of Chemical Factors on Stress Corrosion of Alloy 600 Exposed to the Cooling Medium in Pressurized Water Reactors," *Proceedings of the Fifth International Symposium on Environmental Degradation of Materials in Nuclear Power Systems—Water Reactors, August 25–29*, 1991, pp. 533–538.

Bier, V. M. et al, 1990. *Development and Demonstration of Methods for Nuclear Power Plant Aging Risk Analysis: Bayesian Data Analysis*, EGG-SSRE-8990, April.

Bosnak, R. J., 1987. "Meeting Minutes of 1/15/87 Technical Panel Discussion of Surry-2 Pipe Failure Implications," Memorandum to T.P. Speis, U.S. Nuclear Regulatory Commission, February 4.

Bruemmer, S. M., L. A. Charlot, and C. H. Henager, Jr., 1988. "Microstructure and Microdeformation Effects on IGSCC of Alloy 600 Steam Generator Tubing," *Proceedings: 1987 EPRI Workshop on Mechanisms of Primary Water Intergranular Stress Corrosion Cracking*, EPRI NP-5987SP, Electric Power Research Institute, Palo Alto, September, pp. C3-1 to C3-31.

Campbell, C. A. and S. Fyfitch, 1994. "PWSCC Ranking Model for Alloy 600 Components," *Sixth International Symposium on Environmental Degradations of Materials in Nuclear Power Systems—Water Reactors,* San Diego, California, pp. 863–870.

Cheok, M. C., et al., 1998. "Use of importance measures in risk-informed regulatory applications," *Reliability Engineering and System Safety*, 60, pp. 213-226.

Chexal, V. K. and R L. Jones, 1988. "Implications of the Surry Piping Failure for Other Nuclear and Fossil Units," *International Journal of Pressure Vessels & Piping, 34,* pp. 331-343.

Chexal, B and J. S. Horowitz, 1995. "Chexal-Horowitz Flow-Accelerated Corrosion Model-Parameters and Influences," *Current Perspectives of International Pressure Vessels and Piping Codes and Standards*, PVP-Vol. B, pp. 231-243. American Society of Mechanical Engineers, New York.

Chexal, B., J. S. Horowitz, R. Jones, B. Dooley, C. Wood, 1996. *Flow-Accelerated Corrosion in Power Plants*, EPRI TR-106611, Electric Power Research Institute, Palo Alto.

Chopra, O. K. and H. M. Chung, 1986. "Investigations of the Mechanisms of Thermal Aging of Cast Stainless Steels," presented at the *Metal Component Subcommittee of the Advisory Committee on Reactor Safeguards Meeting, Columbus, Ohio, July 1-2, 1986*, transcript available from the NRC Public Document Room.

Copeland, J. F. and A. J. Giannuzzi, 1984. *Long-Term Integrity of Nuclear Power Plant Components*, EPRI NP-3673-LD, Electric Power Research Institute, Palo Alto.

Coriou, H., et al., 1959. "Corrosion Fissurante Sous Contrainte De L'Inconel Dans L'Eau A Haute Temperature," in *Third Colloque de Metallurgie Corrosion, Centre d' Etudes Nucleaires de Saclay, France,* North Holland Publishing Co., Amsterdam, p. 161.

Cragnolino, G., C. Czajkowski, and W. J. Shack, 1988. *Review of Erosion-Corrosion in Single-Phase Flows*, NUREG/CR-5156, NRC, April.

Davis, T., A. Shafaghi, R. Kurth, and F. Leverenz, 1985. *Importance Ranking Based on Aging Consideration of Components Included in Probabilistic Risk Assessment*, NUREG/CR-4144, April.

Dwight, J. E., 1990. *A Structured Approach to Evaluating Aging of the Advanced Test Reactor*, EGG-M-9054, January.

Edson, J. L., 1990. *Aging Evaluation of Class 1E Batteries: Seismic Testing*, NUREG/CR-5448, EGG-2576, August.

Edson, J. L. and J. E. Hardin, 1987. *Aging of Class 1E Batteries in Safety Systems of Nuclear Power Plants*, NUREG/CR-4457, EGG-2488, July.

Egan, G. R., et al., 1987. *Inspection of Centrifugally Cast Stainless Steel Components in PWRs*, EPRI NP-5131, Electric Power Research Institute, Palo Alto.

EPRI, 1990. *PWR Primary Water Chemistry Guidelines: Revision 2*, EPRI NP-7077, Electric Power Research Institute, Palo Alto, November.

Forsyth, P.J.E., 1969. *The Physical Basis of Metal Fatigue*, Elsevier, New York.

Fuchs, H. O. and R. I. Stephens, 1980. *Metal Fatigue in Engineering*, John Wiley and Sons, New York.

Galyean, W. J. et al., 1993, *ISLOCA Research Program*, NUREG/CR-5928, U.S. Nuclear Regulatory Commission, July.

Gorman, J. A., 1989. *Survey of PWR Water Chemistry*, NUREG/CR-5116, ANL-88-43.

Gorman, J. A., et al., 1991. *Statistical Analysis of Steam Generator Tube Degradation*, EPRI-NP-7493, Electric Power Research Institute, Palo Alto.

Gosselin, S. R., F. V. Ammirato, S. M. Walker, P. O'Regan, V. Dimitrijevic, and R. Gamble, 1996. *Risk-Informed Inservice Inspection Evaluation Procedure*, EPRI-TR-106706, Interim Report, EPRI, Palo Alto, California, June.

Gosselin, S. R., 1997. "EPRI's New In-Service Pipe Inspection Program," *Nuclear News*, American Nuclear Society, La Grange Park, Illinois, November.

Harris, D. O. et al., 1992. *Theoretical and User's Manual for pc-PRAISE, A Probabilistic Fracture Mechanics Computer Code for Piping Reliability Analysis*, NUREG/CR-5864, UCRL-ID-109798.

Hoge, K. G., 1979. *Evaluation of the Integrity of SEP Reactor Vessels*, NUREG-0569.

Hunt, E. S., and J. A. Gorman, 1986. *Status and Suggested Course of Action for Nondenting-Related Primary-Side IGSCC of Westinghouse-Type Steam Generators,* EPRI NP-4594-LD, Electric Power Research Institute, Palo Alto, May 1986.

Hunt, E. S. and D. J. Gross, 1994. *PWSCC of Alloy 600 Materials in PWR Primary System Penetrations*, EPRI TR-103696, EPRI TR-103345, Electric Power Research Institute, Palo Alto, July.

Jarrell, D. B., A. B. Johnson, Jr., P. W. Zimmerman, and M. L. Gore, 1989. *Nuclear Plant Service Water System Aging Degradation Assessment*, NUREG/CR-5379, Vol. 1., NRC, Washington, D.C.

Jonas, O., 1988. *Erosion-Corrosion of PWR Feedwater Piping Survey of Experience, Design, Water Chemistry, and Materials*, NUREG/CR-5149, NRC, Washington D.C., March.

Kao, T., 1998. *Incorporating Flow-Accelerated Corrosion Effects into Probabilistic Risk Assessment*, Ph.D. Thesis, Massachusetts Institute of Technology, September.

Kaplan, S., 1983. "On a 'Two-Stage' Bayesian Procedure for Determining Failure Rates from Experiential Data," *IEEE Transactions on Power Apparatus and Systems*, Vol. PAS 102, No. 1. 195-202.

Kastner, W. and E. Riedle, 1986. "Empirical Model for Calculation of Material Losses Due to Corrosion Erosion," *VGB Kraftwerkstechnik 66*, No. 12, pp. 1023-1029.

Kastner, W., 1987. *Erosion-Corrosion Experiments and Calculation Model,* EPRI Workshop on Erosion-Corrosion of Carbon Steel Piping: Nuclear and Fossil Plants, April 14-15.

Keck, R. G., and P. Griffith, 1987. *Prediction and Mitigation of Erosion-Corrosive Wear in Secondary Piping Systems of Nuclear Power Plants*, NUREG/CR-5007.

Kennedy, A. J., 1963. *Processes of Creep and Fatigue in Metals,* John Wiley and Sons, New York.

Kondic, N. N., 1992. *NRC Research Program on Plant Aging: Listing and Summaries of Reports Issued Though July 1992*, U. S. Nuclear Regulatory Commission, Washington D.C.

Lott, R. G., et al. 1992. "Primary Water Stress Corrosion Crack Growth Rates in Alloy 600 Steam Generator Tubing," *Proceedings of the Fifth International Symposium on Environmental Degradation*

of Materials in Nuclear Power Systems—Water Reactors, Monterey, California, August 25–29, 1992, pp. 525–532.

Lucas, G. E., and G. R. Odette 1986. "Recent Advances in Understanding Radiation Hardening and Embrittlement in Pressure Vessel Steels," *Proceedings of the Second International Symposium on Environmental Degradation of Materials in Nuclear Power Systems-Water Reactors, Monterey California, September 9, 1985*, American Nuclear Society, p. 345.

Meyer, L. C., 1989. *Nuclear Plant Aging Research on High Pressure Injection Systems*, NUREG/CR-4967, EGG-2514, August.

Millett, P. J. and C. J. Wood, 1994. "Mediterranean Reflections—Recent Development in Water Chemistry," *Nuclear Engineering International*, August, pp. 14–15.

Modarres, M., 1993, *What Every Engineer Should Know About Reliability and Risk Analysis*, Marcel Dekker, Inc., New York.

Nedelko, L. and W. Kastner, 1991. "Erosion Corrosion in Nuclear Power Plant Piping," *Symposium on Plant Life Extension (PLEX) of Nuclear Power Plants*, Madrid, April 24-26, p. 1-11.

Nuclear Regulatory Commission, 1982. "Failures in Turbine Exhaust Lines," USNRC Information Notice 82-22, July 9.

Nuclear Regulatory Commission, 1991. "High-Energy Piping Failures Caused by Wall Thinning," USNRC Information Notice 91-18, March 12.

Nuclear Regulatory Commission, 1987. "Feedwater Line Break," USNRC Information Notice 86-106, Supplement 1.

Nuclear Regulatory Commission, 1992. "Rapid Flow-Induced Erosion/Corrosion of Feedwater Piping," USNRC Information Notice No. 92-07.

Nuclear Regulatory Commission, 1998. *450th Advisory Committee on Reactor Safeguards Transcripts*, Washington D.C., March.

Odette, G. R., and G. E. Lucas 1986. "Irradiation Embrittlement of Reactor Pressure Vessel Steels: Mechanisms, Models and Data Correlations," *Radiation Embrittlement of Reactor Pressure Vessel Steels: An International Review*, ASTM STP 909, L. E. Steele (ed.), American Society for Testing and Materials, Philadelphia, p. 206.

Odette, G. R. 1983. "On the Dominant Mechanism of Irradiation Embrittlement of Pressure Vessel Steels," *Scripta Metallurgica, 17*, p. 1183.

Phillips, J. H., 1993. *Demonstration of a Method to Include An Aging Passive Component in a PRA (Draft)*, NUREG/CR-5730, EGG-2646, December.

Poore, W.P., 1996. Personal Communication with W. P. Poore at the Oak Ridge National Laboratory (ORNL), Dec. 6 through 16, 1996.

Rao, G. V. 1994. "Methodologies to Assess PWSCC Susceptibility of Primary Component Alloy 600 Locations in Pressurized Water Reactors," *Sixth International Symposium on Environmental Degradations of Materials in Nuclear Power Systems—Water Reactors,* San Diego, pp. 871–882.

Remy, F. N. and M. Bouchacourt 1992. "Flow-Assisted Corrosion: A Method to Avoid Damage," *Nuclear Engineering and Design*, 133, p. 23-30.

Roberts, E. W., J. L. Edson, and A. C. Udy, 1996. *Aging of Safety Class 1E Transformers in Safety Systems of Nuclear Power Plants*, NUREG/CR-5753, INEL-95/0573, February.

Russell, K. D. et al., 1994. Systems Analysis Programs for Hands-On Integrated Reliability Evaluations (SAPHIRE), U.S. Nuclear Regulatory Commission, NUREG/CR-6116, Washington D.C.

Sanzo, D. P. Kvan, G. Apostolakis, J. Wu, T. Milici, N. Ghoniem, and S. Guarro, 1994. *Survey and Evaluation of Aging Risk Assessment Methods and Applications*, NUREG/CR-6157, NRC, November.

Scarberry, R. C., S. C. Pearman, and J. R. Crum 1976. "Precipitation Reactions in Inconel Alloy 600 and Their Effect on Corrosion Behavior," *Corrosion-NACE*, Vol.32, No. 10, October, pp. 401–406.

Selby, D. L., et al. 1985. *Pressurized Thermal Shock Evaluation of the H. B. Robinson Unit 2 Nuclear Power Plant,* NUREG/CR-4183, ORNL/TM-9567/V1.

Shah, V. N. and P. E. Macdonald, 1993. *Aging and Life Extension of Major Light Water Reactor Components,* Elsevier Science Publishers.

Shah, V. N., A. G. Ware, A. M. Porter, 1997. *Review of Industry Effort to Manage Pressurized Water Reactor Feedwater Nozzle, Piping, and Feedring Cracking and Wall Thinning*, NUREG/CR-6456.

Shah, V. N., S. K. Smith, and U. P. Sinha, 1994. *Insights for Aging Management of Light Water Reactor Components*, NUREG/CR-5314-V5, EGG-2562, March.

Siu, N. O. and G. E. Apostolakis, 1982. "Probabilistic Models for Cable Tray Fires," *Reliability Engineering*, 3:213-227.

Steele, L. E. 1975. *Neutron Irradiation Embrittlement of Reactor Pressure-Vessel Steels*, Technical Report Series No. 163, International Atomic Energy Agency, Vienna, p. 124.

Stein, A. A., and A. R. McIlree 1986. "Relationship of Annealing Temperature and Microstructure to Primary-Side Cracking of Alloy 600 Steam Generator Tubing and the Prediction of Stress Corrosion Cracking in Primary Water," *Proceedings of the Second International Symposium on Environmental Degradation of Materials in Nuclear Power Systems-Water Reactors,* American Nuclear Society, La Grange Park, Illinois, pp.47.

Stoller (S. M. Stoller Corporation), 1989. "Reactor Trip, ESF Actuations - HP Turbine Extraction Steam Line Ruptured - Pipe Thinning - Erosion, Corrosion - Other Problems Noted After Trip," *Nuclear Power Experience*, P.06E.0923.

Stoller (S. M. Stoller Corporation), 1993. "Manual Reactor Trip-High Generator Voltage-Steam in Voltage Regulator Cubicle-Extraction Steam Line Rupture-Erosion/Corrosion-Inadequate Management Oversight," *Nuclear Power Experience*, P.06.E.1211.

Stout, R. D. 1985. "Postweld Heat Treatment Pressure Vessel Steels," *Bulletin 302*, Welding Research Council, New York, p. 1.

Tatone, O. S. and R. S. Pathania 1985. "Steam Generator Tube Performance: Experience with Water-Cooled Nuclear Power Reactors During 1982," *Nuclear Safety, 26, 5*, pp. 623-639.

Theus, G. J., 1986. "Primary Side Stress Corrosion Cracking and Remedial Measures," *Transactions of the American Nuclear Society, 53,* pp. 207-209.

Tillack, D. J., and E. B. Fernsler, 1981. "Heat Treating of Nickel and Nickel Alloys," Metals Handbook Ninth Edition, Volume 4, Heat Treating, American Society for Metals, Metals Park, Ohio, pp. 754–759.

Vesely, W. E., 1987. *Risk Evaluation of Aging Phenomena: the Linear Aging Reliability Model and Its Extension,* NUREG/CR-4769, USNRC, Washington, D. C.

Vesely, W. E., R.E. Kurth, and S.M. Scalzo, 1990. *Evaluation of Core Melt Frequency Effects Due to Component Aging and Maintenance*, NUREG/CR-5510, June.

Vesely, W. E., 1992. *Approaches for Age-Dependent Probabilistic Safety Assessments with Emphasis on Prioritization and Sensitivity Studies*, NUREG/CR-5587, August.

Virginia Power 1987. *Surry Unit 2 Reactor Trip and Feedwater Pipe Failure Report*, Rev. 0.

Vora, J. P., 1993. *NRC Research Program on Plant Aging: Listing and Summaries of Reports Issued Through September*, NUREG-1377, Rev. 4, U.S. Nuclear Regulatory Commission, December.

Wesley, D. A., 1992. *Screening Methods for Developing Internal Pressure Capacities for Components in Systems Interfacing with Nuclear Power Plant Reactor Coolant Systems*, NUREG/CR-5862, U.S. Nuclear Regulatory Commission, May.

Wolford, A. J., C. L. Atwood, 1992. *Aging Data Analysis and Risk Assessment-Development and Demonstration Study*, NUREG/CR-5378, August.

Westinghouse Energy Systems, 1996. *Westinghouse Owners Group Application of Risk-Based Methods to Piping Inservice Inspection Topical Report*, WCAP-14572.

Appendix A

Models and Codes Available for Quantitative Estimates of Aging Damage

Appendix A

Models and Codes Available for Quantitative Estimates of Aging Damage

A-1. Radiation Embrittlement of Ferritic Low-Alloy Steels

USNRC requirements assessing radiation embrittlement of RPVs are specified in the U.S. Code of Federal Regulations (which includes endorsement of the ASME Boiler and Pressure Vessel Code), plant technical specifications, and plant operating procedures. In addition, the USNRC has established further recommendations and requirements through issuance of regulatory guides, branch technical positions, information notices, bulletins, and generic letters. Table A-1 chronologically lists key regulatory rule implementation/changes and guidance since the early 1970s to 1994. These requirements address the primary issues associated with radiation embrittlement of the reactor pressure vessels: operating pressure-temperature curves, pressurized thermal shock (PTS), low upper shelf toughness, and defect evaluation and acceptance. Each U.S. nuclear power plant is required to have a surveillance monitoring program (per Appendix H of 10 CFR 50) to ensure physical measurement of property changes indicative of the embrittling process occurring over time within the reactor pressure vessel wall.

The assessment methodology for radiation embrittlement is very straight forward. Namely, perform post-radiation mechanical testing of reactor pressure vessel material from surveillance capsules in accordance with a prescribed surveillance capsule withdrawal schedule. Once the surveillance capsule data are available, radiation embrittlement can be estimated and pressure/temperature curves can be generated using the methodology given in Appendix G to ASME Section III of the Boiler and Pressure Vessel Code. Radiation embrittlement estimates can be made using the methodology given in Regulatory Guide 1.99, Rev. 2.

Several computer codes have been developed for evaluation of structural integrity of reactor pressure vessel. Only one of these codes, VISA-II Code (Vessel Integrity Analysis Code), is in public domain. The VISA-II Code performs both deterministic and probabilistic analysis to determine reactor vessel failure probability following through-wall cracks caused by PTS events (Simonen et al. 1986). The deterministic portion of the code performs heat transfer, stress, and fracture mechanics calculations for the vessel subjected to a temperature and pressure transient specified by the user. The probabilistic portion of the code performs a Monte Carlo simulation to estimate the probability of vessel failure. Parameters such as initial crack size and position, copper and nickel content, fluence, and the fracture toughness values for crack initiation and arrest are treated as random variables. Linear elastic fracture mechanics methods are used to model crack initiation and growth. The fraction of vessel failures (through-wall cracks) in a large number of simulations provides an estimate of the vessel failure probability.

Table A-1. Key regulatory changes and guidance for RPV integrity.

Date	Regulatory document	Comments
Before 1971	10 CFR Part 50, Domestic Licensing of Production and Utilization Facilities	Very general design criteria in this section were the only requirements for the reactor vessel. Pre-1960 vessels were constructed according to ASME Section VIII; after 1960 according to Section III.
1971	10 CFR 50.55a, Codes and Standards	Professional society codes and standards, including ASME Section XI requirements for reactor vessel inspection, were incorporated by reference into the regulations. 10 CFR 50.55a is periodically updated to reference the latest ASME Code editions.
	10 CFR 50, Appendix A, General Design Criteria (GDC)	The GDC were first developed in 1965 and published for comment in 1967. They were published as a final rule in 1971. The key RPV requirements are contained in GDC 15, Reactor Coolant System Design, GDC 31, Fracture Prevention of Reactor Coolant Pressure Boundary, and GDC 32, Inspection of Reactor Coolant Pressure Boundary.
1973	10 CFR 50, Appendix G—Fracture Toughness Requirements	The bases for this Appendix are (1) ASME Code Section III, Division 1, Rules for Construction of Nuclear Power Plant Components, including Appendix G (Protection Against Non-Ductile Failure) and (2) ASME Code Section XI, Division 1, Rules for Inservice Inspection of Nuclear Power Plant Components.

Date	Regulatory document	Comments
	10 CFR 50, Appendix H—Reactor Vessel material Surveillance Program Requirements	ASTM E 185, "Standard Practice for Conducting Surveillance Tests for Light-Water Cooled Nuclear Power Reactor Vessels," is incorporated by reference.
1975	Standard Review Plan (SRP) 5.3.2—Pressure-Temperature Limits	Guidance on establishing pressure-temperature curves for heatup and cooldown.
	RG 1.99—Effects of Residual Elements on Predicted Radiation Damage to Reactor Vessel Materials	Guidance for predicting radiation damage effects
1977	RG 1.99, Rev. 1—Effects of Residual Elements on Predicted Radiation Damage to Reactor Vessel Materials	Copper and phosphorus are key residual elements affecting the degree of radiation damage.
1983	10 CFR 50.60, Acceptance Criteria for Fracture Prevention Measures for Light Water Nuclear Power Reactors for Normal Operations.	Implemented with revised reference to Appendices G and H.
1985	10 CFR 50.61—Fracture Toughness Requirements for Protection Against Pressurized Thermal Shock Events	PTS Rule requirements first implemented.
1987	RG 1.154—Format and Content of Plant-Specific Pressurized Thermal Shock Safety Analysis Reports for Pressurized Water Reactors	Provides a probabilistic analysis procedure to be used three years before the PTS screening criteria are reached.
1988	RG 1.99, Rev. 2—Effects of Residual Elements on Predicted Radiation Damage to Reactor Vessel Materials	Added nickel and removed phosphorous as a key residual element. New statistical correlation.
1991	10 CFR 50.61—Fracture Toughness Requirements for Protection Against Pressurized Thermal Shock Events	Revised to incorporate RG 1.99, Rev. 2 methodology for determining RT_{PTS}.

Date	Regulatory document	Comments
1992	10 CFR 50.55a	Updated to incorporate the 1989 Edition of ASME Section XI, which requires inspection of 100% of the RPV welds; expedited schedule was added and previously approved relief requests were revoked.
1993–1996	The following new guidance or rule making are being developed: (1) Regulatory Guide on dosimetry (2) Regulatory Guide on evaluation of vessels with low upper shelf energy (3) Regulatory Guide on annealing (4) Standard Review Plan defining course of action for indeterminate vessel condition, information needed to evaluate Justifications for Continued Operation (JCOs), and augmented inspection requirements if PTS screening criterion is exceeded (5) 10 CFR 50 Rule on annealing.	All items except the regulatory guide on dosimetry, are primarily the result of the review of the Yankee Rowe reactor vessel restart program.
	The following regulations or existing guidance are being amended: (1) 10 CFR 50, Appendix G (2) 10 CFR 50, Appendix H (3) 10 CFR 50.61 (4) RG 1.154 (5) RG 1.99 (see comments).	Embrittlement trend data from material surveillance results and from research programs are being evaluated. This evaluation will determine if changes to Regulatory Guide 1.99, Revision 2, are warranted. A decision concerning potential revisions to this guide is expected in 1995.

A-2. Thermal Aging of Cast Stainless Steels

Chopra (1992a,b) has developed two different approaches to determine the extent of the thermal aging of cast stainless steel. These approaches quantify the extent of aging at the PWR operating temperatures [288°C (550°F)] by measuring the room-temperature Charpy impact energy after aging at temperatures in the range of 300 to 400°C (570 to 750°F). The higher aging temperature (400°C) is often employed to accelerate the rate of thermal aging compared with that occurs at normal PWR operating temperatures. The first approach provides a means for estimating the lower bound fracture toughness after long-term thermal aging, whereas the second approach provides means for estimating fracture toughness at a given service time and temperature.

Chopra (1992b) has also developed a procedure for estimating mechanical properties, i.e., CVN and elastic-plastic fracture toughness, of thermally aged cast stainless steel piping components. The procedure is divided into three parts: (a) estimation of lower-bound material properties of steels with unknown chemical composition, (b) estimation of saturation material properties of steels with known chemical composition but unknown service history, and (c) estimation of material properties at time and temperature for steels having known chemical composition and service history. The estimation of lower-bound material properties, required by the first part of the procedure, is based on the worst-case chemical composition (>15% ferrite), which is very conservative for most steels. A more realistic lower bound can be developed if the ferrite content is known.

For the second part of the procedure, the estimation of the saturation (long-term) mechanical properties does not explicitly use the initial properties. So, as discussed, the saturation properties need to be compared with an estimate of the initial mechanical properties. If the initial properties are lower than the saturation properties, then the initial properties are treated as the saturation properties. If the initial properties are not available, the lower-bound initial properties based on the chemical composition may be used.

For the third part of the procedure, the estimation of the material properties at time and temperature requires that the initial properties of the unaged material are known. If the estimated fracture toughness is higher than the minimum initial fracture toughness of the unaged material, the latter is used as the estimated fracture toughness at time and temperature.

A-3. Low-Cycle Fatigue

Cyclic stresses of sufficient magnitude will initiate a crack. Then, during succeeding cycles, the crack will grow until it progresses through the wall. It was shown by Coffin (1954) in a cyclic constant strain range test that the fatigue life of a small, smooth-polished specimen was proportional to the range of strain imposed on the specimen. Since most of the fatigue life of a small smooth specimen is in the precrack phase, it may be inferred that the range of strain determines the onset of crack initiation. Later, it was shown by Paris (1964) that the amount of growth of a given crack under a given cyclic stress correlates almost exactly with the applied stress intensity range, ΔK, which is a function of the crack size, shape, stress level, and geometry.

Fatigue Crack Initiation The PWR main coolant piping is designed and analyzed on the basis of Section III of the ASME Code. The ASME Code provides fatigue design curves that are entirely based on data obtained from in-air tests mainly at room temperature. The ASME design curves were developed by applying a factor of 2 on stress or 20 on cycles, whichever is lower, to the mean failure curve for small, polished specimens. For less than 10,000 cycles, the factor 20 on cycles gives the lower curve. These factors are intended to account for size effects, surface finish, statistical scatter of the data, and differences between laboratory and industry environments, but not the effects of a specific coolant and temperature. The factor 20 on cycles is a product of three subfactors: a subfactor of 2.5 for size, 2.0 for data scatter, and 4.0 for surface finish and atmosphere. Large-scale carbon steel vessel fatigue tests have been performed in air at room temperature for the express purpose of checking the ASME fatigue design curve (Kooistra et al. 1961). It was shown by these tests that cracks may initiate below the ASME fatigue design curves, but that wall penetration is not expected until the fatigue cycles exceed the ASME design curves by about a factor of 3 (Cooper 1992). Recent in-air fatigue tests on ferritic and stainless steel elbows, subject to inplane bending moments at room temperature, have also shown that cracks initiate when the fatigue design curve is reached, and that full-wall penetration occurs when the fatigue cycles exceed the design curve by a factor between 2 and 3 (Kussmaul, et al. 1988).

However, recent results from fatigue tests with small, polished specimens show that the effects of high-temperature oxygenated pure water (simulating a PWR environment) on the fatigue strength of carbon steels are not fully accounted for in the ASME design curves (Terrell 1988, Iida et al. 1988). The results also show that the changes in fatigue strength are primarily caused by the PWR operating temperature rather than the PWR coolant. The failure data curves for these specimens are below the failure data used to develop the ASME design curve for carbon steel. The PWR environment reduces the number of cycles to failure by a maximum of a factor of three. Figure A-1 shows the results of the in-air fatigue tests on smooth SA 106-B steel specimens at room temperature and at a typical PWR operating temperature (288°C). The tests were performed at a load ratio R equal to -1 (R= minimum load/maximum load). The mean data curve at 288°C falls below the ASME mean data curve (room temperature data) in the low-cycle regime by as large as a factor of 3. Therefore, as far as the fatigue behavior at 288°C is concerned, the ASME Section III design curve for the carbon steel represents less than the intended factor of 2 on stress or 20 on cycles. A revised design curve, dashed line in Figure

A-1, could be obtained by applying the factors 2 and 20 to the mean data curve at 288°C; as before, the factors are intended to account for size effect, surface finish, data scatter, and atmosphere. However, any revision of the ASME design curve should be based on comprehensive test results. These tests should account for variables such as types of steel, chemical compositions, test temperatures, and PWR environment.

Fatigue tests with Type 304 and Type 316 stainless steel specimens at 300°C in air and in PWR and BWR water have been performed in Japan (Higuchi and Iida 1992). Again, the failure data from these specimens are generally below the mean failure curve used to develop the ASME design curve for stainless steel. The Japanese data do not indicate clearly whether the observed reduction in fatigue strength was due to the high temperature or the PWR coolant environment. However, the results from these tests indicate that the fatigue design curve for these stainless steels should probably be conservatively shifted downward by a factor of 3 on cycles. Additional fatigue tests with Type 304 and Type 316 stainless steel specimens in a PWR environment should be performed to confirm these results and develop a new design curve. Fatigue test results for thermally aged Grade CF-8M stainless steels indicate that thermal aging has no effect on fatigue-crack initiation as measured with an S-N curve (Buchalet et al., 1986). Similar data for Grades CF-8 and CF-8A stainless steels are needed.

Fatigue Crack Growth in Carbon Steel and Low-Alloy Steel. Cyclic crack growth rates are typically depicted by a relationship involving (a) the maximum stress intensity factor K_{max} (where the stress intensity factor K defines the increase in the applied stress field in the vicinity of the crack tip), and (b) the cyclic stress intensity range ΔK, [which is the difference between the maximum and minimum stress intensity factors (K_{max} - K_{min}) during a given cycle]. In other words,

$$\text{cyclic crack growth rate} = da/dN = f(K_{max}, \Delta K) = f(R,\Delta K)$$

$$= C_o (\Delta K)^n \qquad \text{(A-1)}$$

where variables *a* and *N* in da/dN are crack length and number of cycles, respectively, C_o is a scaling factor, and R is the load ratio (K_{min} /K_{max}). A typical example of fatigue crack growth rates for subsurface flaws (air environment) in low-alloy steel is as follows (ASME 1995). The relationship between the crack growth rate and ΔK, for a given ratio *R*, is linear on a log-log scale:

$$da/dN = (1.99 \times 10^{-10}) S(\Delta K)^{3.726} \text{ in./cycle} \qquad \text{(A-2)}$$

where *S* is a scaling parameter to account for the R ratio. For $0 \le R \le 1$, $S = 25.72(2.88 - R)^{-3.07}$. ASME (1995) provides expressions for S for other values of the ratio R. The applied stress intensity factor K is in $ksi.in^{0.5}$. Reference fatigue crack growth rate curves given by Equations [A-1] and [A-2] are presented in Figure A-2.

Crack growth rates are also influenced by the environment. For surface flaws in a light water reactor environment, the relationship is bilinear on a log-log scale. For high ΔK,

$$da/dN = (1.01 \times 10^{-7}) S (\Delta K)^{1.95} \text{ in./cycle,} \quad \text{(A-3)}$$

where the parameter S is given by

$$\begin{aligned} S &= 1 && (0.0 \le R \le 0.25) \\ &= 3.75R + 0.06 && (0.25 \le R \le 0.65) \\ &= 2.5 && (0.65 \le R \le 1.0) \end{aligned}$$

and for low ΔK,

$$da/dN = (1.02 \times 10^{-6}) S (\Delta K)^{5.95} \text{ in./cycle,} \quad \text{(A-4)}$$

where the parameter S is given by

$$\begin{aligned} S &= 1.0 && (0.0 \le R \le 0.25) \\ &= 26.9R - 5.725 && (0.25 \le R \le 0.65) \\ &= 11.76 && (0.65 \le R \le 1.0) \end{aligned}$$

Equation [A-3] is applied when ΔK is greater than the corresponding value at the intersection of the curves given by Equations [A-3] and [A-4], and Equation [A-4] is applied for smaller ΔKs. Reference fatigue crack growth rate curves given by Equations [A-3] and [A-4] are presented in Figure A-3.

Fatigue Crack Growth in Austenitic Stainless Steels The fatigue crack growth model presented here is based on the EPRI Database for Environmentally Assisted Cracking (EDEAC) (James and Jones 1985). This database includes data from tests conducted at various load ratios, cyclic frequencies, environments, temperatures and neutron irradiation levels. The model presented here can be used for predicting the extension of existing flaws in pressure vessel and piping components exposed to air environments. This model is in the current ASME Code (ASME 1995). The crack growth behavior in the LWR water environment is currently being evaluated.

There are several parameters that may potentially affect fatigue crack growth behavior of austenitic stainless steels in an air environment: heat-to-heat variations, carbon content, grain size, product form, cold work, thermal aging, neutron irradiation, weld metal and weldments, frequency, R-

ratio (mean stress), temperature, and cyclic stress intensity range. However, evaluation of the EDEAC data show that the first three of these parameters (heat-to-heat variations, carbon content, grain size) have little or no influence on the fatigue crack growth behavior of the austenitic stainless steels in an air environment.

Little information is available for the effect of product form on fatigue crack growth behavior of austenitic stainless steels. Based on the limited information, it is assumed that the crack growth behaviors of different product forms of the same wrought alloy do not differ significantly. Fatigue crack growth rates in Grade CF-8 (the cast version of wrought Type 304 SS) have been shown to be equivalent to or slightly lower than growth rates in wrought Type 304 SS. However, there is some uncertainty about the fatigue crack growth rates in Grade CF-8M (the cast version of wrought Type 316 SS). The fatigue crack growth model presented later in the section may be used when data from actual product form are not available. Small amount of cold work that might be introduced incidently into the structure by machining, fabrication, or installation procedures has a little effect on the crack growth rate and it is conservatively represented by the crack growth rate in the air environment. A large amount of cold work (20-25%) is known to produce a small reduction in the fatigue crack growth rate, but such a amount of cold work is generally not present in the LWR pressure vessel and piping components. Thermal aging of austenitic stainless steel components at the operating LWR temperature generally has no deleterious effect on the fatigue crack growth rates in an air environment. This holds true for both base metal and weldments. Often the crack growth rates for the thermally aged components are lower. Neutron irradiation does not produce higher fatigue crack growth rates in austenitic stainless steel base metal and weldments for neutron fluences up to about 1×10^{22} n/cm^2 ($E > 0.1$ MeV) and irradiation temperatures below 900°F.

A significant percentage of actual defects encountered in structural components are at or in the vicinity of welds. Austenitic stainless steel welds have different microstructures than wrought stainless steels. These variations along with several welding variables (weld process, delta ferrite level, flux and filler rods, residual stresses, etc.) can produce variation in the fatigue crack growth behavior. However, in spite of these differences, fatigue crack growth rates in austenitic steel weldments, in the absence of residual stresses are generally equal to or lower than the rates in the wrought austenitic stainless steels under similar conditions. These differences do not justify development of separate model for weldments. Therefore, the weldment data were combined with the data for wrought and cast materials to develop the model.

The main parameters affecting the fatigue crack growth rate in the austenitic stainless steel in the air environment are cyclic frequency, cyclic stress ratio (R-ratio or mean stress effect), temperature, and cyclic stress intensity range. Cyclic frequency effects can be significant for austenitic stainless steel tested in an aggressive environment (e.g. air, water, etc.) at elevated temperature. The crack growth per cycle increases with the decreasing cyclic frequency. Loading wave forms generally do not have a significant effect upon fatigue crack growth behavior of stainless steel in the air environment at LWR

operating temperatures; however, at high temperature (>1100°F) the creep-fatigue interactions should be considered.

The fatigue crack growth model applicable to austenitic stainless steels in air is

$$da/dN = C\ F\ S\ [\Delta K]^{3.3} \qquad \text{(A-5)}$$

where

da/dN = crack growth rate per cycle (in./cycle)
C = correction factor for temperature
F = correction factor for frequency
S = correction factor for R-ratio
R = K_{min}/K_{max}
K = stress intensity factor (ksi.in.$^{0.5}$)
ΔK = $K_{max} - K_{min}$ (ksi.in.$^{0.5}$)

The correction factors for temperature and frequency are given by third degree polynomials as shown in Figures A-4 and A-5, respectively. Use of correction factor for frequency is only recommended for application at 800°F and above where time-dependent effects in air become more pronounced; use below 800°F could lead to overly conservative estimates of time-dependent effects.

The correction factor for R-ratio is given in Figure A-6. When both K_{min} and K_{max} are negative, the correction factor S should be taken as unity. The correction factor S is based on R-ratio data for the temperature in the vicinity of 550 to 600°F. Therefore, the correction factor S should be applied to that temperature range.

The crack growth model presented by Equation [A-5] is validated by the results of some fatigue crack growth experiments that were not used in developing the model. The validation results show that the model presented by Equation [A-5] provides estimates for crack extension in stainless steel in an air environment that are both conservative and reasonably accurate.

This model has been adopted by the ASME Section XI. The reference fatigue crack growth curves for austenitic stainless steels in air environments are presented in Figure A-7.

Equations [A-5] may be used to estimate the cumulative growth of a detected flaw during a specified period of normal operation. This involves identifying design basis transients during the period

and estimating incremental flaw growth for each of the transients in a chronological order. Flaw length and depth are updated at the end of each transient by the incremental flaw growth estimated during the transient. The allowable sizes for flaws oriented either in circumferential or axial direction are defined in the nonmandatory Appendix C of ASME Section XI (ASME 1995).

Environmental Effects The fatigue crack growth curves for austenitic stainless steels in PWR environment are steeper than those in an air environment shown in Figure A-7. But the effect of R-ratio and temperature on the fatigue crack growth rate are very similar. The fatigue crack growth curves for PWR environment are currently being developed. The fatigue crack growth curves for BWR environment will be developed later (Bamford, Jones, and James 1989).

Fatigue Crack Growth Rate in Cast Stainless Steels Several researchers have evaluated the low-cycle fatigue-crack- growth properties of cast stainless steels, mainly of Grade CF-8M. Landerman and Bamford (1978) found that Grade CF-8M stainless steel exhibited about the same fatigue crack-growth resistance as comparable wrought alloys, and that aging at 427°C (800°F) for 3000 h had no significant effect on the fatigue crack-growth resistance in either air or simulated PWR water environments. Slama et al. (1983) also evaluated the fatigue crack-growth resistance of cast stainless steels at both room temperature and 320°C (610°F). They also found that the fatigue crack-growth rate in air was not significantly affected by thermal aging. However, they found that the fatigue-crack-growth rates for aged CF-8M stainless steel increased by as much as a factor of 10 when tested in a simulated PWR water environment, compared to testing in air at 320°C (610°F), but did not exceed the upper-bound design fatigue-crack-growth-rate curve for stainless steels. No fatigue-crack-growth rate results for Grades CF-8 and CF-8A stainless steels in a PWR environment are currently available. These data need to be developed because the main coolant piping in several PWRs are made of these steels.

A-4. High-Cycle Vibrational Fatigue of Welded Piping Connections

There are two approaches for high-cycle vibrational fatigue analysis of socket-welded small-diameter piping connections and fillet welded attachments: (1) ASME Section III fatigue design which is an analysis-based approach, and (2) American Association of State Highway Transportation Officers (AASHTO) fatigue design which is an empirical approach. These two approaches are discussed here and their advantages and limitations have been identified.

ASME Section III Fatigue Design The ASME Code Class 1 piping is subject to ASME Section III fatigue analysis procedures. However, the socket welds of small-diameter piping were not subject to analysis by the ASME Section III Code because of their size and/or location. These procedures are most frequently applied to low-cycle fatigue loading conditions, such as those occur during plant heat up, cool down and other thermal transients, rather than high-cycle fatigue conditions. In additions, the fatigue design curves in ASME Section III are based on small, smooth specimen data rather than actual weldment fatigue data. Therefore, the detrimental effects of weldments on fatigue life are accounted for by the use of fatigue strength reduction factors along with detailed stress analyses of component (Vecchio 1996).

The difficulty with the analytically based approach of ASME Section III is the estimate of a sufficiently accurate local peak stresses including the effects of stress concentrations introduced by weld geometry such as a toe-undercut and fabrication defects such as incomplete penetration. The stress analysis may not accurately estimate the peak stress. If these stress concentrations are present, the fatigue life of a socket-welded piping connection may be significantly reduced or eliminated. Since the ASME Section III fatigue curves include fatigue crack initiation as a significant portion of the total fatigue life, particularly in the high-cycle regime, loss of fatigue crack initiation portion of the total life can result in non-conservative life estimate (Barsom and Vecchio 1995). The laboratory test results supports this assessment. The results show that the fatigue strength reduction factors for socket welds are much larger than the ASME Code values, and therefore, the ASME Section III Code does not always ensure a conservative design for socket-welded piping connections subject to vibrational fatigue (Higuchi et al. 1996). However, it is worth it to notice at this point that, in general, the ASME Section III procedures (NB-3200 and NB-3650) yield conservative lives for vessels and piping subject to low-cycle fatigue (Kooistra et al. 1961, Ware et al. 1995).

AASHTO Fatigue Design In contrast to analysis-based approach such as ASME Section III fatigue design approach, this empirically based approach does not depend on complex stress analysis. Instead, this approach rely on statistically significant data from the fatigue tests of actual or full-sized weldments. With the use of statistical data, the design curves can be specified with known confidence levels with respect to mean. In addition, this approach requires estimate of nominal or net applied stress instead of highly complex local stresses. The effects of stress concentrations caused by weld geometry

and defects, which can not be easily characterized by the stress analysis, are incorporated in the fatigue design curves.

The National Cooperative Highway Research Program (NCHRP), *The Effect of Weldments on the Fatigue Life of Steel Beams,* studies showed that the two important parameters affecting the fatigue life estimated by this approach are the weld type and the nominal applied stress range. The mean stress and material strength had only secondary effects on weldment fatigue life. The mean stress effects are accounted for in the design fatigue curves by virtue of the fact that the welded fatigue test specimens used for developing the design curves contained high tensile residual stresses. These studies also showed that fatigue damage could also occur at weld details located in relatively low stress fields which were subjected to high-cycle loading in excess of $2x10^6$ cycles. The AASHTO design curves were modified in 1974 using the NCHRP results (Barsom and Vecchio 1995). Fatigue analysis of socket-welded connection using appropriate AASHTO fatigue curve has provided results that compare well with the full-size test results (Vecchio 1996).

A-5. Primary Water Stress Corrosion Cracking of Alloy 600 Components

Based on the stress and temperature dependencies as described by Equations [1] and [2] in Section 2.1.5, the damage rate for PWSCC of Alloy 600 can be described by an equation of the form

$$\text{damage rate} \propto \sigma^4 \exp(-Q/RT) \qquad [A\text{-}6]$$

The time to crack initiation, t_i, is given by

$$t_i \propto (\text{damage rate})^{-1}$$

$$= A\sigma^{-4}\exp(Q/RT) \qquad [A\text{-}7]$$

where the constant *A* is a scaling factor determined by using some standard stress level and reference temperature. The value of *A* will change whenever there is a systematic change in the material characteristics, the average stress level at the location of interest, or other conditions that may depend on type of component and differ from plant to plant. The constant *A* for steam generator tube, tube plugs, CRDM nozzles, and other penetrations is likely to be different because different fabrication and installation procedures are used.

Statistical analyses are performed to predict crack initiation times for steam generator tubes. Weibull distribution along with Equation [A-7] is used to predict the times to crack initiation (Lipson

and Sheth 1973, Shah et al. 1992). Similar approach is also used to predict the times to failure, where failure of a tube is defined as the event when the tube is removed from service by plugging or repaired by sleeving. Lognormal distribution instead of Weibull distribution is also used for making similar predictions. Weibull and lognormal distributions are also used for predicting failure times for mechanical plugs for steam generator tubes.

Deterministic analysis are performed to predict PWSCC initiation and growth times in thick-wall components such as CRDM nozzles and pressurizer penetrations. Equation [A-7] may be used for predicting crack initiation. For PWSCC growth, the model developed by P. M. Scott of Framatome may be used (Scott 1991). The Scott model is based on PWSCC growth rate data obtained by Smialowska et al. of Ohio State University. The data were developed at 330°C and included the effects of several different water chemistries. Only those data associated with standard primary water chemistry of 2 ppm Li, 1200 ppm B, and pH = 7.3 were considered in developing the model. The equation fitted to these data is

$$da/dt = 2.8 \times 10^{-11} (K_I\text{-}9)^{1.16} \quad m/sec \qquad [A\text{-}8]$$

where da/dt is a PWSCC growth rate and K is a crack tip stress intensity factor in $MPa.m^{0.5}$. The model presents the PWSCC crack growth rate at 330°C as a function of the applied crack tip stress intensity factor K_I. The equation implies a threshold value of $K_{ISCC} = 9$ $MPa.m^{0.5}$; no crack growth takes place when the applied crack tip intensity factor is less than K_{ISCC}. This value of K_{ISCC} appears to be reasonable because some other test results also indicate that K_{ISCC} for Alloy 600 in primary water would be in the range of 5 to 10 $MPa.m^{0.5}$ (Rebak et al. 1992).

The specimens used by Smialowska et al. for crack growth tests were machined from flattened halves of a short length of steam generator tubing. These specimens are likely to have a significantly higher degree of cold work than that found in steam generator tube roll transition regions (maximum of 2%). Some stress corrosion crack growth rate tests for Alloy 600 performed in 400°C hydrogenated steam environments and in 360°C primary water environments have shown that 5% prior cold work leads to growth rates between 5 to 10 times faster than those observed in materials without cold work (Cassagne and Gelpi 1992). Another factor affecting the crack growth rate is test temperature; crack growth rate is higher for a higher test temperature. Scott made corrections to the above crack growth equation [(Equation (A-8)], by dividing it by 10, to take into account the absence of cold work or a presence of a small amount of cold work. So the PWSCC growth rates for Alloy 600 components at 330°C and no cold work is

$$da/dt = 2.8 \times 10^{-12} (K_I\text{-}9)^{1.16} \quad m/sec. \qquad [A\text{-}9]$$

This equation may be used for predicting crack growth in the CRDM nozzle material, because in the CRDM nozzles cold work is present only in a thin layer of material on the inside surface of the

nozzle, whereas the remaining subsurface material has little cold work. The effects of temperature were added to the Scott model using available Alloy 600 primary water SCC crack growth rates estimated from laboratory test results and field data for steam generator tubes. The estimated activation energy for PWSCC growth in CRDM nozzle materials is 33 Kcal/mole. The modified crack growth model is

$$da/dt = 2.56\ e^{-(33{,}000/RT)}(K_I-9)^{1.16} \qquad [A\text{-}10]$$

The modified Scott model, Equation [A-10], indicates that the crack growth rate is proportional to the increase in stress intensity factor above the threshold (9 $MPa.m^{0.5}$) raised to the 1.16 power.

The available crack growth data for Alloy 600 were for thin steam generator tubes on which the modified model is based. No crack growth data for thick Alloy 600 components such as CRDM nozzles were available at the time the modified model was developed. So the Westinghouse Owners Group initiated a project in 1992 to obtain crack growth rate data for the CRDM nozzle materials. The test materials were obtained from six fabricators of the CRDM nozzles. The test results show that the crack growth rates for the materials with high grain boundary carbides fall at or below the modified Scott model as shown in Figure A-8, whereas the growth rates for materials with low grain boundary carbide coverage fall at or above the modified model as shown in Figure A-9 (Foster, Bamford, and Pathania 1995). The higher PWSCC growth rates for materials with low grain boundary carbides are being further evaluated. The PWSCC growth rate data presented in Figure A-8 and A-9 are based on the laboratory test data and need to be validated in the field.

If the percentage of grain boundary carbides is not known, a recently developed field surface replication technique for the microstructural characterization of Alloy 600 components could be used to accurately determine the percentage of intergranular carbides (Rao 1994). This technique has been successfully demonstrated by determining the intergranular carbides in outer CRDM nozzles at one European plant. The application of this technique takes about 1 to 2 hours.

A-6. Flow-Accelerated Corrosion of Carbon Steel Components

Single-Phase flow-Accelerated Corrosion Single-phase flow-accelerated corrosion tests have been conducted at several British, French, and German laboratories to identify the factors affecting the corrosion rates (rate of metal loss) and to provide data for development of empirical models to estimate the rates (Chexal and Jones 1988, Chexal and Horowitz 1995). Evaluation of the test results and data from the operating plants have identified several factors that affect the flow-accelerated corrosion rates. These factors may be divided in three groups: (a) hydrodynamic variables - fluid velocity, piping configuration (geometry of the flow path), and pipe roughness of pipe inside surface; (b) metallurgical variables - chemical composition including weight percentage of chromium, molybdenum and copper

in the steel; and (c) environmental variables - coolant temperature and water chemistry including dissolved oxygen, ferrous ion concentration, and metallic impurities in water, pH, and the amines used for pH control. Several calculated results using the Chexal-Horowitz model are presented. The calculated results are for the following parameters, with some variations: 102-mm (4-in.) diameter carbon steel elbow, 7 ppb oxygen content, 6.1-m/s (20-ft/s) flow velocity, room temperature [25°C (77°F)] pH of 7, and 0.03 wt% of chromium, molybdenum, and copper content; the variations are noted as appropriate. The pH level at the room temperature is also referred to as *cold pH*.

The hydrodynamic variables affect the rate of mass transfer of the iron ions and other corrosion products to the bulk coolant and thus affect the flow-accelerated corrosion rate. *Fluid velocity* affects the mass transfer. At a relatively low flow velocity, the corrosion rate is controlled by the rate of mass transfer, whereas at higher velocity (still lower than the critical velocity above which metal removal by mechanical process takes place), the mass transfer rate is higher and the corrosion rate is controlled by the chemical reactions at the oxide-coolant and metal-oxide interfaces. Flow-accelerated corrosion is less frequently observed in straight lengths of pipe free from hydro-dynamic disturbances unless the bulk fluid velocity is high. Laboratory studies of the effect of bulk flow velocities, which varied from 2 to 18 m/s, on the corrosion of carbon steel in 150°C (300°F) circulating water show that the corrosion rate increases with an increase in the flow rate and, for a given flow rate, the corrosion rate is about constant.[†] The variable *piping configuration* takes into account the hydrodynamic disturbances (elbows, tees, branch connections, reducers, valves, flow control orifices, etc.) that produce high local fluid velocities and result in a further increase in mass transfer. Experiments have shown that local-flow velocities in elbows can be two to three times the bulk-flow velocities (Bosnak 1987, USNRC 1987a). A rough surface produced by the flow-accelerated corrosion process can be very damaging. The micropits formed by the initial selective attack on the carbon steel microstructure grow until they touch, and thus the surface becomes rough. The dependence of mass transfer on the velocity is greater for a rough surface than for a smooth surface.

Trace amounts of chromium, molybdenum, and copper in carbon steel provide resistance to flow-accelerated corrosion. The corrosion rate is most sensitive to the weight percent (wt%) of the chromium in the steel. The maximum rate is equal to about 3.9 mm/yr (0.155 in/yr) for 0.03 wt% Cr and equal to about 0.4 mm/yr (0.016 in/yr) for 0.50 wt% Cr. Thus a small amount of chromium significantly reduces the flow-accelerated corrosion rate.

Two main environmental variables that affect flow-accelerated corrosion rate are coolant temperature and water chemistry. The water chemistry includes dissolved oxygen, ferrous ion concentration, metallic impurities, and cold pH level. The *coolant temperature* influences both the ferrous ion production and the mass transfer of these ions into the bulk water (Remy and Bouchacourt

---

[†] Feedwater flow in a typical four-loop, 1100-MWe unit is about 6.8 x 10^6 kg/h (15 x 10^6 lb/h), which corresponds to about 4 m/s bulk flow velocity.

1992). As the temperature increases, the ferrous ion concentration at the oxide-water interface decreases almost linearly. On the other hand, as the temperature increases, the ferrous ion diffusivity into the coolant increases, resulting in a mass transfer coefficient that increases about linearly. For most feedwater piping conditions, the maximum corrosion rate occurs at about 150°C (300°F) (Chexal and Horowitz 1995).

The flow-accelerated corrosion rate varies inversely with the level of *dissolved oxygen* in the fluid. As the level of oxygen increases above a threshold value, a less porus oxide layer of hematite, instead of magnetite, is formed. Because the solubility of hematite in the feedwater is several orders of magnitude lower than that of magnetite, the flow-accelerated corrosion rate decreases significantly. Some laboratory test results show that the threshold value for dissolved oxygen is less than 15 ppb (Remy and Bouchacourt 1992). The corresponding results using the Chexal-Horowitz model shows a reduction in the maximum flow-accelerated corrosion rate from about 3.2 to 0.9 mm/yr (0.125 to 0.035 in./yr) as dissolved oxygen content increased from 10 to 30 ppb.

Ferrous ion concentration and metallic impurities in the water affects the flow-accelerated corrosion rate. The increase in the *ferrous ion concentration* in the bulk fluid reduces the mass transfer of ferrous ions from the oxide-coolant interface to the bulk coolant. An increased ferrous ion concentration can reduce or suppress flow-accelerated corrosion when the corrosion process is controlled by mass transfer. Flow-accelerated corrosion rates vary by an order of magnitude over the cold *pH range* of 8.5 to 9.5, which is typical for feedwater systems (Shack and Jonas 1988).

Two-Phase Flow-Accelerated Corrosion Examination of worn extraction piping has identified two distinct *mechanisms* causing damage in the system carrying two-phase coolant: oxide dissolution and droplet-impact wear (Bosnak 1987, Keck and Griffith 1987). The oxide dissolution mechanism is similar to single-phase flow-accelerated mechanism discussed with one exception. Two-phase flow-accelerated corrosion has been observed in piping carrying wet steam. Its occurrence has not been observed in piping carrying dry steam (100% quality). Moisture in the wet steam is essential to dissolve the oxide film. Test results show that the flow-accelerated corrosion rate in a two-phase flow varies with the quality of the steam. It is zero at 100% quality and equal to the single-phase (water) flow value at 0% quality. The erosion-corrosion rate peaks at some intermediate value for quality (Chexal and Horowitz 1990). Field data indicate that the greatest degradation is seen in the piping containing steam with the highest moisture content, such as the turbine crossover piping and the exhaust and extraction piping connected to the high-pressure turbines.

The droplet-impact wear mechanism may be explained as follows. The liquid phase in a steam line generally flows in a thin layer near the main steam line pipe wall, while the vapor forms the core of the flow and moves much faster than the liquid phase. This velocity difference creates shear forces at the liquid-vapor interface; if this force is greater than the surface tension force at the interface, some liquid will be sheared off the liquid layer and carried over with the vapor. This liquid will form

droplets, which will be accelerated by the vapor and become entrained in the vapor core. A fraction of the entrained liquid droplets will impinge on the oxide film on the main steam line inside surface. The impact of liquid droplets on carbon-steel oxide films can produce a matrix of cracks and subsequent fatigue failure of the films, and expose the underlying metal surfaces to the corrosive action of the coolant. The parameters that determine film failure are the oxide hardness, the critical strain, and the fatigue loads required to fracture the oxide film. This wear mechanism occurs under certain conditions at elbows and fittings where the flow changes direction, predominantly on the outside radius of the bend in the direction of the flow, as shown in Figure A-10 (Keck and Griffith 1987). In contrast, damage caused by oxide dissolution occurs on the inside radius of the bend where flow separation causes turbulence (also shown in Figure A-10). The droplet impact wear mechanism requires the presence of droplets, so this mechanism occurs only in piping carrying two-phase flow.

Keck and Griffith (1987) provide simple models for estimating oxide dissolution and droplet-impact wear. The model developed to describe droplet-impact erosion does not strongly depend on temperature, but does strongly depend on flow velocity (fourth power dependence). Therefore, droplet-impact wear is expected to be of importance at high flow velocities.

Computer Model EPRI has developed the computer code CHECWORKS (Chexal-Horwitz Engineering-Corrosion Workstation) for managing flow-accelerated corrosion of nuclear power plant piping. This program has capabilities for estimating parameters (such as local water chemistry and flow rate) that affect corrosion rates, and for predicting corrosion rates and helping to select inspection locations. The computer code is based on data from France, England, and Germany, and on U.S. plant data. The code has been validated using other U.S. plant data. The comparison between the predicted results and measurements show that the code predicts the flow-accelerated corrosion rates within ±50%. The main sources of uncertainties are associated with the original thickness and thickness profile of the piping components, trace amounts of alloy content in the piping material, actual number of hours of operation, plant chemistry history, and discontinuities on the inside surface of the piping.

All PWR and BWR plants in the U.S. use the CHECWORKS code (or its predecessor code CHECMATE) for estimating the flow-accelerated corrosion rates (Chexal and Horowitz 1995). This code is also used by many fossil plants, by the U.S. Navy, and by several overseas utilities. The code has been used for identifying the sites most susceptible to flow-accelerated corrosion, prioritizing the locations that need to be inspected, estimating remaining service life for each susceptible component, and evaluating the effectiveness of different water chemistries and other mitigative actions.

Siemens/KWU in Germany has long been active in researching wall thinning rate estimation caused by flow-accelerated corrosion. The empirical Kastner model was developed in the early 1980s for the calculation of material losses due to flow-accelerated corrosion in single- and two-phase flow (Kastner and Riedle 1986). Kastner's model was based on experiments carried out at Siemens/KWU and on plant data from all known single and two-phase locations (more than 6,000 data points overall),

as well as on theoretical considerations. After the Surry Unit 2 accident in 1986, the WATHEC program based on Kastner's model was developed to perform weak-point analyses at power plants. In 1991, WATHEC was interfaced with the DASY program which handles the recording, management, evaluation, and documentation of the data obtained from non-destructive examinations. These two software packages were continuously improved in cooperation with European utilities to calibrate the predicted wall thinning rates for further plant diagnosis with increased prediction accuracy (Chexal et al., 1996).

A-7. References

ASME 1995. *ASME Boiler and Pressure Vessel Code*, Section XI, Appendix C: Evaluation of Flaws in Austenitic Piping, American Society of Mechanical Engineers, New York, pp. 381-394.

Bamford, W. H., D. P. Jones, and L. A. James 1989. "Flaw Tolerance in Engineering Structures: An Assessment of Current Approaches and Future Needs for Predicting Subcritical Crack Growth," *Proceedings of the Fourth International Symposium on Environmental Degradation of Materials in Nuclear Power Systems - Water Reactors*, pp. 8-1 to 8-27.

Bosnak, R. J. 1987. "Meeting Minutes of 1/15/87 Technical Panel Discussion of Surry-2 Pipe Failure Implications," Memorandum to T.P. Speis, U.S. Nuclear Regulatory Commission, February 4.

Buchalet, C., et al., 1986. "Effect of Long Term Embrittlement on the Critical Defect Sizes in Primary Piping Cast Stainless Elbows," *Proceedings of the Second International Symposium on Environmental Degradation of Materials in Nuclear Power Systems-Water Reactors, Monterey, California, September 9–12, 1985,* American Nuclear Society, LaGrange Park, Illinois, pp. 477–484.

Cassagne, T. and A. Gelpi 1992. "Crack Growth Rate Measurements on Alloy 600 Steam Generator Tubes in Steam and Primary Water," *Proceedings of the 5th International Symposium on Environmental Degradation of Materials in Nuclear Power Systems - Water Reactors*, August 25-29, 1991, Monterey, California, pp. 518-532.

Chexal, B., et al. 1996. *Flow-Accelerated Corrosion in Power Plants*, EPRI TR-106611, Electric Power Research Institute, Palo Alto.

Chexal, V. K. and J. S. Horowitz, 1995. "Chexal-Horowitz Flow-Accelerated Corrosion Model-Parameters and Influences," *Current Perspectives of International Pressure Vessels and Piping Codes and Standards*, PVP-Vol. B, pp. 231-243. American Society of Mechanical Engineers, New York.

Chexal, V. K. and Horowitz, J. S. 1990. "Flow Assisted Corrosion in Carbon Steel Piping, Parameters and Influences," *Proceedings of the Fourth International Symposium on Environmental Degradation of Materials in Nuclear Power Systems—Water Reactors*, D. Cubicciotti (Editor), National Association of Corrosion Engineers, Houston, pp. 9-1 to 9-12.

Chexal, V. K. and R L. Jones 1988. "Implications of the Surry Piping Failure for Other Nuclear and Fossil Units," *International Journal of Pressure Vessels & Piping, 34,* pp. 331-343.

Chopra, O. K. 1992a. "Estimation of Mechanical Properties of Cast Stainless Steels During Thermal Aging in LWR Systems," *Proceedings of the U.S. Nuclear Regulatory Commission Nineteenth Water Reactor Safety Information Meeting*, NUREG/CP-0119, Vol.1, pp.151–178.

Chopra, O. K. 1992b. *Long-Term Aging of Cast Duplex Stainless Steels in LWR Systems*, NUREG/CR-4744, Vol. 6, No.2, ANL-92/32.

Coffin, L. F. 1954. "A Study of the Effects of Cyclic Thermal Stresses on a Ductile Material," *Transactions of the American Society of Mechanical Engineers*, *76*, p. 931.

Cooper, W. E. 1992. "The Initial Scope and Intent of the Section III Fatigue Design Procedures," presented at the *Pressure Vessel Research Council Workshop on Environmental Effects on Fatigue Performance, Clearwater Beach, Florida, January 20, 1992.*

Foster, J. P., W. H. Bamford, and R. S. Pathania 1995. "Initial Results of Alloy 600 Crack Growth Rate Testing in a PWR Environment," *Proceedings of the Seventh International Symposium on Environmental Degradation of Materials in Nuclear Power Systems - Water Reactors, August 7-10, 1995*, NACE International, pp. 25-40.

Higuchi, M. and K. Iida 1992. "Fatigue Strength Data of LWR Structural Materials in Japan (Effects of LWR Water Environment on Fatigue Strength)," *Technical Information from Workshop on Cyclic Life on Environmental Effects in Nuclear Applications, PVRC Volume 2, Clearwater Beach, Florida, January 20–21, 1992,* Welding Research Council, Inc., New York.

Huguchi, M. A. Nakagawa, M. Hayashi, T. Yamauchi, M. Salto, K. Lida, F. Matsuda, and M. Sato, 1996. "A Study on Fatigue Strength Reduction Factor for Small Diameter Socket Welded Pipe Joints," PVP-Vol. 338, *Pressure Vessel and Piping Codes and Standards*, Volume 1, ASME, pp. 11-19.

Iida, K., et al. 1988. "Abstract of DBA Committee Report, 1988—Survey of Fatigue Strength Data of Nuclear Structural Materials in Japan," unpublished article sent to V. N. Shah (K. Iida is Professor Emeritus, University of Tokyo, Tokyo).

James, L. A. and D. P. Jones 1985. "Fatigue Crack Growth Correlations for Austenitic Stainless Steels in Air," *Predictive Capabilities in Environmentally Assisted Cracking,* PVP-Vol. 99, pp. 363-414.

Keck, R. G., and P. Griffith 1987. *Prediction and Mitigation of Erosion-Corrosive Wear in Secondary Piping Systems of Nuclear Power Plants*, NUREG/CR-5007.

Kooistra, L., et al. 1961. "Full Size Pressure Vessel Testing and Its Approach to Fatigue," *Journal of Engineering for Power, Transactions of the American Society of Mechanical Engineers, 86*, 4, pp. 419–28.

Kussmaul, K., et al. 1988. "Deformation and Failure Behavior of Elbows: Experimental Results and analytical Predictions," University of Stuttgart, Germany.

Landerman, E. I., and W. H. Bamford 1978. "Fracture Toughness and Fatigue Characteristics of Centrifugally Cast Type 316 Stainless Steel Pipe after Simulated Thermal Service Conditions," *in Ductility and Toughness Considerations in Elevated Temperature Service,* MPC-8, The American Society of Mechanical Engineers, New York, pp. 99–127.

Paris, P. C. 1964. "The Fracture Mechanics Approach to Fatigue," in *Fatigue—An Interdisciplinary Approach*, I. I. Burke, N. L. Reed, and V. Weiss (eds.), Syracuse Univer-sity Press, Syracuse, New York, pp. 107–132.

Rao, G. V. 1994. "Methodologies to Assess PWSCC Susceptibility of Primary Component Alloy 600 Locations in Pressurized Water Reactors," *Sixth International Symposium on Environmental Degradations of Materials in Nuclear Power Systems—Water Reactors,* San Diego, pp. 871–882.

Rebak, R. B., et al. 1992. "Effects of pH and Stress Intensity on Crack Growth Rate in Alloy 600 in Lithiated + Borated Water at High Temperatures," *Proceedings of the 5th International Symposium on Environmental Degradation of Materials in Nuclear Power Systems - Water Reactors*, August 25-29, 1991, Monterey, California, pp. 511-517.

Remy, F. N. and M. Bouchacourt 1992. "Flow-Assisted Corrosion: A Method to Avoid Damage," *Nuclear Engineering and Design*, 133, p. 23-30.

Scott, P. M. 1991. "An Analysis of Primary Water Stress Corrosion Cracking in PWR Steam Generators," *Proceedings of the Specialists Meeting on Operating Experience with Steam Generators*, Brussels, Belgium, September, 1991, Paper 5.6.

Shack, W. J., and O. Jonas 1988. "Investigation of Erosion-Corrosion in Reactor Piping," presented at the *Workshop on Structural Integrity of Reactor Piping Systms, May 16-19, Tokyo, Japan*, U.S. Nuclear Regulatory Commission and Japanese Ministry of International Trade and Industry.

Shah, V. N. et al. 1992. "Assessment of Primary Water Stress Corrosion Cracking of PWR Steam Generator Tubes," *Nuclear Engineering and Design, 134*, pp. 199-215.

Simonen, F. A., et al. 1986. *Reactor Pressure Vessel Failure Probability Following Through-Wall Cracks Due to Pressurized Thermal Shock Events*, NUREG/CR-4483, PNL-5727.

Slama, G. et al., 1983. "Effect of Aging on Mechanical Properties of Austenitic Stainless Steel Castings and Welds," *SMiRT Postconference Seminar 6, Monterey, California, 1983*.

Terrell, J. B. 1988. *Fatigue Life Characterization of Smooth and Notched Piping Steel Specimens in 288°C Air Environments*, NUREG/CR-5013, MEA-2232.

USNRC 1987. "Feedwater Line Break," USNRC Information Notice 86-106, Supplement 1.

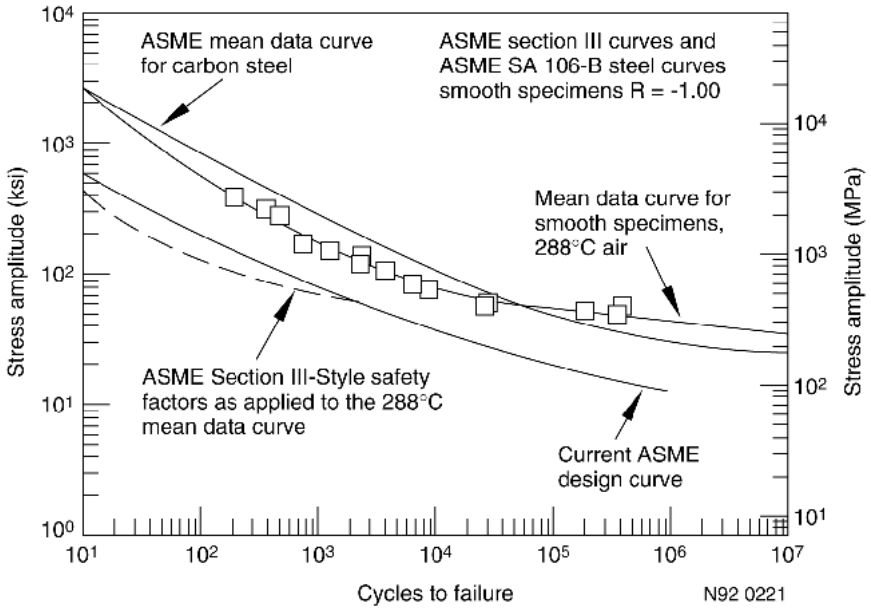

Figure A-1. Fatigue data of SA 106-B carbon steel smooth base metal specimens in air at room temperature and 288 °C (Terrell 1988).

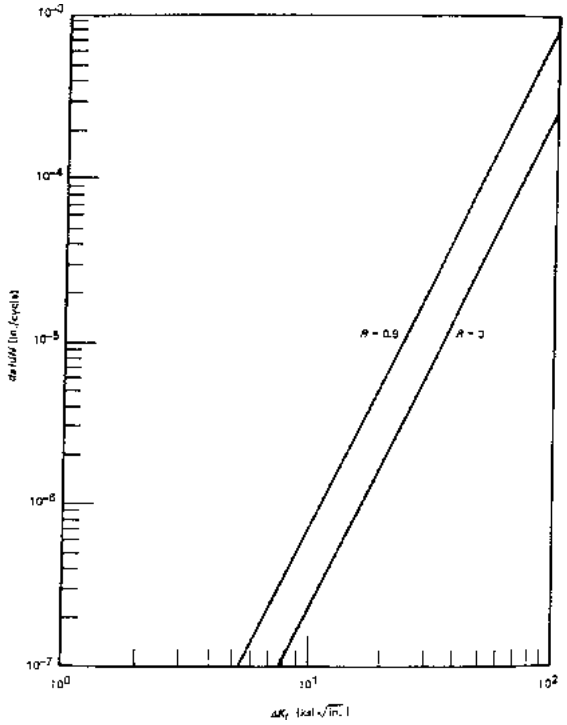

Figure A-2. Reference fatigue crack growth curves for carbon and low alloy ferritic steels exposed to air environments (subsurface flaws).

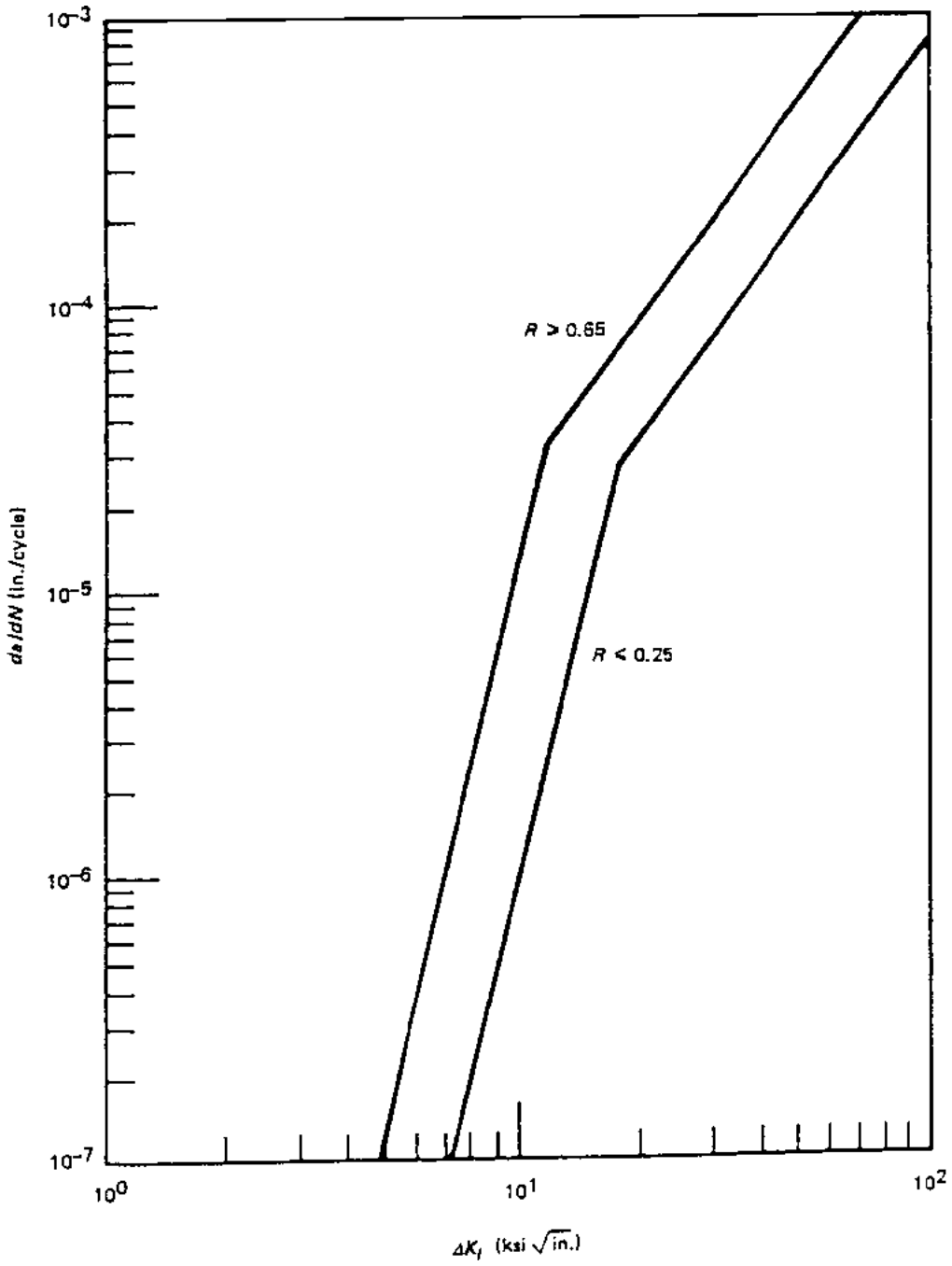

Figure A-3. Reference fatigue crack growth curves for carbon and low alloy ferritic steels exposed to water environments.

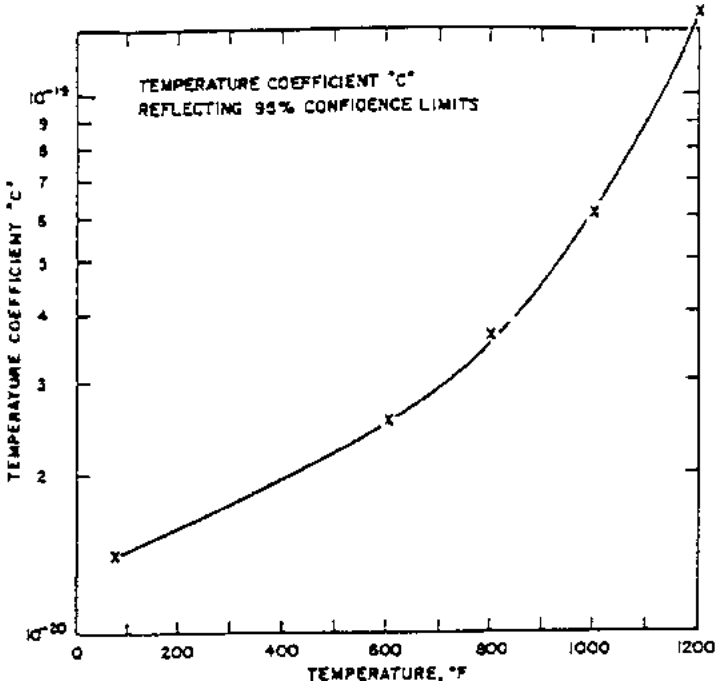

Figure A-4. Coefficient "C" in equation (A-5) as a function of temperature.

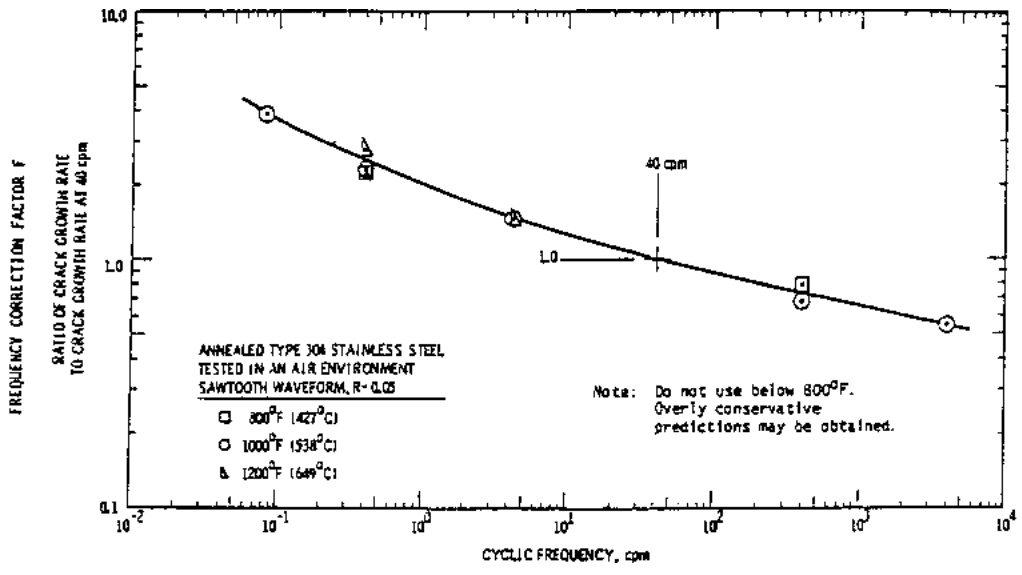

Figure A-5. Frequency correction factor "F" as a function of cyclic frequency in the range 800° –1,000°F.

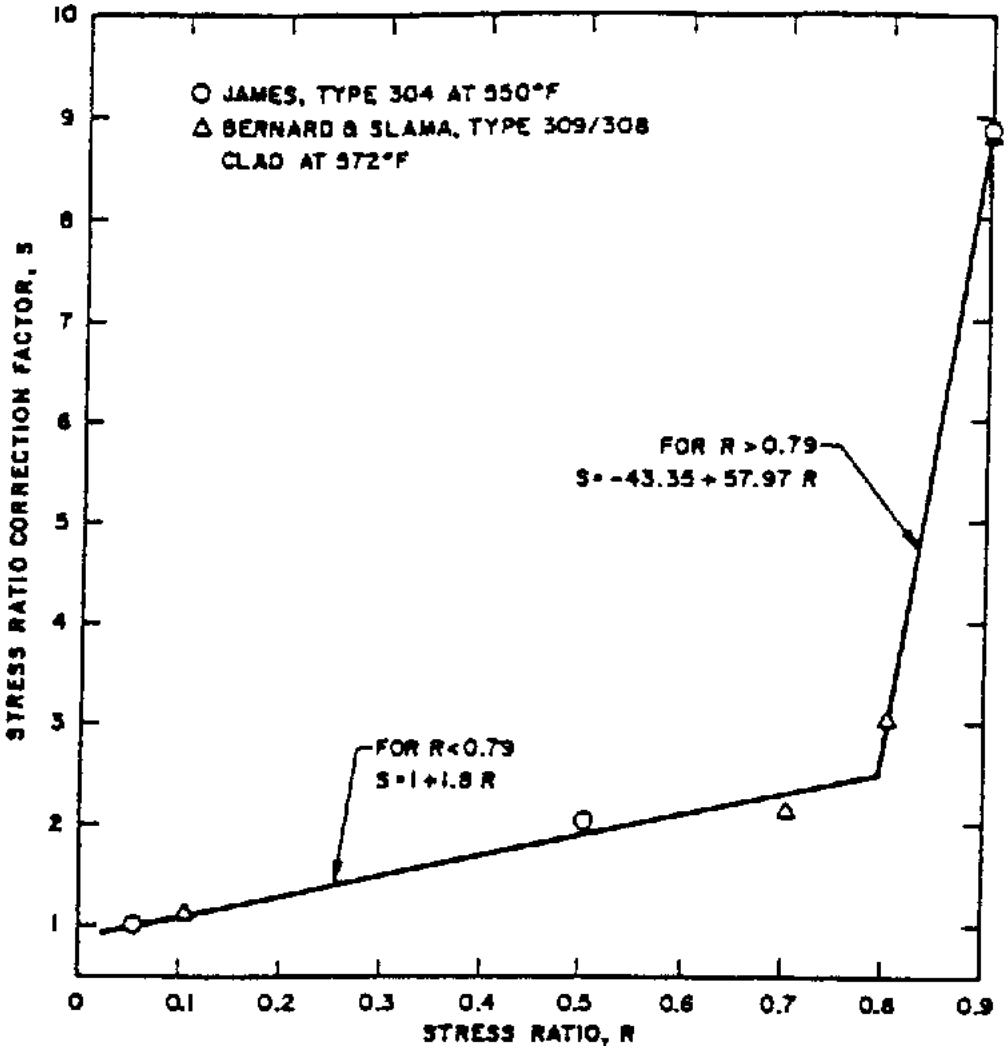

Figure A-6. Ratio correction factor "S" as a function of stress ratio.

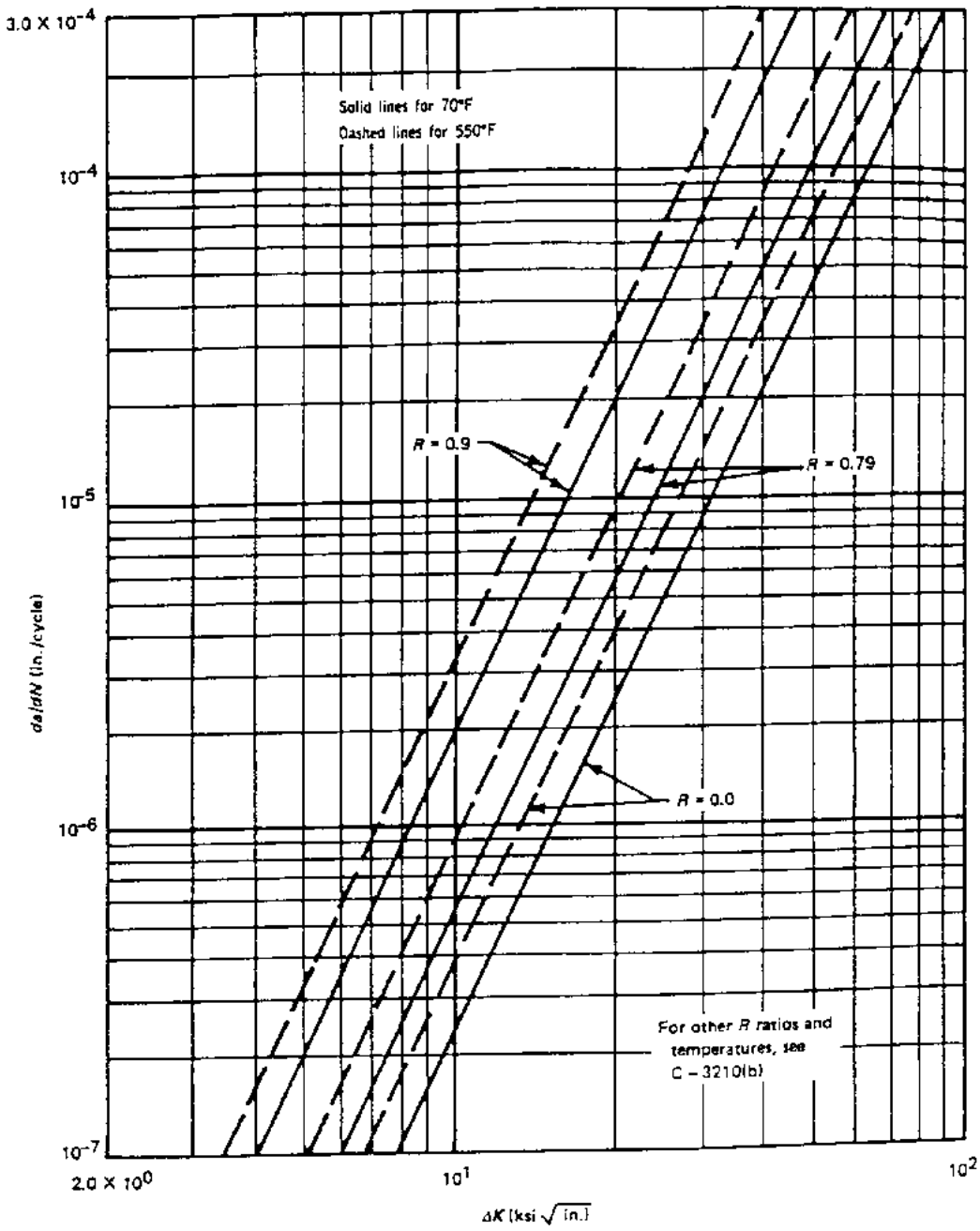

Figure A-7. Reference fatigue crack growth curves for austenitic stainless steels in air environments.

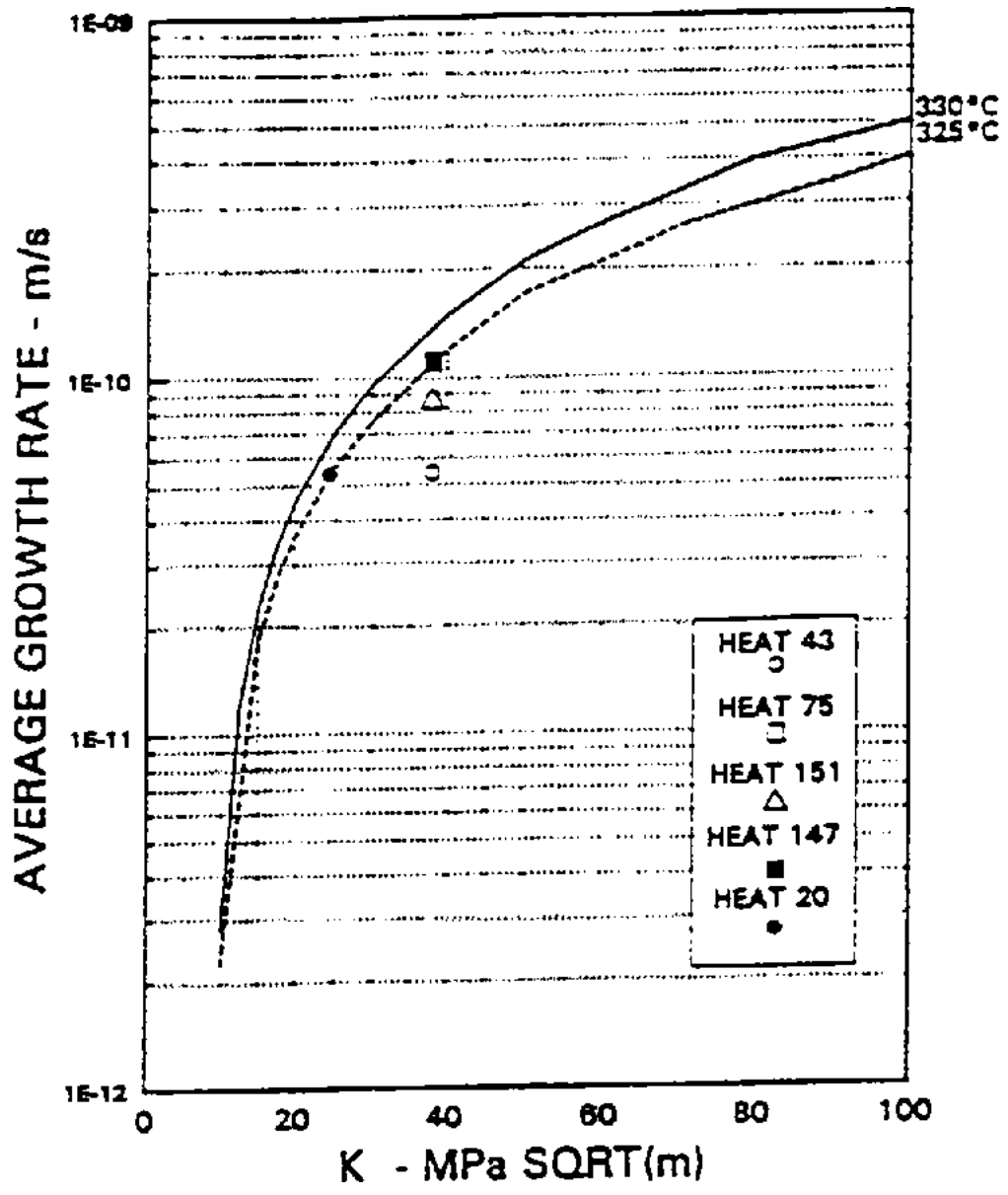

Figure A-8. Comparison of high grain boundary carbide coverage materials (>40%) with the modified Scott model.

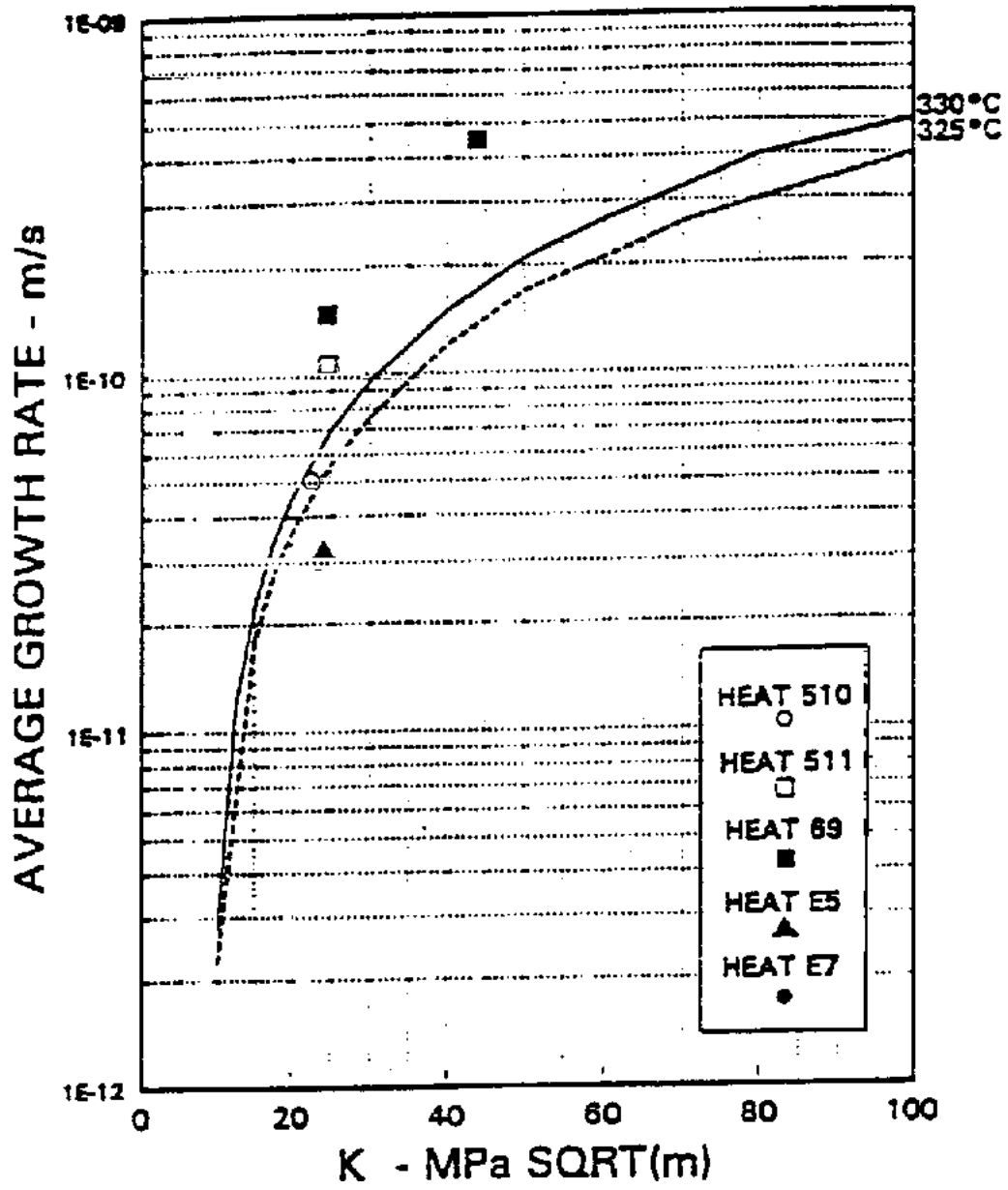

Figure A-9. Comparison of low grain boundary carbide coverage materials (<20%) with the modified Scott model.

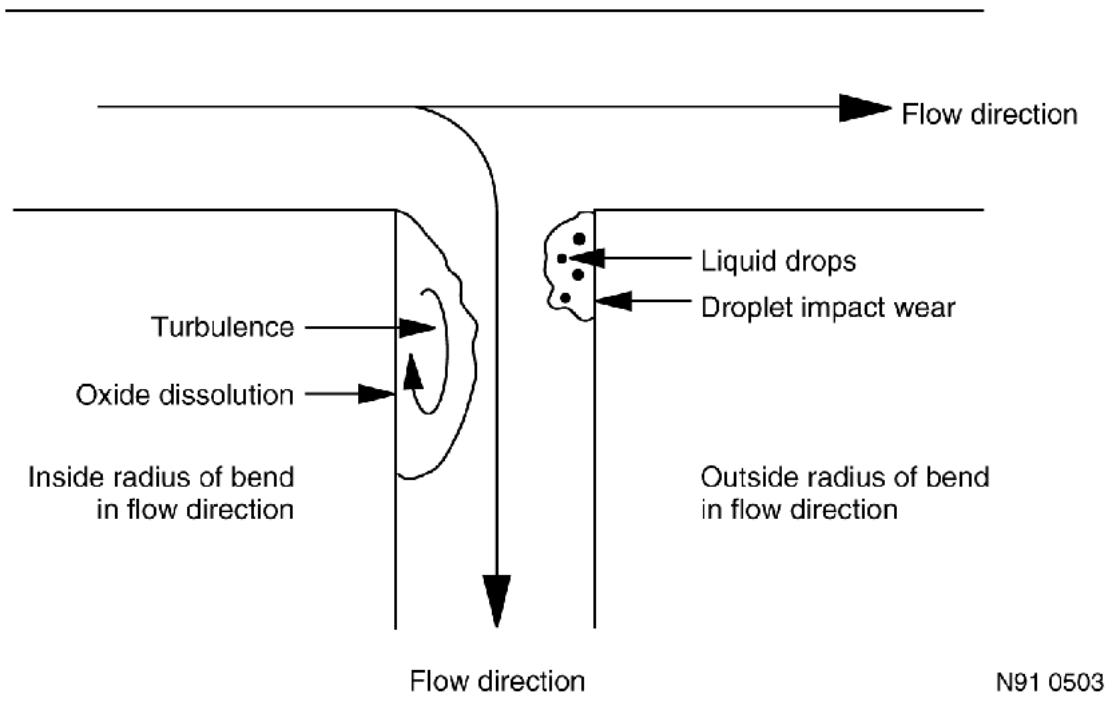

Figure A-10. Potential sites for the two different types of wet steam flow-accelerated corrosion damage.

Appendix B

Field Experience Related to Damage of Passive Components Caused by Selected Degradation Mechanisms

Appendix B

Field Experience Related to Damage of Passive Components Caused by Selected Degradation Mechanisms

B-1. Radiation Embrittlement of Ferritic Low-Alloy Steels

PWR pressure vessel failure will probably only occur when a severe abnormal transient or event occurs. For example, a pressurized thermal shock might cause brittle failure of the vessel when the material properties of the vessel beltline region are severely degraded by radiation embrittlement (i.e., the RT_{NDT} has reached to high temperatures). However, there must also be a defect or crack of critical size present to produce such a failure. Also, an over-load situation combined with radiation-induced low upper-shelf material in the beltline region could lead to low-energy ductile tearing, if, again, a crack is present. The regions of interest in the beltline have extremely low fatigue usage factors, indicating a small probability of initiating a defect or crack. But, defects are possible, as evidenced by the concern over underclad cracks in the 1970s; these manufacturing-induced cracks can result from high-heat-input multipass strip-cladding techniques (at the overlap points), especially for SA508-2 forging steel. However, vessels fabricated in the United States were typically subjected to a single- or multi-layer submerged arc welding process to clad the vessel inside surfaces, which does not cause embrittlement of the heat-affected zone leading to cracks (Griesbach 1984).

The shift in the transition temperature (RT_{NDT} temperature) increases as the reactor vessel gets older. So the severity of a given transient increases as the vessel gets older and RT_{NDT} shifts to higher temperatures. The lowest coolant temperature, T_c, during a transient is an important parameter in determining severity of the transients. The magnitude of T_c in the following six events could have led to a PTS concern if the vessels were older: 110°C (230°F) at TMI-2 on 28 March 1979, 118°C (245°F) at Crystal River-3 on 26 February 1980, 138°C (280°F) at Rancho Seco on 20 March 1978, 143°C (290°F) at Robinson-2 on 28 April 1970, 160°C (320°F) at R. E. Ginna on 25 January 1982, and 177°C (350°F) at Prairie Island-2 (Dircks 1982). The RPV integrity of these PWRs following the transients has been demonstrated by analyses and NDE inspections. In older plants with higher RT_{NDT}, these events will require a detailed analysis to demonstrate RPV integrity.

B-2. Thermal Aging of Cast Stainless Steels

Thermally aged cast stainless steel components with high ferrite content are susceptible to ductile fracture at operating temperatures. The potential for ductile fracture is higher for Grade CF-8M stainless steel than Grade CF-8 stainless steel because Grade CF-8M is likely to experience more reduction in its fracture toughness. In addition, the potential for ductile fracture is higher for statically

cast components than centrifugally cast components. The statically cast components have more fabrication flaws, and the ferrite content can vary significantly from a given nominal value. The potential for ductile fracture is also higher for thermally aged shielded metal-arc welds than for gas-tungsten-arc welds because the former welds have a higher inclusion content and are more susceptible to embrittlement.

Normal PWR operations do not introduce any new flaws in the cast stainless steel components other than those present as fabrication defects. If a drop in the fracture toughness of a cast stainless steel component makes the critical flaw size smaller than a fabrication defect, there is a potential for brittle fracture if transients with low temperatures and coincident high applied stresses occur.

B-3. Low-Cycle Fatigue

Low-cycle fatigue has caused cracking and leakage in PWR high pressure safety injection line, residual heat removal line, PWR steam generator shell girth welds, PWR feedwater nozzles, and other locations. Table B-1 summarizes the fatigue damage locations in the major light water reactor components (ASME Section XI Task Group 1992). (This Table also summarizes fatigue cracking experience with BWR components.) Table B-2 and B-3 summarize the cracking experience with PWR feedwater nozzles. Table B-2 summarizes the experience during 1979-1980; whereas Table B-3 summarizes the experience from 1983 to present. Detail description of the recent feedwater nozzle cracking at Sequoyah, Diablo Canyon, and San Onofre 3 may be found in a report by Shah et al. (1997). Detail description of two cracking events associated with the primary pressure boundary of high pressure injection line is presented here.

A through-wall fatigue crack developed in the heat-affected zone of an elbow weld in the 152-mm (6-in.) safety injection piping of Farley Unit 2, a U.S. PWR, after approximately six years of commercial operation (USNRC 1988a, 1988c). The crack was located downstream of the first check valve from the Loop B nozzle, as shown in Figure B-1, a portion of the safety injection piping that constitutes the primary pressure boundary. The crack was on the inside surface of the weld, extending approximately 120 degrees circumferentially around the underside of the pipe, and about 250-mm (1-in.) of this crack was through-wall. The geometric discontinuities in the weld region might have acted as stress concentration sites (Simos et al. 1990). The crack developed slowly, and the resulting leak rate was 2.7 L/min (0.7 gpm). A metallurgical evaluation, which included surface, metallographic, and fractorgraphic examinations concluded that the failure resulted from fatigue damage caused by thermal cycling, which is a cyclic axial movement of an interface between hot and cold fluids. Such cycling takes place when a column of hot turbulent fluid penetrates a branch line and interacts with a cooler stratified fluid.

Table B-1. Summary of fatigue damage locations in major LWR components.

Mechanism	Causes	Sites with Significant Damage[a]
Low-cycle fatigue	Stratified flows, thermal shocks (intermittent flows), heatups, cool-downs, scrams, frozen snubbers, leaking valves	PWR: High pressure injection makeup lines (2), nozzles (1), and thermal sleeves (5); residual heat removal piping (1); surge lines (3); spray lines; surge nozzle thermal sleeves (1), reactor coolant piping BWR: CRDM return line nozzles (12); CRDM collet housing (4)
High-cycle thermal fatigue	Thermal mixing, thermal striping, leaking valves	PWR: High pressure injection/makeup lines (2), nozzles (1), and thermal sleeves (5); residual heat removal piping (1); cold (1); leg piping (1); reactor coolant pump shafts (1); feedwater nozzles (19) BWR: Feedwater nozzles (18) and CRDM return line nozzles (12)
High-cycle mechanical fatigue	Flow-induced vibrations	PWR: High pressure injection/makeup nozzle thermal sleeves (1); steam generator U-tubes (1); reactor internal fasteners (4); core barrel 91) LWR: Emergency diesel generator piping, pumps, engine parts, heat exchangers, generator windings (3)
	Alternating bending stress	PWR: Reactor coolant pump shafts (9) BWR: Recirculation pump bearing housing attachment welds (3) BWR: Recirculation pump thermowell (1)
	Turbulent flow	Charging pump blocks (17)
	Cyclic pressure loads	
Environmentally assisted fatigue	Secondary coolant in PWRs and thermal and pressure cycles	PWR: Steam generator shell girth welds (3), steam generator feedwater nozzles (3), OTSG tubes (139)
Fretting fatigue	Flow-induced vibrations	PWR: Recirculation steam generator tubes near antivibration bars (1) and near integral preheaters; thimble tubes (13)

a. Numbers in parenthesis are the number of failures identified for that component.

Table B-2. PWR feedwater piping cracking during 1979-1980 (USNRC 1980). (1 in. = 25.4 mm).

Plant	Vendor/steam generator model	Maximum depth[a] (in.)	Circumferential Location	Lines cracked[b]	Comments
Beaver Valley 1	W	0.400	9 o'clock	3 of 3	N[c]
D.C. Cook 1,2	W	Trough-wall	Top	8 of 8	Through-wall cracks in two of the four Unit 2 lines
Ginna	W	0.107	8:30 o'clock	2 of 2	N
Kewaunee	W	0.050	7 o'clock	2 of 2	3-in. auxiliary feed near SG inlet
Millstone 2	CE	0.250	12 o'clock	2 of 2	N
Palisades	CE	0.170	3 & 9 o'clock	2 of 2	Cracks also found at weld in vicinity of horizontal pipe
Point Beach 1,2	W	0.047	3 o'clock	2 of 4	3-in. auxiliary feed near SG inlet
H. B. Robinson 2	W	0.750	9 o'clock	3 of 3	Shallow cracking of nozzle under thermal sleeve
Salem 1	W	0.235	N	4 of 4	N
San Onofre 1	W	0.100	Lower half of reducer	3 of 3	Multiple-branched cracks, fatigue
Surry 1,2	W	0.080	2 & 5 o'clock	6 of 6	N
Turkey Point 3,4	W	N	N	6 of 6	N
Zion 1,2	W	0.088	N	N	N

a. The typical thickness of a feedwater line pipe wall is approximately 13 to 25 mm (0.5 to 1 in.).

b. Number of total feedwater lines into steam generators that were found to be cracked. For example, the D.C. Cook plants are 4-loop Westinghouse units, so all eight lines in the two plants were cracked.

c. Additional information was not found.

Table B-3. PWR feedwater nozzle cracking 1983 to present (Shah, 1997).

Plant	Date	Vendor/steam generator model	Maximum depth	Circumferential location/extent[a]	Lines cracked	Comments
1983 to 1991						
St. Lucie 1	1983	CE	N[b]	N	2/2	safe-end base metal
Maine Yankee	1983	CE	through-wall	leak at bottom of pipe; cracking 11 to 7 o'clock	3/3	existing crack propagated by water hammer; cracking only in pipe side of weld
Beaver Valley 2	1983 1985	W/51M	N	N	N	N
Turkey Point 4	1984	W/44F	N	270° (A), 180° (C) around	2/3	base metal in pipe-to-nozzle weld region
Farley 1	1984	W/51	7-37% through-wall	11-1, 7-9, 4-5 (B only) o'clock	3/3	base metal in pipe-to-nozzle weld region
Trojan	1987	W/51A	0.533 in.	4, 7, 9, 12 o'clock	3/4	base metal in pipe-to-nozzle weld region
Beaver Valley 1	1987	W/51	N	N	3/3	pipe-to-nozzle weld region
Indian Point 2	1989	W/44F	0.347 in. (bore); 0.388 in. (weld)	bottom 120°	2/4	pipe-to-nozzle weld region; upstream piping; nozzle inner bore
1991 to present						
Beaver Valley 1	1992	W/51	N	N	N	N
Sequoyah 1	1992 1993	W/51	through-wall	3 and 9 o'clock	3/4	leak in one line; transition piece; AFW auto/manual
Sequoyah 2	1992 1993	W/51	60% through-wall	most at 3 and 9 o'clock (slightly rotated), one at top	2/4	transition piece; AFW auto/manual
Salem 1	1992	W/51	N	N	4/4	nozzle-to-expander and expander-to-elbow weld areas
Diablo Canyon 1	1992	W/51	0.06	360° around circumference	4/4	base metal in pipe-to-nozzle weld region
Prairie Island 1 & 2	1992	W/51	N	N	N	N
Haddam Neck	1993	W/27	0.25	lower 180°	3/4	base metal in pipe-to-nozzle weld region
Robinson 2	1993	W/44F	N	N	N	N
Turkey Point 3	1993	W/44F	N	N	N	N
San Onofre 3	1993	CE	0.02	3 and 9 o'clock	2/2	AFW on/off prior to 1986; safe end
Farley 2	1993	W/51	N	N	N	N

a. The upper case letter in the parenthesis identifies the affected steam generators. Such identification of affected steam generators was not provided for in all the cracking events reported here.

b. Information was not found.

Field measurements of the temperature distribution in the pipe wall indicated the presence of a stratified flow; top-to-bottom temperature difference near the weld was about 120°C (215°F). The stratified flow was caused by leakage of cold coolant through a nearby faulty globe valve (Valve A in Figure B-1). The dark solid line in Figure B-1 is the flow path for the leaking fluid. Interaction of the stratified fluid with a turbulent penetration from the cold leg into the high-pressure injection line resulted in thermal cycling, which caused a through-wall fatigue crack. The stress and fatigue analyses of the affected safety injection line indicate that the stress range at the inside surface of the piping was about 350 MPa (50 ksi) and about 100,000 to 200,000 cycles were required for the crack to grow through wall (Strauch et al. 1990). This estimate of the number of cycles was supported by the metallurgical evaluation.

Valve leakage in Tihange Unit 1 in Belgium has also caused a through-wall fatigue crack in the base metal of an elbow between the first check valve in the safety injection system and a safety injection nozzle located on the hot leg, as shown in Figure B-2 (Crack 1) (USNRC 1989c). The crack was 89-mm (3.5-in.) long on the inside surface and 41-mm (1.6-in.) long on the outside surface. The crack developed rapidly, and the resulting leak rate was 23 L/min. (6 gpm). During repair of the piping, the inside surface of the check valve body was inspected using dye-penetrant testing, and several other cracks were found. The maximum depth of these cracks, determined by grinding, was about 30% of the wall thickness. A safety valve was installed downstream of the first check valve to mitigate the thermal fatigue loads caused by the leaking coolant. On-line monitoring of leakage from faulty or degraded valves is needed.

Other piping connected to the primary coolant system of a PWR is also susceptible to thermal fatigue damage because of valve leakage. For example, outleakage from the first isolation valve on a 202-mm (8-in.), Type 316 stainless steel residual heat removal line in a Japanese PWR caused a through-wall, unisolatable crack (USNRC 1988d). The crack was located in a weld joint between an elbow and a horizontal pipe section between the hot leg and the valve.

B-4. High-Cycle Vibrational Fatigue of Welded Piping Connections

A review of License Event Reports (LERs) from 1969 to 1980 has identified 84 events of cracking and leaking of small piping [smaller than 102-mm (4-in.) diameter] subject to vibratory fatigue (USNRC 1980). These events are summarized in Table B-4. It was reported that pipe cracking occurred in small lines in most operating plants. The cracking occurred predominantly in socket welds in 3/4-in. to 2-in. diameter vent, drain and instrument lines. The cracking was predominantly near the pumps, and failure was attributed to vibrational fatigue.

Table B-4. Summary of PWR cracking in pipes smaller than 4 inches (10.2 Cm)[†]

System	Plants	Licensee Event Report Citations	Crack Location	Probable Cause
Chemical and volume control	Arkansas 2	1	Most cracks in welds located near pumps	Fatigue caused by vibration
	Calvert Cliffs 1	4		
	Calvert Cliffs 2	5		
	Haddam Neck	2		
	Fort Calhoun 1	2		
	Indian Point 2	3		
	Indian Point 3	1		
	Kewaunee 1	2		
	North Anna 1	1		
	Palisades 1	1		
	Point Beach 2	1		
	R. E. Ginna 1	3		
	Salem 1	1		
	Surry 1	1		
	Turkey Point 3	1		
	Turkey Point 4	3		
	Yankee Rowe	4		
	Zion 1	1		
	Zion 2	1		
Coolant recirculation	Arkansas 2	1	In welds at small tees and nipples, etc.	Vibration
	Calvert Cliffs 2	3		
	Fort Calhoun 1	1		
	Palisades 1	2		
	Point Beach 2	1		
	Salem 1	1		
	Three Mile Island 1	1		
	Indian Point 1	1		
	San Onofre	1		

[†] Leakage occurred in all cracks.

System	Plants	Licensee Event Report Citations	Crack Location	Probable Cause
Residual heat removal	Arkansas 1 D.C. Cook 1 Indian Point 2 Prairie Island 1 Three Mile Island 2 Three Mile Island 1	3 2 3 1 1 1	Most cracks in welds near pumps or valves	Vibration
Reactor coolant cleanup	Calvert Cliffs 1 Calvert Cliffs 2 Kewaunee 1 Trojan 1 Yankee Rowe	3 3 1 1 1	Most cracks in welds in lines located near pumps	Fatigue caused by vibration
Emergency core cooling	Arkansas 2 Beaver Valley 1 Calvert Cliffs 2 Farley 1 Millstone 2 Oconee 2	1 1 1 1 1 1	Most cracks in welds of vent or drain lines	Vibration
Main steam supply	North Anna 1	1	Cracks in weld in instrument lines	Not determined
Condensate feedwater	Three Mile Island 1	1	Crack in socket weld	Vibration
Other engineered safety features	Turkey Point 3	1	Crack in drain line weld	Vibration
Reactor core isolation cooling	Oconee 3	1	Crack in weld in sample line	Vibration
Spent fuel pool	Arkansas 1 Three Mile Island	2 1	In welds HAZ	Not determined IGSCC
Containment heat removal	Indian Point 2	1	Vent to pump weld	Vibration

B-5. Primary Water Stress Corrosion Cracking of Alloy 600 Components

Field experience related to PWSCC damage to Alloy 600 components, steam generator tubes and their plugs, pressurizer penetration, and CRDM nozzles, has been summarized here. Often PWSCC damage has resulted in through wall cracking and leakage.

Steam Generator Tubes As of 1993, at least 61 plants worldwide (19 U.S.) have experienced some degree of PWSCC in the expanded portions of the tubes, which were typically expanded by hard rolling (which introduces high residual stresses at the roll transition region and at regions in some tubes where rolling anomalies occurred). At least 36 plants (22 U.S.) have reported cracking caused by U-bend PWSCC, and five plants (all U.S.) have noted PWSCC at dents. Three foreign plants have also reported PWSCC in the cold leg roll transition of tubes pulled from a steam generator and examined destructively (Tatone and Pathania 1985, Hunt and Gorman 1986, Togo et al. 1985, Gorman and Hunt 1986) and six U.S. plants have identified small numbers of PWSCC indications in the cold leg tube sheet region by nondestructive examination (NDE). The rate of progression of PWSCC increases as the operating temperature and combined residual and applied tensile stresses increase at a particular steam generator tube location.

In general, plant experience has shown that the high stress or temperature locations in steam generators with tubing that was mill annealed at a relatively low temperature (low-temperature mill-annealed tubing) may exhibit PWSCC after 1 to 10 effective full-power years (EFPYs) of operation (Hunt and Gorman 1986, Gorman and Hunt 1986). To date, this degradation mechanism has been limited to RSGs of Westinghouse design (this includes plants built by Westinghouse and plants built by Westinghouse licensees in Europe and Japan, referred to in the remainder of this chapter as Westinghouse type plants), and primarily to plants with low-temperature mill-annealed tubing. PWSCC proceeds more slowly in high-temperature mill-annealed tubing. Plants with high-temperature mill-annealed tubing may experience significant PWSCC after 10 or more EFPYs of operation (Kuchirka and Cunningham 1986, Benson 1988). Certain types of plugs are also susceptible to PWSCC-type degradation, as described below:

- Explosive plugs of Westinghouse design installed in the 1970s have experienced PWSCC, as evidenced by several reports of leaking plugs (Stoller 1982, 1987). Explosive plugs have leaked in at least three plants because of large plastic strains and unfavorable residual stresses at plug corners. The cracking seen in at least one plant was circumferential in orientation and occurred at the top transition of the explosive expansion, i.e., in a pressure boundary region.

- PWSCC has recently been reported as occurring in Babcock & Wilcox mechanically rolled plugs installed in recirculating and once-through steam generators, and has been identified in several different thermally treated Alloy 600 tube plug heats (USNRC 1989b). This PWSCC has occurred in the form of circumferential cracks located in the transition below the roll

expansion, i.e., at the "heel" location, which is not part of the pressure boundary, so that plug integrity is not affected (see Figure B-3). To a lesser extent, degradation in the form of axial cracks in the transition above the roll expansion, i.e., in the "toe" location (part of the pressure boundary), has also been identified. Cracked plugs have only been seen on the hot-leg sides.

- Mechanical plugs of Westinghouse design have experienced PWSCC in the expanded area. These plugs have been installed in large numbers since about 1980. The most significant occurrence of PWSCC in this type of tube plug occurred in February 1989 at North Anna Unit 1 (*Nucleonics Week* 1989a and b, USNRC 1989a, USNRC 1990). The plug involved was made with thermally treated Alloy 600 material. In this incident, circumferential PWSCC occurred nearly through wall all around the circumference of a plug. The remaining ligament broke during a plant transient and allowed the top part of the plug to be propelled up the tube until it hit the U-bend, which it penetrated, causing a significant primary-to-secondary-side leak (tube rupture). The adjacent tube was deformed, but not penetrated, by the impact of the plug top. An extensive investigation concluded that this situation did not pose serious safety concerns, but that widespread corrective action was necessary (Smith 1989).

  It was originally estimated that mechanical plugs potentially susceptible to PWSCC had been installed in about 7000 tubes in Westinghouse steam generators in approximately 20 U.S. PWR plants. However, plugs made with what were thought to be relatively non-susceptible heats have recently experienced significant circumferential cracking at only about 20% of the lifetime estimated by Westinghouse. The USNRC now requires U.S. utilities to implement a program of plug removals, inspections, and repairs for all Westinghouse mechanical plugs fabricated from thermally treated Alloy 600. (USNRC 1991a).

- Welded plugs manufactured by Combustion Engineering have also degraded and resulted in leakage in service. Cracking in these Alloy 600 plugs has occurred in the welded region and is believed to be caused by PWSCC degradation.

Pressurizer Penetrations. PWSCC in the pressurizer penetrations (heaters, sleeves, and instrumentation nozzles) has occurred in the United States and abroad. A summary of Alloy 600 cracking incidents at U.S. PWRs is presented in Table B-6. The information includes unit name, affected component, date of component installation and cracking occurrence, incident summary, and remedial action(s) (O'Neill and Hall 1990). A cracking incident in a non-pressurizer component, steam generator drain pipe, is also included in Table B-1. More than seven pressurizer instrument nozzles and about 22 heater sleeves at 5 PWRs have cracked and several of these nozzles and most of the sleeves have leaked. A similar summary of Alloy 600 cracking incidents in French PWRs (EdF plants) is presented in Table B-6. About 28 instrument nozzles experienced cracking at 7 PWR plants in France. Some selected cracking incidents at the U.S. PWRs are described here.

Table B-5. Summary of pressurizer incidents, domestic.

Plant/Date of Incident	Affected Component	Date of Commercial Operation	Detection Method	Outcome	Remedial Action	Number Cracked
San Onofre-3 / Feb. 1986	instrument nozzles	1983	Leak (0.15 gpm) in vapor space; dye penetrant teseing revealed crack in nozzle	Axial crack in nozzle - suspected PWSCC: intergranular attack, no contaminants, susceptible material, residual weld stresses.	One nozzle replaced in 1986, two in 1987, with more resistant heat of material.	3
Arkansas-2 / Apr 1987	heaters and sleeves	1980 (Sept 1982, Watlow heaters installed)	Boric acid deposits and corrosion found on lower head; leakage from cracked sleeve due to ruptured heater.	Axial + circumferential cracking of heater sheath - PWSCC suspected: Residual + applied stresses, temperature, cold-worked micro-structure.	Removal of all Watlow heaters so pressure boundary sleeve not jeopardized; damaged holes plugged; heaters replaced. Sleeves subsequently restored.	2 heater sheaths 1 sleeve
St. Lucie-2 / Oct 1987	instrument nozzles	1983	Axial indications in two nozzles of four; same heat of material as SONGS-3.	Suspected PWSCC - Met exam never done.	Replaced the four nozzles; potential SL leak evaluation done for seven remaining A600 nozzles - continued operation.	2
Calvert Cliffs-2 / May 1989	heater sleeves	Apr 1977	Boric acid crystal buildup at bottom head indicated leak; verified by LPT. Indications also in instrument nozzles.	Axial cracks in upper 3-4 in. (reamed area); no indications across P.B. weld or in J-weld. PWSCC-cold work by reaming, susceptible microstructure, high yield strength; no threat of unisolable leak.	1) Inspection of pressurizer lower head each outage for leakage. 2) Further testing if necessary. 3) Replace sleeves with Alloy 690. 4) Review of fabrication history of C-E NSSS heater sleeves.	20
Calvert Cliffs-2 / 1989	instrument nozzle	Apr 1977	Leak; boric acid noticed	Axial cracks on ID; nozzle had been reworked, along with three others; PWSCC identified as failure mode.	Replace four nozzles with Alloy 690.	1
Arkansas-1 / 1990	instrument nozzle		Nondestructive examination detected a small, throughwall axial crack		Partial replacement of nozzle and establishing a penetration pressure boundary at the outside surface of the pressurizer shell by placing a weld around the penetration.	1
NON-PRESSURIZER						
Shearon Harris / Jul 1988	S/G drain pipe	May 1987	Boric acid deposits noted by visual examination at bottom of channel head, S/G A + B; ECT detected 100% cracks S/G B + C.	PWSCC suspected; drain pipe hard-rolled into drilled hole; axial orienta-tion of cracks; no cracks observed at weld (cladding-to-drain pipe seal).	Drain line repaired by W.	

Table B-6. Summary of pressurizer incidents, EDF.

Plant/Date of Incident (No. of cycles)	Affected Component	Date of Commercial Operation	Detection Method	Outcome	Remedial Action	Number Cracked
Cattenom-2 / Apr 1989 (1)	instrument nozzle	1987	Dye penetrant	Axial and circum-ferential cracks		3
Nogent-1 / June/July 1989 (1)	instrument nozzle		leakage detected	PWSCC confirmed by met exam; axial cracks in rolled region near weld.	1) Short term: elim-inate penetrations - use external measurements; repair "unacceptable" (14) cracks. 2) Long term: replace all A600 sleeves and nozzles with A690 or SS/I-182.	2
Belleville-1 / 1989 (1)	instrument nozzle	1987	Visual indication (circumferential)	No leak occurred; PWSCC sus-pected; axial and circumferential cracks.		2
Saint Alban-2 / Oct. 1989 (1)	instrument nozzle	1986	Dye penetrant exam showed indication(s)	Axial cracks only - no leaks		5
Flamanville-2 / 1989 (2)	instrument nozzle	1985	Dye penetrant exam showed indication(s)	Axial only		7
Cattenom-1 / 1989 (2)	instrument nozzle	1986	Dye penetrant exam showed indication(s)	Axial only		6
Paluel-2 / 1989 (3)	instrument nozzle	1985	Dye penetrant exam showed indication(s)	Axial only		3

Leak indications were noted in the heater sleeves at Calvert Cliffs Unit 2 (Combustion Engineering plant) in 1989 during a routine inspection (*Inside NRC* 1989). Further investigations revealed indications in 28 of the 120 sleeves; boric acid crystals had formed rings around 20 of the 28 penetrations, verifying that leakage had occurred. The cracks were linear, axial, and confined to the top 2 inches of the sleeve. Detailed evaluation of a damaged sleeve revealed that the cracks originated from the inside surface of the sleeve and propagated through the wall; there were no cracks in the sleeve-to-cladding weld (Pathania and Gilman 1991). No contaminants were found on the fracture surfaces that could account for the observed cracking. Therefore, the failures were attributed to PWSCC. Further inspection revealed cracks on the inside surfaces of several other heater sleeves. Although the Calvert Cliffs Unit 1 heater sleeves were made of the same heat of material as the Calvert Cliffs Unit 2 material, the Unit 1 sleeves did not crack. major difference between the sleeves in the two units was in the amount of cold working performed during installation (O'Neill and Hall 1990). The sleeves in Unit 2 were reamed on the inside surface from 23.0 to 23.2 mm (0.905 to 0.913 in.) to allow for heater installation and then welded to the stainless steel cladding. The sleeves in Unit 1 were welded first and then reamed to allow for installation of the 22.7-mm (0.895-in.) diameter heaters. Therefore, the reaming was more severe in Unit 2, which resulted in higher residual stresses on the inside surface of the Unit 2 pressurizer sleeves. The sleeves were not heat treated to reduce the residual stresses introduced by reaming. All Calvert Cliffs Unit 2 Alloy 600 heater sleeves and the affected penetrations (discussed in next paragraph) were replaced with Alloy 690 sleeves and penetrations; Alloy 690 has a higher chromium content and is immune to PWSCC.

Cracking of Alloy 600 instrument penetrations, some located in the pressurizer vapor space and some in the liquid space, has occurred in three Combustion Engineering plants and one Babcock & Wilcox plant in the U.S. and seven Électricité de France (EDF) plants in France (O'Neill and Hall 1990). All of the cracks in the U.S. plants and five of the EDF plants were axial in orientation, but both axial and short circumferential cracks have been discovered in two French plants. A 34-L/h (0.15-gpm) leak from an instrument penetration at the top of the San Onofre Unit 3 pressurizer head was discovered in 1987. A subsequent liquid penetrant inspection showed crack indications in another San Onofre Unit 3 pressurizer instrument penetration that had previously been inspected and found to be defect-free. The material had a high carbon content (0.065 wt%), a high yield strength [420 MPa (60.9 ksi)], and it is suspected that residual tensile stresses had been introduced during welding. Two penetrations from St. Lucie Unit 2 (which is also a Combustion Engineering plant), made of the same heat of material as the San Onofre penetrations, were also found to have crack-like indications in 1987. Boric acid deposits were found around an instrument penetration at Calvert Cliffs Unit 2 in 1989. Three separate cracks on the inside diameter of the penetration were discovered, extending from just inside the pressurizer to about 19 mm (0.75 in.) through the penetration wall.

Circumferential cracks in the instrument nozzles were discovered at two EDF plants. Although these cracks were small, they are more of a safety concern than the axial cracks, because if they become sufficiently deep, the end of the penetration might blow out and cause a small-break LOCA rather than a small leak. The penetrations were repaired by removing the old instrument

penetration, temper beading an Alloy 182 coating on the outside of the pressurizer, and then welding in a replacement stainless steel penetration.

Control Rod Drive Mechanism Nozzles. In September 1991, a leak from a peripheral CRDM nozzle occurred during a 10-year hydrotest at Bugey 3, a French PWR, which had operated for about 84,000 h (72,000 effective full power hours) since 1979. The hydrotest pressure was 20.7 MPa (3,002 psi). The leak was detected by acoustic emission monitoring, and its rate was about 0.70 L/h (0.003gpm). Visual examination revealed that the leaking crack was oriented axially and located on the downhill side at the elevation corresponding to the lowest portion of the partial penetration weld.

Destructive examination of the damaged Bugey 3 nozzle revealed that the through-wall crack was initiated on the nozzle inside surface and was caused by primary water stress corrosion cracking (PWSCC) and not by fatigue. Such cracking takes place in high-nickel alloys that are exposed to a PWR environment and requires the simultaneous presence of high tensile stresses, high operating temperatures, and a susceptible microstructure. The crack was present prior to the hydrotest, but significant leakage did not occur during operation. The destructive examination also revealed the presence of a small circumferential crack in the base metal on the outside surface of the nozzle. The circumferential crack was connected to the through-wall crack and could be a part of that crack, or the primary coolant that leaked from the through-wall crack could have caused the crack.

As of September 1994, more than 4,181 CRDM nozzles were inspected at 78 overseas and one U.S. PWR plant, and generally short, axial PWSCC cracks were found in 101 nozzles, mostly the peripheral ones. These inspection results are summarized in Table B-6 (Shah, Ware, and Porter 1994). PWSCC of the nozzles has been found at about 35 European PWR plants. About thirty of these plants are in France, two in Sweden, two in Belgium, and one in Switzerland. In early 1994, cracks were found in the CRDM nozzles of a Spanish one-loop plant (Zorita); most of these cracks were axial and in the free span of the nozzles, though some of the cracks were circumferential and located near the partial penetration weld. The cracks were caused by the chemical attack resulting from an intrusion of demineralizer resins into the primary coolant and not by PWSCC. However, PWSCC could have played some role in causing the circumferential cracking near the weld.

B-6. Flow-Accelerated Corrosion of Carbon Steel Components

Flow-accelerated corrosion has been a most destructive corrosion mechanism for high energy carbon steel piping in light water reactors. It has caused rupture of both large- and small-diameter piping carrying either single phase or two-phase flow. Single-phase flow accelerated corrosion has also caused significant wall thinning of carbon steel J-tubes and feedrings within the recirculating steam generators (Roarty 1986, Thailer, Dalal, and Goyette 1995). First we describe few selected events related to single-phase flow and then with two-phase flow.

Table B-7. Summary of control rod drive mechanism nozzle inspection results. [°C = 5/9 (°F-32)][a]

Country	Plant Type	Plants Inspected	Operating Time (EFPH)[b] K Hours	Estimated Head Temp (°F)	Total Penetrations	Penetrations Inspected	Penetrations with Indications
France[c]	CPO	6	80–107	596–599	390	390	19
	CPY	25	40–97	552	1625	1625	52
	1300MW	14	30–51	558–597[d]	1080	1080	18
Sweden	3 Loop	3	75–115	580–606	195	190	8
Switzerland	2 Loop	2	155	575	72	63	2
Japan[e]	2 Loop	3	105–108	590–599	123	107	0
	3 Loop	1	99	610	62	57	0
	4 Loop	1	46	590	74	62	0
Belgium[f]	2 Loop	2	125-140	585	99	99	1 scratch
	3 Loop	5	60–130	549–603	325	133	1 scratch
Spain[g]	3 Loop	4	65-70	610	260	82	0
Brazil[g]	2 Loop	1	25	—	40	40	0
USA	2 Loop	1	—	598	49	49	0
Total		68[h]			4,394	4,181	101

a. This table updates the inspection results previously published by Strosnider (1993).

b. Effective Full Power Hours.

c. As of July 1994 [A. Teissier (EDF), "Strategy for the Maintenance of Pressure Vessel Head Penetrations and Pressurizer Nozzles," presented at the International Symposium on Contribution of Materials Investigation to the Resolution of Problems Encountered in Pressurized Water Reactors (Fontevraud III), September 12-16, 1994].

d. Head temperature was 597°F prior to inspection. Then it was reduced to 589°F by decreasing the hot leg temperature. The temperature was reduced further to 558°F by T_{cold} conversion of the vessel head.

e. As of June 1994, penetrations in 11 additional Japanese plants have been inspected (Iwahashi et al. 1994). The available information suggests that these inspections did not reveal any indications.

f. From *Nucleonics Week*, June 30, 1994, and Daoust 1994. Total numbers of penetrations are estimates.

g. Bamford, W. 1994. "An Integrated Industry Approach to the Issue of Head Penetration Cracking," presented to the USNRC Advisory Committee on Reactor Safeguards, September 9.

h. Total number of plants inspected is 79 including 11 Japanese plants, for which the detailed results are not available.

Single-Phase Flow-Accelerated Corrosion. Flow-accelerated corrosion caused the rupture of the feedwater piping outside the containment at both the Trojan plant in 1985 (Stoller 1985) and Surry Unit 2 in 1986 (Virginia Power 1987). A pressure pulse caused the ultimate rupture of feedwater piping already significantly degraded by flow-accelerated corrosion at both plants. In neither the Trojan nor Surry case was there a leak or any other warning signs indicating incipient failure. As a result of the Surry accident, the NRC staff asked that all utilities with operating nuclear power plants inspect their high-energy carbon steel piping (USNRC 1987b). Various degrees of wall thinning in six BWR feedwater-condensate systems were identified; these systems are reported in Table B-8. Also, the degraded components, fittings, and straight runs in the 27 PWR feedwater-condensate systems identified in that inspection and reported to the NRC are listed in Table B-9 (USNRC 1988c).

Table B-8. BWRs with pipe wall thinning in the feedwater-condensate systems (USNRC 1988c).

Plant	Unit	Commercial Operation	Degraded Components (Fittings or Straight Runs)
Dresden	2	Jan-70	Elbows
Duane Arnold	-	Mar-74	Elbows, reducers, straight runs
Pilgrim	1	Jun-72	Elbows
Oyster Creek	-	May-69	Elbows
River Bend	1	Oct-85	Recirculation line
Perry	-	Jun-86	Straight runs

A potential generic problem was discovered at Catawba Unit 2 in 1991 that may affect all the Westinghouse Model D4, D5, and E steam generators in which a portion of the main feedwater is diverted to the auxiliary feedwater nozzle via the preheater bypass line. (Stoller 1992, USNRC 1992) An example of a preheater system is shown in Figure B-4. The fluid velocity in the 102-mm (4-in.) diameter preheater bypass line and the connecting auxiliary feedwater line was in the range of 9 to 11 m/s (30 to 35 ft/s). The licensee detected several locations in this piping that were at or near the minimum required wall thickness. Examinations revealed that single-phase flow-accelerated corrosion had reduced the nominal 8.56-mm (0.337-in.) wall thickness to 4.70-mm (0.185-in.) in only four operating cycles. This implies a flow-accelerated corrosion rate of about 1.0 mm/cycle (0.04 in./cycle). If the preheater bypass line had ruptured, the break would not have been isolable and would have resulted in the steam generator coolant being released outside containment. Over 27 m (90 ft) of piping was replaced at Catawba Unit 2.

Table B-9. PWR plants with pipe wall thinning in feedwater-condensate systems (USNRC 1988c).

Plant	Unit	Commercial operation	Degraded components (fittings, straight runs)
Arkansas Nuclear One	1	August 1974	Elbows, drain pump discharge piping
Arkansas Nuclear One	2	December 1978	Undefined
Calvert Cliffs	1	October 1974	Elbows, reducers, straight runs
Calvert Cliffs	2	November 1976	Elbows, reducers, straight runs
Callaway	-	October 1984	Recirculation line elbows
Diablo Canyon	1	April 1984	Elbows, straight runs
Diablo Canyon	2	August 1985	Elbows, Y
D.C. Cook	2	March 1978	Elbows
Fort Calhoun	-	August 1973	Elbows, straight run
Haddam Neck	-	July 1967	Recirculation line
Millstone	2	October 1975	Elbows, heater vent piping
North Anna	1	April 1978	Elbows, straight runs
North Anna	2	June 1980	Elbows, straight runs
H. B. Robinson	2	September 1970	Recirculation lines
Rancho Seco	-	September 1974	Straight runs downstream of feedwater isolation valves or main feedwater pumps minimum flow valves
San Onofre	1	June 1967	Reducers, heater drain piping
San Onofre	2	July 1982	Heater drain piping
San Onofre	3	August 1983	Heater drain piping
Salem	1	December 1976	Recirculation line
Salem	2	August 1980	Recirculation line
Shearon Harris	-	October 1986	Recirculation line
Surry	1	July 1972	Fittings
Surry	2	March 1973	Fittings
Sequoyah	1	July 1980	Elbows, straight runs
Sequoyah	2	November 1981	Elbows
Trojan	-	December 1975	Elbows, reducers, straight runs
Turkey Point	3	October 1972	Feedwater pump suction line fittings

Generally, the flow-accelerated corrosion monitoring programs concentrate on inspection of pipe elbows and tee fittings, the sites where local high velocities may be present. However, flow-accelerated corrosion has caused rupture at other feedwater piping sites, such as in the flange of a flow measuring device downstream of an orifice at Loviisa Unit 1 in Finland and in the straight portion of a pipe, located immediately downstream of a level control valve, at Surry Unit 1 and at Millstone Unit 3. Flow-accelerated corrosion has caused significant wall thinning of the feedwater control valve bypass line at both the San Onofre and Diablo Canyon plants. It was surprising to find significant wall thinning and failures of the startup feedwater system piping at both the Wolf Creek and Callaway plants because these systems are used for a very short time period during startup. Investigation of these failure showed that the cause was the flow resulting from the leaking valves on the piping (Chexal et al. 1996).

Two-Phase Flow-Accelerated Corrosion Flow-accelerated corrosion has caused ruptures in two-phase systems at three PWRs: Oconee Unit 2 in 1982, Arkansas Nuclear One Unit 2 in 1989, and Sequoyah Unit 2 in 1993. These three ruptures occurred within 9 to 11 years after commercial operation of the affected plants. Flow-accelerated corrosion caused a 1,219-mm (4-ft) rupture of a 609.6-mm (24-in.)-diameter, long-radius elbow in the feedwater heat extraction line that is supplied steam from the high-pressure turbine exhaust at the Oconee Unit 2 in 1982 (USNRC 1982). The utility established a pipe inspection program for two-phase (steam/water) systems after this incident. After the feedwater piping rupture accident at Surry Unit 2 in 1986, the utility augmented this program to include single phase systems (USNRC 1991b).

In 1989, following the 18 April rupture of a 355.6-mm (14-in.)-diameter steam extraction line at Arkansas Nuclear One Unit 2, pipe inspections revealed significant thinning of other sections of the two-phase steam extraction piping at the plant. The pipe wall was worn from the nominal 9.52-mm (3/8 in.) thickness to a thickness of about 0.79-mm (1/32-in.). The 180-degree fishmouth rupture was about 76.2-mm (3-in.) wide. That prompted the utility to replace more than 30.48-m (100 ft) of carbon steel piping with 2.5% chrome alloy material (Stroller 1989).

A third incident occurred at Sequoyah Unit 2, a 1,148 MWe PWR that has been in commercial operation since 1982. An extraction line to the feedwater heater ruptured and caused a 76- by 152-mm (3- by 6-in.) hole in the line. The cause of this event was a programmatic failure of the erosion/corrosion program resulting from insufficient management of the program (Stoller 1993). To prevent recurrence, an independent review of the erosion/corrosion program for adequacy and completeness was to be performed. The plant was to evaluate appropriate piping systems on both Units 1 and 2 again. Inspections, as well as repair and replacements, were to be performed based on the results of the evaluation. This resulted in a long shutdown for both units.

B-7. Boric Acid Corrosion

Table B-10 presents the summary of boric acid corrosion of carbon steel components in the PWR primary coolant system during 1977 to 1989 period. Most of the leaking events are because of leaking manway gaskets, pump seals, and leaky valves. A review of LERs from 1985 to 1996 is currently being performed and the results will be summarized later.

B-8. Wear

Movement of the in-core neutron flux monitor thimble tubes caused by flow-induced vibrational can wear the tubes and their guides. The thimble tubes in the Westinghouse-designed plants constitute part of the primary pressure boundary. These tubes are supported by (a) guide tubes within the lower vessel region, (b) the core support columns in the region between the bottom support casting and the lower core plate, (c) guide tubes in the fuel assemblies, and (d) high-pressure conduit between the reactor vessel and the seal table. However, a small portion of the thimble tube is directly exposed to the reactor coolant flow as shown in Figures B-5 and B-6. This exposed portion is between the top of the lower core plate and the bottom of the fuel assembly. Many U.S. plants have detected thimble tube wear and several instances of leaks, and thimble tube thinning and leakage have been detected in facilities in France and Belgium. For example, wall thinning was identified in 23 out of 50 thimble tubes in North Anna Unit 1; one tube thinned as much as 49% (USNRC 1987b). Nineteen of the 58 thimble tubes in D. C. Cook Unit 2 were found to have more than 60% wall thinning. Westinghouse sets 60% thinning as a replacement criterion (*Inside NRC* 1988a). More than 70% of the thimble tubes at South Texas Unit 1 showed wear after only 32 weeks of full-flow operation. One thimble tube had 60% of the wall thickness removed by wear (*Nucleonics Week* 1988). Initially, the utility installed flow-limiting devices in an attempt to shield the tubes from cross-flow. When the problem continued, the utility removed the previously installed flow limiting devices, installed thicker-walled tubes, and installed both a manual isolation valve and a magnetic ball check valve on each tube (*Inside NRC* 1988b).

Although Combustion Engineering and Babcock & Wilcox plants also contain in-core flux monitoring instrumentation, the support and sealing designs are different from the Westinghouse design, and no problems have been reported.

Reactor internals keys and pins may also experience wear over plant lifetime. The core barrel at the Palisades plant was loosened by wear caused by flow-induced vibrational (Fry et al. 1974). The wear occurred where the core barrel was clamped between the pressure vessel and vessel head (see Figure B-7). Movement of the control rod assemblies causes wear of their guide tubes.

Table B-10. Summary of boric acid corrosion of carbon steel.

Date	Plant (NRC Notice, etc.)	Corroded component	Type of corrosion	Source of Leakage
1977	St. Lucie	Steam Generator Manway Closure Studs	Corrosion Wastage	Manway Gasket Leakage
1978	St. Lucie	Pressurizer Manway Closure Studs	Corrosion Wastage	Manway Gasket Leakage
1979	Zion,, Unit 1	CVCS Valve	Erosion/Corrosion	Unknown
*5/80	Fort Calhoun I&E Notice 80-27	Reactor Coolant Pump Studs	Wastage: 2.4 in. Max. in 14 months	Pump Case/Cover Interface
6/80	Calvert Cliffs Units 1 & 2	Reactor Coolant Pump Studs Steam Generator Manway Studs	Corrosion Wastage	Leaky Gasket
1/81	Calvert Cliffs Units 1 & 2	Suction Piping to Reactor Coolant Pumps	1/8 in. Corrosion Wastage	Leaky Pump Seal Pressure Lines/ Bleed Off Lines
7/81	Kewaunee	Instrument Isolation Valve's Bonnet	---	Leaking Valve's Diaphragm
2/81	Oconee Units 1 & 2	Reactor Coolant Pump Studs	Corrosion Wastage	Leaky Gasket
1981	Arkansas 1	Steam Generator Manway Closure Studs	Corrosion Wastage	Leaking Closure Gasket
1981	D.C. Cook 2	Check Bonnet Bolts	Corrosion Wastage	Valve Body to Bonnet Gasket Leakage
*3/82	Maine Yankee I&E Notice 82-06	Steam Generator's Manway Closure Studs	Corrosion Wastage and Cracks	Small Primary Coolant Leak
*10/86	ANO-1 I&E Notice 86-108	High Pressure Injection Nozzle attached to Cold Leg	½ in. Corrosion Wastage	Leaky Isolation Valve
*3/87	Turkey Point Unit 4 I&E Notice 86-108 Supplement 1	Reactor Vessel Head, Closing Studs and CRDM	Corrosion Wastage	Leaky Lower Instrument Tube Seal (500 lbs. of boric acid crystals formed)
*8/87	San Onofre Unit 2 I&E Notice 86-108 Supplement 2	Bolts on Valve Packing Follower Plate in Shutdown Cooling system	Corrosion Wastage	Leaky Valve Packing
*8/87	Salem Unit 2 I&E Notice 86-108 Supplement 2	Reactor Vessel Head	Corrosion Wastage 360 mils	Seal Weld on Instrument Penetration (crystals)
5/88	Millstone Unit 2	RPV Nozzles 1A & 1B	Corrosion .060 mils	RPV "O" Rings
12/89	ANO-1	CRD Housing Nut Rings	Corrosion Wastage	Leaking Gaskets CRDM Flanges

* IE Information Notices were issued.

B-9. References

Benson, J. 1988. "Application of an F* Probe at Connecticut Yankee," presented at the *EPRI Steam Generator Workshop, Myrtle Beach, South Carolina, June 7-9.*

Chexal, B., et al. 1996. *Flow-Accelerated Corrosion in Power Plants*, EPRI TR-106611, Electric Power Research Institute, Palo Alto.

Fry. D. N., et al. 1974. *Analysis of Neutron-Density Oscillations Resulting From Core Barrel Motion in the Palisades Nuclear Power Plant*, ORNL-TM-4570, Oak Ridge National Laboratory.

Gorman, J. A., and E. S. Hunt 1986. *Status of Cracking and Remedial Measures for PWR Steam Generators with Full-Depth Expanded Tubing,* EPRI NP-4459-LD, Electric Power Research Institute, Palo Alto.

Hunt, E. S., and J. A. Gorman 1986. *Status and Suggested Course of Action for Nondenting-Related Primary-Side IGSCC of Westinghouse-Type Steam Generators,* EPRI NP-4594-LD, Electric Power Research Institute, Palo Alto, May 1986.

Inside NRC 1989. "BG&E Assesses Pressurizer Leaks for Evidence of Corrosion Cracking," *Inside NRC 11,* l4, p. 11.

Inside NRC 1988a. "NRC to Require Thimble Tube Inspections after Cook-2 Reports Problems," August 1, pp. 1-2.

Inside NRC 1988b. "NRC Staff was Planning to Issue a Low-Power License for Houston Lighting & Power Co.'s STP-2," December 19, p. 11.

Kuchirka, P. J., and J. W. Cunningham 1986. *Examination of Steam Generator Tubes R18C53HL and R18C43HL from the Jose Cabrera (Zorita) Nuclear Power Station*, EPRI NP-4760-LD, Electric Power Research Institute, Palo Alto.

Nucleonics Week 1989a. "NRC Deciding if PWRs Should Shut to Replace Faulty Tube Plugs," *Nucleonics Week, 30*, 13, March 30.

Nucleonics Week 1989b. "North Anna Plug Failure Shows Threat of Intergranular Cracking," *Nucleonics Week, 30*, 11, March 16.

Nucleonics Week 1988. "STP-1 Operating Time Limited as Thimble Tubes Keep Thinning," October 27, 1988, p. 6.

O'Neill, A. S., and J. F. Hall, 1990. *Literature Survey of Cracking of Alloy 600 Penetrations in PWRs*, EPRI NP-7094, Electric Power Research Institute, Palo Alto.

Pathania, R. and J. Gilman, 1991. "Corrosion-Related Degradation in Pressure Vessels," presented at the *SMiRT 11 Post Conference Seminar No. 2: Assuring Structural Integrity of Steel Reactor Pressure Boundary Components, Taipei, Taiwan, August 26-28.*

Shah, V. N., et at. 1997. *Review of Industry Effort to Manage Pressurized Water Reactor Feedwater Nozzle, Piping, and Feedring Cracking and Wall Thinning*, NUREG-CR-6456.

Shah, V. N., A. G. Ware, A. M. Porter 1994. *Assessment of Pressurized Water Reactor Control Rod Drive Mechanism Nozzle Cracking,* NUREG/CR-6245, EGG-2715, p. 9.

Simos, N., et al. 1990. "Assessment of Thermal Fatigue Crack Propagation in Safety Injection PWR Lines," *System Interaction with Linear and Nonlinear Characteristics,* PVP Volume 187, American Society of Mechanical Engineers, New York, pp. 65–72.

Smith, E. R. 1989. "North Anna Unit 1 Steam Generator Tube Leak Event," *Eighth Annual EPRI Steam Generator, NDE Workshop at Williamsburg, Virginia,* August, 1989.

Stoller (S. M. Stoller Corporation), 1993. "Manual Reactor Trip-High Generator Voltage-Steam in Voltage Regulator Cubicle-Extraction Steam Line Rupture-Erosion/Corrosion-Inadequate Management Oversight," *Nuclear Power Experience*, P.06.E.1211.

Stoller (S. M. Stoller Corporation) 1992. "IN 92-07 re: Rapid Flow-Induced Erosion/Corrosion of FW Piping - Westinghouse SG Design Deficiency," *Nuclear Power Experience*, PWR-2, VI.E.1131.

Stoller (S. M. Stoller Corporation) 1987. "Tube Plug Leak Exceeded Tech Spec Limit," PWR-2, V, D, January, p. 144.

Stoller (S. M. Stoller Corporation) 1985. "Heater Drain Pump Discharge Pipe Ruptured, Personnel Burned--FW Pressure Transient During Turbine, Reactor Trips--Pipe Eroded/Corroded," *Nuclear Power Experience*, PWR-2, III.

Stoller (S. M. Stoller Corporation) 1982. "Tubes, Plugs Leaked," PWR-2, V, D, October, p. 87.

Stout, R. D. 1985. "Postweld Heat Treatment Pressure Vessel Steels," *Bulletin 302*, Welding Research Council, New York, p. 1.

Su, N. T., 1990. *Special Study Report – Review of Thermal Stratification Operating Experience*, AEOD/S902, U.S. NRC.

Strauch, P. L., et al. 1990. "Stratification Issues and Experience in Operating Power Plants," *High Pressure Technology, Fracture Mechanics, and Service Experience in Operating Power Plants, ASME Pressure Vessels and Piping Conference, Nashville, Tennessee, June 1990*, PVP Vol. 192, pp. 85–92.

Tatone, O. S. and R. S. Pathania 1985. "Steam Generator Tube Performance: Experience with Water-Cooled Nuclear Power Reactors During 1982," *Nuclear Safety, 26, 5*, pp. 623-639.

Togo, et al. 1985. "Preventing Tube Degradation in Japan," *Nuclear Engineering International, 30,* 365, pp.43-44.

USNRC 1992. "Rapid Flow-Induced Erosion/Corrosion of Feedwater Piping," USNRC Information Notice No. 92-07.

USNRC 1991a. "Failure of Westinghouse Steam Generator Tube Mechanical Plugs," NRC Bulletin 89-01 Supp. 2, June 28, 1991.

USNRC, 1991b. "High-Energy Piping Failures Caused by Wall Thinning," USNRC Information Notice 91-18, March 12.

USNRC 1990. "Failure of Westinghouse Steam Generator Tube Mechanical Plugs," NRC Bulletin 89-01 Supp. 1, November 14, 1990.

USNRC 1989a. "Failure of Westinghouse Steam Generator Tube Mechanical Plugs," NRC Bulletin 89-01, May 15, 1989.

USNRC 1989b. "Potential for Stress Corrosion Cracking in Steam Generator Tube Plugs Supplied by Babcock & Wilcox," USNRC Information Notice 89-65.

USNRC 1989c. "Thermal Stresses in Piping Connected to Reactor Coolant Systems," USNRC Bulletin 88-08, Supplement 3.

USNRC 1988a. "Safety Injection Pipe Failure," USNRC Information Notice 88-01.

USNRC 1988b. "Thermal Stresses in Piping Connected to Reactor Coolant Systems," USNRC Bulletin 88-08.

USNRC 1988c. "Summary Responses to NRC Bulletin 87-01: Thinning of Pipe Walls in Nuclear Power Plants," USNRC Information Notice 88-17, April 22.

USNRC 1988d. "Thermal Stresses in Piping Connected to Reactor Coolant Systems," USNRC Bulletin 88-08, Supplement 2.

USNRC 1987a. "Feedwater Line Break," USNRC Information Notice 86-106, Supplement 1.

USNRC 1987b. "Thimble Tube Thinning in Westinghouse Reactors," USNRC Information Notice 87-44, September 16.

USNRC, 1982. "Failures in Turbine Exhaust Lines," USNRC Information Notice 82-22, July 9.

Virginia Power 1987. *Surry Unit 2 Reactor Trip and Feedwater Pipe Failure Report*, Rev. 0.

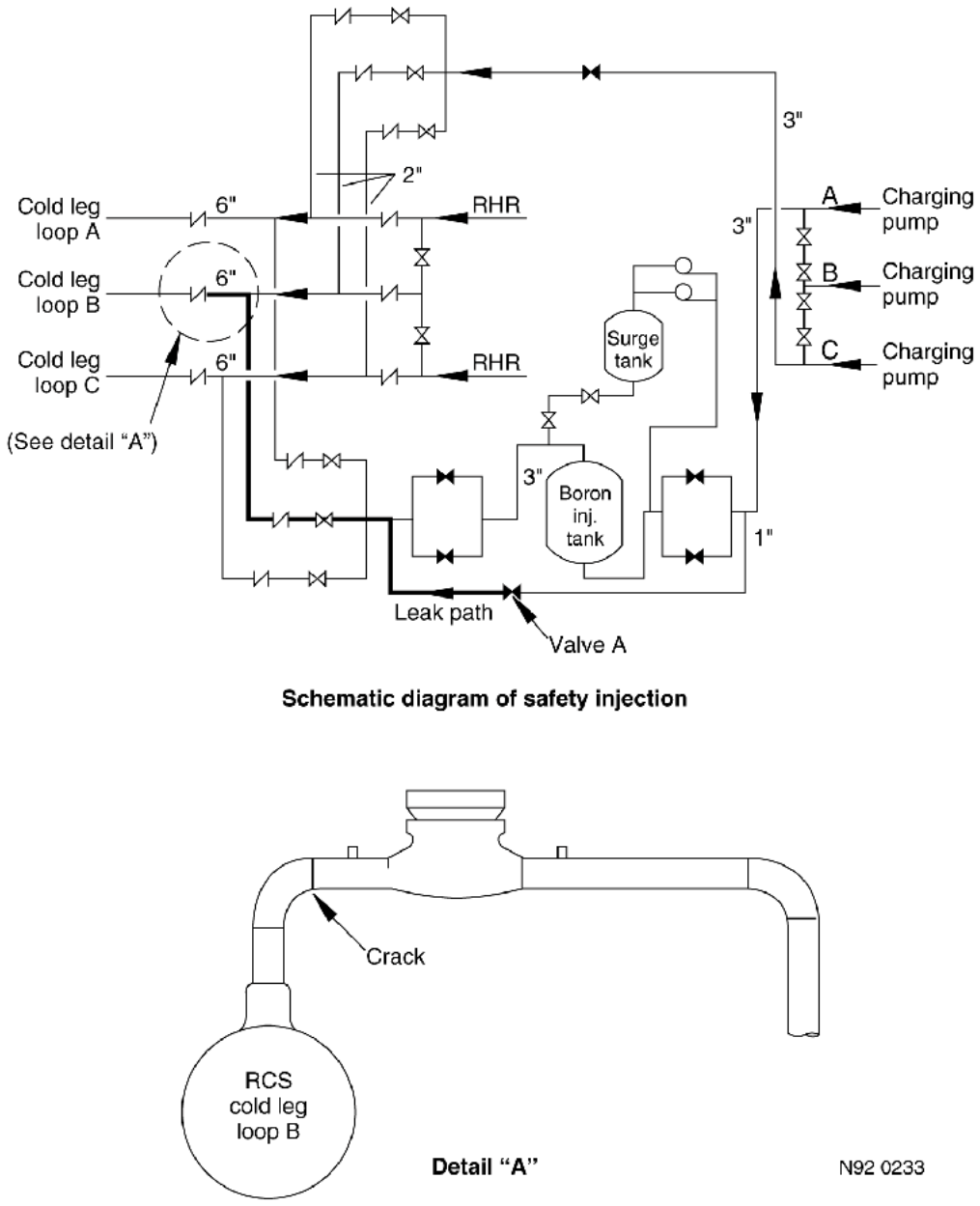

Figure B-1. Schematic diagram of a safety injection and residual heat removal system in a three-loop Westinghouse plant (Su 1990).

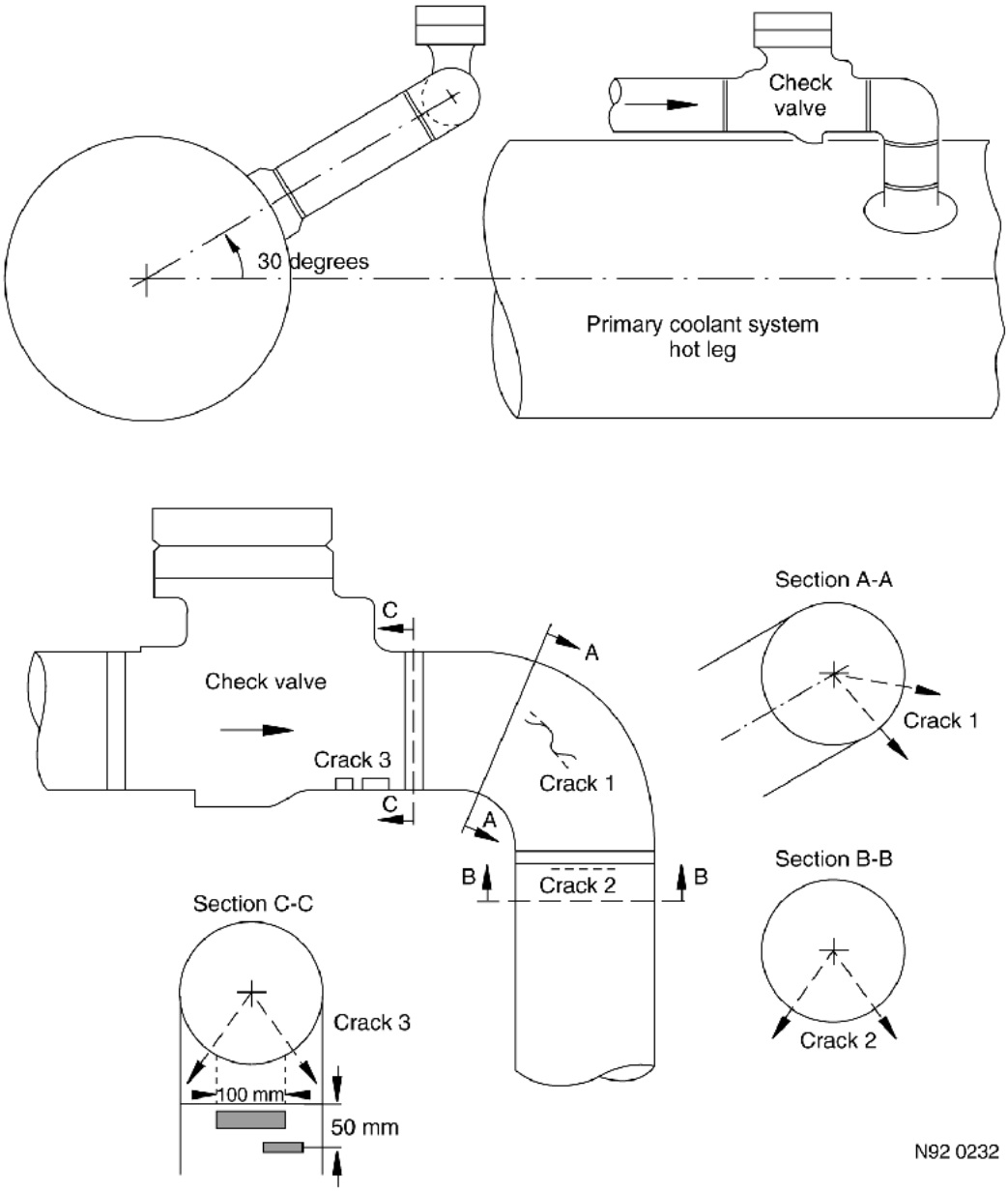

Figure B-2. Location of the cracks in the base metal and welds in the safety injection piping in Tihange Unit 1 (Su 1990).

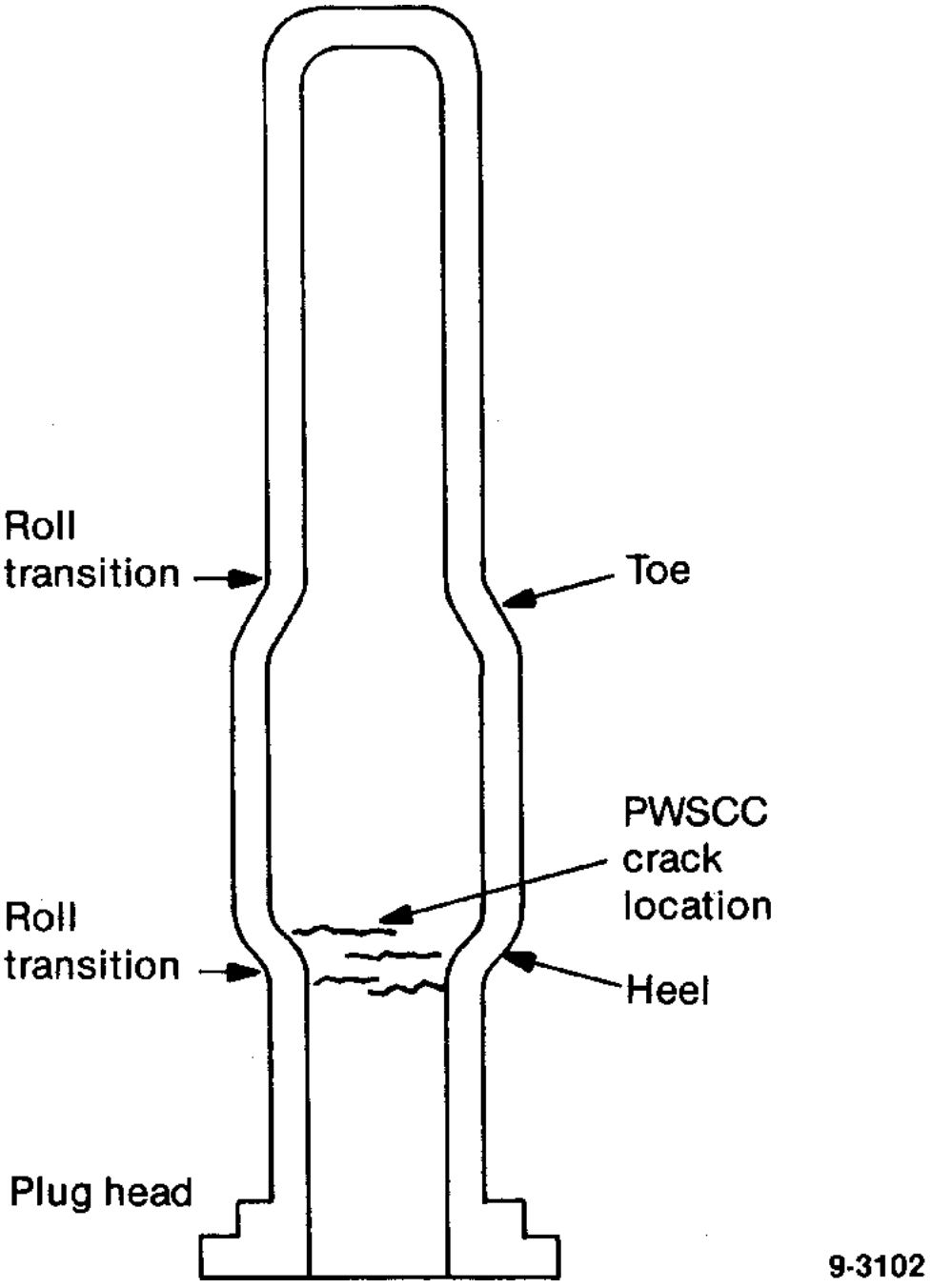

Figure B-3. PWSCC cracks in rolled plug supplied by Babcock & Wilcox (USNRC 1989b).

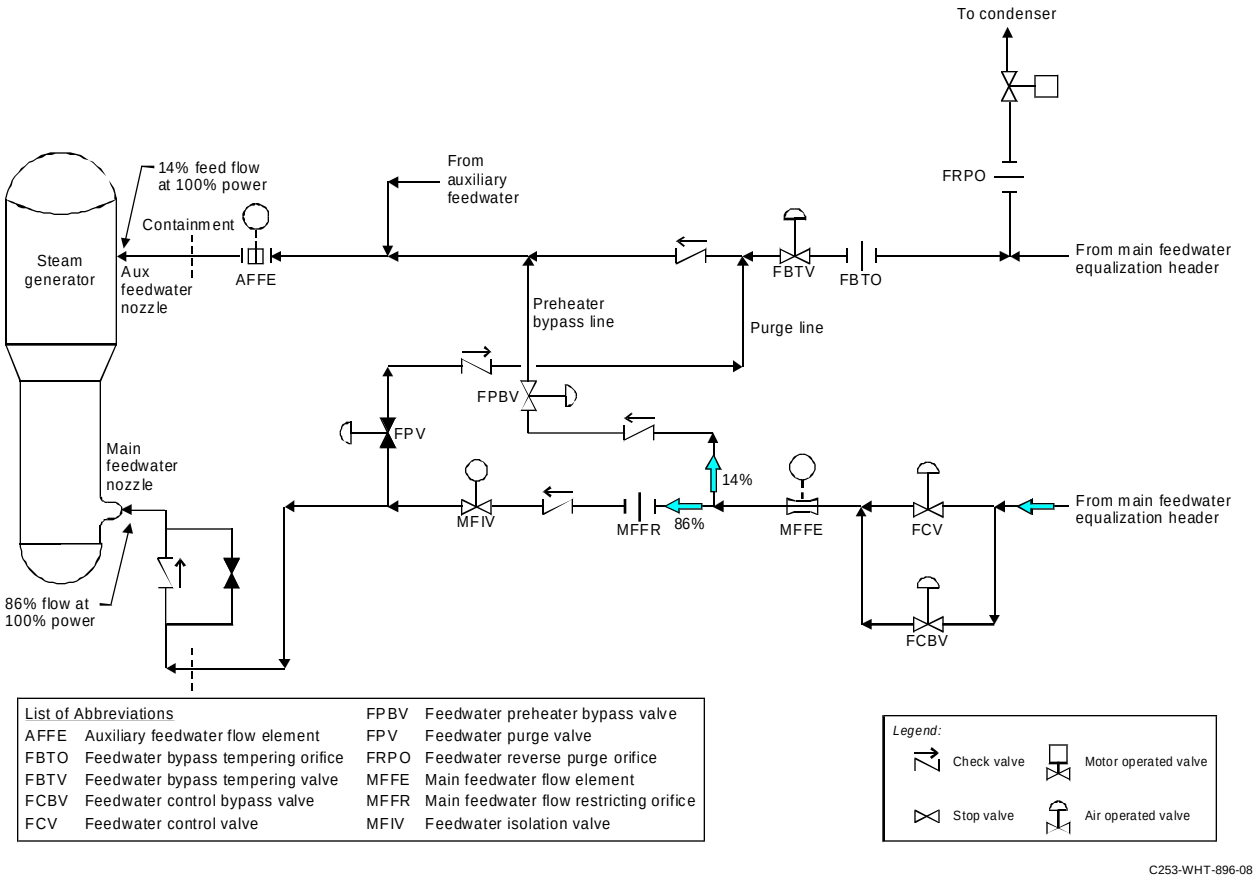

Figure B-4. Schematic of a feedwater system for a Westinghouse plant with steam generators equipped with preheaters.

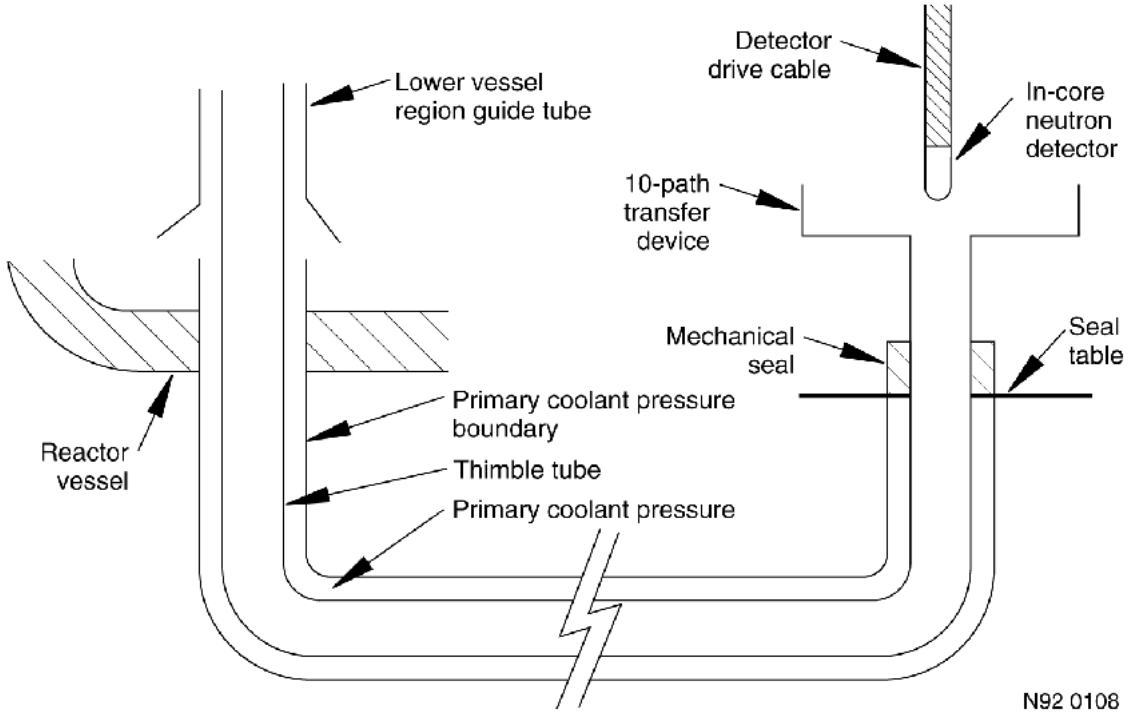

Figure B-5. Westinghouse flux thimble tube routing.

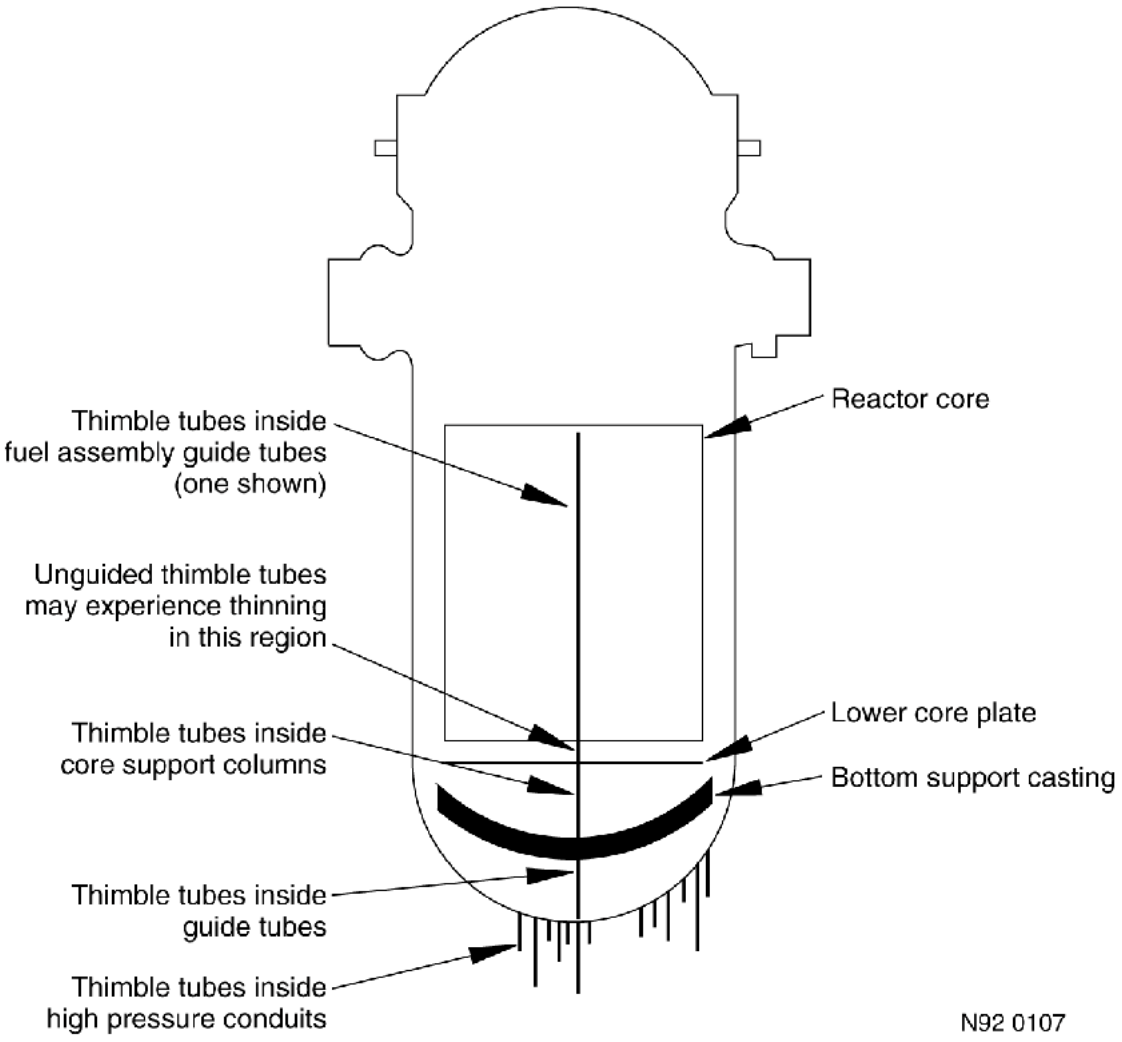

Figure B-6. Westinghouse in-core instrument guides (USNRC 1987b).

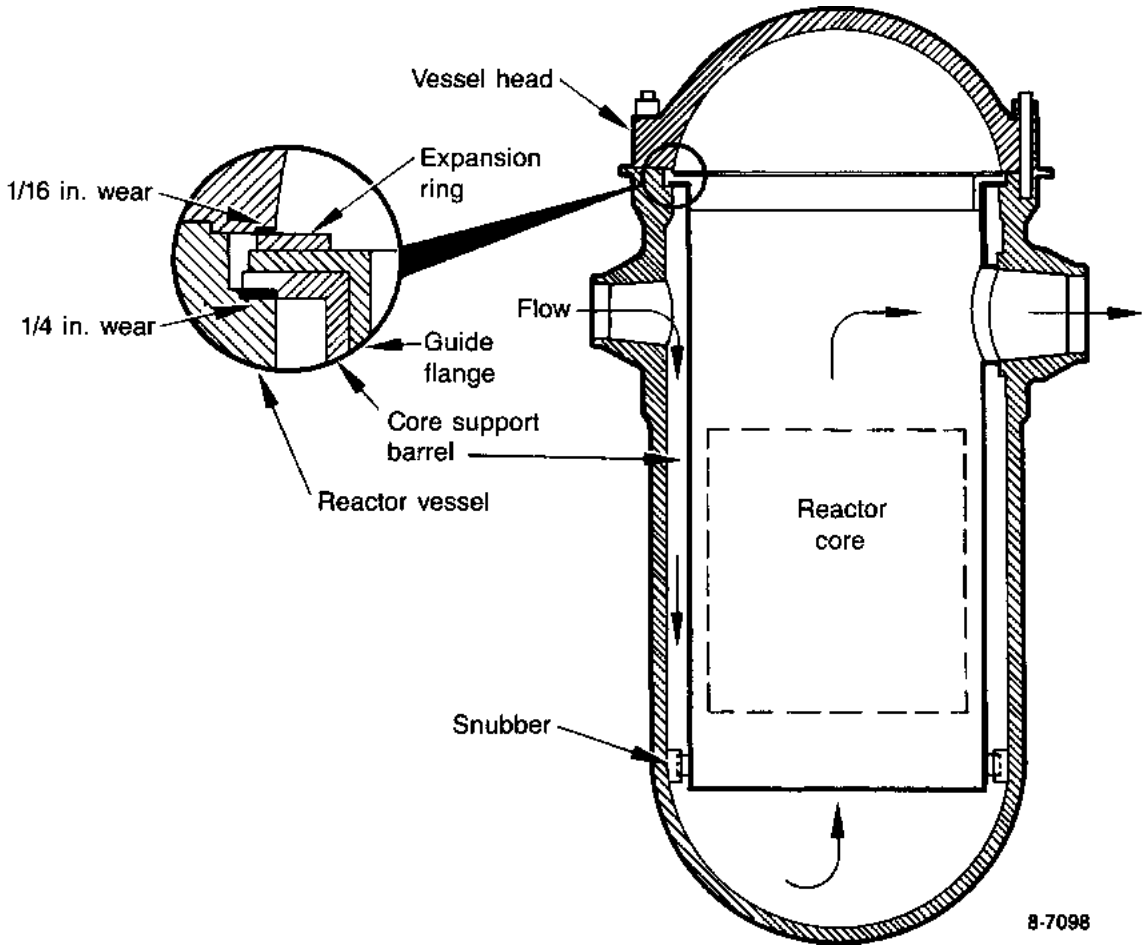

Figure B-7. Palisades core barrel wear (Fry et al. 1974).

Appendix C

Modeling of Radiation Embrittlement

APPENDIX C

Modeling of Radiation Embrittlement

The main concern relating to radiation embrittlement damage of PWR reactor pressure vessels is loss of fracture toughness and increase in ductile-to-brittle transition temperature of vessel materials. When a vessel is subjected to a pressurized thermal shock (PTS) transient, a preexisting crack in the vessel wall might be induced to propagate completely through the wall and result in vessel rupture. In a PTS event, an overcooling transient imposes simultaneously both low temperature and high pressure, and concurrent high tensile stresses on the inside surface of the vessel wall.

Before 1980 it was postulated that the most severe overcooling event for a PWR vessel is associated with a large-break loss-of-coolant accident (LOCA). This overcooling event had been analyzed and it was concluded that probability of resulting vessel failure was less than 10^{-6} at a 99% confidence level if the vessel was built to the specifications of the ASME Boiler and Pressure Vessel Code (White 1983). However, the addition of pressure stresses to the thermal stresses was not considered in the analysis because it was expected that during a large-break LOCA the reactor coolant system will remain at low pressure.

Since 1980, however, non-LOCA type thermal hydraulic transients have occurred in at least six operating commercial PWRs, where pressure vessels were subjected to unanticipated loadings: Robinson-2 in 1970, Rancho Seco in 1978, TMI-2 in 1979, Crystal River-3 in 1980, Ginna in 1982, and Prairie Island-2 (Dircks 1982). These transients have raised concern that the probability of pressure vessel rupture may be larger than previously considered. The transients may have caused a rapid cooling of the vessel internal surface, with resulting temperature distributions leading to significant tensile stresses. If such transients were to occur when the vessel is pressurized, the resulting additional tensile stresses would compound the problem significantly.

The reactor pressure vessels of significant PTS concern are the older vessels that have relatively high copper and nickel concentrations, primarily in the welds. The combined role of three factors has raised a significant concern about structural integrity of reactor pressure vessels: (1) reduced fracture toughness because of radiation embrittlement, (2) reduction in fracture toughness caused by low temperature in the transients, and (3) high tensile stresses at the inner surface during these transients.

The area of the vessel of particular concern during a PTS event is the beltline region, which is directly across from the core, where (a) radiation embrittlement damage is the greatest, (b) thermal shock effect could be severe, and (c) rupture of the vessel could preclude flooding of the vessel.

PTS events are analyzed in three steps: (1) identify significant overcooling transients that potentially could result in PTS, (2) estimate the frequency of through-wall cracks in the vessel wall subject to a given overcooling transient, and (3) estimate vessel rupture probability following through-wall cracks. The following brief outline of the PTS analysis:

> In the first step, thousands of hypothetical overcooling events were constructed and quantified using computer-generated event trees. All scenarios with a frequency greater than 10^{-7} per reactor year were explicitly considered, and those with lower frequency were grouped together. Then, thermal hydraulic analyses were performed for all the identified scenarios. In the second step, the temperature of the vessel wall and the stresses in the wall were estimated deterministically. Then, probabilistic fracture mechanics analysis was performed to estimate the conditional through-wall cracking for each scenario. In the third step, probabilistic fracture mechanics analyses were performed to estimate vessel rupture probability following through-wall cracks. This Appendix focuses on Step 2.

C.1 Probability of Through-Wall Cracks in the Vessel Wall

Several computer codes have been developed for calculating through-wall crack probability. Two of these codes include OCA-P (overcooling accident - probabilistic approach) developed at the Oak Ridge National Laboratory (Cheverton and Ball 1984) and VISA-II (Vessel Integrity Simulation Analysis) developed at the Pacific Northwest Laboratory (Simonen et al. 1986). These codes perform Monte Carlo analysis, which means that through-wall cracking probability is estimated by performing a large number of deterministic evaluations with random values selected for various parameters. This report describes input parameters for the VISA-II code, causes of uncertainty in these parameters, assumed distributions of these parameters, and sensitivity of calculated failure probability to the alternatives to the assumed distribution. The description of the input parameters presented is from the report by Simonen et al. (1986) and, therefore, the quantitative data presented here represent those available in the early 1980s.

The VISA II code is divided into two parts to define *stress* and *strength* models needed for Monte Carlo analyses. The deterministic part defines the *stress* model; the probabilistic part defines the *strength* model. In the first part, a deterministic fracture mechanics analysis is performed for a temperature and pressure transient defined by the user of the code. This analysis estimates values of crack-tip temperatures and applied stress intensity factors for several crack depths. These values are used by the probabilistic analysis performed in the second part. The second part treats flaw depth and fracture toughness of vessel materials as random variables. The sampled values of fracture toughness are compared with the stress intensity factors (estimated in the first part) at a sampled flaw depth to determine crack initiation and growth. The proportion of through-wall cracks in a large number of passes through the simulation loop is an estimate of the conditional probability of through-wall cracking (vessel failure).

C.1.1 Stress Model in the VISA II Code. The VISA II code uses closed form solutions for heat transfer and stress calculations. It uses influence coefficients for calculating applied stress intensity factors. The inputs for the deterministic analysis include (a) pressure and temperature of the reactor coolant as a function of time for a given PTS transient, (b) surface heat transfer coefficient, (c) material properties, and (d) wall thickness and radius of the vessel. Effects of cladding are included in the heat transfer and stress analysis.

C.1.2 Strength Model in the VISA II Code. For each pass through the simulation loop, simulated values of initial RT_{NDT}, fluence at the inner wall, flaw (crack) size, flaw location, and copper and nickel contents are selected from their respective distribution. These sampled values, as discussed later, are eventually used to determine the fracture toughness. With these values fixed for a given pass, the code performs time history analysis for a given transient. At the end of each time step, the simulated value of the fracture toughness is compared with the applied stress intensity factor at the crack tip. If the fracture toughness is less than the applied stress intensity factor, crack initiation occurs, otherwise, the simulation moves to the next time step. If crack initiation occurs, the crack is extended 0.25 in. and the crack arrest toughness, K_{Ia}, is simulated. If crack arrest occurs, the simulation moves to the next time step; otherwise, the crack is extended another 0.25 in., and a new value of K_{ia} is simulated. This process continues until either the crack becomes a through-wall crack or the transient is completed.

Each simulation pass results in one of the three outcomes: (1) no crack growth, (2) crack growth followed by crack arrest, or (3) a through-wall crack. The conditional probability of through-wall cracks is obtained by dividing the number of simulations (passes) that resulted in through-wall cracking by the total number of simulations that were made. The relevance of the estimated probability depends on the correctness of the fracture mechanics algorithm and the validity of the probability distributions of the random variables used in the analysis.

Simulated Fracture Toughness. For each time step, the sampled value of fluence at the crack tip is calculated. Then, the value of the shift in RT_{NDT} is calculated using sampled values of copper and nickel and the attenuated fluence. The calculated value of the shift is then added to the sampled initial RT_{NDT} to obtain the adjusted RT_{NDT}, which is used to estimate the simulated fracture toughness. This fracture toughness is compared with the applied stress intensity factor determined in the first part of the VISA-II code.

Vessel Simulation. An entire embrittled beltline region is simulated in the VISA-II code. The user provides a table of data that characterize each weld and plate that constitutes the beltline region. These data include copper and nickel contents, initial RT_{NDT}, and weld volumes and orientation (either longitudinal or circumferential). The flaws are assumed to be randomly located within the vessel wall.

C.2 Probability Distributions Used in the VISA II Code

The VISA-II code focuses on welds in the beltline region because they are more likely to have flaws and are more susceptible to damage from radiation than plates in the beltline region. Therefore, weld behavior is likely to dominate the through-wall cracking probability. The size of cracks in the weld material has the greatest uncertainty of the random variables considered in the VISA-II code. The other random variables considered in the code include copper and nickel contents, initial RT_{NDT}, trend curve for shift in RT_{NDT}, irradiation fluence, and fracture toughness,

Flaw Size Distribution. The VISA-II code uses the modified OCTAVIA flaw distribution. This distribution provides the probability P_s, that the deepest crack in the weld volume of the beltline region falls into a particular crack-size interval. For example, the probability for the deepest crack to be in the crack-size interval of 0.375 to 0.75 in. is 0.025. The user can define other flaw size distributions such as Marshall distribution and a distribution developed by Dufresne and Lucia. The comparison of these three flaw size distributions is presented in Table C-1.

Table C-1. A comparison of three flaw-depth distributions.

Depth (inches)		Probability Distribution		
		OCTAVIA	Marshall	Dufresne/Lucia
0.125	(0–0.1875)	0.847225	0.72614885	0.99535924
0.25	(0.1875–0.375)	0.125	0.19853597	0.00405525
0.5	(0.375–0.75)	0.025	0.06946752	0.00058543
1.0	(0.75-1.25)	0.0022	0.00562507	0.00000009
1.5	(1.25–1.75)	0.000425	0.00021033	0.00000000
2.0	(1.75–2.25)	0.0001	0.00001118	0.0
2.5	(2.25–2.75)	0.00003	0.00000096	0.0
3.0	(2.75–3.25)	0.000015	0.00000011	0.0
3.5	(3.25+)	0.000005	0.00000000	0.0

The user must specify the number of expected flaws in the beltline region of a given vessel. However, the expected number of flaws in the beltline region is known only with great uncertainty. Use of one flaw in the beltline region is suggested so that the output of the code is consistent with the prior calculations performed for USNRC.

The code assumes that the flaws are in the weld and are uniformly distributed within the weld material. Higher probabilities are given to welds having greater volume. The flaws are assumed to be randomly located along the length of each weld, typically at the inside surface of the vessel. However, VISA-II provides an option to allow the flaws to have random locations through the thickness of the vessel wall. All flaws in longitudinal welds are assumed to have axial orientation, and the ones in circumferential welds have circumferential orientation.

The contribution of flaws in the base metal (plates) to through-wall cracking in the vessel wall is neglected because often the embrittlement of the weld metal is much greater than that of the base metal. However, for some vessels the base metal toughness may be lower than the weld metal toughness. The VISA-II code can be used to analyze these vessels by treating each plate of the beltline region as a weld.

Causes for Uncertainty — Considerable uncertainty is associated with the selection of a flaw-size distribution. The flaw-size distribution discussed here is derived from sparse and/or incomplete data often lacking sound theoretical basis. For example, the OCTAVIA distribution is obtained by quantifying *experience* and *expert engineering* judgement and is not supported by specific experimental measurements. Three main reasons for the uncertainty in relevant flaw-size data are as follows:

1. There is a question about how to quantify the flaw size, that is, how many dimensions are needed to adequately define the flaw size. Flaw depth is considered to be the most important dimension, and most distributions define only flaw depth as an independent variable. However, there are some attempts to define both flaw-depth and length as independent variables.

2. It is difficult to size flaws with nondestructive examination (NDE) methods. Flaws with depth as small as 0.25 in. can lead to vessel failure, but it is difficult to detect flaws smaller than 0.5 in. with the NDE methods available in the early 1980s, and even more difficult to size them.

3. The distribution of flaw sizes differs by material and location. The distribution of flaw sizes in weld metal differs from that for steel plate, and underclad flaws (in heat-affected zone) are more likely than flaws in weld metal. The flaw size distributions employed in the VISA-II code do not account for these differences.

Sensitivity of Through-Wall Cracking Probability to Flaw Distribution — The simulated probability of vessel failure (through-wall cracking), when other inputs are held constant, is almost proportional to the probability assigned to flaw depth in the critical range between 0.25 and 1.0 in. Flaws smaller than 0.25-in. depth do not often result in failure (in simulations) and flaws greater than 1.0-in. depth are not frequent enough to have significant effect. Since the probability distributions

presented in Table 8 differ by two orders of magnitudes in the critical depth range (0.25 to 1.0 in.), there is great uncertainty associated with the choice of a flaw distribution: the probability of flaw depth between 0.25 to 1.0 in. is 0.1522 for OCTAVIA, 0.2736 for Marshall, and 0.00464 for Dufresne/Lucia distribution. Therefore, among these three distributions, the Marshall distribution is expected to yield the highest, the Octavia distribution intermediate, and the Dufresne/Lucia distribution the lowest vessel failure probabilities. Any increase in the knowledge of distribution of flaw sizes, especially depths, would result in corresponding decrease in the uncertainty of failure probability estimates.

Calculated failure probabilities are sensitive to flaw position, flaw length, and preservice inspection. Burried flaws compared to surface flaws, finite length flaws compared to infinite length flaws, and preservice inspection compared to no inspection, each reduces the calculated failure frequency by about two orders of magnitude.

Copper Content Distribution. The VISA II code assumes a truncated normal distribution for copper content, with a lower limit of 0.08 and upper limit of 0.4 wt%.[†] The user must specify the mean and the standard deviation of the distribution for each weld and plate of the vessel. Based on the limited data available in the early 1980s, the typical values for the mean copper content are in the range of 0.1 to 0.35 wt% for welds, and 0.05 to 0.2 wt% for base metal, with standard deviation in the range of 0.02 to 0.07 wt%. A standard deviation of 0.025 was used for several analyses performed for the USNRC.

Causes for Uncertainties — The uncertainty in copper content resulted from welding practices and steel making practices. A copper coated weld wire was used for welding to enhance electrical conductivity during welding and to reduce corrosion of weld wire. Since the thickness of coating was not controlled, copper content varies from weld to weld and it is different at different depths in a given weld, if different weld wires were used to complete the weld. Use of automotive scrap in steel making resulted in copper contents in vessel plates. The copper contents in the welds and plates were not controlled because their detrimental effect in radiation environment was not known.

Sensitivity of Through-Wall Cracking to Copper Content Distribution. The assumed standard deviation can significantly affect the calculated frequency of vessel failure. Increasing the standard deviation from 0.025 to 0.065, typically increased the failure probability by a factor 2 to 5. In some exceptional cases, the failure probability increased by one to two orders of magnitudes. For simulations in which vessel failures are predicted, the simulated copper contents are typically less than two standard deviations above the mean. The lower standard deviation, 0.025 wt% of copper, corresponds to a well characterized weld, and the higher standard deviation, 0.065 wt% of copper, corresponds to a poorly characterized weld.

[†] Some newer vessels have a copper content lower than 0.08 wt%.

Nickel Content Distribution. VISA-II assumes truncated normal distribution for nickel content. There is no truncation at the upper limit, but the lower limit is truncated at zero. The user has to specify the mean and standard deviations of distribution for each weld and plate of the vessel. Mean nickel contents for vessel materials vary from nearly 0.0 to as much as 1.0 wt%. The standard deviation has been taken as 0.0 for most calculations performed for the NRC.

Causes for Uncertainty — The uncertainty in nickel content is generally smaller than that in copper content because nickel was intentionally alloyed into both the weld metal and the base metal. An exception is the welding practice in which a pure nickel wire was added in a three-wire welding procedure. The variable feed rate of the nickel wire will cause greater variation in nickel content as compared to the case in which nickel was alloyed into the welding wire in a controlled manner.

Sensitivity of Through-Wall Cracking Probability to Nickel Content Distribution — Failure probabilities are relatively insensitive to uncertainties in the standard deviation of nickel content. Increasing the standard deviation for nickel content from 0.0 to 0.05wt% did not increase the failure probability by more than 30%. However, increasing the standard deviation from 0.0 to 0.15 wt% nickel increased the probability by factors as large as 2 to 3. The 0.05 wt% standard deviation corresponds to a weld made with nickel alloyed into the weld wire. The 0.15 wt% standard deviation corresponds to a possible uncertainty for a weld made using a pure nickel weld wire. The failure probability increases with nickel content, especially when copper content is high.

Initial RT_{NDT} Distribution. The property of initial RT_{NDT} has been studied extensively, and the normal distribution is a good approximation to the measured data. This distribution is assumed for initial RT_{NDT} in the VISA-II code. The mean value and standard deviation for each weld and plate in the vessel are input variables. Typical values for standard deviation have been 17°F for plates and 24°F for welds.

Causes for Uncertainties — The uncertainty in measuring the initial RT_{NDT} results from metallurgical variability and test variability. Initial RT_{NDT} is established from Charpy impact tests instead of fracture toughness tests because Charpy tests require small test specimens that can be easily irradiated, whereas fracture toughness tests require large test specimens. However, the Charpy test is a high rate impact test, whereas the fracture toughness test is performed at much slower rates. Therefore, the Charpy tests do not represent crack initiation and growth behavior in the thick-walled PWR vessels.

Sensitivity of Through-Wall Cracking Probability to Initial RT_{NDT} Distribution — Since the normal distribution is well established as an initial RT_{NDT} distribution, sensitivity of the failure probability to other distribution has not been evaluated.

Fluence Distribution. The distribution of fluence at the inner surface of the vessel wall is assumed to be normal in the VISA-II code. Data available in the early 1980s indicate that the fluence at the inner wall is known within 30 percent. There is no truncation of the normal fluence, except the calculated fluences that are less than zero are excluded. The user can specify the mean fluence to be the same at all locations of the inner wall, in which case the practice has been to use the peak value of the estimated fluence variation. The user has the option to follow a less conservative approach by prescribing the spatial variation of fluence along each weld and specifying a standard deviation of less than a typical value of 30 percent of the mean.

The neutron fluence attenuates as it penetrates the vessel wall. The attenuated fluence, f(x), at the crack tip is calculated using an exponential decay function

$$f(x) = f_0 e^{-ax},$$

where x is the distance in inches between the crack tip and the vessel inner surface, a is the decay factor, and f_0 is the simulated fluence at the inner surface. The VISA-II code uses $a = 0.24$, which is consistent with NRC RG 1.98, Rev. 2.

Causes for Uncertainties — The estimate of neutron fluence at a postulated crack tip requires establishing the fluence at a reference location, that is, surveillance capsule location, and extrapolation to the location of the crack tip. The quality of dosimetry and extrapolation techniques determines the uncertainty. Analysis results indicate that the standard deviations are within the range of 15 to 30 percent of the mean fluence value.

Sensitivity of Through-Wall Cracking Probability to Fluence Distribution — It is expected that the reasonable variations in the assumed standard deviation of fluence will not cause significant variations in the calculated failure frequency because the shift in RT_{NDT}, which is discussed next, weekly depends on fluence (one-fourth power dependence).

Shift in RT_{NDT} (ΔRT_{NDT}). The shift in RT_{NDT} depends on the fluence and the copper and nickel contents in the vessel materials. There are three different trend curves in the VISA-II code to calculate the shift. However, now the shift is generally calculated using the trend curve given in Regulatory Guide 1.99, Rev. 2, which is based on a large number of surveillance data, and the other trend curves are not used. Therefore, there is no uncertainty associated with the use of trend curve.

In the VISA-II code, the variable ΔRT_{NDT} is either treated as a definite variable or as a random variable. Treating ΔRT_{NDT} as a definite variable is appropriate because it is believed that the observed variability in the calculated values of the shift is due to uncertainties in the measured values of fluence and copper content, which are already accounted for in the VISA-II code. However, as an alternative

to simulation of fluence, and copper and nickel contents, the code provides an option to simulate ΔRT_{NDT} as a random variable.

Adjusted RT_{NDT}. The adjusted RT_{NDT} is defined as a reference temperature of the nil-ductility transition for the vessel materials. This reference temperature is used to determine the fracture toughness at the crack tip. The adjusted RT_{NDT} is calculated by adding the simulated value of initial RT_{NDT}, the calculated shift, and the error in the adjusted RT_{NDT}. The error is simulated from a normal distribution centered at zero, that is, the error can be positive or negative. The standard deviation, σ, for the error is determined as follows:

$$\sigma = (\sigma_I^2 + \sigma_\Delta^2)^{0.5}$$

where σ_I is the standard deviation of the initial RT_{NDT}, and σ_Δ is the standard deviation of the shift in RT_{NDT}. These standard deviations are specified by the user.

Fracture Toughness. In VISA-II code, the mean values for the fracture toughness for crack initiation, K_{Ic}, and arrest, K_{Ia}, are given as a function of $(T\text{-}RT_{NDT})$, where T is the temperature at the crack tip. These curves of fracture toughness as a function of temperature were developed by testing the unirradiated pressure vessel materials. These curves are indexed to RT_{NDT}, so the x-axis of the curves become $(T\text{-}RT_{NDT})$. These curves for mean fracture toughness are truncated at some maximum stress intensity value as defined by the user. In certain PTS evaluations performed by the NRC staff, the curves were truncated at 200 ksi·$in^{1/2}$.

The distributions of K_{Ic} and K_{Ia} about their mean values are assumed to be normal, with a user-specified standard deviation as a percent of the mean value. The suggested value of standard deviation is 10% of the mean value. The distributions are truncated at the user specified standard deviations. The suggested value is 3.0 standard deviations.

Causes for Uncertainty in Unirradiated Fracture Toughness — The uncertainty in the measured fracture toughness results from microstructural inhomogeneities in the steels and from variability in the measurement methods. Brittle fracture is affected by a critical number and/or size of carbides within a characteristic distance from the crack tip, whereas ductile fracture is affected by a critical strain within a characteristic distance from the crack tip.

Sensitivity of Through-Wall Cracking Probability to Fracture Toughness Distribution — The calculated probability of failure has been found to only weekly depend on the standard deviation of fracture toughness. Increasing the standard deviation from 10 to 20% of the mean caused an increase in calculated probability of failure by about a factor of 1.5 to 3.0. Although this increase is significant, it is much smaller than the effects caused by the use of alternative assumptions related to

flaw distribution. The 10% uncertainty is well established at low values of fracture toughness (ductile-to-brittle transition zone) but not at higher values of fracture toughness (upper shelf or ductile fracture zone).

For the cases where vessel failures are predicted, the simulated fracture toughness are typically about one standard deviation below the mean and only rarely less than two standard deviations below the mean. Therefore, the distributions that are well established within one to two standard deviations are appropriate for use in the VISA-II code. Preliminary evaluations show that the shape of the distribution (either normal or Weibull) does not strongly affect the failure probabilities. The main reason for the lack of sensitivity is that the simulated failures usually occur in the ductile-to-brittle transition zone where the Weibull distribution is relatively symmetrical and, therefore, is similar in shape to the normal distribution.

Crack Detection Model. The VISA-II code allows the user to take into account the inservice inspection results. First, the size and location of the crack is simulated in the Monte Carlo analysis. The code then considers the probability of flaw detection that the user has specified as input to the analysis. If the simulated inspection results in a predicted flaw detection, then it is assumed that this flaw is repaired and, therefore, does not cause vessel failure.

The use of simulated inspection is meaningful if the inservice inspection is capable to detect the flaws that were not detected and repaired at the time of preservice inspection and vessel fabrication. Note that the flaw size distributions used in the Monte Carlo analyses are intended to represent only those flaws that are not detected at the time of fabrication and preservice inspection.

The VISA-II code has algorithms to estimate the probability of flaw detection by two types of inspection: a near surface examination of the clad/vessel interface and a volumetric examination of the entire wall. To determine whether the flaw will be detected, the code generates a random number between 0.0 and 1.0 and compares it with the probability of detection. The flaw is said to be detected if the random number is less than or equal to the probability of detection.

Appendix D

Results of PRA-Based Event Screening Using SWIM Index

APPENDIX D

Results of PRA-Based Event Screening Using SWIM Index

To begin the selection of potential aging-important SSCs, cut sets for the Surry IPE model were generated using a truncation level of 1E-13/yr. From these cut sets, the basic event importance measures [including Fussell-Vesely (F-V), risk increase ratio (RIR, also known as risk achievement worth, or RAW)] were calculated. These importance measures were then evaluated to obtain a single ranked list of events using the Smith Weighted Importance Measure (SWIM) index. The SWIM index is a type of importance measure that allows an analyst to combine information from the F-V list of events with the RIR list of events (with a user selected weighting factor) in order to work with a single, ranked list of basic events.

Advantages to using the SWIM index over separate lists of importance measures are (1) the results are contained in a single list rather than two (or more) importance measure lists, (2) events are ranked against each other even for cases where one event has a high F-V (and low RIR) while another event has a high RIR (and low F-V), and (3) the analyst can weight one result characteristic over another (e.g., RIR is more important than F-V so weight RIR measures higher than F-V measures). A complete derivation for the SWIM was provided in Section 4.3.2. In summary, the SWIM index is defined as:

$$SWIM = \left(W_{FV}\right)^{WF_{FV}} + \left(W_{RIR}\right)^{WF_{RIR}}$$

where WF_{FV} = the weighting factor for the F-V measure
WF_{RIR} = the weighting factor for the RIR measure

and

$$W_{FV} = I_{FV}$$

$$W_{RIR} = \left(1 - \frac{1}{I_{RIR}}\right)^{7.64}$$

where I_{FV} = the F-V importance measure for the i'th event
I_{RIR} = the RIR importance measure for the i'th event

Since the scaled risk threshold in the SWIM derivation was chosen to be 0.005, any event with a SWIM value of 0.005 or larger can be considered to be risk significant. As such, these events would pass the risk-based part of the screening. But, the SWIM list still would be evaluated for those events (and their related "passive" components) with respect to applicable aging mechanisms.

The results of the SWIM importance measure analysis are shown in Table D-1. The events shown in Table D-1 represent a single sorted list of basic events from the nominal Surry IPE model sorted based upon the SWIM index. Only those events that could be considered risk significant (i.e., F-V > 0.005 or RIR > 2) are included in the table. Along with the basic event name, an event description is included along with the event probability.

In Table D-1, the events that are labeled as "n/a" are presumed (for this study) to not be affected by aging or are outside the current scope of the analysis demonstration. These events include: operator errors (e.g., 1RSHEP-SFLNG-PT6), maintenance activities (e.g., 1EEBUS-UM-1H), recovery actions (e.g., HEP-1ECA3:2), success/complemented events (e.g., C-LT02), plugging events (e.g., 1SIMV--PG-1SI24), and electrical systems (e.g., 1RPBKR-CC-RTARTB). Events that are left blank under the "applicability" column would be candidates for further aging-related investigations. The passive piping components are not included in the events shown in Table D-1. Once these event are incorporated into the PRA model, they could be sorted and evaluated based upon their individual risk significance.

The events shown in Table D-1 represent (primarily) active components. For these events, potential aging mechanism will need to be identified (if any) in order to associate a physics-based reliability model to the particular basic event. It may be possible that many of these events could be susceptible to corrosion, fatigue, or wear mechanisms. The passive components that appear in the list and those that will be added to the list as the analysis progresses will be evaluated based upon the aging mechanisms identified in Section 2. Specifically, the area of corrosion will be investigated as part of the demonstration project.

Table D-1. Basic event importance measure results and applicability to the aging analysis for the Surry IPE PRA model (sorted by the SWIM index) for events with F-V > 0.005 or RIR > 2.

Event	Probability	F-V	RIR	SWIM	Applicability	Event Description
IE-T8	5.9E-04	2.2E-01	3.8E+02	1.200		LOSS OF SWITCHGEAR ROOM COOLING
1FWCKV-CC-275889	6.3E-05	5.3E-02	8.4E+02	1.044		CCF 3/3 FL CHECK VALVES 1FW27
IE-VX	1.6E-06	2.1E-02	1.3E+04	1.021		INTERFACING LOCA
IE-T4	5.0E-06	1.0E-02	2.0E+03	1.006		LOSS OF RCP COOL/INJECT
IE-A	5.0E-04	6.3E-02	1.3E+02	1.005		LARGE LOCA
IE-RX	2.7E-07	3.6E-03	1.4E+04	1.003		VESSEL RUPTURE
1RPBKR-CC-RTARTB	1.3E-05	1.1E-02	8.1E+02	1.001	n/a	Common-cause failure 2/2 REACTOR TRIP BREAKERS
1RSHEP-SFLNG-PT6	8.0E-05	2.5E-02	3.1E+02	1.000	n/a	TEST FLANGES LEFT BLANKED AFTER 1-PT-17.6
1SICKV-CC-798285	6.3E-05	2.1E-02	3.2E+02	0.997		CCF 3/3 CHECK VALVES S1-79
1CSMV--PG-1CS25	4.5E-05	1.5E-02	3.4E+02	0.993	n/a	N.O. VALVE CS-25 PLUGGED IN STANDBY
1SIMOV-CC-867842	2.5E-04	4.2E-02	1.5E+02	0.992		CCF 3/3 FC OF CL HH DISCH MOVS 1867C
1RPROD-LF-CRODS	1.8E-06	1.4E-03	7.9E+02	0.992		Control rods fail to insert due to MECHANICAL BINDING
IE-S1	1.0E-03	7.1E-02	7.2E+01	0.971		MEDIUM LOCA
1SICKV-CC-224225	6.3E-05	1.1E-02	1.5E+02	0.961		CCF 2/2 FC OF CHECK VALVES SI225 AND SI224
1EEBUS-LU-1H	1.2E-05	1.6E-03	1.3E+02	0.945	n/a	4160v Bus Bar 1H Loss of Function 1-EE-BUS-1H
1EEBUS-UM-1H	7.3E-06	9.4E-04	1.3E+02	0.944	n/a	BUS BAR UNSCHEDULED MAINTENANCE
1EEBUS-LU-1H-1	1.2E-05	1.4E-03	1.2E+02	0.938	n/a	480v Bus 1H-1 Loss Of Function 1-EE-BUS-1H-1
1EEBUS-LU-1H-480	1.2E-05	1.4E-03	1.2E+02	0.938	n/a	Bus Bar Loss of Function 1-EE-BUS-1H
1EEBUS-UM-1H-1	7.3E-06	8.4E-04	1.2E+02	0.937	n/a	BUS BAR UNSCHEDULED MAINTENANCE
1EEBKR-SO-14H15	3.4E-05	3.3E-03	1.0E+02	0.929	n/a	Breaker 14H15 Spuriously Opens 1-EE-BKR-14H15
1EEBKR-SO-15H7	3.4E-05	3.3E-03	1.0E+02	0.929	n/a	Breaker 15H7 Spuriously Opens 1-EE-BKR-15H7
1EETFM-LP-1H1	1.9E-05	1.9E-03	1.0E+02	0.928	n/a	Transformers Fails To Supply Power 1-EE-TX-1H1
1EEBKR-SO-14H14	3.4E-05	2.5E-03	7.7E+01	0.907	n/a	Breaker 14H14 Spuriously Opens 1-EE-BKR-14H14
1EEBUS-LU-1H1-1	1.2E-05	9.2E-04	7.7E+01	0.906	n/a	480v MCC 1H1-1 Loss of Function 1-EE-BUS-1H1-1
1EEBUS-UM-1H1-1	7.3E-06	5.4E-04	7.6E+01	0.904	n/a	480V MCC 1H1-1 unavailable DUE TO MAINTENANCE
1EGEDG-CC-123	7.5E-05	4.9E-03	6.6E+01	0.895	n/a	COMMON CAUSE FAILURE OF EDG #1/2/3
1EGEDG-CC-13	1.1E-04	6.4E-03	5.7E+01	0.880	n/a	COMMON CAUSE FAILURE OF EDG #1 AND EDG #3
1SICKV-FC-1SI25	6.3E-04	2.7E-02	4.4E+01	0.867		CHECK VALVE 1-SI-25 FAILS TO OPEN
1SICKV-FC-1SI410	6.3E-04	2.7E-02	4.4E+01	0.867		CHECK VALVE 1-SI-410 FAILS TO OPEN
1RSMOV-CC-104AD	2.5E-04	1.2E-02	4.9E+01	0.867		CCF 4/4 FC OF INLET ISO VALVES 1-SW-MOV-104A/D
1RSMOV-CC-105AD	2.5E-04	1.2E-02	4.9E+01	0.867		CCF 4/4 FC OF OUT ISO VALVES 1-SW-MOV-105A/D
1EE-LOOP-24	2.1E-04	1.0E-02	4.9E+01	0.864	n/a	Loss of offsite power within 24 HRS OF REACTOR TRIP
1SIMV--PG-1SI24	5.5E-04	2.4E-02	4.4E+01	0.863	n/a	MANUAL VALVE 1-SI-24 PLUGGED IN STANDBY
1EGEDG-CC-12	1.1E-04	5.2E-03	4.6E+01	0.851	n/a	COMMON CAUSE FAILURE OF EDG #1 AND EDG #2
1SIMOV-CC-1115BD	2.5E-04	1.1E-02	4.4E+01	0.850		CCF 2/2 FC OF LCV 1115B AND LCV 1115D TO OPEN
1SIMOV-CC-1115CE	2.5E-04	1.1E-02	4.4E+01	0.850		CCF 2/2 FO OF LCV-1115C AND 1115E TO CLOSE
1SWCKV-PG-1SW130	3.0E-06	1.4E-04	4.8E+01	0.850	n/a	CHECK VALVE 1-SW-130 PLUGS DURING MISSION
1CESTR-CC-SUMPPG	5.0E-05	2.0E-03	4.2E+01	0.834		COMMON CAUSE BLOCKAGE OF CONTAINMENT SUMP
1EEBUS-LU-1J-480	1.2E-05	5.0E-04	4.2E+01	0.833	n/a	Bus Bar 1J 480v Loss of Function 1-EE-BUS-1J
1EEBUS-LU-1J-1	1.2E-05	5.0E-04	4.2E+01	0.833	n/a	480v Bus 1J-1 Loss of Function 1-EE-BUS-1J-1
1EEBUS-LU-1J	1.2E-05	5.0E-04	4.2E+01	0.833	n/a	4160v Bus Bar 1J Loss of Function 1-EE-BUS-1J
1EEBUS-UM-1J-1	7.3E-06	2.9E-04	4.1E+01	0.829	n/a	BUS BAR UNSCHEDULED MAINTENANCE
1EEBUS-UM-1J	7.3E-06	2.9E-04	4.1E+01	0.829	n/a	BUS BAR UNSCHEDULED MAINTENANCE
1EEBAT-CC-1A-1B	1.1E-06	3.7E-05	3.6E+01	0.804		COMMON CAUSE FAILURE OF BOTH DC BATTERIES
1SIPSB-CC-FS1A1B	4.4E-04	1.2E-02	2.8E+01	0.767		CCF 2/2 PS OF PUMPS 1A AND 1B TO START
1RPRPS-LF-INPUT	1.4E-06	3.9E-05	2.9E+01	0.763	n/a	NO INPUT SIGNAL FROM REACTOR TRIP PROTECTION

Event	Probability	F-V	RIR	SWIM	Applicability	Event Description
1SIMOV-CC-1860AB	2.5E-04	6.7E-03	2.8E+01	0.761		CCF 2/2 FC FAILURE OF SUMP VALVES 1860A AND B
1SICKV-CC-46A46B	6.3E-05	1.7E-03	2.8E+01	0.757		CCF 2/2 FC OF CHECK VALVES SI-46A AND SI-46B
1SICKV-CC-FC5058	6.3E-05	1.7E-03	2.8E+01	0.757		CCF 2/2 FC OF CHECK VALVES 50 AND 58 TO OPEN
1SICKV-CC-FC4756	6.3E-05	1.7E-03	2.8E+01	0.756		CCF 2/2 FC OF CHECK VALVES SI-47 AND SI-56
1FWHEP-FULLRECRC	1.4E-03	3.2E-02	2.3E+01	0.748	n/a	Operator fails to restore full RECIRC VLVS 1-FW-625/6/7 & 631
1IAIAS-LF-OUTIA	2.5E-04	6.2E-03	2.6E+01	0.743		Outside containment instrument air system loss of function
1FWCKV-LEAKAGE	1.0E-04	2.3E-03	2.4E+01	0.724		UNDETECTED LKG THRU CKVS 27
1FWCKV-CC-131136	6.3E-05	1.5E-03	2.4E+01	0.723		CCF 2/2 FC CHECK VALVES 1FW131
1EEBKR-SO-14J11	3.4E-05	7.7E-04	2.4E+01	0.722	n/a	Breaker 14J11 Spuriously Opens 1-EE-BKR-14J11
1EEBUS-LU-1H1-2	1.2E-05	2.8E-04	2.4E+01	0.721	n/a	480v MCC 1H1-2 Loss of Function 1-EE-MCC-1H1-2
1EEBKR-SO-15J7	3.4E-05	7.7E-04	2.4E+01	0.721	n/a	Breaker 15J7 Spuriously Opens 1-EE-BKR-15J7
1EETFM-LP-1J1	1.9E-05	4.3E-04	2.4E+01	0.721	n/a	Transformer Fails To Supply Power 1-EE-TX-1J1
HEP-1ECA3:1	2.7E-03	5.0E-02	2.0E+01	0.721	n/a	1-ECA-3.1 SGTR w/ loss of RX coolant subcooled recovery
1EEBUS-UM-1H1-2	7.3E-06	1.7E-04	2.4E+01	0.720	n/a	480V MCC 1H1-2 UNAVAILABLE DUE TO MAINTENANCE
1EEBUS-LU-1J1-2	1.2E-05	2.8E-04	2.4E+01	0.719	n/a	480v MCC 1J1-2 Loss of Function 1-EE-MCC-1J1-2
1EEBUS-UM-1J1-2	7.3E-06	1.6E-04	2.4E+01	0.719	n/a	480V MCC 1J1-2 UNAVAILABLE DUE TO MAINTENANCE
1FWCKV-CC-425772	6.3E-05	1.4E-03	2.3E+01	0.717		CCF 3/3 FC CHECK VALVES 1FW142
1FWMOV-SO-24H60B	1.2E-05	2.7E-04	2.3E+01	0.712		Motor operated valve transfers open - 24 H1-FW-MOV-260B
1FWMOV-SO-24H60A	1.2E-05	2.7E-04	2.3E+01	0.712		Motor operated valve transfers open- 24 H1-FW-MOV-260A
1SICKV-CC-FC5361	6.3E-05	1.3E-03	2.1E+01	0.690		CCF 2/2 FC OF CHECK VALVES SI-53 AND SI-61
1EEBUS-LU-VBII	1.2E-05	2.3E-04	2.0E+01	0.677	n/a	Vital Bus Bar 1-II Loss of Function 1-EE-VTB-II
1RHHCV-SO-1605	1.2E-05	2.3E-04	2.0E+01	0.674		Flow control valve 1-RH-FCV-1605 SPURIOUS OPENS
1CCTNK-LF-1CCTK1	2.7E-06	5.0E-05	2.0E+01	0.674		Insufficent CC pump NPSH surge tank 1-CC-TK1 loss of function
RECOVER-T8	2.8E-02	2.2E-01	8.7E+00	0.611	n/a	Recovery from T8 initiator VIA ESR U-2 FANS OR B/U CHL
1CSLIC-CC-100	4.6E-04	6.8E-03	1.6E+01	0.609	n/a	CCF 3/4 LF RWST Level Channels 1-CS-LC-100A
IE-S2	2.1E-02	1.8E-01	9.5E+00	0.609		SMALL LOCA
1VSFAN-FR-1FMO7	9.9E-05	1.3E-03	1.5E+01	0.584	n/a	1-VS-AC-7 FAN MOTOR FAILS TO RUN FOR MISSION
1VSACU-LF-1VSAC7	3.4E-05	4.7E-04	1.5E+01	0.583	n/a	LOSS OF FUNCTION IN AIR HANDLING UNIT 1-VS-AC-7
IE-T7	1.6E-02	1.3E-01	8.9E+00	0.529		STEAM GENERATOR TUBE RUPTURE
1SIHEP-MOV-1890C	8.0E-04	7.5E-03	1.0E+01	0.471	n/a	Locked open valve 1-SI-MOV-1890C inadvertently closed
1EEBKR-SO-14J16	3.4E-05	2.9E-04	9.7E+00	0.438	n/a	Breaker 14J16 Spuriously Opens 1-EE-BKR-14J16
1EEBUS-LU-1J1-1	1.2E-05	1.1E-04	9.7E+00	0.437	n/a	480v MCC 1J1-1 Loss of Function 1-EE-BUS-1J1-1
1EEBUS-LU-1ADC	1.2E-05	1.0E-04	9.5E+00	0.427	n/a	BUS BAR 1A DC LOSS OF FUNCTION
HEP-1E0-18	1.4E-03	1.2E-02	9.2E+00	0.427	n/a	1-E-0 RX TRIP OR SI STEP 18 verify ventilation alignment
1SIMOV-PG-1890C	8.2E-04	6.6E-03	9.1E+00	0.417	n/a	N.O. MOV 1-SI-1890C PLUGGED DRNG STNDBY
1EEBUS-UM-1J1-1	7.3E-06	5.6E-05	8.7E+00	0.396	n/a	480V MCC 1J1-1 unavailable DUE TO MAINTENANCE
HEP-1OP14:1-5:2	2.7E-03	1.8E-02	7.8E+00	0.370	n/a	OP-14.1 RHR STEP 5.2 OPEN TV-CC-109
1RSHEP-OPEN-VLVS	8.0E-05	5.7E-04	8.1E+00	0.367	n/a	MANUAL VALVES LEFT OPEN AFTER 1-PT-17.4
1RSHEP-SFLNG-PT4	8.0E-05	5.7E-04	8.1E+00	0.367	n/a	SPECTACLE FLANGE LEFT BLANKED AFTER 1-PT-17.4
1SIMOV-PG-1865C	8.2E-04	5.6E-03	7.9E+00	0.360	n/a	N.O. OPEN MOV SI-1865C PLUGGED IN STANDBY
1SIMOV-PG-1865A	8.2E-04	5.6E-03	7.9E+00	0.360	n/a	N.O. OPEN MOV SI-1865A PLUGGED IN STANDBY
1SICKV-FC-1SI147	6.3E-04	4.4E-03	7.9E+00	0.360		CHECK VALVE 1-SI-147 FAILS CLOSED
1SICKV-FC-1SI109	6.3E-04	4.4E-03	7.9E+00	0.359		CHECK VALVE SI-109 FAILS CLOSED (FAILS TO OPEN)
1SICKV-FC-1SI145	6.3E-04	4.4E-03	7.9E+00	0.359		CHECK VALVE SI-145 FAILS CLOSED (FAILS TO OPEN)
1SICKV-FC-1SI107	6.3E-04	4.4E-03	7.9E+00	0.359		CHECK VALVE SI-107 FAILS CLOSED (FAILS TO OPEN)
HEP-1ECA3:2	1.6E-03	1.1E-02	7.7E+00	0.357	n/a	1-ECA-3.2 SGTR w/ loss of RX coolant saturated recovery
HEP-1ES1:4	4.8E-04	3.2E-03	7.8E+00	0.352	n/a	OPERATOR fails to initiate HOT LEG RECIRCULATION
1SICKV-CC-229228	6.3E-05	4.3E-04	7.8E+00	0.349		CCF 2/2 FC OF CHECK VALVES SI-228 AND SI-229
1EEBUS-LU-1BDC	1.2E-05	7.9E-05	7.5E+00	0.336	n/a	Bus Bar 1B DC Loss of Function

Event	Probability	F-V	RIR	SWIM	Applicability	Event Description
1EEBAT-LP-1A	4.5E-04	2.7E-03	7.0E+00	0.313		Battery 1A Electrical Failure 1-EE-B-1A
IE-T1	7.7E-02	2.1E-01	3.5E+00	0.292	n/a	LOSS OF OFFSITE POWER
1EGEDG-CC-23	1.1E-04	5.9E-04	6.2E+00	0.260	n/a	COMMON CAUSE FAILURE OF EDG #2 AND EDG #3
1EGEDG-FS-1	7.9E-03	3.6E-02	5.5E+00	0.250	n/a	EDG #1 Start Failure
HEP-AP12:01-11	2.7E-03	1.2E-02	5.6E+00	0.236	n/a	AP-12:01 loss INTKE CANAL step 11 verify CW/SW isolation
1EEBKR-SO-14H13	3.4E-05	1.5E-04	5.4E+00	0.207	n/a	Breaker 14H13 Spuriously Opens 1-EE-BKR-14H13
1EEBKR-SO-15H8	3.4E-05	1.4E-04	5.3E+00	0.201	n/a	Breaker 15H8 Spuriously Opens 1-EE-BKR-15H8
HEP-1FRH:1-5	2.7E-03	1.1E-02	5.1E+00	0.199	n/a	1-FR-H.1 LOSS 2ND HEAT SINK step 5 check SG LEVELS
C-LT02	8.9E-01	2.0E-01	1.0E+00	0.195	n/a	TURBINE DRIVEN AFW AVAILABLE COMPLEMENT
1EEBKR-SO-14J14	3.4E-05	1.4E-04	5.2E+00	0.194	n/a	Breaker 14J14 Spuriously Opens 1-EE-BKR-14J14
1FWPSB-CC-MDP3AB	7.0E-04	2.5E-03	4.6E+00	0.153		CCF 2/2 FS MDP - COMMON CAUSE FAILURE
1EGEDG-FR-1	1.3E-02	4.1E-02	4.0E+00	0.152	n/a	EDG #1 Fails To Run For six hours
1FWCKV-FC-1FW273	6.3E-04	2.2E-03	4.4E+00	0.143		CHECK VALVE FAILS TO OPEN 1-FW-273
1FWCKV-FC-1FW272	6.3E-04	2.2E-03	4.4E+00	0.143		CHECK VALVE FAILS TO OPEN 1-FW-272
C-L04	9.9E-01	1.4E-01	1.0E+00	0.143	n/a	AUX FEEDWATER OPERABLE COMPLEMENT S1
2FWMOV-CC-160AB	2.5E-04	8.5E-04	4.4E+00	0.141		CCF 2/2 FC CCF FTO 2-FW-MOV-160A/B
1FWPSB-FR-24HP3A	7.9E-04	2.5E-03	4.2E+00	0.127		MD PUMP -STNDBY SYS FAILS TO RUN - 24 HR1-FW-P-3A
1FWHEP-1FW155156	8.0E-04	2.5E-03	4.1E+00	0.123	n/a	OPERATOR fails to RESTORE VALVES 1-FW-155 AND -156
1FWCKV-FC-1FW157	6.3E-04	2.0E-03	4.1E+00	0.122		CHECK VALVE FAILS TO OPEN 1-FW-157
HEP-1ECA0:0-7	2.7E-03	7.7E-03	3.9E+00	0.111	n/a	1-ECA-0.0 loss all AC step 7 conserve INTAKE CANAL water
CU01	2.0E-02	4.6E-02	3.2E+00	0.105	n/a	NO CORE UNCOVERY before RECOVERY of offsite power
B04	5.0E-01	1.0E-01	1.1E+00	0.101	n/a	RECOVER OFFSITE POWER
C-D103	1.0E+00	9.5E-02	1.0E+00	0.095	n/a	HIGH PRESSURE INJECTION COMPLEMENT
1FWPSB-UM-1FWP3A	2.7E-03	7.0E-03	3.6E+00	0.092	n/a	MD STNDBY PUMP UNSCHDL MAINT. 1-FW-P-3A
C-Q02	9.8E-01	9.2E-02	1.0E+00	0.092	n/a	RCS BOUNDARY INTACT COMPLEMENT
1FWPSB-TM-1FWP3A	5.7E-04	1.5E-03	3.6E+00	0.087	n/a	MD pump -STDBY SYS sched. test and maintenance 1-FW-P-3A
IE-T5B	6.0E-03	1.3E-02	3.2E+00	0.072	n/a	LOSS OF DC BUS 1B
IE-T5A	6.0E-03	1.3E-02	3.2E+00	0.072	n/a	LOSS OF DC BUS 1A
2EGEDG-UM-2	6.8E-02	6.8E-02	1.9E+00	0.071	n/a	EDG #2 Unavailable Due To Unscheduled Maintenance
1EGEDG-FS-3	7.9E-03	1.7E-02	3.1E+00	0.067	n/a	EDG #3 Start Failure
HEP-1E3-15	8.9E-02	6.6E-02	1.7E+00	0.067	n/a	1-E-3 SGTR STEP 15 INITIATE RCS COOLDOWN
C-LT01	9.6E-01	6.5E-02	1.0E+00	0.065	n/a	TURBINE DRIVEN AFW AVAILABLE COMPLEMENT
2CWMOV-CC-06A00A	2.5E-04	5.8E-04	3.3E+00	0.064		COMMON CAUSE FAILURE OF MOV'S 206A AND 200A
1CWMOV-CC-06D00D	2.5E-04	5.8E-04	3.3E+00	0.064		COMMON CAUSE FAILURE OF CW-MOV'S 106D AND 100D
2CWMOV-CC-06C00C	2.5E-04	5.8E-04	3.3E+00	0.064		COMMON CAUSE FAILURE OF MOV'S CW-206C AND 200C
1CWMOV-CC-06A00A	2.5E-04	5.8E-04	3.3E+00	0.064		COMMON CAUSE FAILURE OF CW MOV'S 106A AND 100A
1CWMOV-CC-06B00B	2.5E-04	5.8E-04	3.3E+00	0.064		COMMON CAUSE FAILURE OF CW MOV'S 106B AND 100B
2CWMOV-CC-06D00D	2.5E-04	5.8E-04	3.3E+00	0.064		COMMON CAUSE FAILUROF CW MOV'S 206D AND 200D
2CWMOV-CC-06B00B	2.5E-04	5.8E-04	3.3E+00	0.064		COMMON CAUSE FAILURE OF CW-MOV'S 206B AND 200B
1CWMOV-CC-06C00C	2.5E-04	5.8E-04	3.3E+00	0.064		COMMON CAUSE FAILURE OF CW MOV'S 106C AND 100C
C-O02	9.5E-01	6.4E-02	1.0E+00	0.064	n/a	OPERATOR cooldown and DEPRESSURIZE complement
1EGEDG-UM-1	1.1E-02	2.2E-02	2.9E+00	0.063	n/a	EDG #1 Unavailable Due To Unscheduled Maintenance
1EGEDG-FR-3	1.3E-02	2.5E-02	2.9E+00	0.062	n/a	EDG #3 Fails To Run For six hours
1FWCKV-FO-1FW172	3.4E-03	7.5E-03	3.2E+00	0.062		CHECK VALVE FAILS TO CLOSE 1-FW-172
HEP-1E3-3	2.3E-02	3.7E-02	2.6E+00	0.061	n/a	1-E-3 SGTR STEP 3 ISOLATE RUPTURED SG
C-D101	1.0E+00	6.1E-02	1.0E+00	0.061	n/a	HIGH PRES INJECTION COMPLEMENT
C-D203	9.9E-01	5.5E-02	1.0E+00	0.055	n/a	ACCUMULATOR INJECTION COMPLEMENT
HEP-1ES1:2-S2	5.3E-02	4.7E-02	1.8E+00	0.049	n/a	1-ES-1.2 post-LOCA cooldown and DEPRESSURIZATION
1EGEDG-TM-1	5.7E-04	1.1E-03	2.9E+00	0.043	n/a	EDG #1 Unavailable Due To Scheduled Test or Maintenance

Event	Probability	F-V	RIR	SWIM	Applicability	Event Description
2EGEDG-FR-2	1.3E-02	2.1E-02	2.5E+00	0.042	n/a	EDG #2 Fails To Run For six hours
HEP-1FRC:1-12-S2	3.1E-01	4.1E-02	1.1E+00	0.041	n/a	1-FR-C.1 IN ADC CC step 12 DEPRESS all intact SGS - S223
REC-6H-DG-MECH	6.0E-01	3.9E-02	1.0E+00	0.039	n/a	Failure to recover MECH FAULTS IN DG IN SIX HOURS
1FWCKV-FO-1FW157	3.4E-03	6.1E-03	2.8E+00	0.039		CHECK VALVE FAILS TO CLOSE 1-FW-157
2EGEDG-FS-2	7.9E-03	1.2E-02	2.5E+00	0.034	n/a	EDG #2 Start Failure
1CHCKV-FO-1CH267	3.4E-03	5.8E-03	2.7E+00	0.033		CHECK VALVE CH-267 FAILS OPEN (FAILS TO CLOSE)
2FWTRB-FR-24HP2	1.1E-01	3.2E-02	1.3E+00	0.032		TURBINE DRIVEN PUMP FAILS TO RUN - 24 HR 2-FW-P-2
CHP-XTIE-SUCCESS	8.0E-01	3.0E-02	1.0E+00	0.030	n/a	SUCCESSFUL CROSS TIE OF UNIT 2 CHARGING
1MSRV--CC-101ABC	1.0E-03	1.6E-03	2.6E+00	0.025		CCF 3/3 FC CCF - SG PORV - FC 1-MS-RV-101A/B/C
1SICKV-FC-1SI225	6.3E-04	1.0E-03	2.6E+00	0.025		CHECK VALVE 225 FAILS TO OPEN
1FWTRB-FS-1FWP2	2.5E-02	2.2E-02	1.8E+00	0.024		TURBINE DRIVEN PUMP FAILS TO START 1-FW-P-2
1SIMOV-CC-1867CD	2.5E-04	4.0E-04	2.6E+00	0.024		CCF 2/2 FC OF MOV'S 1867C AND 1867D
1EEUPS-LF-1B-2	7.2E-04	1.1E-03	2.6E+00	0.023	n/a	Uninterruptable Power Supply 1B-2 Fails
1EEUPS-LF-1A-2	7.2E-04	1.1E-03	2.5E+00	0.023	n/a	Uninterruptable Power Supply 1A-2 Fails
1EEHS--LF-SVB	2.7E-05	4.2E-05	2.6E+00	0.023	n/a	MANUAL transfer switch 480V MCC TO SEMI VITAL BUS
1EEBUS-LU-SVB-1	1.2E-05	1.9E-05	2.6E+00	0.023	n/a	SEMI VITAL BUS BAR LOSS OF FUNCTION 1-EE-SVB-1
1FWTRB-FR-24HP2	1.1E-01	2.2E-02	1.2E+00	0.022		TURBINE DRIVEN PUMP FAILS TO RUN - 24HR1-FW-P-2
1FWTRB-FR-12HP2	5.7E-02	2.2E-02	1.4E+00	0.022		TURBINE DRIVEN PUMP FAILS TO RUN - 12HR1-FW-P-2
IE-T3	2.0E+00	2.2E-02	1.0E+00	0.022	n/a	TRANSIENT WITH MFW AVAILABLE
1EEBKR-SO-35VBIV	3.4E-05	5.2E-05	2.5E+00	0.021	n/a	Breaker 35 on Panel 120v 1-IV Spuriously Opens
C-FM01	9.9E-01	2.1E-02	1.0E+00	0.021	n/a	ISLOCA BREAK SIZE SMALLER THAN S1 COMPLEMENT
1EEBKR-SO-35-III	3.4E-05	5.2E-05	2.5E+00	0.021		Breaker 35 on Panel 120v 1-III Spuriously Opens
1EEBUS-LU-VBIV	1.2E-05	1.8E-05	2.5E+00	0.020	n/a	Vital Bus Bar 1-IV Loss of Function 1-EE-VTB-IV
1FWPSB-U2-MODE45	2.1E-01	2.0E-02	1.1E+00	0.020	n/a	PROB THAT UNIT 2 IS SHUTDOWN
1EEBUS-LU-VBIII	1.2E-05	1.8E-05	2.5E+00	0.020	n/a	Vital Bus Bar 1-III Loss of Function 1-EE-VTB-III
B02	3.0E-01	2.0E-02	1.0E+00	0.020	n/a	RECOVER OFFSITE POWER
1CHHEX-LU-1CHE5A	2.1E-04	3.1E-04	2.5E+00	0.020		HEAT EXCHANGER 1-CH-E-5A LOSS OF FUNCTION
2EEBKR-SO-25H7	3.4E-05	5.0E-05	2.5E+00	0.020	n/a	Breaker 25H7 Spuriously Opens 2-EE-BKR-25H7
2EEBKR-SO-24H11	3.4E-05	5.0E-05	2.5E+00	0.020	n/a	Breaker 24H11 Spuriously Opens 2-EE-BKR-24H11
2EETFM-LP-2H1	1.9E-05	2.8E-05	2.5E+00	0.019	n/a	Transformers Fail To Supply Power 2-EE-TX-2H1
REC-OPEN-RSSWVLV	1.3E-01	1.9E-02	1.1E+00	0.019	n/a	Failure to locally open RS SERVICE WATER VALVE IN 2HR
2EEBKR-SO-24J15	3.4E-05	4.9E-05	2.5E+00	0.019	n/a	Breaker 24J15 Spuriously Opens 2-EE-BKR-24J15
2EEBKR-SO-25J7	3.4E-05	4.9E-05	2.5E+00	0.019	n/a	Breaker 25J7 Spuriously Opens 2-EE-BKR-25J7
IE-T6	6.7E-02	1.9E-02	1.3E+00	0.019		LOSS OF CIRCULATING WATER PUMPS
2EEBUS-LU-2H-480	1.2E-05	1.8E-05	2.5E+00	0.018	n/a	Bus Bar Loss of Function 2-EE-BUS-2H (480v)
2EEBUS-LU-2H-1	1.2E-05	1.8E-05	2.5E+00	0.018	n/a	480v Bus 2H-1 Loss Of Function 2-EE-BUS-2H-1
1EGEDG-UM-3	8.1E-03	9.5E-03	2.2E+00	0.018	n/a	EDG #3 Unavailable Due To Unscheduled Maintenance
2EETFM-LP-2J1	1.9E-05	2.8E-05	2.5E+00	0.018	n/a	Transformer Fails To Supply Power 2-EE-TX-2J1
2EEBUS-LU-2H	1.2E-05	1.8E-05	2.5E+00	0.018	n/a	4160v Bus Bar 2H Loss of Function 2-EE-BUS-2H
2EEBUS-LU-2J	1.2E-05	1.8E-05	2.4E+00	0.018	n/a	4160v Bus Bar 2J Loss of Function 2-EE-BUS-2J
2EEBUS-LU-2J-1	1.2E-05	1.8E-05	2.4E+00	0.018	n/a	480v Bus 2J-1 Loss of Function 2-EE-BUS-2J-1
2EEBUS-LU-2J-480	1.2E-05	1.8E-05	2.4E+00	0.018	n/a	Bus Bar 2J 480v Loss of Function 2-EE-BUS-2J (480v)
1SWTCV-SC-108A	1.2E-05	1.7E-05	2.4E+00	0.017		N.O. temp. control valve 1-SW-TCV-108 SPURIOUS CLOSES
1RCPORV-DMDSBO	4.5E-01	1.6E-02	1.0E+00	0.016	n/a	PROB OF PORV DEMAND - SBO
B03	4.0E-01	1.6E-02	1.0E+00	0.016	n/a	RECOVER OFFSITE POWER
2EEBUS-UM-2H-1	7.3E-06	1.0E-05	2.4E+00	0.016	n/a	BUS BAR UNSCHEDULED MAINTENANCE
2EEBUS-UM-2H	7.3E-06	1.0E-05	2.4E+00	0.016	n/a	BUS BAR UNSCHEDULED MAINTENANCE
1FWTRB-UM-1FWP2	1.9E-02	1.4E-02	1.7E+00	0.015	n/a	TURBINE-DRIVEN PUMP UNSCHLD MAINT. 1-FW-P-2
PROB-O03	1.0E-01	1.5E-02	1.1E+00	0.015	n/a	NO SEAL LOCA PRIOR TO COOLDOWN TREE T4

Event	Probability	F-V	RIR	SWIM	Applicability	Event Description
C-O202	1.0E+00	1.5E-02	1.0E+00	0.015	n/a	SGTR OPERATOR COOLDOWN LATE COMPLEMENT
1RTTMR-LF-2-B	8.0E-04	1.0E-03	2.3E+00	0.013	n/a	Output Timer 2 Fails To Energize Train B
1RTTMR-LF-2-A	8.0E-04	1.0E-03	2.3E+00	0.013	n/a	Output Timer 2 Fails To Energize Train A
1RTRLY-LF-2X-B	2.7E-04	3.4E-04	2.3E+00	0.013	n/a	Output Relay 2X Fails To Energize Train B
1RTRLY-LF-2X-A	2.7E-04	3.4E-04	2.3E+00	0.013	n/a	Output Relay 2X Fails To Energize Train A
1VSPAT-CC-MER3&5	1.1E-04	1.4E-04	2.3E+00	0.012		CCF 5/5 FR 24 HR 1-VS-P-1A B C D E FAIL (AIR
PROB-M02	2.9E-01	1.2E-02	1.0E+00	0.012	n/a	Number of FW events above 40% power EQN:M02 TREE:TH
1EEBKR-SO-15J8	3.4E-05	4.1E-05	2.2E+00	0.011	n/a	BREAKER 15J8 SPURIOUSLY OPENS 1EEBKR-SO-15J8
IE-TS1	4.4E-06	5.3E-06	2.2E+00	0.010		STEAM BREAK IN CONTAINMENT
C-O201	1.0E+00	1.0E-02	1.0E+00	0.010	n/a	SGTR OPERATOR COOLDOWN LATE COMPLEMENT
C-Y03	5.1E-01	1.0E-02	1.0E+00	0.010	n/a	CORE COOLING REC. EQN: C-Y03
1CHPAT-FR-24HP1A	7.9E-04	9.3E-04	2.2E+00	0.010		CHARGING PUMP 1A FAILS TO RUN FOR 24 HOURS
2FWTRB-FS-2FWP2	2.5E-02	9.7E-03	1.4E+00	0.010		TURBINE DRIVEN PUMP FAILS TO START 2-FW-P-2
1EGEDG-TM-3	5.7E-04	6.7E-04	2.2E+00	0.010	n/a	EDG #3 Unavailable Due To Scheduled Test or Maintenance
1MSCKV-FO-MS102B	3.4E-03	3.6E-03	2.0E+00	0.009		CHECK VALVE FAILS OPEN 1-MS-NRV-102B
1MSCKV-FO-MS102C	3.4E-03	3.6E-03	2.0E+00	0.009		CHECK VALVE FAILS OPEN 1-MS-NRV-102C
2EEBUS-UM-2J-1	7.3E-06	8.5E-06	2.2E+00	0.009	n/a	BUS BAR UNSCHEDULED MAINTENANCE
2EEBUS-UM-2J	7.3E-06	8.5E-06	2.2E+00	0.009	n/a	BUS BAR UNSCHEDULED MAINTENANCE
IE-T2A	6.5E-01	9.0E-03	1.0E+00	0.009		RECOVERABLE LOSS OF MFW
B12AVE	1.1E-01	9.0E-03	1.1E+00	0.009	n/a	Time averaged probability of Non-recovery AC IN 12 HOURS
1FWPSB-FS-1FWP3A	7.0E-03	6.1E-03	1.9E+00	0.009		MD PUMP -STNDBY SYS FAILS TO START 1-FW-P-3A
1MSMV--LK-1MS157	5.0E-02	8.6E-03	1.2E+00	0.009		SG C PORV BLOCKED DUE TO LEAKAGE
1MSMV--LK-1MS119	5.0E-02	8.6E-03	1.2E+00	0.009		SG B PORV BLOCKED DUE TO LEAKAGE
1RCRV--FO-PCV55C	2.5E-02	8.5E-03	1.3E+00	0.009		PWR OP RELIEF VALVE FAILS OPEN PCV-1455C
1RCRV--FO-PCV456	2.5E-02	8.2E-03	1.3E+00	0.008		PWR OP RELIEF VALVE FAILS OPEN PCV-1456
REC-XTIE-RWST	4.6E-03	4.3E-03	1.9E+00	0.008	n/a	FAIL TO XTIE RWST FROM UNIT 2
1SIPSB-FS-1SIP1B	7.0E-03	5.8E-03	1.8E+00	0.008		MD STNDBY PUMP 1-SI-P-1B FAILS TO START
1SIPSB-FS-1SIP1A	7.0E-03	5.8E-03	1.8E+00	0.008		MD STNDBY PUMP 1-SI-P-1A FAILS TO START
1SIMOV-FC-1860B	7.0E-03	5.8E-03	1.8E+00	0.008		MOTOR operated valve SI-1860B fails closed (FAILS to OPEN)
1SIMOV-FO-1862B	7.0E-03	5.8E-03	1.8E+00	0.008		MOTOR OPERTD VALVE SI-1862B FAILS OPEN
1FWCKV-FC-1FW58	6.3E-04	7.1E-04	2.1E+00	0.008		CHECK VALVE FAILS TO OPEN 1-FW-58
1FWCKV-FC-1FW89	6.3E-04	7.1E-04	2.1E+00	0.008		CHECK VALVE FAILS TO OPEN 1-FW-89
1SIMOV-FO-1862A	7.0E-03	5.8E-03	1.8E+00	0.008		MOTOR operated valve SI-1862A fails open (FAILS to CLOSE)
1SIMOV-FC-1860A	7.0E-03	5.8E-03	1.8E+00	0.008		MOTOR operated valve SI-1860A fails closed (FAILS to OPEN)
2FWPSB-UM-2FWP3B	1.6E-02	7.9E-03	1.5E+00	0.008	n/a	MD STNDBY PUMP UNSCHDL MAINT. 2-FW-P-3B
2FWPSB-UM-2FWP3A	1.6E-02	7.9E-03	1.5E+00	0.008	n/a	MD STNDBY PUMP UNSCHDL MAINT. 2-FW-P-3A
1FWCKV-FO-1FW142	3.4E-03	3.4E-03	2.0E+00	0.008		CHECK VALVE FAILS TO CLOSE 1-FW-142
1FWCKV-FC-1FW27	6.3E-04	7.0E-04	2.1E+00	0.008		CHECK VALVE FAILS TO OPEN 1-FW-27
B02_B04	6.0E-01	7.6E-03	1.0E+00	0.008	n/a	Non-recovery AC power in 2 HOURS GIVEN B04 (REC 1HR)
1EGEDG-FR-1-1HR	2.2E-03	2.2E-03	2.0E+00	0.007	n/a	EDG #1 FAIL TO RUN FOR 1 HOUR
2FWTRB-UM-2FWP2	1.9E-02	7.1E-03	1.4E+00	0.007	n/a	TURBINE-DRIVEN PUMP UNSCHLD MAINT. 2-FW-P-2
1EEBKR-SO-14J1	3.4E-05	3.7E-05	2.1E+00	0.007	n/a	Breaker 14J1 Spuriously Opens 1-EE-BKR-14J1
1EEBKR-SO-14H1	3.4E-05	3.7E-05	2.1E+00	0.007	n/a	Breaker 14H1 Spuriously Opens 1-EE-BKR-14H1
1MSTCV-CC-105AB	1.8E-03	1.8E-03	2.0E+00	0.007		CCF 2/2 FTO of STEAM DUMP valves 1-MSTCV-CC-105A/B
1MSMV--LK-1MS86	5.0E-02	6.8E-03	1.1E+00	0.007		SG A PORV BLOCKED DUE TO LEAKAGE
REC-XTIE-RWST-C1	8.0E-01	6.8E-03	1.0E+00	0.007	n/a	FAIL TO XTIE RWST FROM U-2
HEP-1ES1:3	5.8E-02	6.8E-03	1.1E+00	0.007	n/a	1-ES-1.3 TRANSFER TO COLD LEG RECIRCULATION
1EETFM-LP-1J	1.9E-05	2.1E-05	2.1E+00	0.007	n/a	Transformer Fails To Supply Power 1-EE-TX-1J
1EETFM-LP-1H	1.9E-05	2.1E-05	2.1E+00	0.007	n/a	Transformer Fails to Supply Power 1-EE-TFM-1H

Event	Probability	F-V	RIR	SWIM	Applicability	Event Description
IE-T2	1.5E-01	6.5E-03	1.0E+00	0.007		LOSS OF MFW
C-QS01	9.7E-01	6.1E-03	1.0E+00	0.006	n/a	STEAM GENERATOR ISOLATION COMPLEMENT
HEP-AP12:01-10	2.7E-03	2.5E-03	1.9E+00	0.006	n/a	AP-12:01 LOSS INTKE CANAL STP 10
1MSMV--FO-1MS87	1.3E-04	1.3E-04	2.0E+00	0.006		MANUAL VALVE FAILS OPEN 1-MS-87
2EGEDG-TM-2	5.7E-04	5.7E-04	2.0E+00	0.006	n/a	EDG #2 Unavailable Due To Scheduled Test or Maintenance
1SWDDP-CC-1A1B1C	2.1E-03	1.9E-03	1.9E+00	0.006		COMMON CAUSE FAILURE ESW PUMPS 1-SW-P-1A
1VSFAN-FS-1FMO6	2.0E-03	1.8E-03	1.9E+00	0.006	n/a	1-VS-AC-6 FAN MOTOR FAILS TO START 1-VS-FMO-6
REC-INAIR-LOCAL	1.0E-01	5.5E-03	1.0E+00	0.005	n/a	FAIL TO RECOVER INSTR. AIR LOCALLY VIA AP 40.00
1EEBUS-UM-1H-480	7.3E-06	7.4E-06	2.0E+00	0.005	n/a	BUS BAR UNSCHEDULED MAINTENANCE
1EEBUS-UM-1J-480	7.3E-06	7.4E-06	2.0E+00	0.005	n/a	BUS BAR UNSCHEDULED MAINTENANCE
1FWPSB-U2-SBOQS	8.0E-02	5.2E-03	1.1E+00	0.005		U2 IN SBO WITH A STUCK OPEN SG RV
1TMSOV-FC-20-ET	1.8E-02	5.0E-03	1.3E+00	0.005		EHC/auto stop OIL low pressure SOV (FAILS TO OPEN)
1TMSOV-FC-ASO	1.8E-02	5.0E-03	1.3E+00	0.005		EHC/auto stop OIL interface valve (FAILS TO OPEN)
REC-XTIE-RWST-C3	1.0E-01	5.0E-03	1.0E+00	0.005	n/a	CROSS TIE of RWST FM U-2 PER ECA 1.3 after HEP for RHR
1RTRLY-LF-63-B	2.7E-04	2.6E-04	2.0E+00	0.005	n/a	2/4 RWST Level or 2/2 PB Master Logic Train B Relay 63
1RTHEP-RMT-RF-B	2.7E-04	2.6E-04	2.0E+00	0.005	n/a	RMT/REFUEL Key Switch Left In REFUEL Position
1RTHEP-TEST-SW-B	2.7E-04	2.6E-04	2.0E+00	0.005	n/a	Test Switch Left In TEST Not OPERATE Train B
1RTHEP-TEST-SW-A	2.7E-04	2.6E-04	2.0E+00	0.005	n/a	Test Switch Left In TEST Not OPERATE Train A
1RTRLY-LF-63-A	2.7E-04	2.6E-04	2.0E+00	0.005	n/a	2/4 RWST Level or 2/2 PB Master Logic Train A Relay 63
1RTHEP-RMT-RF-A	2.7E-04	2.6E-04	2.0E+00	0.005	n/a	RMT/REFUEL Key Switch Left In REFUEL Position

Appendix E

Source Code for the SAPHIRE "Compound"
FAC Calculation

APPENDIX E

Source Code for the SAPHIRE "Compound" Calculation Library for FAC

As discussed in the body of this report, various piping basic events were incorporated into the Surry IPE model. These piping events were considered to be susceptible to FAC and, as such, required an investigation as to their aging-related failure probability. To perform the FAC probability calculation, a "plug-in" module was developed for SAPHIRE. The details of the calculation performed by the FAC plug-in are discussed in Sections 3.6 and 4.5. While the module was written in MODULA-2, any programming language capable of compiling a Microsoft Windows™ dynamic link library (.DLL) could be used.

```
MODULE PLUGPIPE;
  <*/CALLS:SageSystem*>

(**
  This module is used to create the PIPE (Flow Accelerated Corrosion DLL).
*)
%IF DLL %THEN
<*/DLL*>
%END
%IF DLL %THEN
FROM WINX IMPORT
  IsInit;
%END
IMPORT EXCEPTIONS;
IMPORT WinAux;

FROM SetLib IMPORT
  SetSize, SetToEmpty, Include, SetPopulation;

FROM ModSys IMPORT
  CARD32, BitSet, BIT16;

FROM MoveLib IMPORT
  MoveLeft;

FROM SYSTEM IMPORT
  ADDRESS, CAST, ADR, TSIZE;

FROM StorageX IMPORT
  ALLOCATE, DEALLOCATE;
```

```
FROM StringsX IMPORT
  Assign, Compare, CompareResult, Concat;

FROM MathLib IMPORT Exp, Sqrt;

FROM BaseDef IMPORT
  RealPtr, EventRec;
FROM PlugDef IMPORT
  Parameter, EventRecPtr, PNAME, ParamRec, InputRec, ProcRec, ProcRecArray, ProcPtr, ProcDes,
  NoneVar, CardVar, CardArray, CharVar, CharArray, RealVar, RealArray, BoolVar, BoolArray,
  PtrVar, PtrArray, IntVar, IntArray, InOut;

CONST
  NumSamples = 250;
  Seed       = 1254.0;

CONST
  ProcArray : ARRAY OF ProcRec = {
    {"PLUGPIPE_IsSaphPlugIn", "IsSaphPlugIn", 1, FALSE, 9, 0,
      {{"ProcCount",     CardVar+InOut},
       {"ProcRecArray",  PtrVar+InOut},
       {"",              NoneVar},
       {"",              NoneVar},
       {"",              NoneVar},
       {"",              NoneVar},
       {"",              NoneVar},
       {"",              NoneVar},
       {"",              NoneVar},
       {"",              NoneVar},
       {"",              NoneVar},
       {"",              NoneVar},
       {"",              NoneVar},
       {"",              NoneVar},
       {"",              NoneVar},
       {"",              NoneVar},
       {"",              NoneVar},
       {"",              NoneVar},
       {"",              NoneVar},
       {"",              NoneVar},
       {"",              NoneVar},
       {"",              NoneVar}},
      {{"",       "N",  0.0,  1, 0.0, 1.0},
       {"",       "N",  0.0,  1, 0.0, 1.0},
       {"",       "N",  0.0,  1, 0.0, 1.0},
       {"",       "N",  0.0,  1, 0.0, 1.0},
       {"",       "N",  0.0,  1, 0.0, 1.0},
       {"",       "N",  0.0,  1, 0.0, 1.0},
       {"",       "N",  0.0,  1, 0.0, 1.0},
```

```
   {"",       "N",  0.0,  1, 0.0, 1.0},
   {"",       "N",  0.0,  1, 0.0, 1.0},
   {"",       "N",  0.0,  1, 0.0, 1.0},
   {"",       "N",  0.0,  1, 0.0, 1.0},
   {"",       "N",  0.0,  1, 0.0, 1.0},
   {"",       "N",  0.0,  1, 0.0, 1.0},
   {"",       "N",  0.0,  1, 0.0, 1.0},
   {"",       "N",  0.0,  1, 0.0, 1.0},
   {"",       "N",  0.0,  1, 0.0, 1.0},
   {"",       "N",  0.0,  1, 0.0, 1.0},
   {"",       "N",  0.0,  1, 0.0, 1.0},
   {"",       "N",  0.0,  1, 0.0, 1.0},
   {"",       "N",  0.0,  1, 0.0, 1.0}}},

{"PLUGPIPE_ReleasePlugIn", "ReleasePlugIn", 2, FALSE, 2, 0,
  {{"ProcCount",     CardVar},
   {"ProcRecArray",  PtrVar+InOut},
   {"",              NoneVar},
   {"",              NoneVar},
   {"",              NoneVar},
   {"",              NoneVar},
   {"",              NoneVar},
   {"",              NoneVar},
   {"",              NoneVar},
   {"",              NoneVar},
   {"",              NoneVar},
   {"",              NoneVar},
   {"",              NoneVar},
   {"",              NoneVar},
   {"",              NoneVar},
   {"",              NoneVar},
   {"",              NoneVar},
   {"",              NoneVar},
   {"",              NoneVar},
   {"",              NoneVar},
   {"",              NoneVar}},
  {{"",       "N",  0.0,  1, 0.0, 1.0},
   {"",       "N",  0.0,  1, 0.0, 1.0},
   {"",       "N",  0.0,  1, 0.0, 1.0},
   {"",       "N",  0.0,  1, 0.0, 1.0},
   {"",       "N",  0.0,  1, 0.0, 1.0},
   {"",       "N",  0.0,  1, 0.0, 1.0},
   {"",       "N",  0.0,  1, 0.0, 1.0},
   {"",       "N",  0.0,  1, 0.0, 1.0},
   {"",       "N",  0.0,  1, 0.0, 1.0},
   {"",       "N",  0.0,  1, 0.0, 1.0},
   {"",       "N",  0.0,  1, 0.0, 1.0},
   {"",       "N",  0.0,  1, 0.0, 1.0},
```

```
   {"",       "N",  0.0,  1, 0.0, 1.0},
   {"",       "N",  0.0,  1, 0.0, 1.0},
   {"",       "N",  0.0,  1, 0.0, 1.0},
   {"",       "N",  0.0,  1, 0.0, 1.0},
   {"",       "N",  0.0,  1, 0.0, 1.0},
   {"",       "N",  0.0,  1, 0.0, 1.0},
   {"",       "N",  0.0,  1, 0.0, 1.0},
   {"",       "N",  0.0,  1, 0.0, 1.0},
   {"",       "N",  0.0,  1, 0.0, 1.0}}},

{"PLUGPIPE_GetFunctionDescription", "GetFunctionDescription", 3, FALSE, 3, 0,
  {{"FuncName",     CharArray},
   {"Description",  CharArray+InOut},
   {"Result",       CardVar+InOut},
   {"",             NoneVar},
   {"",             NoneVar},
   {"",             NoneVar},
   {"",             NoneVar},
   {"",             NoneVar},
   {"",             NoneVar},
   {"",             NoneVar},
   {"",             NoneVar},
   {"",             NoneVar},
   {"",             NoneVar},
   {"",             NoneVar},
   {"",             NoneVar},
   {"",             NoneVar},
   {"",             NoneVar},
   {"",             NoneVar},
   {"",             NoneVar},
   {"",             NoneVar},
   {"",             NoneVar}},
  {{"",       "N",  0.0,  1, 0.0, 1.0},
   {"",       "N",  0.0,  1, 0.0, 1.0},
   {"",       "N",  0.0,  1, 0.0, 1.0},
   {"",       "N",  0.0,  1, 0.0, 1.0},
   {"",       "N",  0.0,  1, 0.0, 1.0},
   {"",       "N",  0.0,  1, 0.0, 1.0},
   {"",       "N",  0.0,  1, 0.0, 1.0},
   {"",       "N",  0.0,  1, 0.0, 1.0},
   {"",       "N",  0.0,  1, 0.0, 1.0},
   {"",       "N",  0.0,  1, 0.0, 1.0},
   {"",       "N",  0.0,  1, 0.0, 1.0},
   {"",       "N",  0.0,  1, 0.0, 1.0},
   {"",       "N",  0.0,  1, 0.0, 1.0},
   {"",       "N",  0.0,  1, 0.0, 1.0},
   {"",       "N",  0.0,  1, 0.0, 1.0},
   {"",       "N",  0.0,  1, 0.0, 1.0},
   {"",       "N",  0.0,  1, 0.0, 1.0},
   {"",       "N",  0.0,  1, 0.0, 1.0},
   {"",       "N",  0.0,  1, 0.0, 1.0},
   {"",       "N",  0.0,  1, 0.0, 1.0},
```

```
   {"",       "N",  0.0,  1, 0.0, 1.0},
   {"",       "N",  0.0,  1, 0.0, 1.0},
   {"",       "N",  0.0,  1, 0.0, 1.0},
   {"",       "N",  0.0,  1, 0.0, 1.0},
   {"",       "N",  0.0,  1, 0.0, 1.0}}},

{"PLUGSUPER_GetParameterDescription", "GetParameterDescription", 4, FALSE, 4, 0,
  {{"FuncName",     CharArray},
   {"ParamName",    CharArray},
   {"Description",  CharArray+InOut},
   {"Result",       CardVar+InOut},
   {"",             NoneVar},
   {"",             NoneVar},
   {"",             NoneVar},
   {"",             NoneVar},
   {"",             NoneVar},
   {"",             NoneVar},
   {"",             NoneVar},
   {"",             NoneVar},
   {"",             NoneVar},
   {"",             NoneVar},
   {"",             NoneVar},
   {"",             NoneVar},
   {"",             NoneVar},
   {"",             NoneVar},
   {"",             NoneVar},
   {"",             NoneVar}},
  {{"",       "N",  0.0,  1, 0.0, 1.0},
   {"",       "N",  0.0,  1, 0.0, 1.0},
   {"",       "N",  0.0,  1, 0.0, 1.0},
   {"",       "N",  0.0,  1, 0.0, 1.0},
   {"",       "N",  0.0,  1, 0.0, 1.0},
   {"",       "N",  0.0,  1, 0.0, 1.0},
   {"",       "N",  0.0,  1, 0.0, 1.0},
   {"",       "N",  0.0,  1, 0.0, 1.0},
   {"",       "N",  0.0,  1, 0.0, 1.0},
   {"",       "N",  0.0,  1, 0.0, 1.0},
   {"",       "N",  0.0,  1, 0.0, 1.0},
   {"",       "N",  0.0,  1, 0.0, 1.0},
   {"",       "N",  0.0,  1, 0.0, 1.0},
   {"",       "N",  0.0,  1, 0.0, 1.0},
   {"",       "N",  0.0,  1, 0.0, 1.0},
   {"",       "N",  0.0,  1, 0.0, 1.0},
   {"",       "N",  0.0,  1, 0.0, 1.0},
   {"",       "N",  0.0,  1, 0.0, 1.0},
   {"",       "N",  0.0,  1, 0.0, 1.0},
```

```
   {"",       "N",  0.0,  1, 0.0, 1.0}}},

 {"PLUGPIPE_FACRATE", "FACRATE", 5, TRUE, 4, 18,
   {{"NumEvents", CardVar},
    {"ProbArray", PtrArray},
    {"Event Rec", PtrVar},
    {"Result",    CardVar+InOut},
    {"",          NoneVar},
    {"",          NoneVar},
    {"",          NoneVar},
    {"",          NoneVar},
    {"",          NoneVar},
    {"",          NoneVar},
    {"",          NoneVar},
    {"",          NoneVar},
    {"",          NoneVar},
    {"",          NoneVar},
    {"",          NoneVar},
    {"",          NoneVar},
    {"",          NoneVar},
    {"",          NoneVar},
    {"",          NoneVar},
    {"",          NoneVar},
    {"",          NoneVar}},
   {{"Geom. Factor",      "E",  0.0,  1, 0.0,   10.0},
    {"Flow Veloc.",       "E",  0.0,  1, 0.0,   100.0},
    {"pH Value",          "E",  0.0,  1, 7.0,   9.39},
    {"Oxy. Content",      "E",  0.0,  1, 0.0,   30.0},
    {"Cr & Mb %",         "E",  0.0,  1, 0.0,   25.0},
    {"Temp.(Cel.)",       "E",  0.0,  1, 0.0,   3000.0},
    {"Expos. Time",       "E",  0.0,  1, 200.0, 1000000.0},
    {"Steam Quality",     "E",  0.0,  1, 0.0,   100.0},
    {"Mass Flux",         "E",  0.0,  1, 0.0,   10000.0},
    {"Water Density",     "E",  0.0,  1, 0.0,   100.0},
    {"Void Fraction",     "E",  0.0,  1, 0.0,   50000.0},
    {"Pipe Dens.",        "E",  0.0,  1, 0.0,   50000.0},
    {"Pipe Fail.Stress",  "E",  0.0,  1, 0.0,   200.0},
    {"Uncert. Factor",    "E",  0.0,  1, 0.0,   1.0},
    {"Pipe Thickness",    "E",  0.0,  1, 0.0,   1.0},
    {"Hoop Strain",       "E",  0.0,  1, 0.0,   1.0},
    {"Pipe Radius",       "E",  0.0,  1, 0.0,   1.0},
    {"Pipe Load",         "E",  0.0,  1, 0.0,   1.0},
    {"",                  "N",  0.0,  1, 0.0,   1.0},
    {"",                  "N",  0.0,  1, 0.0,   1.0}}},

 {"PLUGPIPE_FAILUREPRESSURE", "FAILUREPRESSURE", 6, TRUE, 4,  18,
   {{"NumEvents", CardVar},
```

```
   {"ProbArray", PtrArray},
   {"Event Rec", PtrVar},
   {"Result",    CardVar+InOut},
   {"",          NoneVar},
   {"",          NoneVar},
   {"",          NoneVar},
   {"",          NoneVar},
   {"",          NoneVar},
   {"",          NoneVar},
   {"",          NoneVar},
   {"",          NoneVar},
   {"",          NoneVar},
   {"",          NoneVar},
   {"",          NoneVar},
   {"",          NoneVar},
   {"",          NoneVar},
   {"",          NoneVar},
   {"",          NoneVar},
   {"",          NoneVar},
   {"",          NoneVar}},
  {{"Geom. Factor",      "E",  0.0,  1, 0.0,   10.0},
   {"Flow Veloc.",       "E",  0.0,  1, 0.0,   100.0},
   {"pH Value",          "E",  0.0,  1, 7.0,   9.39},
   {"Oxy. Content",      "E",  0.0,  1, 0.0,   30.0},
   {"Cr & Mb %",         "E",  0.0,  1, 0.0,   25.0},
   {"Temp.(Cel.)",       "E",  0.0,  1, 0.0,   3000.0},
   {"Expos. Time",       "E",  0.0,  1, 200.0, 1000000.0},
   {"Steam Quality",     "E",  0.0,  1, 0.0,   100.0},
   {"Mass Flux",         "E",  0.0,  1, 0.0,   10000.0},
   {"Water Density",     "E",  0.0,  1, 0.0,   100.0},
   {"Void Fraction",     "E",  0.0,  1, 0.0,   50000.0},
   {"Pipe Dens.",        "E",  0.0,  1, 0.0,   50000.0},
   {"Pipe Fail.Stress",  "E",  0.0,  1, 0.0,   200.0},
   {"Uncert. Factor",    "E",  0.0,  1, 0.0,   1.0},
   {"Pipe Thickness",    "E",  0.0,  1, 0.0,   1.0},
   {"Hoop Strain",       "E",  0.0,  1, 0.0,   1.0},
   {"Pipe Radius",       "E",  0.0,  1, 0.0,   1.0},
   {"Pipe Load",         "E",  0.0,  1, 0.0,   1.0},
   {"",                  "N",  0.0,  1, 0.0,   1.0},
   {"",                  "N",  0.0,  1, 0.0,   1.0}}},


{"PLUGPIPE_CAPACITYLOAD", "CAPACITYLOAD", 7, TRUE, 4, 18,
  {{"NumEvents", CardVar},
   {"ProbArray", PtrArray},
   {"Event Rec", PtrVar},
   {"Result",    CardVar+InOut},
```

```
     {"",          NoneVar},
     {"",          NoneVar},
     {"",          NoneVar},
     {"",          NoneVar},
     {"",          NoneVar},
     {"",          NoneVar},
     {"",          NoneVar},
     {"",          NoneVar},
     {"",          NoneVar},
     {"",          NoneVar},
     {"",          NoneVar},
     {"",          NoneVar},
     {"",          NoneVar},
     {"",          NoneVar},
     {"",          NoneVar},
     {"",          NoneVar}},
    {{"Geom. Factor",      "M",  Seed,  NumSamples, 0.0,   10.0},
     {"Flow Veloc.",       "M",  Seed,  NumSamples, 0.0,   100.0},
     {"pH Value",          "M",  Seed,  NumSamples, 7.0,   9.39},
     {"Oxy. Content",      "M",  Seed,  NumSamples, 0.0,   30.0},
     {"Cr & Mb %",         "M",  Seed,  NumSamples, 0.0,   25.0},
     {"Temp.(Cel.)",       "M",  Seed,  NumSamples, 0.0,   3000.0},
     {"Expos. Time",       "M",  Seed,  NumSamples, 200.0, 1000000.0},
     {"Steam Quality",     "M",  Seed,  NumSamples, 0.0,   100.0},
     {"Mass Flux",         "M",  Seed,  NumSamples, 0.0,   10000.0},
     {"Water Density",     "M",  Seed,  NumSamples, 0.0,   100.0},
     {"Void Fraction",     "M",  Seed,  NumSamples, 0.0,   50000.0},
     {"Pipe Dens.",        "M",  Seed,  NumSamples, 0.0,   50000.0},
     {"Pipe Fail.Stress",  "M",  Seed,  NumSamples, 0.0,   200.0},
     {"Uncert. Factor",    "M",  Seed,  NumSamples, 0.0,   1.0},
     {"Pipe Thickness",    "M",  Seed,  NumSamples, 0.0,   1.0},
     {"Hoop Strain",       "M",  Seed,  NumSamples, 0.0,   1.0},
     {"Pipe Radius",       "M",  Seed,  NumSamples, 0.0,   1.0},
     {"Pipe Load",         "M",  Seed,  NumSamples, 0.0,   1.0},
     {"",                  "N",  0.0,  1, 0.0,   1.0},
     {"",                  "N",  0.0,  1, 0.0,   1.0}}}};

DesArray : ARRAY OF ProcDes = {
  { {"This function returns information about the procedures exportable from this dll."},
    {""},
    {""}},
  { {"This function releases memory allocated during the setup of this dll."},
    {""},
    {""}},
  { {"This function returns a description of an exportable function."},
    {""},
```

```
      {""}},
    { {"This function returns a description of a parameter of an exportable function."},
      {""},
      {""}},
     { {"Calculates the KASTNER Flow Accelarated Corrosive action and returns it as the
probability of this event."},
      {"Inputs are Geometric Factor, Flow Velocity, pH Value, Oxygen Content, Chromium and Mb
percent, Temperature(C),"},
       {"Exposure Time, Steam Quality %, Mass Flux, Water Density, and Void Fraction.  (1.0
generally indicates an error)."}},
   { {"Calculates the failure pressure for a pipe segment and returns it as the probability of
this event."},
     {"Inputs are Geometric Factor, Flow Velocity, pH Value, Oxygen Content, Chromium and Mb
percent, Temperature(C),"},
       {"Exposure Time, Steam Quality %, Mass Flux, Water Density, and Void Fraction.  (1.0
generally indicates an error)."}},
    { {"Calculates the probability of failure of a pipe segment given a load pressure and
returns it as the probability of this event."},
     {"Inputs are Geometric Factor, Flow Velocity, pH Value, Oxygen Content, Chromium and Mb
percent, Temperature(C),"},
      {"Exposure Time, Steam Quality %, Mass Flux, Water Density, and Void Fraction."}}};

  ParamDesArray : ARRAY OF ProcDes = {
    { {"Geometric Factor : The of the pipe.  0.0 <= x <= 10.0 "},
      {""},
      {""}},
    { {"Flow Velocity : Meters/Second. 0.0 <= x <= 100.0 "},
      {""},
      {""}},
    { {"pH Value : 7 <= x <= 9.39"},
      {""},
      {""}},
    { {"Oxygen Content : 0.0 <= x <= 30.0"},
      {""},
      {""}},
    { {"Chromium/Molybdenum content : 0.0 <= x <= 2500.0"},
      {""},
      {""}},
    { {"Temperature : Degrees Celsius.  0 <= x <= 3000. "},
      {""},
      {""}},
    { {"Exposure Time : Hours. 0.0 <= x <= 1,000,000.0"},
      {""},
      {""}},
    { {"Steam Quality : Percent. 0.0 <= x <= 100.0 (Only used if two-phase flow). "},
      {""},
      {""}},
    { {"Mass Flux Rate : Kg / (m**2 sec) (Only used if two-phase flow)"},
```

```
   {""},
   {""}},
 { {"Water Density : Saturation. Kg/m**3 0.0 <= x <= 10000.0 (Only used if two-phase flow)"},
   {""},
   {""}},
 { {"Void Fraction : Percent. 0.0 <= x <= 100.0 (Only used if two-phase flow)"},
   {""},
   {""}},
 { {"Pipe Density : Kg/m**3. 0.0 <= x <= 50000.0"},
   {""},
   {""}},
 { {"Pipe Failure Stress : Ksi. 0.0 <= x <= 200.0"},
   {""},
   {""}},
 { {"Uncertainty Factor : Model Uncertainty Factor. 0.0 <= x <= 1.0"},
   {""},
   {""}},
 { {"Pipe Thickness : Original. cm 0.0 <= x <= 100.0"},
   {""},
   {""}},
 { {"Hoop Strain : Percent. 0.0 <= x <= 100.0"},
   {""},
   {""}},
 { {"Pipe Radius : cm. Initial Inside Pipe Radius. 0.0 <= x <= 1000.0"},
   {""},
   {""}},
 { {"Pipe Load : Amount of pressure on the pipe"},
   {""},
   {""}},
 { {"Geometric Factor : The of the pipe.  0.0 <= x <= 10.0 "},
   {""},
   {""}},
 { {"Flow Velocity : Meters/Second. 0.0 <= x <= 100.0 "},
   {""},
   {""}},
 { {"pH Value : 7 <= x <= 9.39"},
   {""},
   {""}},
 { {"Oxygen Content : 0.0 <= x <= 30.0"},
   {""},
   {""}},
 { {"Chromium/Molybdenum content : 0.0 <= x <= 2500.0"},
   {""},
   {""}},
 { {"Temperature : Degrees Celsius.  0 <= x <= 3000. "},
   {""},
```

```
  {""}},
{ {"Exposure Time : Hours. 0.0 <= x <= 1,000,000.0"},
  {""},
  {""}},
{ {"Steam Quality : Percent. 0.0 <= x <= 100.0 (Only used if two-phase flow). "},
  {""},
  {""}},
{ {"Mass Flux Rate : Kg / (m**2 sec) "},
  {""},
  {""}},
{ {"Water Density : Saturation. Kg/m**3 0.0 <= x <= 10000.0"},
  {""},
  {""}},
{ {"Void Fraction : Percent. 0.0 <= x <= 100.0"},
  {""},
  {""}},
{ {"Pipe Density : Kg/m**3. 0.0 <= x <= 50000.0"},
  {""},
  {""}},
{ {"Pipe Failure Stress : Ksi. 0.0 <= x <= 200.0"},
  {""},
  {""}},
{ {"Uncertainty Factor : Model Uncertainty Factor. 0.0 <= x <= 1.0"},
  {""},
  {""}},
{ {"Pipe Thickness : Original. cm 0.0 <= x <= 100.0"},
  {""},
  {""}},
{ {"Hoop Strain : Percent. 0.0 <= x <= 100.0"},
  {""},
  {""}},
{ {"Pipe Radius : cm. Initial Inside Pipe Radius. 0.0 <= x <= 1000.0"},
  {""},
  {""}},
{ {"Pipe Load : Amount of pressure on the pipe"},
  {""},
  {""}},
{ {"Geometric Factor : The of the pipe.  0.0 <= x <= 10.0 "},
  {""},
  {""}},
{ {"Flow Velocity : Meters/Second. 0.0 <= x <= 100.0 "},
  {""},
  {""}},
{ {"pH Value : 7 <= x <= 9.39"},
  {""},
  {""}},
```

```
{ {"Oxygen Content : 0.0 <= x <= 30.0"},
  {""},
  {""}},
{ {"Chromium/Molybdenum content : 0.0 <= x <= 2500.0"},
  {""},
  {""}},
{ {"Temperature : Degrees Celsius.  0 <= x <= 3000. "},
  {""},
  {""}},
{ {"Exposure Time : Hours. 0.0 <= x <= 1,000,000.0"},
  {""},
  {""}},
{ {"Steam Quality : Percent. 0.0 <= x <= 100.0 (Only used if two-phase flow). "},
  {""},
  {""}},
{ {"Mass Flux Rate : Kg / (m**2 sec) "},
  {""},
  {""}},
{ {"Water Density : Saturation. Kg/m**3 0.0 <= x <= 10000.0"},
  {""},
  {""}},
{ {"Void Fraction : Percent. 0.0 <= x <= 100.0"},
  {""},
  {""}},
{ {"Pipe Density : Kg/m**3. 0.0 <= x <= 50000.0"},
  {""},
  {""}},
{ {"Pipe Failure Stress : Ksi. 0.0 <= x <= 200.0"},
  {""},
  {""}},
{ {"Uncertainty Factor : Model Uncertainty Factor. 0.0 <= x <= 1.0"},
  {""},
  {""}},
{ {"Pipe Thickness : Original. cm 0.0 <= x <= 100.0"},
  {""},
  {""}},
{ {"Hoop Strain : Percent. 0.0 <= x <= 100.0"},
  {""},
  {""}},
{ {"Pipe Radius : cm. Initial Inside Pipe Radius. 0.0 <= x <= 1000.0"},
  {""},
  {""}},
{ {"Pipe Load : Amount of pressure on the pipe"},
  {""},
  {""}}};
```

```
VAR
  msg      : ARRAY[0..63] OF CHAR;

PROCEDURE IsSaphPlugIn(VAR procCnt       : CARDINAL;
                       VAR procArray     : ADDRESS) : CARDINAL [EXPORT];
VAR
  i, j  : CARDINAL;
  k     : CARDINAL;
  strOk : BOOLEAN;
BEGIN
  procCnt   := HIGH(ProcArray)+1;
  procArray := ADR(ProcArray);
  RETURN 11;
END IsSaphPlugIn;

PROCEDURE ReleasePlugIn(    procCnt       : CARDINAL;
                        VAR procArray     : ADDRESS) : CARDINAL [EXPORT];
BEGIN
  RETURN 1;
END ReleasePlugIn;


PROCEDURE GetFunctionDescription(    funcName : ARRAY OF CHAR;
                                 VAR des1     : ARRAY OF CHAR;
                                 VAR des2     : ARRAY OF CHAR;
                                 VAR des3     : ARRAY OF CHAR;
                                 VAR result   : CARDINAL) [EXPORT];
VAR
  i     : CARDINAL;
  strOk : BOOLEAN;
BEGIN
  result := 0;
  des1   := "";
  des2   := "";
  des3   := "";

  FOR i := 0 TO HIGH(ProcArray) DO
    IF Compare(ProcArray[i].dispName, funcName) = equal THEN
      Assign(DesArray[i].line1, des1, strOk);
      Assign(DesArray[i].line2, des2, strOk);
      Assign(DesArray[i].line3, des3, strOk);
      result := 1;
      BREAK;
    END;
  END;
END GetFunctionDescription;
```

```
PROCEDURE GetParameterDescription(    funcName  : ARRAY OF CHAR;
                                      paramName : ARRAY OF CHAR;
                                  VAR des1     : ARRAY OF CHAR;
                                  VAR des2     : ARRAY OF CHAR;
                                  VAR des3     : ARRAY OF CHAR;
                                  VAR result   : CARDINAL) [EXPORT];
VAR
  i      : CARDINAL;
  j      : CARDINAL;
  desIdx : CARDINAL;
  strOk  : BOOLEAN;
BEGIN
  result := 0;
  des1   := "";
  des2   := "";
  des3   := "";
  desIdx := 0;

  FOR i := 0 TO HIGH(ProcArray) DO
    IF Compare(ProcArray[i].dispName, funcName) = equal THEN
      FOR j := 0 TO HIGH(ProcArray[i].inputList) DO
        IF Compare(ProcArray[i].inputList[j].dispParamName, paramName) = equal THEN
          Assign(ParamDesArray[j+desIdx].line1, des1, strOk);
          Assign(ParamDesArray[j+desIdx].line2, des2, strOk);
          Assign(ParamDesArray[j+desIdx].line3, des3, strOk);
          result := 1;
          BREAK;
        END;
      END;
    ELSE
      desIdx := desIdx + VAL(CARDINAL, ABS(ProcArray[i].inputCnt));
    END;
  END;
END GetParameterDescription;


PROCEDURE CalcFacRate(k           : REAL;          (* geometrical factor
*)
                      w           : REAL;          (* flow velocity m/s
*)
                      pH          : REAL;          (* pH Value
*)
                      g           : REAL;          (* oxygen content microg/kg
*)
                      h           : REAL;          (* percent of CR and MB in steel
*)
                      tKelvin     : REAL;          (* Temperature (Kelvin)
*)
```

```
                      time         : REAL;          (* Exposure Time in hours
*)
                      steamQual    : REAL;          (* Percent of steam in pipe
*)
                      massFlux     : REAL;          (* kg/m2s Mass Flux
*)
                      h2oDensity   : REAL;          (* Density of water at saturation (kg/m3)
*)
                      voidFraction : REAL) : REAL;  (* Void Fraction
*)
VAR
  N       : REAL;
  fofTime : REAL;
  B       : REAL;
  velocity: REAL;
  answer  : REAL;
BEGIN
  IF (pH < 7.0) THEN
    pH := 7.0;
  END;

  IF (pH > 9.39) THEN
    RETURN 1.0;
  END;

  IF (g > 30.0) THEN
    RETURN 1.0;
  END;


  IF (h >= 0.0) AND (h < 0.5) THEN
    N := -0.0875*h - (1.275E-5 * tKelvin*tKelvin) + (1.078E-2*tKelvin) - 2.15;  (* for 0.0 <=
h < 0.5  *)
  ELSE
   N := ((-1.29E-4 * tKelvin*tKelvin) + (0.109*tKelvin) - 22.07) * 0.154*Exp(-1.2*h);   (* for
0.5 <= h <= 5.0 *)
  END;

  IF steamQual = 0.0 THEN
    velocity := w;
  ELSE
    velocity := (massFlux/h2oDensity)*((1.0-steamQual) / (1.0-voidFraction));
  END;

  B       := -10.5*Sqrt(h) - (9.375E-4 * tKelvin*tKelvin) + (0.79*tKelvin) - 132.5;

  IF (time <= 9.600000E+4) THEN
```

```
   fofTime := 9.999934E-1 + (-3.356901E-7*time) + (-5.624812E-11*time*time) + (3.849972E-16 *
time * time * time);
  ELSE
    fofTime := 0.79;
  END;

   answer := (6.35*k*(B*Exp(N*velocity)*(1.0- (0.175 * (pH-7.0) * (pH - 7.0))) * 1.8 *
Exp(-0.118*g) + 1.0) * fofTime);
  RETURN answer;
END CalcFacRate;

PROCEDURE FACRATE(    numEvents : CARDINAL;
                  VAR events    : ARRAY OF Parameter;
                      evRecAdr  : ADDRESS;
                  VAR result    : CARDINAL) [EXPORT];
VAR
  evPtr        : EventRecPtr;
  k            : REAL;
  w            : REAL;
  pH           : REAL;
  g            : REAL;
  h            : REAL;
  tKelvin      : REAL;
  time         : REAL;
  stQual       : REAL;
  massFlux     : REAL;
  h2oDensity   : REAL;
  voidFraction : REAL;
  epsilon      : REAL;

BEGIN
  evPtr  := CAST(EventRecPtr, evRecAdr);

  IF (numEvents < 13) THEN
    result := 0;
    evPtr^.prob := 1.0;
    RETURN;
  END;

  k            := events[0].event^.prob;              (* geometrical factor
       *)
  w           := events[1].event^.prob;               (* flow velocity m/s
       *)
  pH           := events[2].event^.prob;               (* pH Value
       *)
  g           := events[3].event^.prob;                (* oxygen content microg/kg
       *)
```

```
  h            := events[4].event^.prob/100.0;         (* percent of chromium and molybdenum
in steel *)
  tKelvin      := events[5].event^.prob + 273.15;      (* Temperature (Kelvin)
       *)
  time         := events[6].event^.prob;               (* Exposure Time in hours
       *)
  stQual       := events[7].event^.prob/100.0;          (* Percent of steam in flow
       *)
  massFlux     := events[8].event^.prob;               (* kg/m2s Mass Flux
       *)
  h2oDensity    := events[9].event^.prob;                 (* Density of water at saturation
(kg/m3)      *)
  voidFraction := events[10].event^.prob/100.0;         (* Void Fraction  (percent)
       *)
  epsilon      := events[13].event^.prob;               (* Uncertainty Factor
      *)

  (*  Multiply FAC Rate by uncertainty before outputting.
  *)

    evPtr^.prob  :=  CalcFacRate(k,  w,  pH,  g,  h,  tKelvin,  time,  stQual,  massFlux,
h2oDensity,voidFraction)*epsilon;
  result := 1;
END FACRATE;


PROCEDURE CalcFailPress(k            : REAL;         (* geometrical factor
      *)
                        w            : REAL;         (* flow velocity m/s
      *)
                         pH           : REAL;          (* pH Value
      *)
                         g            : REAL;         (* oxygen content microg/kg
      *)
                         h            : REAL;        (* percent of chromium and molybdenum in
steel *)
                        tKelvin      : REAL;         (* Temperature (Kelvin)
      *)
                         time         : REAL;          (* Exposure Time in hours
      *)
                         steamQual    : REAL;         (* Percent of steam in flow
      *)
                         massFlux     : REAL;         (* kg/m2s Mass Flux
 *)
                        h2oDensity   : REAL;        (* Density of water at saturation (kg/m3)
*)
                          voidFraction : REAL;          (* Void Fraction
 *)
                         pipeDens     : REAL;         (* Pipe Density in in micrograms/cm3
      *)
```

```
                        pipeFS      : REAL;         (* Pipe Failure Stress K/si
     *)
                       epsilon      : REAL;         (* Uncertainty Factor
     *)
                        origWall    : REAL;         (* Original Pipe thickness (inches)
     *)
                        hoopStrain  : REAL;          (* Pipe Hoop strain (percent)
     *)
                       radius       : REAL) : REAL;  (* Initial inside pipe radius
     *)
VAR
  erodedWall : REAL;
  answer     : REAL;
BEGIN
  (* Use uncertainty factor E
     f_c(x,t) = sigma_f * (W_original - E*W_c(t))/((r + E*W_c(t))(1 + 0.25* epsilon_f(hoop
strain)))
  *)
  erodedWall  := ((CalcFacRate(k, w , pH, g, h, tKelvin, time, steamQual,
                               massFlux, h2oDensity,voidFraction) * time)/pipeDens) * epsilon;
  answer := (pipeFS * (origWall-erodedWall))/((radius + erodedWall) * (1.0 + 0.25*hoopStrain))
* 1000.0;
  RETURN answer;
END CalcFailPress;

PROCEDURE FAILUREPRESSURE(    numEvents : CARDINAL;
                          VAR events    : ARRAY OF Parameter;
                              evRecAdr  : ADDRESS;
                          VAR result    : CARDINAL) [EXPORT];
VAR
  evPtr        : EventRecPtr;
  k            : REAL;
  w            : REAL;
  pH           : REAL;
  g            : REAL;
  h            : REAL;
  tKelvin      : REAL;
  time         : REAL;
  pipeDens     : REAL;
  pipeFS       : REAL;
  epsilon      : REAL;
  origWall     : REAL;
  hoopStrain   : REAL;
  radius       : REAL;
  massFlux     : REAL;
  h2oDensity   : REAL;
  voidFraction : REAL;
  stQual       : REAL;
```

```
BEGIN
  evPtr  := CAST(EventRecPtr, evRecAdr);

  IF (numEvents < 17) THEN
    result := 0;
    evPtr^.prob := 1.0;
    RETURN;
  END;

  k             := events[0].event^.prob;            (* geometrical factor
    *)
  w            := events[1].event^.prob;            (* flow velocity m/s
    *)
  pH            := events[2].event^.prob;            (* pH Value
    *)
  g             := events[3].event^.prob;           (* oxygen content microg/kg
    *)
  h             := events[4].event^.prob/100.0;      (* percent of chromium and molybdenum in
steel *)
  tKelvin      := events[5].event^.prob + 273.15;   (* Temperature (Kelvin)
    *)
  time          := events[6].event^.prob;            (* Exposure Time in hours
    *)
  stQual       := events[7].event^.prob/100.0;      (* Steam Quality by percent
    *)
  massFlux      := events[8].event^.prob;            (* kg/m2s Mass Flux
    *)
  h2oDensity    := events[9].event^.prob;           (* Density of water at saturation (kg/m3)
    *)
  voidFraction := events[10].event^.prob/100.0;     (* Void Fraction
    *)
  pipeDens     := events[11].event^.prob*1000.0;    (* Pipe Density in in micrograms/cm3
    *)
  pipeFS       := events[12].event^.prob;           (* Pipe Failure Stress K/si
    *)
  epsilon      := events[13].event^.prob;           (* Uncertainty Factor
    *)
  origWall     := events[14].event^.prob;           (* Original Pipe thickness (inches)
    *)
  hoopStrain   := events[15].event^.prob/100.0;     (* Pipe Hoop strain (percent)
    *)
  radius       := events[16].event^.prob;           (* Initial inside pipe radius
    *)
  evPtr^.prob  := CalcFailPress(k, w, pH, g, h, tKelvin, time, stQual,
                                massFlux, h2oDensity,voidFraction, pipeDens, pipeFS,
                                epsilon, origWall, hoopStrain, radius);
  result := 1;
END FAILUREPRESSURE;
```

```
PROCEDURE CAPACITYLOAD(    numEvents : CARDINAL;
                       VAR events    : ARRAY OF Parameter;
                           evRecAdr  : ADDRESS;
                       VAR result    : CARDINAL) [EXPORT];
VAR
  evPtr        : EventRecPtr;
  k            : REAL;
  w            : REAL;
  pH           : REAL;
  g            : REAL;
  h            : REAL;
  tKelvin      : REAL;
  time         : REAL;
  stQual       : REAL;
  massFlux     : REAL;
  h2oDensity   : REAL;
  voidFraction : REAL;
  pipeDens     : REAL;
  pipeFS       : REAL;
  epsilon      : REAL;
  origWall     : REAL;
  hoopStrain   : REAL;
  radius       : REAL;
  load         : REAL;
  capacity     : REAL;
  failCnt      : CARDINAL;
  i            : CARDINAL;
BEGIN
  evPtr  := CAST(EventRecPtr, evRecAdr);

  IF (numEvents < 18) THEN
    result := 0;
    evPtr^.prob := 1.0;
    RETURN;
  END;
  failCnt   := 0;

  FOR i := 1 TO NumSamples DO
    k            := events[0].unc^[i-1];           (* geometrical factor
    *)
    w            := events[1].unc^[i-1];           (* flow velocity m/s
    *)
    pH           := events[2].unc^[i-1];           (* pH Value
    *)
    g           := events[3].unc^[i-1];           (* oxygen content microg/kg
    *)
```

```
    h            := events[4].unc^[i-1];            (* amount of chromium and molybdenum in
steel  *)
    tKelvin      := events[5].unc^[i-1] + 273.15;   (* Temperature (Kelvin)
    *)
    time         := events[6].unc^[i-1];            (* Exposure Time in hours
    *)
    stQual       := events[7].unc^[i-1]/100.0;      (* Steam Quality by percent
    *)
    massFlux     := events[8].unc^[i-1];            (* kg/m2s Mass Flux
    *)
    h2oDensity   := events[9].unc^[i-1];           (* Density of water at saturation (kg/m3)
    *)
    voidFraction := events[10].unc^[i-1];           (* Void Fraction
    *)
    pipeDens     := events[11].unc^[i-1]*1000.0;    (* Pipe Density in in micrograms/cm3
    *)
    pipeFS       := events[12].unc^[i-1];          (* Pipe Failure Stress K/si
    *)
    epsilon      := events[13].unc^[i-1];          (* Uncertainty Factor
   *)
    origWall     := events[14].unc^[i-1];           (* Original Pipe thickness (inches)
    *)
    hoopStrain   := events[15].unc^[i-1]/100.0;     (* Pipe Hoop strain (percent)
    *)
    radius       := events[16].unc^[i-1];          (* Initial inside pipe radius
    *)

    capacity := CalcFailPress(k, w, pH, g, h, tKelvin, time, stQual,
                              massFlux, h2oDensity, voidFraction, pipeDens, pipeFS,
                              epsilon, origWall, hoopStrain, radius);
    load := events[17].unc^[i-1];

    IF load > capacity THEN
      INC(failCnt);
    END;
  END;

  evPtr^.prob := FLOAT(failCnt) / FLOAT(NumSamples);

  result := 1;
END CAPACITYLOAD;

BEGIN
%IF DLL %THEN
  IF IsInit THEN
    RETURN TRUE;
  ELSE
    RETURN FALSE;
  END;
```

```
%ELSE
  IsSaphPlugIn;
%END
EXCEPT
  EXCEPTIONS.GetMessage (msg);
  (*WinAux.ControlExceptionProc (msg);*)
END PLUGPIPE.
```

NRC FORM 335 (2-89)
NRCM 1102, 3201. 3202

U.S. NUCLEAR REGULATORY COMMISSION

BIBLIOGRAPHIC DATA SHEET

(See Instructions on the reverse)

1. REPORT NUMBER (Assigned by NRC, Add Vol., Supp., Rev., and Addendum Numbers, if any.)
NUREG/CR-5632

2. TITLE AND SUBTITLE
Incorporating Aging Effects into Probabilistic Risk Assessment — A Feasibility Study Utilizing Reliability Physics Models

3. DATE REPORT PUBLISHED
MONTH: August
YEAR: 2001

4. FIN OR GRANT NUMBER
W6329

5. AUTHOR(S)
C. L. Smith, V. N. Shah, T. Kao, G. Apostolakis

6. TYPE OF REPORT
Technical

7. PERIOD COVERED (Inclusive Dates)

8. PERFORMING ORGANIZATION - NAME AND ADDRESS (If NRC, provide Division, Office or Region, U.S. Nuclear Regulatory Commission, and mailing address; if contractor, provide name and mailing address.)
Idaho National Engineering and Environmental Laboratory
Bechtel BWXT Idaho, LLC.
P.O. Box 1625
Idaho Falls, ID 83415-3850

9. SPONSORING ORGANIZATION - NAME AND ADDRESS (If NRC, type "Same as above"; If contractor, provide NRC Division, Office or Region, U.S. Nuclear Regulatory Commission, and mailing address.)
Office of Nuclear Regulatory Research
U.S. Nuclear Regulatory Commission
Washington, DC 20555-0001

10. SUPPLEMENTARY NOTES

11. ABSTRACT (200 words or less)

Traditional PRAs include active components but not passive systems, structures, and components (SSCs) because the passive SSCs are much more reliable than the active ones. The objective of the paper is to evaluate the feasibility of incorporating aging effects into PRAs so that risk impact of aging can be estimated. We have evaluated this feasibility by incorporating into PRA a flow-accelerated corrosion model, the KWU model developed by Kastner and Riedle, which estimates wall thinning. For this purpose, we have used the PRA model developed for the Surry Individual Plant Examination. In addition, we have employed a *load-capacity* model based upon a *reliability physics* model and simplifying assumptions for estimating failure caused by flow-accelerated corrosion. We have demonstrated that the results and insights gained from the NRC Nuclear Power Aging Research Program and other NRC and industry programs related to materials degradation can be integrated into the existing PRA models. However, our evaluation represents feasibility of such integration and *should not* be construed to represent either relative or absolute magnitude of risk posed by flow-accelerated corrosion in PWRs.

12. KEY WORDS/DESCRIPTORS (List words or phrases that will assist researchers in locating the report.)
PWR, probabilistic risk assessments, PRA, reliability physics, NPAR, aging, failure rate, flow-accelerated corrosion, embrittlement, fatigue, erosion, load-capacity, wall thinning, FAC

13. AVAILABILITY STATEMENT
Unlimited

14. SECURITY CLASSIFICATION
(This page)
Unclassified
(This report)
Unclassified

15. NUMBER OF PAGES

16. PRICE